



Université  
de Toulouse

# THÈSE

En vue de l'obtention du

## DOCTORAT DE L'UNIVERSITÉ DE TOULOUSE

**Délivré par :**

Institut National Polytechnique de Toulouse (INP Toulouse)

**Discipline ou spécialité :**

Réseaux, Télécommunications, Systèmes et Architecture

---

**Présentée et soutenue par :**

M. JEAN BAPTISTE PAGOT

le mardi 20 décembre 2016

**Titre :**

Modeling and Monitoring of New GNSS Signal Distortions in the Context of  
Civil Aviation

---

**Ecole doctorale :**

Mathématiques, Informatique, Télécommunications de Toulouse (MITT)

**Unité de recherche :**

Laboratoire de Télécommunications (TELECOM-ENAC)

**Directeur(s) de Thèse :**

M. OLIVIER JULIEN

M. PAUL THEVENON

**Rapporteurs :**

M. GONZALO SECO-GRANADOS, UNIVERSIDAD AUTONOMA DE BARCELONE

Mme LETIZIA LO PRESTI, POLITECNICO DE TURIN

**Membre(s) du jury :**

Mme LETIZIA LO PRESTI, POLITECNICO DE TURIN, Président

M. OLIVIER JULIEN, ECOLE NATIONALE DE L'AVIATION CIVILE, Membre

M. PAUL THEVENON, ECOLE NATIONALE DE L'AVIATION CIVILE, Membre



*I will remember that I didn't make the world, and it doesn't satisfy my equations.  
I will never sacrifice reality for elegance without explaining why I have done so.  
Nor will I give the people who use my model false comfort about its accuracy.  
Instead, I will make explicit its assumptions and oversights.*

*From the The Modelers' Hippocratic Oath*



# Abstract

Global Navigation Satellite Systems (GNSS) is used nowadays in various fields for navigation and positioning including safety-of-life applications. Among these applications is civil aviation that requires a very high quality of service for the most demanding phases of flight. The quality of the GNSS service is typically based on four criteria (integrity, accuracy, availability and continuity), that have to meet International Civil Aviation Organization (ICAO) requirements. To meet these requirements any source of potential service degradations has to be accounted for.

One such example is GNSS signal distortions due to the satellite payload which can manifest in two ways:

- Nominal signal distortions generated by healthy satellites due to payload imperfections. This type of perturbation can limit the accuracy of the GNSS measurements and result in the unavailability of the service for some very stringent phases of flight. To mitigate their impact, a precise characterization of these distortions and a knowledge of their effects on civil aviation GNSS receivers are necessary.
- Non-nominal distortions that are triggered by a satellite payload failure. Non-nominal distortions, also called Evil WaveForms (EWFs) are rare events that may pose an integrity risk if the signal remains used by the airborne receiver. The strategy proposed by ICAO to deal with the EWF challenge is to characterize threatening distortions by the definition of a Threat Model (TM) and to build an appropriate monitor, referred to as Signal Quality Monitor (SQM) that will be able to detect any distortion from the TM that could lead to a position integrity failure. This task is performed by GNSS augmentation systems including Ground Based Augmentation Systems (GBAS) and Satellite Based Augmentation Systems (SBAS). The current monitors are based on the analysis of the correlation function.

Supported by the groundwork performed by civil aviation on signal distortions for the GPS L1 C/A signal, this dissertation aims at proposing new distortions models associated to the new Global Positioning System (GPS) and Galileo signals that will be used by civil aviation after 2020.

One important characteristic of GNSS signal distortions is that although they impact all users of the distorted signal, the consequence on the estimated pseudorange is dependent upon the GNSS receiver setting. This makes arduous the estimation of the impact of signal distortions on a GNSS user. The receiver parameters that have an influence on the pseudorange measurement estimated from distorted signals (nominal or non-nominal distortions) are listed. In addition illustrations to show the influence of these parameters on the GNSS receiver signal processing are proposed.

The thesis first looks at the nominal distortions through GPS L1 C/A and Galileo E1C signals. Different types of observations are used based on correlation or chip domain visualization, and using high-gain and omnidirectional antennas.

This investigation allows to:

- compare results with the state-of-the-art to validate the receiver processing software developed for this study,
- confirm published results and provide new results,

- make a comparison between nominal distortions observed from measurements collected with a high-gain dish antenna and with an omnidirectional antenna.

The conclusions of the analysis are that the nominal distortions are relatively constant over years and that a precise characterization of nominal distortions is difficult notably because it is challenging to isolate signal distortions induced by the satellite from distortions induced by the receiver.

After the observation of nominal distortions, the dissertation investigates the non-nominal distortions due to the payload failure. In particular, new TMs for new signals (GPS L5, Galileo E5a and Galileo E1C) are proposed. To define these TMs, the same parameters as the ones used to define the ICAO TM for GPS L1 C/A are used. The main work then consists in defining the range of the TMs parameters for the new signals. The limitation of the range of these parameters is based on two criteria: the impact of a distortion on a reference station and the impact of a distortion on differential users. It is noticeable that the new proposed TMs are larger than the GPS L1 C/A ICAO TM, resulting in an increase by a factor 100 of the number of considered threats.

Then, the dissertation investigates the SQM that would be necessary to protect a civil aviation user against the TMs for new GNSS signals. The new SQM is based on current receiver technologies, in particular the ability to use many correlator outputs from the same signal. The main contribution is to propose an innovative representation to test and compare the SQMs performance whatever the received signal  $C/N_0$  is. This representation is based on several assumptions but a strategy is exposed to still be able to use this representation if all assumptions are not fulfilled. From this representation, new SQMs (for each signal) are designed, their performances are assessed, and optimization processes are described to reduce their complexity.

The concluding chapter of the dissertation reviews the main contributions of this Ph.D.. In addition perspectives for future works that could be conducted from the study performed in this Ph.D. are exposed.

# Résumé

Le GNSS est actuellement présent dans de nombreux domaines et permet le positionnement et la navigation. De nombreuses applications tirent profit du service apporté par le GNSS à l'exemple des applications portant sur la sécurité des personnes. Parmi ces applications, l'aviation civile a besoin d'une qualité de service très élevée et fiable, notamment pendant les phases de vol les plus exigeantes. Cette qualité de service est généralement basée sur quatre critères (l'intégrité, la précision, la disponibilité et la continuité) qui se doivent de respecter les exigences fixées par l'Organisation de l'Aviation Civile Internationale (OACI). Afin de satisfaire ces exigences, toutes les sources de dégradations potentielles du service doivent être prises en compte.

Les distorsions des signaux GNSS générées par la charge utile du satellite sont un exemple de problème qui doit être pris en compte par l'aviation civile. Elles peuvent se manifester de deux manières différentes:

- Les distorsions nominales générées par les satellites en fonctionnement normal. Ces distorsions sont causées par des imperfections au niveau de la charge utile du satellite. Elles limitent la précision des mesures obtenues grâce au GNSS et cela peut entraîner une indisponibilité du service pendant les phases de vol les plus contraignantes. Pour atténuer leur impact, il est nécessaire de caractériser de manière précise ces distorsions et de connaître leurs effets sur les récepteurs GNSS de l'aviation civile.
- Les distorsions non nominales générées lors d'une panne de la charge utile d'un satellite. Les distorsions non nominales, aussi appelées EWFs sont des événements rares qui peuvent poser des problèmes d'intégrité si des signaux affectés par de telles distorsions sont utilisés par un récepteur embarqué. Afin de répondre à la problématique liée aux EWFs, la stratégie proposée par l'OACI est tout d'abord de caractériser par le biais d'un modèle de menaces (aussi appelé TM) les distorsions qui pourraient menacer les utilisateurs. Ensuite le but est de mettre au point un système permettant de détecter les distorsions du TM pouvant entraîner des pertes d'intégrité. Ce système de détection est appelé SQM et est implémenté dans les systèmes d'augmentation du GNSS tels que le GBAS et le SBAS. Les détecteurs actuels sont basés sur une analyse de la fonction de corrélation.

En utilisant les travaux réalisés dans le passé par l'aviation civile dans le cadre du signal GPS L1 C/A, un but de cette thèse est de proposer de nouveaux modèles de distorsions associés aux nouveaux signaux GPS et Galileo qui vont être utilisés par l'aviation civile après 2020.

Une importante propriété des distorsions des signaux GNSS est que, bien qu'elles impactent tous les utilisateurs du signal déformé, la conséquence sur la pseudo-distance estimée dépend du récepteur GNSS. Cela rend compliqué l'estimation de l'impact d'une distorsion sur les récepteurs GNSS. Les paramètres ayant une influence sur la mesure de pseudo-distance estimée à partir d'un signal déformé (que ce soit par une distorsion nominale ou non nominale) sont listés. De plus, des illustrations sont proposées afin de montrer l'influence de ces paramètres sur le traitement du signal opéré par le récepteur GNSS.

Tout d'abord, cette thèse aborde le problème des déformations nominales affectant les signaux GPS L1 C/A et Galileo E1C. Différentes observations sont réalisées à partir de la visualisation de la fonction

de corrélation ou du signal et par l'utilisation d'antennes à haut gain et d'une antenne omnidirectionnelle.

Cette étude permet de :

- comparer les résultats avec ceux présents dans la littérature afin de valider le bon fonctionnement du traitement du signal implémenté dans le récepteur virtuel mis au point dans le cadre de cette thèse,
- confirmer les résultats déjà publiés et fournir de nouveaux résultats,
- faire une comparaison entre les distorsions nominales observées à partir de collectes réalisées grâce à une antenne parabolique à haut gain et à une antenne omnidirectionnelle.

Les conclusions de cette analyse sont que les distorsions nominales sont relativement constantes au fil des années et qu'une caractérisation précise des distorsions nominales est rendue compliquée étant donné la difficulté d'isoler la distorsion du signal induite par le satellite de celle induite par le récepteur.

Après l'observation des distorsions nominales, cette thèse aborde le sujet des distorsions non nominales du signal, causées par une panne de la charge utile. Dans ce cadre, de nouveaux TMs pour les nouveaux signaux (GPS L5, Galileo E5a et Galileo E1C) sont proposés. La définition de ces TMs est basée sur les mêmes paramètres que ceux utilisés pour définir le TM de l'OACI pour le signal GPS L1 C/A. Le travail consiste alors en la limitation des valeurs que peuvent prendre les paramètres en ce qui concerne les nouveaux signaux. Cette limitation est fondée sur deux critères : l'impact d'une distorsion sur la station de référence et l'impact de la distorsion sur un utilisateur différentiel. Il est à noter que les nouveaux TMs proposés lors de cette étude sont plus larges (environ d'un facteur 100) que le TM défini par l'OACI pour le signal GPS L1 C/A.

La dernière étape de cette thèse se focalise sur l'étude de SQMs capables de protéger un utilisateur de l'aviation civile contre les distorsions des TMs proposés pour les nouveaux signaux. Les SQMs envisagés utilisent les technologies actuellement disponibles au niveau récepteur. En particulier, de nombreuses sorties de corrélateurs estimées à partir d'un même signal sont utilisées. La principale contribution est de proposer une représentation innovante afin de tester et de comparer les performances de SQMs quel que soit la valeur du  $C/N_0$ . Cette représentation est basée sur plusieurs hypothèses mais une stratégie qui permet d'utiliser cette représentation quand les hypothèses ne sont pas toutes vérifiées est exposée. A partir de cette représentation, de nouveaux SQMs sont définis pour chaque signal. Les performances de ces SQMs sont estimées et un processus d'optimisation permettant de réduire la complexité des SQMs est décrit.

En guise de conclusion, les principales contributions de cette thèse sont résumées dans le dernier chapitre. De plus, les perspectives qui pourraient être envisagées et les travaux futurs qui pourraient être entrepris en continuité de cette thèse sont exposés.



# Acknowledgements

Many people have contributed to the completion of this work and the writing of this manuscript and I want to acknowledge them. Among them, my supervisors, Olivier Julien and Paul Thevenon who played important role during this three last years. They gave me a part of their vast knowledge making possible the achievement of this Ph.D. thesis. Thank you for your patience, your time, your help, your kindness and for teaching me rigor.

I gratefully acknowledge Professor Letizia Lo Presti and Associate Professor Gonzalo Seco-Granados for reviewing my Ph.D. thesis, providing me some interesting comments and participating as a member of the jury for the thesis defense. I would also like to thank Doctor Eric Phelts, who came from the other side of the Atlantic to attend the thesis defense and who helped me, several times, to understand this so particular topic of EWF.

This Ph.D. thesis would not have been possible without the co-funding of ENAC, ESA and Capgemini. For this reason, I thank more particularly Margaux Cabantous, Denis Maillard and Olivier Sabaloue, my preferred interlocutors with Capgemini, for their responsiveness, the quality of their remarks and the time spent to exchange ideas. I also want to thank Francisco Amarillo Fernandez, my ESA supervisor who found some of his time, although always extremely busy, to speak about technique as well as economic issues related to GNSS. He gave me the chance to spend a nine months stimulating experience at ESTEC. This stay has been the opportunity to meet a lot of people and especially colleagues, for some months, from the TEC-ETN section who made this stay pleasant and formative. I would also like to thank Jaron Samson for his interest in my work and his helpful support and Yoan Gregoire for sharing with me some useful data collections.

Je remercie Christophe Macabiau, qui en plus d'avoir éveillé mon intérêt pour la recherche, m'a proposé de faire cette thèse.

Même si aux vues du contenu de cette thèse on peut penser que j'ai passé trois années sans dormir, sans manger et sans quitter mon clavier d'ordinateur, la vérité est tout autre. En effet, bien que le cadre professionnel de l'ENAC ait été un atout majeur lors de ces trois dernière années, il ne faut pas oublier que les collègues des laboratoires SIGNAV et EMA m'ont permis de passer d'agréables moments que ce soit en pause, en soirée ou encore en conférence. C'est pour cela que je tiens à remercier Anaïs et ses potins, Rémi et sa fameuse idée de me faire lire Dune (allez, je suis presque à la fin), Alexandre alias Monsieur unités internationales, Carl et ses cheese cakes, Amany pongiste à ses heures perdues, Axel et non pas Alex, Antoine qui fait vivre Linux magazine, Jérémy et son aide précieuse en toutes circonstances, Giuseppe qui a bien tenter de me faire apprendre l'italien mais je ne pense pas avoir été un élève modèle, Christophe le "biker", Sara et ses pâtisseries (même si il n'y a pas que la nourriture dans la vie), Ludo l'artiste du grand nord, Alyzé ou l'agence de voyage au top, Anne-Christine que j'aimerais bien voir jouer un jour au badminton, et Hélène et sa bonne humeur.

Je souhaite aussi un bon courage à Ikhlal qui reprend le flambeau de l'étude des EWFs et à tous ceux qui soutiendront leur thèse dans les prochains mois: Enik qui... a été assis en face de moi depuis le début et ce n'est pas rien, Quentin qui n'ayant pas assez de ma présence au travail a accepté une colocation, Capucine voleuse de colocataire, Johan et ses actions à la paillote, Jade, Enzo et Seif.

Et puis il y a aussi tous ceux qui ont déjà fini leur thèse depuis quelque temps: Marion, Philipe, Myriam, Jimmy et Leslie. Pour finir avec le monde professionnel, je souhaite remercier Cathy et Collette pour leur patience.

Je remercie aussi mes amis, ceux qui ont eu le courage de relire certaines parties de la thèse (en fait je ne vois que Cédric et Elie) mais aussi les autres qui m'ont supporté, entre autre, pendant les week-ends et les vacances. Une pensée pour Ludo qui nous a quitté bien trop tôt, toujours à proposer des remarques intéressantes quel que soit le sujet abordé.

Je tiens à remercier mes parents pour leur soutien et l'éducation qu'ils m'ont apportés, deux bases solides qui m'ont permis d'arriver jusqu'ici. Et puis, il y a aussi bien sûr mes deux petites sœurs pour leur enthousiasme (ça arrive) et leur dynamisme, et les autres membres de ma famille. J'espère pouvoir trouver un plus de temps à passer avec vous maintenant que ces trois années sont terminées. Pour finir, merci à Roxanne pour sa patience, son aide et son soutien. Merci d'être à mes côtés.

# Table of Contents

ABSTRACT.....	3
RESUME.....	5
ACKNOWLEDGEMENTS.....	7
TABLE OF CONTENTS .....	9
LIST OF FIGURES.....	15
LIST OF TABLES.....	21
ABBREVIATIONS .....	23
1 INTRODUCTION .....	27
1.1 Thesis Motivations.....	27
1.2 Thesis Objectives.....	28
1.3 Thesis Contributions .....	29
1.4 Thesis Outline .....	31
2 GNSS BACKGROUND.....	33
2.1 PVT Computation using GNSS core constellations.....	33
2.1.1 GNSS positioning principles	33
2.1.2 GNSS structure	35
2.1.3 Pseudorange measurement errors	37
2.2 Civil Aviation Operational Requirements .....	41
2.2.1 Accuracy	41
2.2.2 Integrity	42
2.2.3 Availability	42
2.2.4 Continuity	42
2.2.5 Civil aviation SiS requirements	43
2.3 Augmentation of core constellation systems for civil aviation .....	43
2.3.1 Accuracy improvement	45
2.3.2 Integrity monitoring	50

<b>2.4</b>	<b>Focus on SBAS .....</b>	<b>51</b>
2.4.1	SBAS architecture	51
2.4.2	SBAS differential pseudorange measurement concept	53
2.4.3	SBAS integrity risk allocation	54
2.4.4	Comparison between SBAS and GBAS	55
<b>2.5</b>	<b>Conclusions.....</b>	<b>55</b>
<b>3</b>	<b>GNSS SIGNALS STRUCTURE AND RECEIVER PROCESSING.....</b>	<b>57</b>
<b>3.1</b>	<b>Signals of interest description .....</b>	<b>58</b>
3.1.1	General GNSS signal structure	58
3.1.2	GPS L1 C/A signal structure	60
3.1.3	GPS L5 signal structure	61
3.1.4	Galileo E5a signal structure	63
3.1.5	Galileo E1 OS signal structure	64
3.1.6	Discussion about power spectral density and correlation function	67
3.1.7	Signals structures summary	68
<b>3.2</b>	<b>Analog processing of GNSS receiver .....</b>	<b>68</b>
3.2.1	Antenna	69
3.2.2	RF front-end	69
3.2.3	Analog to digital converter (ADC)	70
3.2.4	Signal expression at the output of the analog section	70
<b>3.3</b>	<b>Digital processing of GNSS receiver .....</b>	<b>72</b>
3.3.1	Correlation process	72
3.3.2	Acquisition	78
3.3.3	Tracking	79
<b>3.4</b>	<b>Conclusions.....</b>	<b>88</b>
<b>4</b>	<b>IMPACT OF GNSS SIGNAL DISTORTIONS ON SIGNAL PROCESSING.....</b>	<b>89</b>
<b>4.1</b>	<b>Category of GNSS signal distortions.....</b>	<b>89</b>
4.1.1	Nominal distortions	90
4.1.2	Non-nominal distortions	95
4.1.3	Origin of GNSS signal distortions	98
<b>4.2</b>	<b>Example of signal distortion .....</b>	<b>101</b>
<b>4.3</b>	<b>Impact of GNSS signal distortions on the receiver.....</b>	<b>102</b>
4.3.1	RF front-end and antenna equivalent filters	103
4.3.2	Impact on tracking loops	103
4.3.3	Effect of nominal distortions on the tracking bias	106
4.3.4	Conclusions about the impact of distortions on a user and differential considerations	109
<b>4.4</b>	<b>Non-nominal signal distortions and SBAS .....</b>	<b>110</b>
4.4.1	Necessity to model threatening distortions	110
4.4.2	Necessity to detect non-nominal distortions	112
4.4.3	Estimation of the Maximum Undetected Differential Error (MUDE)	113

<b>4.5</b>	<b>Visualization of GNSS signal distortions.....</b>	<b>115</b>
4.5.1	Standard deviation and general considerations	115
4.5.2	Chip domain observable method	116
4.5.3	Correlation function observable	120
4.5.4	Comparison of chip domain and correlation function domain observables	122
<b>4.6</b>	<b>Conclusions.....</b>	<b>124</b>
<b>5</b>	<b>NOMINAL DISTORTIONS.....</b>	<b>125</b>
<b>5.1</b>	<b>Setups definition and high-gain dish antenna measurements.....</b>	<b>126</b>
5.1.1	Data collections from high-gain dish antennas	126
5.1.2	Software overview	127
<b>5.2</b>	<b>Chip observation from high-gain dish measurements.....</b>	<b>128</b>
5.2.1	GPS L1 C/A	128
5.2.2	Galileo E1C	130
<b>5.3</b>	<b>Correlation function observable from high-gain dish measurements.....</b>	<b>131</b>
5.3.1	GPS L1 C/A	132
5.3.2	Galileo E1C pilot component	135
<b>5.4</b>	<b>Conclusions and problems related to the observation of nominal distortions with high-gain dish antennas .....</b>	<b>139</b>
<b>5.5</b>	<b>Nominal differential tracking errors studied from an omnidirectional antenna and inter-PRN biases</b>	<b>141</b>
5.5.1	Omnidirectional antenna measurements setup	142
5.5.2	Data set 1 results and introduction of the inter-PRN bias	142
5.5.3	Comparison of results obtained from the three different data sets	145
5.5.4	Conclusions about the observation of nominal distortions with an omnidirectional antenna	146
<b>5.6</b>	<b>Comparison between estimated inter-PRN biases and the state-of-the-art .....</b>	<b>147</b>
5.6.1	High-gain dish antenna inter-PRN biases (Leeheim)	147
5.6.2	Omnidirectional antenna inter-PRN biases	148
5.6.3	Conclusion about the estimation of inter-PRN biases	149
<b>5.7</b>	<b>Conclusions.....</b>	<b>149</b>
<b>6</b>	<b>NON-NOMINAL DISTORTIONS.....</b>	<b>153</b>
<b>6.1</b>	<b>GPS L1 C/A Threat Model .....</b>	<b>153</b>
6.1.1	ICAO Threat Model definition	154
6.1.2	Impact on differential users	157
<b>6.2</b>	<b>Generalization to other modulations .....</b>	<b>160</b>
6.2.1	Difficulties to translate GPS L1 C/A case to other modulations	160
6.2.2	Proposition of a new methodology to define the TS	161
<b>6.3</b>	<b>TM-A like propositions for new signals .....</b>	<b>164</b>
6.3.1	Galileo E5a and GPS L5 TM-A	164
6.3.2	Galileo E1C TM-A	166
6.3.3	Summary of the proposed TM-A for new signals	170

<b>6.4</b>	<b>TM-B like proposition for new signals .....</b>	<b>171</b>
6.4.1	Lower limit for $\sigma$ and $fd$ parameters	171
6.4.2	Upper limit for $\sigma$ and $fd$ parameters	173
6.4.3	Number of tests to cover the entire proposed TM	177
6.4.4	Summary on the proposed TM-B for new signals	182
<b>6.5</b>	<b>TM-C like propositions for new signals .....</b>	<b>184</b>
<b>6.6</b>	<b>Conclusions.....</b>	<b>185</b>
<b>7</b>	<b>SIGNAL QUALITY MONITORING OF NEW SIGNALS .....</b>	<b>187</b>
<b>7.1</b>	<b>SQM requirements and performance assessment .....</b>	<b>187</b>
7.1.1	Maximum tolerable ERRor (MERR)	188
7.1.2	Tests and metrics	191
7.1.3	Minimum Detectable Error (MDE) definition 7.1.4	193
	Targeted requirements ( $Pffd$ , $Pmd$ and TTA) 7.1.5	195
	Theoretical estimation of the MDE	197
7.1.6	Conclusions	200
<b>7.2</b>	<b>Parameters with an influence on SQM performance .....</b>	<b>201</b>
7.2.1	Tested distortions	201
7.2.2	Receiver configurations 7.2.3	202
	Definition of reference SQMs	203
<b>7.3</b>	<b>SQM performance assessment: example on GPS L1 C/A .....</b>	<b>204</b>
7.3.1	A representation to assess SQM performance	205
7.3.2	Scale change to assess SQM performance function of $CN0$	206
7.3.3	Estimation of the equivalent theoretical $CN0$ at a reference station	208
7.3.4	Comparison of SQMs	210
7.3.5	Conclusions	212
<b>7.4</b>	<b>Results on new signals .....</b>	<b>212</b>
7.4.1	Metrics standard deviations vs $CN0$ abacuses for new signals	213
7.4.2	Performance of a SQM based on all available metrics	213
7.4.3	Optimization of the SQM	216
7.4.4	Conclusions about optimal SQM on new signals	226
<b>7.5</b>	<b>Conclusions.....</b>	<b>227</b>
<b>8</b>	<b>CONCLUSION AND RECOMMENDATIONS FOR FUTURE WORKS.....</b>	<b>229</b>
<b>8.1</b>	<b>Conclusions.....</b>	<b>229</b>
<b>8.2</b>	<b>Recommendations for future work.....</b>	<b>232</b>
	REFERENCES.....	235
	APPENDIX A. CORRELATOR OUTPUTS AND CDO STANDARD DEVIATIONS.....	243
<b>A.1</b>	<b>Theoretical derivation of standard deviations .....</b>	<b>243</b>

A.1.1	Correlation function observable	243
A.1.2	Chip Domain Observable	246
A.2	CDO and correlator outputs standard deviations estimated from simulations .....	247
APPENDIX B.	THEORETICAL AND SIMULATED METRICS STANDARD DEVIATIONS.....	251
B.1	Theoretical derivation of some metrics standard deviations.....	251
B.2	Theoretical VS simulated $\sigma_{metric}$ .....	252
APPENDIX C.	LIST OF SIGNALS COLLECTED FROM HIGH-GAIN DISH ANTENNAS .....	255
APPENDIX D.	NOMINAL DISTORTION PARAMETERS .....	257
APPENDIX E.	FEATURES OF TESTED FILTERS.....	259
APPENDIX F.	DISTORTIONS TO TEST ON THE PROPOSED TMS.....	263
F.1	Number of tests on area 1 for Galileo E5a, GPS L5 and GPS L1 C/A.....	263
F.1.1	Galileo E5a and GPS L5 area 1	263
F.1.2	GPS L1 C/A area 1	264
F.2	Number of tests on area 2.....	266
F.2.1	Galileo E1C area 2	266
F.2.2	Galileo E5a and GPS L5 area 2	268
F.2.3	GPS L1 C/A area 2	268
F.3	Conclusion about the number of distortions to test .....	269
APPENDIX G.	PROPERTIES OF TM-B DISTORTIONS AT $\sigma_{fd}$ AND $\sigma_{fd}^2$ CONSTANT .....	271
G.1	$\sigma_{fd}$ ratio .....	271
G.2	$\sigma_{fd}^2$ ratio .....	273





# List of Figures

<b>Figure 2-1.</b> SiS integrity risk allocation example.....	50
<b>Figure 2-2.</b> SBAS general architecture [Chatre, 2003].....	52
<b>Figure 2-3.</b> General SBAS fault tree, SiS integrity risk allocation.....	54
<b>Figure 2-4.</b> General fault tree, ground system SiS integrity risk allocation. ....	54
<b>Figure 3-1.</b> General structure of a GNSS receiver.....	57
<b>Figure 3-2.</b> Galileo and GPS frequency plans [GSA, 2010]. ....	58
<b>Figure 3-3.</b> Normalized PSD (on the left) and normalized autocorrelation function (on the right) of the GPS L1 C/A signal. ....	61
<b>Figure 3-4.</b> Normalized PSD (on the left) and normalized autocorrelation function (right) of the GPS L5 quadrature component. ....	63
<b>Figure 3-5.</b> Correlation function terms used to defined CBOC autocorrelation function. ....	66
<b>Figure 3-6.</b> Normalized PSD of the Galileo E1 signal (on the left) and normalized autocorrelation function (right) of the Galileo E1C signal. ....	66
<b>Figure 3-7.</b> Chip shapes and autocorrelation functions for different signals. ....	68
<b>Figure 3-8.</b> Influence of the filter bandwidth on chip shapes.....	70
<b>Figure 3-9.</b> Illustration of the code correlation process for different code delays between the incoming signal and the local replica.....	75
<b>Figure 3-10.</b> Correlation functions between a CBOC(6,1,1/11)-modulated signal and a CBOC(6,1,1/11)-modulated signal (blue) or a BOC(1,1)-modulated signal (red). ....	76
<b>Figure 3-11.</b> Correlation functions for different pre-correlation filters.....	77
<b>Figure 3-12.</b> Example of GPS L1 C/A acquisition grids. On the left, a signal is acquired, whereas on the right no signal is found by the receiver. ....	79
<b>Figure 3-13.</b> General structure of a DLL. Dashed block is outside the DLL.....	80
<b>Figure 3-14.</b> Examples of S-curves for an unfiltered GPS L1 C/A signal and different DLL discriminators, $CS = 0.2$ chip. In blue is the early minus late discriminator, in orange the DP discriminator, in yellow the EMLP and in purple the early minus late normalized by the early plus late.....	82
<b>Figure 3-15.</b> Example of PLL standard deviations due to all sources of errors function of the C/N0 [Kaplan and Hegarty, 2006].....	84
<b>Figure 3-16.</b> General structure of a PLL. Dashed block is outside the PLL.....	85
<b>Figure 3-17.</b> S-curve of the atan PLL discriminator.....	85
<b>Figure 3-18.</b> Example of PLL standard deviations due to all sources of errors function of the C/N0 [Kaplan and Hegarty, 2006].....	87
<b>Figure 4-1.</b> Example of delay between rising and falling transitions zero-crossings (GPS L1 C/A, PRN 4). ....	92
<b>Figure 4-2.</b> Results about delay between rising and falling transitions zero-crossings for different signals (GPS L1 C/A and one GPS L5) [Wong et al., 2010]. ....	92
<b>Figure 4-3.</b> Results about analog nominal distortions (GPS L1 C/A in red and one GPS L5 in blue) [Wong et al., 2010]. ....	93
<b>Figure 4-4.</b> Imbalance between I and Q channels and 10 MHz ringing [Gunawardena and van Graas, 2012b].....	95

<b>Figure 4-5.</b> Spectrum of signals transmitted by a healthy satellite (left) and SV 19 during its failure (right).....	96
<b>Figure 4-6.</b> Chip domain representation of signals transmitted by a healthy satellite (left) and the SV 19 during the failure (right).....	97
<b>Figure 4-7.</b> Nominal (orange) and distorted (blue) BPSK(1)-modulated signals on ten chips. ....	101
<b>Figure 4-8.</b> Nominal (orange) and distorted (blue) CBOC(6,1,1/11,-)-modulated signals on ten chips. ....	102
<b>Figure 4-9.</b> Nominal (orange) and distorted (blue) BPSK(10)-modulated signals on ten chips. ....	102
<b>Figure 4-10.</b> EML S-curves for a nominal signal (dashed plots) and a distorted signal (continuous plots) BPSK(1) modulated and different correlator spacing's: 0.2 chip (red), 0.35 chip (blue).....	105
<b>Figure 4-11.</b> Nominal (orange) and distorted (blue) EML S-curves for BPSK(1) (top left), for CBOC(6,1,1/11) (top right) and BPSK(10) (bottom) modulations.....	106
<b>Figure 4-12.</b> Tracking error induced by different GPS L1 C/A signals at different correlator spacing's [Wong, 2014]. One curve corresponds to one PRN.....	107
<b>Figure 4-13.</b> Receiver parameters having an influence on the impact of GNSS signal distortions on pseudorange measurements.....	109
<b>Figure 4-14.</b> Summary of civil aviation and DFMC SBAS receivers configurations in terms of bandwidth and correlator spacing.....	115
<b>Figure 4-15.</b> Illustration of the CDO concept. ....	117
<b>Figure 4-16.</b> Example of nominal (blue) and distorted (orange) CDO for BPSK(1) (top left), CBOC(6,1,1/11) (top right) and BPSK(10) (bottom) modulations.....	118
<b>Figure 4-17.</b> Block scheme summarizing CDO algorithm.....	119
<b>Figure 4-18.</b> Illustration of the correlation function observable concept. ....	120
<b>Figure 4-19.</b> Nominal (blue) and distorted (orange) correlation function observables for BPSK(1) (top left), CBOC(6,1,1/11) (top right) and BPSK(10) (bottom) modulations.....	122
<b>Figure 5-1.</b> Chip domain observable of rising and falling transitions,.....	129
<b>Figure 5-2.</b> Superposition of results from Stanford University [Wong et al., 2010] with results obtained by another set of collected data (Leeheim and CNES). Visualization of the delay between rising and falling transitions. ....	130
<b>Figure 5-3.</b> Chip domain observable on positive and negative chips,.....	131
<b>Figure 5-4.</b> Difference between correlation functions affected by nominal distortions and the ideal unfiltered correlation function. GPS L1 C/A.....	133
<b>Figure 5-5.</b> Tracking error function of the correlator spacing for different GPS L1 C/A PRNs (reference at CS = 0.1 chip).....	134
<b>Figure 5-6.</b> Difference between correlation functions affected by nominal distortions and an ideal unfiltered correlation function. Galileo E1C. ....	136
<b>Figure 5-7.</b> Difference between correlation functions affected by nominal distortions and an ideal unfiltered correlation function. Galileo E1C and E1B. (PRN 14 only) ....	137
<b>Figure 5-8.</b> Difference between nominal distortions on the correlation functions of the E1C and the E1B components.....	138
<b>Figure 5-9.</b> Tracking error function of the correlator spacing for different Galileo E1C PRNs (reference at CS = 0.25 chip).....	139
<b>Figure 5-10.</b> Comparison of nominal distortions for the same PRN making the difference of correlation functions with and without nominal distortions. In red, data were collected by the CNES, in blue, by the DLR.....	140

<b>Figure 5-11.</b> Comparison of differential tracking biases entailed by nominal distortions for the same PRN (reference at CS = 1 chip).....	140
<b>Figure 5-12.</b> Chip domain comparison of nominal distortions for the same PRN.....	141
<b>Figure 5-13.</b> Difference between chip domain observables obtained from the same PRN.....	141
<b>Figure 5-14.</b> EML discriminator outputs multiplied by $c$ (reference CS at 0.1 chip) recorded with an omnidirectional antenna and process by a NovAtel GIII receiver. ....	143
<b>Figure 5-15.</b> Differential tracking errors (reference at 0.1 chip and user at 1 chip) recorded with an omnidirectional antenna and processed by the NovAtel GIII. ....	144
<b>Figure 5-16.</b> Sky-plots at the beginning of the data set 1 collection (left) and at the end of the data set 1 collection, 1 h after (right). ....	144
<b>Figure 5-17.</b> Superposition of inter-PRN biases estimated from high-gain dish antenna measurements with results obtained in [Wong, 2014]. (reference at 0.1 chip and user at 1 chip).....	148
<b>Figure 5-18.</b> Superposition of inter-PRN biases estimated from omnidirectional antenna measurements with results obtained in [Wong, 2014]. (reference at 0.1 chip and user at 1 chip)....	149
<b>Figure 6-1.</b> Illustration of the ICAO TM-A impact on the signal (left) and on the correlation function (right). The nominal signal is in blue, the distorted one in orange.....	154
<b>Figure 6-2.</b> Illustration of the ICAO TM-B impact on the signal (left) and on the correlation function (right). The nominal signal is in blue, the distorted one in orange.....	155
<b>Figure 6-3.</b> Illustration of the ICAO TM-C impact on the signal (left) and on the correlation function (right). The nominal signal is in blue, the distorted one in orange.....	156
<b>Figure 6-4.</b> Impact of the TM-A (at top on the left), the TM-B (at top on the right), and the TM-C (at bottom) on the worst differential tracking error. ....	159
<b>Figure 6-5.</b> Impact of the TM-A for GPS L5 and Galileo E5a signals for different $\Delta$ . On the left, impact on the reference station tracking error. On the right, impact on the worst differential tracking error. ....	164
<b>Figure 6-6.</b> Distorted GPS L5/Galileo E5a correlation functions for different values of $\Delta$ filtered by a 6 <sup>th</sup> -order Butterworth (24 MHz). ....	165
<b>Figure 6-7.</b> Galileo E1 signal generation block scheme [Navipedia, 2015]. ....	166
<b>Figure 6-8.</b> Impact of digital distortion 1 on the signal (left), and on the correlation function (right). ....	167
<b>Figure 6-9.</b> Impact of digital distortion 2 on the signal (left), and on the correlation function (right). ....	167
<b>Figure 6-10.</b> Galileo E1C signal generation unit and digital distortions. ....	168
<b>Figure 6-11.</b> CBOC signals affected by different digital distortions on the top and associated correlation functions on the bottom.....	169
<b>Figure 6-12.</b> Tracking error for TM-A1 and TM-A2 and different delta values ( $\Delta$ and $\Delta_{11}$ ).....	170
<b>Figure 6-13.</b> Tracking errors entail by low $f_d$ distortions on a reference station for different signals. ....	172
<b>Figure 6-14.</b> Tracking error entails by low $\sigma$ distortions on a reference station, GPS L1 C/A.....	172
<b>Figure 6-15.</b> Worst differential tracking error for different signal distortion parameters. On the right, only the 1 m limit is shown. Blue limits give the remaining conservative TM. Red limit underlines that the TM cannot be bounded for high $\sigma$ values. Galileo E1C. ....	173
<b>Figure 6-16.</b> Worst differential tracking error for different signal distortion parameters. On the right, only the 1 m limit is shown. Blue limits give the remaining conservative TM. Red limit underlines that the TM cannot be bounded for high $\sigma$ values. Galileo E5a and GPS L5. ....	173

<b>Figure 6-17.</b> Worst differential tracking error for different signal distortion parameters. On the right, only the 1 m limit is shown. Blue limits give the remaining conservative TM. Red limit underline that the TM cannot be bounded for high $\sigma$ values. GPS L1 C/A.....	174
<b>Figure 6-18.</b> Differential tracking errors in meter generated by a TM-B distortion, function of $\sigma$ and $f_d$ for signals of interest.....	175
<b>Figure 6-19.</b> Impact of highly attenuated TM-B distortions on the correlation function. ....	175
<b>Figure 6-20.</b> Tracking errors affecting the reference in meter generated by TM-B distortions, function of $\sigma$ and $f_d$ . Blue rectangles represent area 2 limits, black lines area 1 upper limits.....	176
<b>Figure 6-21.</b> $\sigma = 1$ Mnepers/s increment in the traditional $\sigma$ TM representation. Points represent tested distortions.....	177
<b>Figure 6-22.</b> $\sigma f_d = 1$ nepers/s/Hz/MHz increment in the traditional $\sigma$ TM representation. Points represent tested distortions.....	178
<b>Figure 6-23.</b> Example of a TS grid (GPS L1 C/A ICAO TM).....	179
<b>Figure 6-24.</b> $\Delta err\_dist$ as a function of $\sigma$ associated to the TS grid from Figure 6-23 (GPS L1 C/A ICAO TM). ....	179
<b>Figure 6-25.</b> Example of TS grid (Galileo E1C, area 1 of the proposed TM-B).....	180
<b>Figure 6-26.</b> $\Delta err\_dist$ as a function of $\sigma$ associated to the zone 1 of the selected TS grid (Galileo E1C, area 1 of the proposed TM-B).....	181
<b>Figure 6-27.</b> $\Delta err\_dist$ as a function of $\sigma$ associated to the zone 2 of the selected TS grid (Galileo E1C, area 1 of the proposed TM-B).....	181
<b>Figure 6-28.</b> $\Delta err\_dist$ as a function of $\sigma$ associated to the zone 3 of the selected TS grid (Galileo E1C, area 1 of the proposed TM-B).....	182
<b>Figure 6-29.</b> Summary of reasons that are considered to limit TSs.....	183
<b>Figure 6-30.</b> Area 1 (black) and area 2 (red) in the $\sigma f_d$ representation (left) and in the $\sigma$ representation (right) for Galileo E5a and GPS L5 signals. ....	184
<b>Figure 7-1.</b> Acceptable values of maximum L5 and L1 biases for DFMC SBAS.....	191
<b>Figure 7-2.</b> Difference between the detection threshold and the MDE. ....	194
<b>Figure 7-3.</b> Kmetric, j factors if metrics are totally dependent (red plot) or totally independent (blue plot) function of the sub-tests number. ....	198
<b>Figure 7-4.</b> Theoretical and simulated metrics standard deviations on a BPSK(1)-modulated signal for $CN_0 = 30$ dB-Hz and $T_{int} = 1$ s. ....	199
<b>Figure 7-4.</b> Correlator outputs used to design the SQM (represented in green).....	203
<b>Figure 7-5.</b> Example of worst differential tracking errors function of TestMDE.....	205
<b>Figure 7-6.</b> Comparison of SQM performances considering that the reference station is operating at $CN_0 = 35$ dB-Hz (left) and $CN_0 = 38$ dB-Hz (right).....	206
<b>Figure 7-7.</b> Example of worst differential errors function of $CN_0$ .....	207
<b>Figure 7-8.</b> Example of reference station metrics standard deviations compared to theoretical values. One curve corresponds to one iso- $CN_0$ . ....	209
<b>Figure 7-9.</b> Simple ratio metrics performance thresholds for different $CN_0$ and different distance to the prompt.....	210
<b>Figure 7-10.</b> Comparison of two SQMs performance. ....	211
<b>Figure 7-11.</b> Metric (simple ratio) standard deviations values. One curve corresponds to one iso- $CN_0$ . Galileo E1C signal on the left, Galileo E5a (and GPS L5 signal) on the right. ....	213
<b>Figure 7-12.</b> Reference SQM performance considering the proposed Galileo E1C TM. ....	214
<b>Figure 7-13.</b> Reference SQM performance considering the proposed Galileo E5a TM. ....	215

<b>Figure 7-14.</b> Distorted correlation function (in red) that induces the step around 26 dB-Hz on Galileo E5a and GPS L5 SQM performance. ....	215
<b>Figure 7-15.</b> Algorithm to optimize the SQM at a given working point. ....	217
<b>Figure 7-16.</b> SQME1C_optimal1 (in red) and SQME1C_optimal2 (in blue) performances compared to baseline SQM (in green) considering the proposed Galileo E1C TM. ....	219
<b>Figure 7-17.</b> SQME5a_optimal1 and SQME5a_optimal2 performances considering the proposed Galileo E5a TM (also valid for GPS L5). MUDE = 2.78 m for $CN0 = 25.3$ dB-Hz. ....	220
<b>Figure 7-18.</b> SQME5a_optimal3 and SQME5a_optimal4 performances considering the proposed Galileo E5a TM (also valid for GPS L5). MUDE = 0.61 m for $CN0 = 39$ dB-Hz. ....	221
<b>Figure 7-19.</b> Algorithm of SQM optimization at all $CN0$ values. ....	223
<b>Figure 7-19.</b> Correlator outputs used in the optimal SQM (Galileo E1C). ....	224
<b>Figure 7-20.</b> SQME1C_optimal_all1 performance (in red) compared to the baseline SQM performance (in green). ....	225
<b>Figure 7-21.</b> SQME5a_optimal_all1 performance (in red) compared to the baseline SQM performance (in green). ....	226
<b>Figure A-1.</b> Correlator outputs and associated standard deviation in case 1. ....	248
<b>Figure A-2.</b> Bins value and associated standard deviation in case 2. ....	248
<b>Figure A-3.</b> Bins value and associated standard deviation in case 3. ....	249
<b>Figure B-1.</b> Theoretical (continuous line) and simulated (dotted line) metrics standard deviations on BPSK(1) signal. ....	252
<b>Figure B-2.</b> Theoretical (continuous line) and simulated (dotted line) metrics standard deviations on CBOC(6,1,1/11) signal. ....	252
<b>Figure B-3.</b> Theoretical (continuous line) and simulated (dotted line) metrics standard deviations on BPSK(10) signal. ....	253
<b>Figure E-1.</b> Amplitude, phase and differential group delay of the 6 <sup>th</sup> -ordre Butterworth filter used in simulations. ....	259
<b>Figure E-2.</b> Amplitude, phase and differential group delay of resonator filter type with a constant group delay equal to zero used in simulations. ....	260
<b>Figure E-3.</b> Amplitude, phase and differential group delay of resonator filter type with a concave group delay and a 150 ns differential group delay used in simulations. ....	260
<b>Figure E-4.</b> Amplitude, phase and differential group delay of a 6 <sup>th</sup> -order Butterworth filter for the amplitude and the smallest order Butterworth filter leading to a differential group delay higher than 150 ns for the phase used in simulations. ....	261
<b>Figure E-5.</b> Chip distortion induces by the four different filters. ....	261
<b>Figure F-1.</b> Example of TS grid (Galileo E5a and GPS L5, area 1 of the proposed TM). ....	264
<b>Figure F-2.</b> $\Delta err\_dist$ associated to the selected TS grid (Galileo E5a and GPS L5, area1 of the proposed TM). ....	264
<b>Figure F-3.</b> Example of TSs grid (GPS L1 C/A, area 1 of the proposed TM). ....	265
<b>Figure F-4.</b> $\Delta err\_dist$ associated to the selected TS grid for GPS L1 C/A area 1. On the left it corresponds to zone 1, on the middle to zone 2 and on the right to zone 3. ....	265
<b>Figure F-5.</b> Example of a TS grid in the $\sigma_{fd2}$ representation (Galileo E1C, area2 of the proposed TM). ....	266
<b>Figure F-6.</b> Example of a TS grid in the $\sigma$ representation (Galileo E1C, area2 of the proposed TM). ....	267
<b>Figure F-7.</b> $\Delta err\_dist$ associated to the TS grid from Figure F-6 (Galileo E1C, area2 of the proposed TM). ....	267

<b>Figure F-8.</b> $\Delta err\_dist$ values (Galileo E5a and GPS L5, area2 of the proposed TM). .....	268
<b>Figure F-9.</b> $\Delta err\_dist$ values (GPS L1 C/A, area2 of the proposed TM).....	269
<b>Figure G-1.</b> Signal shape for different $f_d$ but the same $\sigma f_d$ . GPS L1 C/A. ....	271
<b>Figure G-2.</b> Average distortion first peakovershoot in % (left) and standard deviation associated to the average (right) function of $\sigma f_d$ . GPS L1 C/A.....	272
<b>Figure G-3.</b> Signal shape for different $f_d$ but the same $\sigma f_d = 3$ nepers/Hz. Galileo E1C.....	272
<b>Figure G-4.</b> Signal shape for different $f_d$ but the same $\sigma f_d = 2.4$ nepers/Hz. Galileo E5a.....	273
<b>Figure G-5.</b> Signals (left) and correlation functions (right) for several $f_d$ but the same $\sigma f_d^2 = 1$ nepers/s/Hz/MHz. GPS L1 C/A signal. ....	273
<b>Figure G-6.</b> Signals (left) and correlation functions (right) for several $f_d$ but the same $\sigma f_d^2 = 3$ nepers/s/Hz/MHz. GPS L1 C/A signal. ....	274
<b>Figure G-7.</b> Correlation function distortions for several $f_d$ (1: 5: 16 MHz) but the same $\sigma f_d^2 = 1$ nepers/s/Hz/MHz. Galileo E1C on the right and Galileo E5a on the left.....	274
<b>Figure G-8.</b> Differential tracking error on a Galileo E1C signal in the $\sigma/f_d^2$ representation.....	275

# List of Tables

<b>Table 2-1.</b> Space segment of four GNSS. ....	36
<b>Table 2-2.</b> Order of magnitude of code measurement errors. ....	41
<b>Table 2-3.</b> Civil Aviation Signal-in-Space Requirements. ....	44
<b>Table 2-4.</b> GPS L1 C/A pseudorange measurement errors order of magnitude before and after applying differential corrections. ....	49
<b>Table 2-5.</b> Space segment of the two SBASs of interest: WAAS and EGNOS [Navipedia, 2015] and [GALILEO LA, 2015]. ....	52
<b>Table 2-6.</b> Ground segment of the two SBASs of interest. [Navipedia, 2015] and [GALILEO LA, 2015]. ....	52
<b>Table 3-1.</b> Characteristics of Galileo and GPS signals of interest. ....	60
<b>Table 4-1.</b> Results about delay between rising and falling transitions zero-crossings for different signals (GPS L5, Galileo E5a and Galileo E1 OS) [Thoelert et al., 2014]. ....	93
<b>Table 4-2.</b> Characteristics of GPS L1 C/A civil aviation receivers parameters with an influence on code pseudorange measurements defined by ICAO [ICAO, 2006]. ....	114
<b>Table 4-3.</b> Characteristics of expected civil aviation receivers parameters with an influence on code pseudorange measurements for different signals. ....	114
<b>Table 5-1.</b> Antennas and digitizers features. ....	126
<b>Table 5-2.</b> Tracking parameters used in the setup. ....	128
<b>Table 5-3.</b> Comparison of nominal distortion parameters for GPS L1 C/A signal. ....	129
<b>Table 5-4.</b> Inter-PRN biases for different PRNs with associated satellite elevations at the beginning and at the end of the data collection. (data set 1). ....	144
<b>Table 5-5.</b> Inter-PRN biases for different PRNs with associated satellite elevations at the beginning and at the end of the data collection. (data sets 1, 2 and 3). ....	146
<b>Table 6-1.</b> ICAO TS defined for GPS L1 C/A signals. ....	157
<b>Table 6-2.</b> Reference receiver and user receiver configurations used to estimate tracking errors and differential tracking errors in chapter 6 for GPS L1 C/A signal. ....	158
<b>Table 6-3.</b> Reference receiver and user receiver configurations used to estimate tracking error and differential tracking error in chapter 6 for new signals. ....	163
<b>Table 6-4.</b> Digital parameters proposed range for Galileo E1C, Galileo E5a and GPS L5. ....	171
<b>Table 6-5.</b> Analog parameters proposed range for different signals on area 1. ....	174
<b>Table 6-6.</b> Analog parameters proposed range for different signals on area 2. ....	177
<b>Table 6-7.</b> Proposed TM-B parameters range for different signals using two representations. ....	184
<b>Table 6-8.</b> Proposed TM-C parameters range for different signals. ....	185
<b>Table 6-9.</b> Summary of proposed TM parameters range for different signals. ....	186
<b>Table 7-1.</b> Static MERR values for WAAS for L1-only and dual-frequency users [Phelts et al., 2013]. ....	190
<b>Table 7-2.</b> Definition of MDE, MERR and MUDE. ....	200
<b>Table 7-2.</b> GPS L1 C/A TM used to estimate SQM performance. ....	201
<b>Table 7-3.</b> Galileo E1C, Galileo E5a and GPS L5 TMs used to estimate SQM performance for different signals (in bold differences with proposed TMs from chapter 6). ....	202

<b>Table 7-4.</b> Reference receiver and user receiver configurations used to estimate SQM performance for different signals. ....	202
<b>Table 7-5.</b> SQM performance considering all available metrics.....	226
<b>Table A-1.</b> Description of the different tested cases. ....	247
<b>Table A-2.</b> Description of the different tested cases. ....	249
<b>Table C-1.</b> Information about GPS L1 C/A data collections. In blue are highlighted signals collected by CNES. ....	255
<b>Table C-2.</b> Information about Galileo E1C data collections. ....	256
<b>Table D-1.</b> Information about GPS L1 C/A data collections. In blue are highlighted results obtained from CNES measurements. ....	257
<b>Table D-2.</b> Information about GPS L1 C/A data collections. In blue are highlighted results obtained from CNES measurements. ....	258



# Abbreviations

AAIM	Aircraft Autonomous Integrity Monitoring
ABAS	Aircraft Based Augmentation System
ADC	Analog to Digital Convertor
AFS	Atomics Frequency Standard
AGC	Automatic Gain Controller
APV	Approach Procedure with Vertical guidance
ARAIM	Advanced Receiver Autonomous Integrity Monitoring
ARNS	Aeronautical Radio Navigation Services
BPSK	Binary Phase Shift Keying
BDT	BeiDou Time
C/A	Coarse/Acquisition
CAT	CATegory
CBOC	Composite Binary Offset Carrier
CDO	Chip Domain Observable
CMCU	Clock Monitoring and Control Unit
CPF	Central Processing Facility
DFMC	Dual-Frequency Multi-Constellation
DFRE	Dual-Frequency Range Error
DGNSS	Differential Global Navigation Satellite System
DLL	Delay Lock Loop
DME	Distance Measuring Equipment
DP	Dot Product
DSSS	Direct Sequence Spread Spectrum
ECEF	Earth-Centered Earth-Fixed
EGNOS	European Geostationary Navigation Overlay Service
EML	Early Minus Late
EMLP	Early Minus Late Product
ENAC	Ecole Nationale de l'Aviation Civile
ESA	European Spatial Agency
EWf	Evil WaveForm
FAA	Federal Aviation Administration
FGUU	Frequency Generation and Up-conversion Unit
FLL	Frequency Lock Loop
FOC	Fully Operational Capability
GAD	Ground Accuracy Designator
GaAs	Gallium Arsenide
GBAS	Ground Based Augmentation System
GEAS	GNSS Evolutionary Architecture Study
GEO	Geostationary Earth Orbit
GIVE	Grid Ionospheric Vertical Error
GNSS	Global Navigation Satellite Systems

## *Abbreviations*

GPS	Global Positioning System
GSA	european GNSS Agency
GSO	Geosynchronous earth Orbit
GST	Galileo Satellite Time
GUS	Ground Uplink Station
ICAO	International Civil Aviation Organization
IF	Intermediate Frequency
ITU	International Telecommunication Union
LAAS	Local Area Augmentation System
LNA	Low Noise Amplifier
LoS	Line-of-Sight
LPV	Localizer Performance with Vertical guidance
MCC	Master Control Center
MDE	Minimum Detectable Error
MDR	Minimum Detectable Ratio
MDU	Mission Data Unit
MEO	Medium Earth Orbit
MERR	Maximum tolerable ERROR
MEWF	Most Evil WaveForm
MI	Misleading Information
MOPS	Minimum Operational Performance Standards
MUDE	Maximum Undetectable Differential Error
NAVIC	NAVigation Indian Constellation
NDU	Navigation Data Unit
NLES	Navigation Land Earth Station
NGSU	Navigation Signal Generation Unit
OMUX	Output MULTiplex
OS	Open Service
PLL	Phase Lock Loop
PRN	Pseudo-Random Noise
PSD	Power Spectral Density
PVT	Position Velocity Time
QZSS	Quasi-Zenith Satellite System
RABF	Radio frequency Antenna Beam Forming
RAIM	Receiver Autonomous Integrity Monitoring
RF	Radio Frequency
RIMS	Ranging Integrity Monitoring Station
RNSS	Radio Navigation Satellite System
RTCA	Radio Technical Commission for Aeronautics
SARPs	Standard And Recommended Practices
SAW	Surface Acoustic Waves
SBAS	Satellite Based Augmentation System
SiS	Signal-in-Space
SISA	Signal-In-Space Accuracy
SNR	Signal to Noise Ratio
SPS	Signal Performance Standard
SQM	Signal Quality Monitor

SSPA	Solid State Power Amplifier
SV	Satellite Vehicle
TEC	Total Electron Content
TM	Threat Model
TS	Threat Space
TTA	Time-To-Alert
TWTA	Traveling Wave Tube Amplifier
UDRE	User Differential Range Error
UDS	User Design Space
UERE	User Equivalent Range Error
UIVE	User Ionospheric Vertical Error
URA	User Range Accuracy
VCO	Voltage Control Oscillator
WAAS	Wide Area Augmentation System
WMS	WAAS Master Station
WRS	Wide area Reference Station



# 1 Introduction

## 1.1 Thesis Motivations

Global Navigation Satellite Systems (GNSS) play an important role on the world economy as well as on our everyday life. Even if GPS (Global Positioning System) is the well-known standard-bearer of GNSS, it only represents a part of the GNSS that is used nowadays in various fields for navigation and positioning including safety-of-life applications. Among these applications is civil aviation that requires a very high quality of service for the most demanding phases of flight. The quality of the GNSS service is typically based on four criteria (integrity, accuracy, availability and continuity), that have to meet International Civil Aviation Organization (ICAO) requirements. To meet these requirements any source of potential service degradations has to be accounted for.

Different errors affect GNSS signals (including ionospheric error, tropospheric error, multipath, satellite clock and ephemeris inaccuracies, signal distortions and noise). Despite the fact that errors from different sources can be present on a GNSS signal, this Ph.D. is focused on one potential source of degradation: GNSS signal distortions due to the satellite payload. These distortions can manifest in two ways:

- Nominal signal distortions generated by healthy satellites due to payload imperfections. This type of perturbation can limit the accuracy of the GNSS measurements and result in the unavailability of the service for some very stringent phases of flight.
- Non-nominal distortions that are triggered by a satellite payload failure. Non-nominal distortions, also called Evil WaveForms (EWFs) are rare events that may pose an integrity risk if the distorted signal remains used by the airborne receiver.

Even if nominal and non-nominal GNSS signal distortions are two different topics with two specific problematics, both signal distortions impact in the same way (even if the order of magnitude is different) the GNSS receiver processing. One important characteristic of GNSS signal distortions is that they impact all users of the distorted signal. Nevertheless, the consequence of a signal distortion on the estimated pseudorange is dependent upon the GNSS receiver setting and this makes arduous the estimation of the impact of signal distortions on a GNSS user due to the large variety of existing GNSS receiver configurations.

On the one hand, the study of GNSS signal nominal distortions aims at quantifying precisely the impact of distortions on different GNSS users. Indeed, these distortions are unavoidable, present all the time and have to be taken into account by anticipating their effects on users even if they are dependent upon several parameters and cannot be characterized easily.

On the other hand, non-nominal distortions study has two aims. First to model the expected distortions that could appear due to a payload failure. These models are referred to as Threat Models (TMs). Then to develop techniques that are able to detect non-nominal distortions of TMs that induce hazardous error on the considered airborne users. Even if these distortions are hard to predict, their scarcity and their considerable impact on the user are at the origin of differences that exist between nominal and non-nominal distortions studies. In order to deal with the EWF problem, civil aviation operations are

## 1. Introduction

supported by Ground Based Augmentation system (GBAS) or/and Satellite Based Augmentation System (SBAS). In GBAS and SBAS, a dedicated monitor is implemented to detect non-nominal signal distortions: the Signal Quality Monitor (SQM).

The GNSS signal distortions topic is not recent and has been subject to many publications regarding the GPS L1 C/A signal, the oldest and the most widely used signal. This Ph.D. thesis takes place in the context of GNSS signals and constellations modernization. Supported by the groundwork performed by civil aviation on signal distortions for the GPS L1 C/A signal, this dissertation aims at proposing new distortions models associated to the modernized GPS and Galileo signals that will be used by civil aviation users after 2020. Investigations on Galileo E1C, Galileo E5a and GPS L5 signals are developed because these signals should be used in the future by airborne receivers.

Without proof that the quality of new signals aided by augmentation systems permits to meet civil aviation requirements, the standardization of these signals to civil aviation users can be compromised. The challenges are by consequence considerable and assessments of signal distortions on new signal in nominal conditions as well as the definition of TM and system to detect non-nominal distortions are of primary importance.

Even if the dissertation contributions can be extended to GBAS (with some slight differences), this work is focused on SBAS and more precisely on the European SBAS: EGNOS (European Geostationary Navigation Overlay Service). EGNOS already provides a support to civil aviation users on GPS L1 C/A signal that has been validated and the aim is to generalize the concept to Galileo E1C, Galileo E5a and GPS L5 signals and the Dual-Frequency Multi-Constellation (DFMC) SBAS context.

### 1.2 Thesis Objectives

The global objective of this dissertation is to tackle the problem of signal distortions generated at satellite level in both nominal and non-nominal cases in the context of GNSS modernization. More precisely a focus is made on Galileo E1C, Galileo E5a pilot component and on GPS L5 pilot component signals. To be compared with studies about distortions on GPS L1 C/A signal, a detailed analysis of GPS L1 C/A signal is also required.

Objectives of this Ph.D. thesis can be divided in four sub-objectives:

- 1) The review of the state-of-the-art on GNSS signal distortions.
  - Sort and select relevant publications about nominal distortions in the context of this Ph.D. thesis.
  - Understand problematics related to EWF, understand why the ICAO TM has been adopted and see if other possibilities to deal with the problem of EWF can be found in the state-of-the-art. In addition, a clear description of SQM is required.
- 2) The investigation of nominal signal distortions on new GNSS signals.
  - Visualize on real signals nominal distortions that can affect GPS L1 C/A, Galileo (E1C and E5a pilot component only) and GPS L5 pilot component signals, and isolate the satellite contribution from the receiver contribution.
  - Assess the impact of nominal distortions on GNSS receivers. For that, different antennas and receivers have to be tested to collect the different signals.

- Synthetize results and as a final challenge, characterize nominal distortions that affect the different signals.
- 3) The investigation of non-nominal distortions on new GNSS signals.
  - Discuss about the relevance to adapt the GPS L1 C/A ICAO TM to new modulations and question the TM concept.
  - Propose TMs for new signals and justify the methodology that leads to these TMs.
- 4) The investigation of a SQM adapted to the proposed TM for new GNSS signals.
  - Define performance objectives that the SQM has to achieve in terms of probability of false alarm, probability of missed detection and maximum tolerable error entailed by undetected signal distortions. Two cases have to be considered: the single frequency (GPS L1 C/A and GALILEO E1C) and the DFMC contexts.
  - Estimate performance that can be reached by SQM in terms of integrity and accuracy.
  - Compare SQM performance on new modulations to SQM performance on GPS L1 C/A that has been already validated.
  - Optimize the SQM by finding the simplest SQM design that is able to meet targeted performance objectives.

### 1.3 Thesis Contributions

Meeting objectives detailed in the previous section, the main contributions of the Ph.D. are listed and can be divided in four main categories.

- 1) Bring a clear understanding of issues related to GNSS signal distortions.
  - A list of receiver parameters that have an influence on the pseudorange measurements estimated from distorted signals is exposed. In addition, the influence of these parameters on the GNSS receiver signal processing is illustrated.
  - An exhaustive list of GNSS signal distortions that summarizes outcomes found in the state-of-the-art is provided. Additionally, based on GPS L1 C/A satellite payload considerations, most likely sources of these distortions are listed.
- 2) Bring new and additional results on GNSS signal nominal distortions.
  - A Matlab® program that is able to process real data collected from different high-gain dish antennas was developed. It gives the possibility to estimate the chip domain observable and a large number of correlator outputs (upto one thousand) on GPS L1 C/A, GPS L5, Galileo E5 and Galileo E1C signals.
  - Observations of nominal distortions on GPS L1 C/A and Galileo E1C signals from a high-gain dish antenna in the chip domain and on the correlation function are presented.
  - A comparison of nominal distortions that affect signal measurements collected from high-gain dish antenna and from omnidirectional antenna is detailed. Similar phenomena as identified in the state-of-the-art are noticed.
  - From results obtained on GPS L1 C/A signals, it appears that nominal distortions are relatively constant over years but that a precise characterization of nominal distortions is difficult notably because it is challenging to isolate signal distortions induced by the satellite from distortions induced by the receiver.

## 1. Introduction

- Based on works performed in [Wong, 2014] a parameter that permits to quantify the impact of nominal distortions on a user is proposed: the inter-PRN bias.
- 3) Propose new TMs for Galileo E5a, GPS L5 and Galileo E1C signals in a DFMC context.
- A comprehensive history of the EWF threat regarding GPS L1 C/A signal is exposed. The strategy adopted by ICAO in the past on the GPS L1 C/A signal is applied to define TMs on new signals. It appears that to define these TMs, the same parameters as the ones used to define the ICAO TM for GPS L1 C/A can be considered. This choice is justified by the observation of nominal distortions, the lack of knowledge about satellite payload and the absence of EWF observation on new signals.
  - The relevance of the TM concept is put into question.
  - A method is introduced to limit the range of these parameters thanks to two criteria: the impact of a distortion on a reference station and the impact of a distortion on considered differential users.
  - Based on the current GPS L1 C/A ICAO TM and a detailed methodology, TMs for Galileo E5a, GPS L5 and Galileo E1C are proposed. A Matlab® program has been implemented to generate signals distorted by the different TMs.
  - A discussion about the number of distortions to test in a given TM is undertaken.
- 4) Propose SQMs regarding new proposed TMs and assess their performance.
- An innovative representation is proposed to test and compare theoretically the SQMs performance whatever the received signal  $C/N_0$  is.
  - A Matlab® program that is able to estimate metrics values on correlation function distorted by proposed TMs has been implemented. In addition, the software permits to estimate the differential tracking error induced by a distortion on different users. From metrics values and differential tracking errors, the ability of a SQM to protect differential users is assessed..
  - Simplified SQMs are proposed. The aim is to reduce the number of SQM metrics still reaching performances targeted in this Ph.D..

In addition to a presentation given at the ENAC ITSNT 2016 as an invited speaker, six papers have been published in the context of this Ph.D..

- [Pagot et al., 2015] presented at ION ITM 2015 conference shows nominal distortions that affect GPS L1 C/A signals on the chip domain and the correlation function domain from high-gain dish antennas data collections.
- [Pagot et al., 2016a] presented at Navitec 2016 conference also focuses SQM design for Galileo E1C and Galileo E5a signals.
- [Pagot et al., 2016b] presented at ION ITM 2016 conference exposes a strategy to design TM and this strategy is used to define TM on Galileo E5a and Galileo E1C signals.
- [Pagot et al., 2016c] presented at ION GNSS+ 2016 conference deals with the SQM design for Galileo E1C and Galileo E5a signals.
- [Thevenon et al., 2014] presented at Navitec 2014 conference gives details on the chip domain observable and on its capacity to visualize non-nominal distortions.
- [Julien et al., 2017] accepted to be presented at ION ITM 2017 conference presents an extended TM definition and its associated SQM.



## 1.4 Thesis Outline

The dissertation is structured as follows:

Chapter 2 introduces the background which permits to understand the GNSS signal distortions problematic. A general overview of GNSS is given before exposing the civil aviation context which is focused in this Ph.D.. More precisely ICAO requirements definitions are presented and concepts of augmentation systems, crucial to meet these stringent requirements, are described. Finally the SBAS is presented as it is the original augmentation system targeted in this study.

Chapter 3 is a more technical chapter which synthetizes the GNSS receiver processing. This chapter is important because it gives the background necessary to understand how a GNSS signal is processed and explains the impact of a signal distortion on the final pseudorange measurement. The analog and the digital sections of the receiver are presented separately. In addition, GNSS signals of interest are presented: GPS L1 C/A, Galileo E1C, Galileo E5a pilot component and GPS L5 pilot component. Mathematical time-domain expression, power spectral density and correlation function of the different signals are provided.

Chapter 4 is the first chapter dedicated to signal distortions. First of all, nominal and non-nominal distortions are described based on the state-of-the-art. This description includes a speculation about the origin of these distortions on GPS L1 C/A signal. Secondly, different impacts of signals distortions on the receiver processing are listed. Then, the issue related to non-nominal distortions in a civil aviation context is detailed. It is seen that it is necessary to model and detect non-nominal distortions that could affect a GNSS signal. Finally, this chapter describes in details two strategies to observe signal distortions: look at distortions in the chip domain and look at distortions on the correlation function.

Chapter 5 synthetizes results on nominal distortions obtained by the observation of real data collections from high-gain dish and from omnidirectional antennas. After a brief introduction to the different setups that were used to collect the different GNSS signals, the effects of nominal distortions at different levels of the receiver processing are observed. From data collected with high-gain dish antennas on GPS L1 C/A and Galileo E1C signals, three observables are used to quantify the impact of signal distortions on users: the chip domain, the correlation function and the S-curve zero-crossing. From high-gain dish antenna measurements, it appears that a wrong or an absence of antenna calibration induces an additional distortion on the measurement which cannot be separated from the nominal distortion generated by the payload. This is the reason why the S-curve zero-crossing observable is also provided based on measurements collected on GPS L1 C/A signal with an omnidirectional antenna. This kind of antenna does not need any calibration because a normalization can be achieved using all visible signals collected at a given time. Finally, inter-PRN tracking biases are estimated from the omnidirectional antenna data collection and appear consistent with results provided in the state-of-the-art.

Chapter 6 deals with the proposition of new TMs for Galileo E5a, Galileo E1C and GPS L5. After a detailed description of the current GPS L1 C/A TM adopted by ICAO, it is proposed to assume that same parameters are relevant to characterize threatening distortions on new modulations. Based on two criteria (the impact of a distortion on a reference station and the impact of a distortion on differential users) the parameters range is limited. Finally TMs similar to the ICAO GPS L1 C/A TM-A, TM-B and TM-C are proposed for each signal of interest.

## *1. Introduction*

Chapter 7 is a thorough study of SQM on new modulations regarding TMs proposed in the previous chapter. Firstly, definitions provided by ICAO on SQM are presented. Secondly an innovative method is exposed that is able to test and compare theoretically the SQMs performance whatever the received signal  $C/N_0$  is. Then, based on this representation and on TMs proposed in chapter 6, performances of reference SQMs are assessed for the different signals. Finally, a method to optimize the SQM is described. The aim is to reduce the number of SQM metrics still reaching targeted performances.

Chapter 8 draws conclusions from main results of this Ph.D. and makes recommendations for works that could be addressed in the future.

## 2 GNSS background

The main purpose of GNSS is to allow users to estimate their Position, Velocity and Time (PVT). The work performed in this Ph.D. thesis focuses on the use of GNSS in a civil aviation context, and more precisely in the context of two augmentation systems: SBAS and GBAS. The main objective of this chapter is to expose GNSS concepts related to its civil aviation use.

Section 2.1 presents the concepts of GNSS positioning. After the introduction of pseudo-ranging and multilateration notions, GNSS segments are described. This section also defines the different errors affecting pseudorange measurements.

Section 2.2 defines the performances requirements criteria that have to be met for the use of GNSS in civil aviation.

Section 2.3 describes augmentation systems used by civil aviation to meet performances requirements. In particular, the notion of differential correction is presented.

Section 2.4 proposes a focus on SBAS which is the augmentation system of interest for this Ph.D. thesis.

Finally, a conclusion about this chapter is given in section 2.5.

### 2.1 PVT Computation using GNSS core constellations

In this section, the PVT estimation technique based on the multilateration concept is first introduced. It uses pseudorange measurements that are described in this section. The GNSS structure is then exposed. To finish, errors having an impact on pseudorange measurements and consequently on the PVT computation are overviewed.

#### 2.1.1 GNSS positioning principles

The primary purpose of GNSS is to allow an autonomous user to compute its PVT. The user's position is commonly evaluated in the Earth-Centered Earth-Fixed coordinate system (ECEF). Information needed by the user to estimate its PVT are carried by an electromagnetic wave emitted by GNSS satellites. The transmitted signal reaches the earth with a remarkably low power. For instance, the minimum received power on ground, measured at the output of a RHCP 0 dBi polarized receiver antenna, is -157 dBW for Galileo E1 OS/Sol signals and -155 dBW for Galileo E5a and E5b signals (for satellite elevation angle higher than 10°) [GSA, 2010]. A part of the information necessary to the user is contained in the time delay caused by the propagation of the electromagnetic waves between satellites and users. The time delay estimated from the signal  $i$  is sometimes called  $PT_i$  (Propagation Time).

The propagation time is estimated by comparing the time at the emission and the time at the reception of the signal. The time at the emission is given in the satellite time frame whereas the time at the

## 2. GNSS background

reception is computed in the receiver time frame. Because the two clocks are not synchronised, a clock bias has to be considered between the satellite and the receiver.

Multiplying  $PT_i$  by the velocity of the wave in space  $c$  (the speed of light), it is possible to estimate the range between the satellite and the receiver. This range estimated for signal  $i$ , affected by errors and by the clock bias between the satellite and the receiver is called pseudorange ( $\rho_i$ ) and is defined by:

$$\rho_i = PT_i \times c$$

To assess its PVT, the user has to estimate the position of the  $i^{th}$  satellite at the origin of the signal  $i$ . A model based on several parameters exists to forecast satellites position. These parameters are sent by satellites via the navigation message and are called ephemeris.

An important remark is that the satellite time may be different from the GNSS constellation time and the difference is satellite-dependent. By consequence, a second important information is sent by the satellite to the user via the navigation message: the clock correction parameters which allow the user to estimate from a model the difference between the satellites and the constellation time. After applying the clock corrections, pseudoranges only include the bias between the constellation time and the receiver. By consequence, after clock corrections, all pseudoranges are affected by the same receiver clock bias  $\delta t_u$ .

Four unknowns must thus be estimated by the user: three for the position ( $x_u, y_u, z_u$ ) and one for the receiver time offset with respect to the constellation reference time  $\delta t_u$ . To compute the four parameters at least four measurements from four different satellites are necessary.

Two types of pseudorange measurements can be extracted from the received satellite signal: carrier phase and code pseudorange measurements.

After correction by the satellite clock term, these clock corrected pseudoranges can be modeled as:

$$\rho_u^i = R_u^i + \delta t_u + errors_{\rho,u}^i \quad (2-1)$$

$$\varphi_u^i = R_u^i + \delta t_u + errors_{\varphi,u}^i + \lambda N^i \quad (2-2)$$

with

$$R_u^i = \sqrt{(x_u - x_{sat,i})^2 + (y_u - y_{sat,i})^2 + (z_u - z_{sat,i})^2} \quad (2-3)$$

where

- $\rho_u^i$  is the code pseudorange measurement estimated from satellite  $i$  in meter.
- $R_u^i$  is the geometric distance in meter between the user and the  $i^{th}$  satellite.
- $[x_u, y_u, z_u]^T$  is the true user's position vector in the reference system.
- $[x_{sat,i}, y_{sat,i}, z_{sat,i}]^T$  is the true position of the  $i^{th}$  satellite in the reference system.
- $c$  is the speed of light in meter/second.
- $errors_{\rho,u}^i$  ( $errors_{\varphi,u}^i$ ) groups all pseudorange errors (respectively all phase measurement errors) related to the propagation medium (tropospheric, ionospheric, bias harder to model), the synchronization errors (due to multipath, interference, thermal noise) and the correction/model uncertainty (satellite clock correction, tropospheric and ionospheric delay, and ephemeris). These errors are detailed in the next section (2.1.3) and are given in meter.
- $\delta t_u = c(\Delta t_u)$  is the clock bias between the receiver time and the constellation time in meter.
- $\varphi_u^i$  is the carrier phase pseudorange measurement in meter.

- $\lambda$  is the carrier wavelength in meter.
- $N^i$  is the carrier phase measurement ambiguity, constant over time as long as the carrier phase synchronization is maintained by the receiver.

In most of GNSS receivers, a least square algorithm is adopted to estimate the four unknowns from at least four pseudorange measurements. Nevertheless other methods exist, such as the Kalman filter.

### 2.1.2 GNSS structure

GNSS are composed of three different complementary segments that are described in the following:

- the space segment,
- the ground segment,
- the user segment.

#### 2.1.2.1 The space segment

This segment consists of satellites that are orbiting around the earth in order to send signals toward the earth that will be used for positioning and timing. The satellite orbit/constellation can generally be chosen according to the desired coverage area:

- Worldwide coverage: a constellation of generally around thirty Medium Earth Orbit satellites (MEO) are used, orbiting at an altitude close to 20 000 km. A minimum number of such satellites (typically at least twenty-four) allows to provide a worldwide service, meaning that any user on earth would see at least four satellites of a given constellation in an open sky environment. Typical core global-coverage GNSS constellations such as GPS, Galileo, GLONASS and BeiDou are described in Table 2-1. ([ESA, 2015], [Navipedia, 2015] and [GPS.gov, 2015])
- Regional coverage: GeoSynchronous earth Orbit (GSO) or Geostationary Earth Orbit (GEO) satellites can be used for regional coverage. GSO vehicles are satellites that are not fixed in the earth frame contrary to GEO satellites. GSO satellites ground track results in an “eight” ground track figure. GEO is a particular GSO with zero inclination and zero eccentricity. All GEO satellites are orbiting at an altitude equal to 35 786 km. BeiDou uses such satellites to enhance its coverage over the Asian area. Some other systems, such as NAVIC or QZSS are entirely based on regional systems that can be complemented by core constellations [Navipedia, 2015].

Note that all these satellites typically transmit multiple signals over multiple frequency bands. Such diversity allows the system to provide several types of positioning services to different communities. The signals and frequency bands associated to civil aviation users will be described later on, in chapter 3.

## 2. GNSS background

Constellations	GPS	GALILEO	GLONASS	COMPASS (BeiDou)
Political entity	United States	European Union	Russia	China
Orbital altitude	20 200 km (MEO)	23 222 km (MEO)	19 100 km (MEO)	21 528 km (MEO) 35 786 km (GEO GSO)
Orbit type	Circular	Circular	Circular	Circular
Orbit period	11 h 58 min 2 s	14 h 05 min	11 h 15 min	12 h 38 min
Number of orbits	6	3	3	3
Inclination of orbits	55°	56°	64.8°	55°
Minimum number of satellites	24	24	24	27 (MEO)+ 3 (GSO) + 5 (GEO)
Frequencies (MHz)	L1(1575.42) L2(1227.60) L5(1176.45)	E1(1575.42) E6(1278.75) E5b (1207.14) E5a (1176.45)	L1 (1602) L2 (1246) L3 (1201)	B1 (1561.098) B1-2 (1589.742) B3(1268.52) B2(1207.14)
Reference system	WGS84	ITRF	PZ-90.02	CGCS2000
Reference time	GPS time	GST (Galileo System Time)	GLONASS time	BDT (BeiDou Time)

**Table 2-1.** Space segment of four GNSS.

### 2.1.2.2 The ground segment

The role of the ground segment is:

- to monitor the satellite constellation,
- to compute the precise satellite ephemeris and satellite clock corrections,
- to generate the navigation message and upload it to the space segment. The navigation message contains the information required by any user receiver to compute its position, such as the satellite position and the satellite clock corrections,
- to perform stations keeping operations.

As a consequence, a ground segment is typically composed of:

- sensor stations that are distributed over the world and monitor the satellite positions and the transmitted signals of all satellites,
- a master control station (with a possible redundancy) that gathers all the information from the sensor stations and extracts all the necessary information to build the navigation message,

- upload stations that can upload the navigation message to all satellites in view,
- the network that link all these stations.

### 2.1.2.3 The user segment

Generally, this segment consists of antennas and receivers that are able to process at least some of the signals sent by the satellites to provide a PVT to the user. A typical receiver is composed of three processing stages:

- A RF front-end whose aim is to pre-condition the received analog signal and digitize it. It is typically composed of a Low Noise Amplifier (LNA), a frequency down-conversion stage, a selective filter stage and a quantization/sampling stage.
- A signal processing unit in charge of acquiring and getting the receiver synchronized with the incoming signals of interest.
- A data processing stage in charge of reading the navigation message, forming the pseudorange measurements, applying the appropriate corrections to the pseudoranges, and computing the PVT.

The two first processing stages are described in more details in chapter 3.

Each receiver has different variants according to the system (GPS/GALILEO, etc.). These variants are mainly on software and models but also on the processing used by the different systems. An important remark is that the user does not have to communicate with the satellites. There can be an unlimited number of simultaneous users.

### 2.1.3 Pseudorange measurement errors

As introduced, the pseudorange measurement model is affected by different independent sources of errors all grouped in the  $errors_{\rho,u}^i$  (or  $errors_{\varphi,u}^i$ ) term. In this section, a list of the main sources of errors is given and a measurement model is defined. Orders of magnitude of these errors are discussed as a conclusion.

#### 2.1.3.1 Different sources of errors

A precise description and modeling of each error type can be found in the literature, for example in [Kaplan and Hegarty, 2006]. A brief overview of each error is proposed in the following:

- the receiver noise,
- ionospheric effect,
- tropospheric effect,
- multipath,
- clock and ephemeris inaccuracies.

The satellite payload, the satellite antenna, the receiver antenna and the receiver processing channel are also sources of pseudorange errors. These errors are induced by signal delays and signal distortions generated at satellite level and at receiver level as detailed in next chapters.

## 2. GNSS background

### 2.1.3.1.1 Receiver noise

The pseudorange estimation is based on the synchronization of the receiver with the digitized incoming signal (thus providing the receiver with the capability to estimate the time of arrival of a specific part of the incoming signal). This synchronization mechanism, also called tracking, will be presented later. The noise affecting a digitized incoming signal has a direct impact on this synchronization and consequently on the pseudorange measurement. The repercussion on the pseudorange can be modeled as an additive Gaussian noise affecting the measurement.

The magnitude of this noise depends upon the setting of the tracking loop, the received signal strength, the antenna as well as upon the modulation of the signal of interest.

### 2.1.3.1.2 Ionospheric effect

The ionosphere is a dispersive medium located approximatively between 70 km and 1000 km above the earth's surface. Because of free electrons which create an electric field, electromagnetic waves do not travel at the vacuum speed of the light as they cross this region. The signal group delay and by consequence the code pseudorange measurement are delayed in proportion to the number of electrons encountered, referred to as the Total Electron Content (TEC), whereas the carrier phase measurement is advanced by the same amount. The ionospheric delay is frequency-dependent. The delay on the code pseudorange measurement  $\varepsilon_{iono}^i$  is modeled by:

$$\varepsilon_{iono}^i(f) \approx -\frac{40.3 \times TEC}{f^2} \quad (2-4)$$

where

- $f$  is the carrier frequency of the signal in hertz.

GNSS receivers systematically try to mitigate the ionospheric effect applying corrections. Different algorithms exist to estimate ionospheric delays:

- GPS receivers apply the Klobuchar ionospheric model and Galileo receivers the NeQuick ionospheric model. These model parameters are embedded in the navigation message.
- SBAS provides users with its own ionospheric delay correction model by the means of an ionospheric grid.
- Another method consists of combining pseudorange measurements from the same satellite but on two different frequencies, exploiting the fact that the ionosphere is a dispersive medium, meaning that the ionospheric delay is frequency-dependent. This method called dual-frequency iono-free combination removes the first order ionospheric delay.
- The use of differential measurements is also a means to compensate the ionospheric effect as presented in 2.3.1.1.

### 2.1.3.1.3 Tropospheric effect

The troposphere is a non-dispersive medium (for frequencies up to 15 GHz) located between about 40 km and the earth's surface. Within this medium, the group and the carrier phase delays are delayed by the same amount compared to free space propagation. This delay, which leads to a pseudorange measurement bias, is function of the tropospheric refractive index, which is dependent upon the local temperature, pressure, and relative humidity.



GNSS receivers can estimate and correct their own tropospheric delay according to different models, usually fairly accurately. Civil aviation, for instance, recommends the UNB3 tropospheric model to be applied by airborne receivers [RTCA, 2006].

The use of differential measurements is also a means to compensate tropospheric effect as presented in 2.3.1.1.

#### 2.1.3.1.4 Multipath error

Multipath are GNSS signal replicas induced by the reflection and/or the diffraction of GNSS signals on obstacles encountered during the signal propagation. This phenomenon is environment-dependent. At receiver level, interferences exist between the Line of Sight (LoS – the only signal corresponding to the true satellite/receiver distance) and reflected/diffracted signals. Thus, the receiver sees multiple versions of the GNSS signal, each with different times of arrival, signal levels and carrier phases. The consequence is that multipath induces an error on the receiver synchronization with the LoS signal of interest. There are usually three types of methods used to mitigate the multipath at different stages of the receiver signal processing:

- at the antenna level, by carefully choosing antenna characteristics and location, in order to limit the power of the multipath entering the receiver,
- at the signal processing level by discriminating the LoS from the multipath. Tens of techniques were developed as the MRDLL [Laxton and DeVilbiss, 1997], the MEDLL [Townsend et al., 2000], the deconvolution technique [Dragunas and Borre, 2011], etc.,
- at the PVT computation level by trying to detect and exclude measurement with biases (high residual values).

#### 2.1.3.1.5 Clock and ephemeris inaccuracies

Satellites clocks are highly stable but cannot remain fully synchronized with the constellation time. This is the reason why the navigation data message contains a clock correction field. Despite the satellite clock correction, some residual errors can affect the receiver. In the same way, ephemeris transmitted in the navigation data message, which contains the information of satellites positions, can be affected by some imprecisions because of the difficulty to forecast changes of satellites orbit. These inaccuracies entail equivalent residual error on pseudorange measurements. Assuming that the distribution of the clock and ephemeris inaccuracies (projected on the vector between the satellite and the user) is a zero mean Gaussian random variable, the standard deviation of the error budget attributed to the clock and ephemeris together is called URA (User Range Accuracy) for GPS and SISA (Signal-In-Space Accuracy) for Galileo. These parameters are broadcast in the navigation message.

#### 2.1.3.2 Measurement error models

The error term which appears in the pseudorange measurements definition gathers the pseudorange measurement bias induced by different sources:

$$errors_p^i = \varepsilon_{p,Noise}^i + \varepsilon_{Tropo}^i + \varepsilon_{Iono}^i + \varepsilon_{p,MP}^i + \varepsilon_{clock\&eph}^i \quad (2-5)$$

$$errors_\varphi^i = \varepsilon_{\varphi,Noise}^i + \varepsilon_{Tropo}^i - \varepsilon_{Iono}^i + \varepsilon_{\varphi,MP}^i + \varepsilon_{clock\&eph}^i \quad (2-6)$$

where

## 2. GNSS background

- $\varepsilon_{\rho,Noise}^i$  ( $\varepsilon_{\phi,Noise}^i$ ) is the error induced by the receiver noise on the code (respectively the carrier phase) pseudorange measurement.
- $\varepsilon_{Tropo}^i$  is the error induced by the tropospheric delay (after applying UNB3 tropospheric model) on the pseudorange measurement.
- $\varepsilon_{Iono}^i$  is the error induced by the ionospheric delay (after applying ionospheric models such as Klobuchar and NeQuick etc.) on the pseudorange measurement.
- $\varepsilon_{\rho,MP}^i$  ( $\varepsilon_{\phi,MP}^i$ ) is the error induced by the multipath (after applying multipath mitigation techniques) on the code (respectively on the carrier phase) pseudorange measurement.
- $\varepsilon_{clock\&eph}^i$  is the error induced by the satellite clock and ephemeris inaccuracies on the pseudorange measurement.

It is usually assumed that components of  $errors_{\rho}^i$  and  $errors_{\phi}^i$  are independent and can be modeled by zero-mean normal distributions that overbound the real error distributions. The total error induced on the pseudorange measurement model, also called User Equivalent Range Error (UERE), has a variance equal to:

$$\sigma_{UERE}^2 = \sigma_{Noise}^2 + \sigma_{Tropo}^2 + \sigma_{Iono}^2 + \sigma_{MP}^2 + \sigma_{clock\&eph}^2 \quad (2-7)$$

where

- $\sigma_{UERE}^2$  is the variance of all residual errors affecting the pseudorange measurement.
- $\sigma_{Noise}^2$  is the variance of the receiver noise affecting the pseudorange measurement.  $\sigma_{Noise}^2$  is lower on carrier phase than on code measurement.
- $\sigma_{Tropo}^2$  is the variance of the tropospheric delay affecting the pseudorange measurement.
- $\sigma_{Iono}^2$  is the variance of the ionospheric delay affecting the pseudorange measurement.
- $\sigma_{MP}^2$  is the variance of the error entailed by multipath affecting the pseudorange measurement.
- $\sigma_{clock\&eph}^2$  is the variance of the satellite clock error plus the ephemeris error affecting the pseudorange measurement.

### 2.1.3.3 Code pseudorange measurement error order of magnitude

Order of magnitude for these five components are given as an example for a single frequency receiver not using any augmentation system. All values given in Table 2-2 are dependent upon several parameters and characteristics of the GNSS receiver. Values given in Table 2-2 have to be considered as order of magnitude and represent the impact of the different errors on a typical receiver.

- $\sigma_{Tropo}$  is evaluated for a satellite elevation angle  $\theta$  equal to 5° (highest value) and equal to 75° (lowest value). It corresponds to the residual tropospheric model after applying the UNB3 model. Values are estimated from formulas defined in [RTCA, 2006].
- $\sigma_{Iono}$  is evaluated for a receiver latitude  $\gamma$  equal to 45° and a satellite elevation angle  $\theta$  equal to 5° (highest value) and equal to 75° (lowest value). GPS results are provided after applying the Klobuchar ionospheric model, whereas Galileo results are provided after applying the NeQuick ionospheric model [Montloin, 2014]. Even if in general  $\sigma_{Iono}$  is lower after applying the NeQuick model than the Klobuchar model, at this latitude, the two models reach same performance.

- $\sigma_{Noise}$  and  $\sigma_{MP}$  are provided for information only and give an idea of expected standard deviations in a clear sky environment with high-end receiver equipment [GSA, 2014]. The standard deviation associated to multipath is considered for a satellite elevation equal to  $45^\circ$  and can be higher for lower satellite elevations. Values are available only for GPS L1 C/A signal.
- $\sigma_{clock\&eph}$  is linked to the integrity performance requirement. ESA specifies a Galileo SISA value for both nominal and degraded modes of 0.85 m [Oehler et al., 2006]. GPS URA depends upon the satellite technology and therefore upon the considered modernization step of the GPS constellation. For the study we will assume, as GPS performance, current GPS SiS performance [Smitham, 2014].

The use of dual-frequency (for example GPS L1 C/A with GPS L5 or Galileo E1 with Galileo E5) mitigates the ionospheric impact (as detailed for example in [Montloin, 2014]) and, in counterpart, increases the noise and multipath error components. The term  $\sigma_{Iono}$  can be neglected for dual-frequency receiver when comparing its magnitude to other errors.

	GPS L1 C/A	GPS L5	Galileo E1C	Galileo E5a
$\sigma_{Noise}$ (m)	0.5	N/A	N/A	N/A
$\sigma_{Tropo}$ (m)	0.2 – 1.5	0.2 – 1.5	0.2 – 1.5	0.2 – 1.5
$\sigma_{Iono}$ (m)	4.6 – 13.7	8.2 – 24.5	4.6 – 13.7	8.2 – 24.5
$\sigma_{MP}$ (m)	0.2	N/A	N/A	N/A
$\sigma_{clock\&eph}$ (m)	0.85	0.85	0.85	0.85

**Table 2-2.** Order of magnitude of code measurement errors.

## 2.2 Civil Aviation Operational Requirements

Civil aviation is a very specific field in the sense that it is fully attached to the notion of safety-of-life. As a consequence, any system used by civil aviation is related to the fact that it has to provide performance according to very stringent requirements. For the use of GNSS in civil aviation, the GNSS Signal-in-Space (SiS) has to fulfil requirements defined through four parameters:

- the accuracy,
- the availability,
- the continuity,
- the integrity.

The four terms are defined below from official sources.

### 2.2.1 Accuracy

*In navigation, the accuracy of an estimated or measured position of a craft (vehicle, aircraft, or vessel) at a given time is the degree of conformance of that position with the true position of the craft at that time [SSF, 2008]. Accuracy requirement is based on the concept that the probability of the estimated position being inside the accuracy bound (maximum allowable position error) has to be at least 0.95.*

## 2. GNSS background

### 2.2.2 Integrity

*Integrity is a measure of the trust that can be placed in the correctness of the information supplied by the total system. Integrity includes the ability of a system to provide timely and valid warnings to the user (alerts) when the system must not be used for the intended operation (or phase of flight) [ICAO, 2006]. Three parameters are defined relatively to the notion of integrity:*

- *The alert limit: To ensure that the position error is acceptable, an alert limit is defined that represents the largest position error allowable for a safe operation. The position error cannot exceed this alert limit without annunciation [ICAO, 2006].*
- *Time to alert: Time-to-Alert is the maximum allowable elapsed time from the onset of a positioning failure until the equipment annunciates the alert [RTCA, 2006].*
- *Integrity Risk: The integrity risk is the probability of providing a signal that is out of tolerance without warning the user in a given period of time [Martineau, 2008].*

In practice to satisfy ICAO SiS integrity requirement, the following condition must be fulfilled:

$$P(PE > AL \ \& \ \text{no alert within TTA}) < IR \quad (2-8)$$

where

- *TTA* is the Time-To-Alert which comprises the delay necessary to detect the positioning failure and transmit this information to the pilot.
- *PE* is the Position Error.
- *P(A)* means the probability of event *A*.
- *AL* is the Alert Limit.
- *IR* is the Integrity Risk.

### 2.2.3 Availability

*The availability of a navigation system is the ability of the system to provide the required function and performance at the initiation of the intended operation. Availability is an indication of the ability of the system to provide usable service within the specified coverage area. Signal availability is the percentage of time that navigational signals transmitted from external sources are available for use [RTCA, 2006].*

### 2.2.4 Continuity

*Continuity of service of a system is the capability of the system to perform its function without unscheduled interruptions during the intended operation. More specifically, continuity is the probability that the specified system performance will be maintained for the duration of a phase operation, presuming that the system was available at the beginning of that phase operation, and predicted to exist throughout the operation [RTCA, 2006].*

These requirements are not met by core GNSS constellations alone and especially accuracy and integrity have to be improved for stringent operations, such as approach. Even with GNSS modernization and the availability of new signals (for instance on the L5 frequency band),

requirements cannot be met. As a consequence, augmentations systems are necessary for GNSS to be usable by civil aviation.

### 2.2.5 Civil aviation SiS requirements

Table 2-3 presents SiS performances requirements defined in the civil aviation context [ICAO, 2006]. The operation LPV-200 is not defined in the SARPs but in a document [FAA, 2008] dedicated to SBAS.

## 2.3 Augmentation of core constellation systems for civil aviation

For GNSS to meet civil aviation operational requirements that demand highest level of performance, there is a need to use augmentation system that can improve GNSS performance. Civil aviation augmentations are mostly working on two aspects:

- improvement of the accuracy of the pseudoranges,
- improvement of the integrity of the PVT solution.

Obviously, this has to be done keeping in mind the continuity and availability of the solution. Different augmentation systems exist and are adopted by civil aviation:

- ABAS (Aircraft Based Augmentation Systems) which consists in the integration of information provided by GNSS with information provided on-board by the aircraft. Indeed, if redundant measurements are available (typically, more than four pseudorange measurements), it is possible to perform a consistency check between the measurements in order to detect biased measurements. The two ABASs that can be used by civil aviation users are the RAIM (Receiver Autonomous Integrity Monitoring) which is based on an on-board algorithm that uses only GNSS information and the AAIM (Aircraft Autonomous Integrity Monitoring) which uses GNSS combined with other on-board sensors such as baro-altimeter and inertial measurement units.
- SBAS (Satellite Based Augmentation system) which is based on additional satellites and ground stations that provide to the user additional information to improve its performance. SBAS provides this information at the continental coverage. SBASs are studied in details later in this section. WAAS (Wide Area Augmentation System), the United States' SBAS and EGNOS (European Geostationary Navigation Overlay Service), the European's SBAS support En-Route, Terminal and Approach operations. It provides CAT I equivalent vertical guidance (also called LPV-200) at any qualifying runway [SBAS IWG, 2014].
- GBAS (Ground Based Augmentation System) which consists of a single ground station that provides to user with additional information to improve its performance. GBAS coverage is local, typically 50 km around the ground station, which is enough to cover all aircraft approaching an airport. GBAS provides CAT I service but research programs are currently conducting to enable CAT III approach service [FAA, 2016a].

## 2. GNSS background

Typical operation	Accuracy horizontal 95%	Accuracy vertical 95%	Time to Alert	Integrity	Continuity	Availability	Horizontal alert limit	Vertical alert limit
En-route	3.7 km	N/A	5 min	$1 \cdot 10^{-7}/h$	$1 \cdot 10^{-4}/h$ to $1 \cdot 10^{-8}/h$	0.99 to 0.99999	7.4 km (oceanic/continental low density traffic) 3.7 km (continental)	N/A
En-route, Terminal	0.74 km	N/A	15 s	$1 \cdot 10^{-7}/h$	$1 \cdot 10^{-4}/h$ to $1 \cdot 10^{-8}/h$	0.99 to 0.99999	1.85 km	N/A
Initial Approach, Intermediate, NPA, Departure	220 m	N/A	10 s	$1 \cdot 10^{-7}/h$	$1 \cdot 10^{-4}/h$ to $1 \cdot 10^{-8}/h$	0.99 to 0.99999	556 m	N/A
Approach operations with vertical guidance (APV1)	16 m	20 m	10 s	$1 \cdot 2 \cdot 10^{-7}$ in any approach	$1 \cdot 8^{-6}$ per 15 s	0.99 to 0.99999	40 m	50 m
Approach operations with vertical guidance APV2	16 m	8 m	6 s	$1 \cdot 2 \cdot 10^{-7}$ in any approach	$1 \cdot 8^{-6}$ per 15s	0.99 to 0.99999	40 m	20 m
CAT I	16 m	6 m to 4 m	6 s	$1 \cdot 2 \cdot 10^{-7}$ in any approach	$1 \cdot 8^{-6}$ per 15s	0.99 to 0.99999	40 m	35 m to 10 m
LPV-200	16 m	4 m	6.2 s	$2 \cdot 10^{-7}/h$ per approach (150 s)	$1 \cdot 8^{-6}$ per 15s	0.99 or N/A depending on the coverage zone	40 m	35 m

**Table 2-3. Civil Aviation Signal-in-Space Requirements.**

### 2.3.1 Accuracy improvement

The accuracy of the pseudorange measurement is one of the performance criteria improved by augmentation systems and several ways exist to perform this task. For instance the RAIM algorithm allows removing pseudorange measurements affected by large bias from the PVT computation whereas AAIM also integrates on-board sensors measurements to increase the pseudorange measurement accuracy. SBAS and GBAS use differential corrections to meet accuracy requirements. As the study focuses on SBAS applications, the concept of differential corrections is detailed in this section. Another method presented in 2.3.1.2 used by civil aviation airborne to increase the accuracy of pseudorange measurements is the smoothing of pseudorange measurements.

#### 2.3.1.1 Differential corrections

In the literature, this technique is called DGPS for Differential GPS when applied only on GPS signals and DGNSS in a more general way. The term DGNSS is used in this document to generalize the differential concept to all GNSS signals.

The concept of differential GNSS is to improve the accuracy of the user pseudorange measurements  $\rho_u^i$  by providing corrections  $\Delta\rho_{corr}^i$  computed by a set of reference stations.

For pseudorange errors that are correlated in space and time, it is interesting for the user who derives a pseudorange measurement to have access to an estimate of these errors from a nearby reference station. Knowing the precise location of the reference station, it is possible to evaluate these errors that affect the reference by comparing the actual pseudorange measurements with respect to the theoretical pseudorange measurements.

##### 2.3.1.1.1 Time correlation of the error

The time correlation of an error gives the rapidity with which the error is varying in time. An error highly correlated in time means that the error varies slowly over time. Issues appear when an error is poorly correlated in time. In this condition, to be efficient, the correction associated to the error should be applied instantaneously. The problem is that in general, a DGNSS user cannot apply corrections in real time. Indeed, the correction has to be estimated by the reference, transmitted, received by the DGNSS user and applied on measured pseudoranges.

A time correlation model is standardized by ICAO and consists of a first order Gauss-Markov [RTCA, 2009] described by:

$$\dot{x} = -\frac{1}{\tau}x + w \quad (2-9)$$

where

- $x$  is the Gauss-Markov random process with a zero mean and a variance equal to  $\sigma_x$ .
- $w$  is the driving noise of the Gauss-Markov process with a zero mean and a variance equal to  $\sigma_w$ .
- $\tau$  is the correlation time of the error in second.

## 2. GNSS background

The relation between the standard deviation of the random process and the standard deviation of the driving noise is given by:

$$\sigma_w^2 = \sigma_x^2 \left(1 - e^{-\frac{\Delta t}{\tau}}\right) \quad (2-10)$$

where  $\Delta t$  is the sampling time interval at which the process is observed in second.

An overview of the time correlation of different errors is given to understand the global impact of each error component. Orders of magnitude of error variations in time are proposed in the literature.

- $\varepsilon_{Tropo}^i$  and  $\varepsilon_{clock\&eph}^i$  are highly correlated in time, by consequence it is not problematic if corrections are applied several seconds after their estimations. The correlation time of  $\varepsilon_{clock\&eph}^i$  can be assumed equal to 7200 s but can be reduced to 3600 s based on the average satellite visibility whereas the correlation time of  $\varepsilon_{Tropo}^i$  can be assumed equal to 1800 s [RTCA, 2009].
- $\varepsilon_{Iono}^i$  is generally highly correlated in time and this correlation depends upon the latitude. When the ionosphere is disturbed (geomagnetic storms, scintillations, etc.), the time correlation can decrease significantly. The correlation time of  $\varepsilon_{Iono}^i$  can be assumed equal to 1800 s [Salos, 2012].
- $\varepsilon_{MP}^i$  and  $\varepsilon_{Noise}^i$  are poorly correlated in time. As a consequence they cannot be corrected by differential corrections. The time correlation of  $\varepsilon_{MP}^i$  depends upon the time over which measurements are averaged to derive the pseudorange measurements. In civil aviation, the time correlation of the  $\varepsilon_{MP}^i$  can take value between 1 and 100 s. The highest value is obtained when smoothing is applied on measurements. The time correlation of the  $\varepsilon_{Noise}^i$  is in general equal to 1 s in civil aviation applications and depends upon receiver setting [Vezinet, 2014].

### 2.3.1.1.2 Spatial correlation of the error

The spatial correlation of an error gives the rapidity with which the error is varying in space. An error highly correlated in space means that the error varies slowly over distance. Issues appear when an error is poorly correlated in space. In this condition, to be efficient, the correction associated to the error should be applied in an area very close to the location of the reference station. In real conditions reference and user locations are different and depending on the error spatial correlation, the correction will be more or less efficient. The distance between the DGNSS user and the reference is called baseline.

An overview of the space correlation of the different errors is given to understand the global impact of each error component. Orders of magnitude of errors variations in space are proposed in [Pullen, 2011].

- $\varepsilon_{clock\&eph}^i$  is highly correlated in space, by consequence it is not problematic if corrections are applied at a location several tens of kilometers from the station providing the estimation. As an order of magnitude, considering that the standard deviation of the error distribution is equal to zero at the reference location, the standard deviation of the error at a distance *baseline* in km from the reference is equal to  $0.1 \text{ mm} \times \text{baseline}$  in optimistic conditions and  $0.6 \text{ mm} \times \text{baseline}$  in pessimistic conditions [Kaplan and Hegarty, 2006].
- $\varepsilon_{Iono}^i$  is, most of the time, highly correlated in space. Even with baselines of tens of kilometers, DGNSS corrections decrease greatly the  $\varepsilon_{Iono}^i$  term. When the ionosphere is disturbed, the space correlation decreases and this term is more difficult to compensate. As an order of



magnitude, considering that the standard deviation of the residual error distribution is equal to zero at the reference location, the standard deviation of the error at a distance *baseline* in km from the reference is equal to  $0.2 \text{ cm} \times \text{baseline}$  in the case of undisturbed ionosphere and  $4 \text{ cm} \times \text{baseline}$  in the case of disturbed ionosphere [Kaplan and Hegarty, 2006].

- $\varepsilon_{Tropo}^i$  is more affected by a difference in height between the user and the reference station than a horizontal distance. This is the reason why, in GBAS, the vertical component which arises from the height difference between ground station and aircraft is corrected using the standardized nominal model given in [RTCA, 2008]. Considering baseline of several kilometres, DGNSS corrections decrease significantly the  $\varepsilon_{Tropo}^i$  term. As an order of magnitude, considering that the standard deviation of the error distribution is equal to zero at the reference location, the standard deviation of the error at a distance *baseline* in km from the reference is equal to  $1 \text{ cm} \times \text{baseline}$  in optimistic conditions and  $4 \text{ cm} \times \text{baseline}$  in pessimistic conditions. This value is estimated considering that the user and the reference are at the same height [Kaplan and Hegarty, 2006] or that tropospheric error due to height difference has been compensated.
- $\varepsilon_{MP}^i$  is poorly correlated in space. This error component is dependent upon the receiver environment. The consequence is that multipath cannot be corrected by DGNSS even if the baseline is of some meters. On the contrary, multipath experienced at the reference station will be added to the differential user pseudoranges.
- $\varepsilon_{Noise}^i$  is not correlated in space and depends also upon the receiver. DGNSS cannot compensate this error component even if the baseline is of some centimeters.

#### 2.3.1.1.3 Differential corrections concept

A simplified differential correction model is proposed to illustrate the DGNSS concept. A more comprehensive definition of SBAS differential corrections is discussed in 2.4.

It is assumed that the error affecting the measurement *i* is decomposed into two parts, the error differentially corrected  $\varepsilon_{diff}^i$  and a smaller error term that is not taken into account by the differential correction  $\varepsilon_{other}^i$ . The error affecting the user (*u*) pseudorange measurement can be written as:

$$errors_{\rho,u}^i = \varepsilon_{other,u}^i + \varepsilon_{diff,u}^i \quad (2-11)$$

and the error affecting the reference receiver (*rr*) can be written as:

$$errors_{\rho,rr}^i = \varepsilon_{other,rr}^i + \varepsilon_{diff,rr}^i \quad (2-12)$$

The pseudorange measurement estimated by the reference can be modeled as:

$$\rho_{rr}^i = R_{rr}^i + \delta t_{rr} + \varepsilon_{other,rr}^i + \varepsilon_{diff,rr}^i \quad (2-13)$$

where

- $R_{rr}^i$  is the geometric distance between the reference station and the satellite at the origin of signal *i*.
- $\delta t_{rr}$  is the clock bias between the reference receiver and the satellite constellation time, in second.

## 2. GNSS background

Knowing the precise location of the reference station allows to remove the term  $R_{rr}^i$ . The differential correction  $\Delta\rho_{\varepsilon_{diff},corr}^i$  is introduced and has the expression:

$$\Delta\rho_{\varepsilon_{diff},corr}^i = \delta t_{rr} + \varepsilon_{other,rr}^i + \varepsilon_{diff,rr}^i \quad (2-14)$$

The user code pseudorange corrected by  $\Delta\rho_{\varepsilon_{diff},corr}^i$  is noted  $\rho_{u,\varepsilon_{diff},corr}^i$  and can be written as a function of the uncorrected user pseudorange  $\rho_u^i$  and the correction  $\Delta\rho_{\varepsilon_{diff},corr}^i$  as:

$$\rho_{u,\varepsilon_{diff},corr}^i = \rho_u^i - \Delta\rho_{\varepsilon_{diff},corr}^i \quad (2-15)$$

with  $\rho_u^i$  the pseudorange measurement estimated by the user and modeled by:

$$\rho_u^i = R_u^i + \delta t_u + \varepsilon_{other,u}^i + \varepsilon_{diff,u}^i \quad (2-16)$$

where

- $R_u^i$  is the geometric distance between the user and the satellite at the origin of signal  $i$ .
- $\delta t_u$  is the clock bias between the user receiver and the satellite constellation times, in second.

Finally the pseudorange corrected by the term  $\varepsilon_{diff}$  can be modeled as:

$$\rho_{u,\varepsilon_{diff},corr}^i = R_u^i + \delta t_{urr} + \varepsilon_{other,u}^i + \varepsilon_{other,rr}^i + \Delta\varepsilon_{diff,urr}^i \quad (2-17)$$

where

- $\delta t_{urr} = \delta t_u - \delta t_{rr}$  is the difference between user and reference station clock offsets in second.
- $\Delta\varepsilon_{diff,urr}^i = \varepsilon_{diff,u}^i - \varepsilon_{diff,rr}^i$  is the residual pseudorange errors on the user pseudorange of the error corrected differentially.

$\delta t_{urr}$  induces the same bias to all pseudorange measurements. This common bias  $\delta t_{urr}$  is consequently integrated in the time unknown (clock bias) of the user PVT solution. The term  $\delta t_{urr}$  which appears in the corrected pseudorange measurement expression is compensated in the same way as  $\delta t_u$ .

It can be seen from the definition of  $\rho_{u,\varepsilon_{diff},corr}^i$  that the error term  $\Delta\varepsilon_{diff,urr}^i$  which alters the corrected pseudorange is the difference between the errors affecting the user and the reference. If both receivers are influenced by the same errors, then the differential correction will have removed all errors. However, if there is a poor spatial and time correlation of the error component, error will be different at reference and user levels and will not be completely compensated and will even be amplified by DGNSS corrections (terms  $\varepsilon_{other,u}^i$  and  $\varepsilon_{other,rr}^i$  are added).

### 2.3.1.2 Pseudorange smoothing

In DGNSS applications used in civil aviation, the pseudorange measurement is smoothed at reference station and user receiver levels using the carrier phase measurement. This step is of primary importance in order to decrease the impact of errors poorly time correlated (receiver noise, some multipath), since the magnitude of carrier phase tracking errors is significantly lower than that of code pseudorange measurements. The smoothing equation is given in the steady state ( $k \geq n$ ) by:

$$\hat{\rho}^i(k) = \frac{1}{n}\rho^i(k) + \frac{n-1}{n}[\hat{\rho}^i(k-1) + (\varphi^i(k) - \varphi^i(k-1))] \quad (2-18)$$

where

- $\hat{\rho}^i$  is the smoothed code pseudorange measurement from the signal  $i$  in meter.
- $\rho^i$  is the unsmoothed code pseudorange measurement from the signal  $i$  in meter.
- $n = S/T$  is the normalized smoothing time with  $S$  the filter time constant and  $T$  the epoch duration.
- $\varphi^i$  is the carrier phase measurement from the signal  $i$  in meter.
- $k$  represents the epoch of measurements estimation.

It is noticeable that the difference of carrier phase pseudoranges removes the ambiguity affecting the carrier phase measurement if no carrier phase tracking disruption has occurred between the two epochs.

As an example, regarding GBAS and SBAS, civil aviation airborne receivers shall utilize a maximum standardized 100-second time constant carrier smoothing [ICAO, 2006]. GBAS users can also use a 30-second smoothing constant.

After smoothing, it is estimated that the standard deviation attributed to noise and multipath is of the order of a few tens of centimeters [RTCA, 2004].

### 2.3.1.3 Code pseudorange measurement errors after differential corrections

As an order of magnitude, expected standard deviations of the three code pseudorange measurement errors  $\varepsilon_{clock\&eph}^i$ ,  $\varepsilon_{Iono}^i$  and  $\varepsilon_{Tropo}^i$  using DGPS compared to a standalone L1 C/A GPS receiver are presented in [Kaplan and Hegarty, 2006]. Values of the three errors after differential corrections are dependent upon the baseline between the user and the reference. It is assumed that:

- the time correlation of errors is neglected (corrections are estimated, sent and applied instantaneously),
- the Klobuchar ionospheric model is applied before differential corrections,
- the UNB3 tropospheric model is applied on pseudorange measurements before the differential correction,
- the tropospheric error due to a difference of height between the reference and the user is not considered and
- when two differential correction values are provided, the lowest value consists of optimistic conditions and the highest value of pessimistic conditions.

	Before differential corrections	After differential corrections
$\sigma_{Noise}$	0.5 m	0.7 m
$\sigma_{Tropo}$	0.2 – 1.5 m	$1 - 4 \text{ cm/km} \times \text{baseline in km}$
$\sigma_{Iono}$	4.3 – 13.7 m	$0.2 - 4 \text{ cm/km} \times \text{baseline in km}$
$\sigma_{MP}$	0.2 m	0.3 m
$\sigma_{clock\&eph}$	0.85 m	$0.1 - 0.6 \text{ mm/km} \times \text{baseline in km}$

**Table 2-4.** GPS L1 C/A pseudorange measurement errors order of magnitude before and after applying differential corrections.

## 2. GNSS background

The standard deviation of  $\varepsilon_{Noise}^i$  and  $\varepsilon_{MP}^i$  increases after applying the differential correction and are independent from the baseline. The influence of the multipath and the noise that affect the reference receiver and the airborne are added.

### 2.3.2 Integrity monitoring

In a DGNSS system, the accuracy can be improved by sending corrections to the user but a second important information is the quality of the correction and the trust that can be put on the correction (including the trust in the GNSS). This second information is related to the integrity issue and is provided by the augmentation system. In civil aviation, an integrity risk is allocated to hazardous failures depending on the phase of flight.

The overall integrity risk is allocated to different identified conditions through an integrity risk allocation tree. The tree depends upon the approach type. In particular an integrity risk is allocated to the SiS threats that correspond to hazardous failures focused in this Ph.D. thesis. An example of integrity risk allocation tree for the SiS is presented in Figure 2-1.

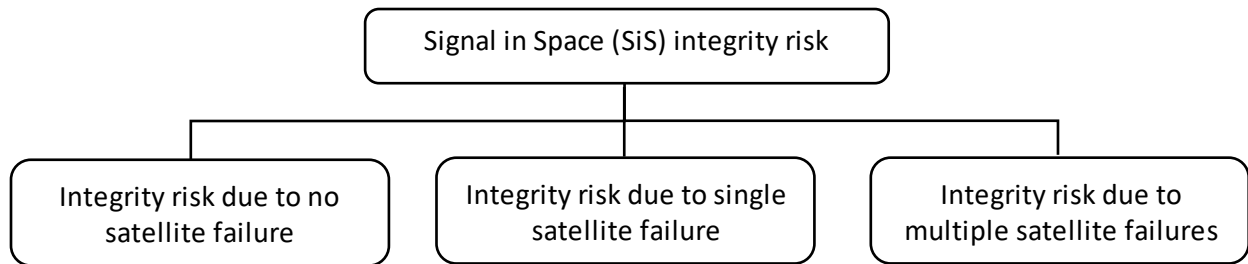


**Figure 2-1.** *SiS integrity risk allocation example.*

Then for each identified condition, an integrity monitoring function is implemented under the form of either:

- a fault detection monitor,
- a protection level computation.

Both integrity monitoring functions are tackled in this section.

#### 2.3.2.1 Fault detection monitors

Different specific monitors are implemented to protect GNSS users against identified failures. The monitor is generally based on an observable whose value is compared to a threshold estimated from the distribution of that observable in nominal conditions. The performance of a fault detection monitor is assessed by testing the capability of a monitor to detect failures defined by a model. The threshold is computed from statistical analysis.

Different monitors exist such as the Signal Quality Monitor (SQM) which aims at detecting hazardous signal distortions. SQM is extensively discussed in chapter 7. Many other monitors exist to detect other precisely identified failures. For example, GBAS monitors the following threats:

- satellite signal deformation (EWF),
- low satellite signal power,

- excessive code-carrier divergence,
- broadcast of erroneous GPS ephemeris data,
- excessive range acceleration,
- ionospheric spatial-gradient anomaly,
- tropospheric gradient anomaly.

#### 2.3.2.2 Protection levels concept

Two protection levels are defined: one horizontally and one vertically. The definition of both protection levels is provided in [RTCA, 2006].

*The Horizontal Protection Level (HPL) is the radius of a circle in the horizontal plane (the local plane tangent to the WGS-84 ellipsoid), with its center being at the true position, that describes the region assured to contain the indicated horizontal position.*

*The Vertical Protection Level (VPL) is half the length of a segment on the vertical axis (perpendicular to the horizontal plane of WGS-84 ellipsoid), with its center being at the true position, that describes the region assured to contain the indicated vertical position.*

The protection level computation is dependent upon the augmentation system. In GBAS and SBAS, the protection level is assumed to protect a user that applies the SBAS or GBAS corrections and only use the non-faulty satellites, i.e. satellites whose measurements have been monitored successfully by the ground reference station(s), for the computation of its PVT. At each epoch, HPL or VPL are computed by the user receiver by combining parameters transmitted by the ground segment, airborne parameters and the user geometry w.r.t. the satellites used in the position computation.

In other words, the protection level computed by SBAS and GBAS users assumed that corrected pseudoranges are affected by nominal errors only, and not by failures.

The ABAS protection level differs from GBAS and SBAS concepts in that sense that it takes into account that one measurement might be faulty (and that ABAS monitor might not detect certain faults).

## 2.4 Focus on SBAS

After the description of the SBAS architecture, the concept of SBAS differential correction which allows the user to improve pseudorange measurement accuracy is described. Then, the SBAS integrity risk allocation is deepened. Finally, a comparison between SBAS and GBAS is proposed to have a better understanding of augmentation systems.

### 2.4.1 SBAS architecture

Figure 2-2 gives an overview of the SBAS architecture [Chatre, 2003]:

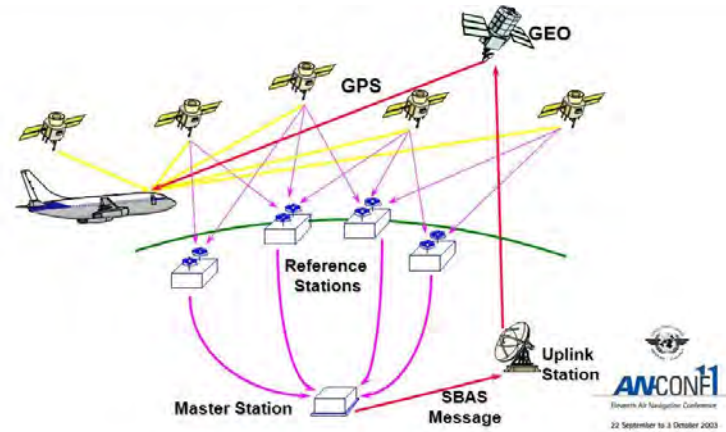


**Figure 2-2.** SBAS general architecture [Chatre, 2003].

The SBAS space segment consists of Geostationary Earth Orbit (GEO) satellites. Some characteristics of the two SBASs that are targeted in this study are given in Table 2-5. Ground stations send information via uplink stations to SBAS satellites that transmit the information to all SBAS users in the area covered by the satellites.

SBAS	WAAS	EGNOS
Political entity	United States	European Union
Orbital height	GEO (35 786 km)	GEO (35 786 km)
Orbital slot	Inmarsat 4F3 (98° W) Galaxy 15 (133° W) Telesat Anik F1R (107.3° W)	Inmarsat-3 AOR-E (15.5° W) Inmarsat-3 IOR-W (25.0° E) ESA-Artemis (21.5° E)
Number of satellites	3	3
Frequencies	L1 (1575.42 Mhz)	L1 (1575.42 Mhz)

**Table 2-5.** Space segment of the two SBASs of interest: WAAS and EGNOS [Navipedia, 2015] and [GALILEO LA, 2015].

Considering SBAS ground segment, WAAS and EGNOS are controlled and managed by different ground stations as summarized in Table 2-6.

	WAAS	EGNOS
Central processing facilities	WAAS Master Station (WMS): 3	Master Control Center (MCC): 4
Uplinks facilities	Ground Uplink Station (GUS): 6	Navigation Land Earth Station (NLES): 6
Monitoring facilities	Wide area Reference Station (WRS) : 38	Ranging Integrity Monitoring Station (RIMS) : 36
	Operational Control Centers : 2	Performance Assessment and Checkout Facilitie: 2

**Table 2-6.** Ground segment of the two SBASs of interest ([Navipedia, 2015] and [GALILEO LA, 2015]).

More details about WAAS and EGNOS are given respectively in [RTCA, 2006] and in [Westbrook et al., 2000] or [Brocard et al., 2000]. In EGNOS, specific and independent Ranging Integrity Monitoring Stations are dedicated to the monitoring of signal distortions: the RIMS-C.

The SBAS user segment is based on the same principles as classical GNSS receivers: L-band receiver/processors and antennas are necessary to process SBAS satellite signals. As the information carried by SBAS satellite signals is different from information carried by GPS or Galileo signals, a dedicated software processing has to be implemented.

SBAS users also have the possibility to use SBAS signals as ranging sources to increase the number of pseudorange measurements (not all SBAS provide this service).

#### 2.4.2 SBAS differential pseudorange measurement concept

SBAS provides three corrections to users which estimate their PVT from GPS L1 C/A signals [RTCA, 2006]:

- Fast corrections: they are intended to correct errors that change rapidly in time such as GNSS satellite clock errors. Fast corrections are common to all users.
- Long-term corrections: they are intended to correct errors that change slowly in time such as errors due to the atmospheric and long-term satellite clock and ephemeris errors.
- Ionospheric corrections: a wide-area vertical ionospheric delay model is provided to the user at points on a reference grid. The ionospheric delay is estimated at user level by interpolation of delays available on the reference grid (at least three points are necessary for the interpolation) and by projection of the ionospheric delay in the direction of the user.

SBAS principles are defined in this section based on EGNOS definitions [RTCA, 2006].

In EGNOS system, the code pseudorange measurement correction is defined as:

$$\hat{\rho}_{u,corr}^i = \hat{\rho}_u^i + TC_i + IC_i + PRC_i(t_{i,of}) + RRC_i(t_{i,of}) \times (t - t_{i,of}) + \Delta t_{sv}^i(t) \quad (2-19)$$

with

$$RRC_i(t_{i,of}) = \frac{PRC_{i,current} - PRC_{i,previous}}{\Delta t}$$

$$\Delta t = t_{i,of} - t_{of,previous}$$

$$\Delta t_{sv}^i(t) = a_{f_0} + a_{f_1}(t - t_0) + a_{f_{G0}}$$

where

- $PRC_i$  is the fast pseudorange correction associated to signal  $i$ .
- $PRC_{i,current}$  is the most recent fast pseudorange correction associated to signal  $i$ .  
 $PRC_{i,current} = PRC_i(t_{i,of})$ .
- $PRC_{i,previous}$  is the previous fast pseudorange correction associated to signal  $i$ .
- $t_{i,of}$  is the time of applicability of the most recent fast pseudorange correction associated to signal  $i$ .
- $t_{i,of,previous}$  is the time of applicability of the previous fast pseudorange correction associated to signal  $i$ .
- $TC_i$  is the tropospheric delay estimated by the user for the signal  $i$  from a UNB3 tropospheric model.

## 2. GNSS background

- $IC_i$  is the ionospheric delay estimated for the signal  $i$  from the grid ionospheric model defined by RTCA [RTCA, 2006] and send by SBAS satellites.
- $\Delta t_{sv}^i$  is the long term satellite error correction associated to signal  $i$ .
- $a_{f_0}$  is the clock offset error correction.
- $a_{f_1}$  is the clock drift error correction.
- $a_{f_{G0}}$  is an additional correction used for GLONASS satellites. It is set to zero for GPS satellites.
- $t_0$  is the time of the day applicability.

Still considering EGNOS, after differential corrections, the standard deviation associated to the ionospheric error is approximately equal to 0.5 m ([GSA, 2014]) instead of being between 4.3 and 13.7 m. The standard deviation of the clock and ephemeris error for users augmented by EGNOS was estimated at 0.3 m assuming that the user apply the most recent correction (sent every 6 s) instead of 0.85 m before corrections [Salos, 2012].

### 2.4.3 SBAS integrity risk allocation

In SBAS, the integrity risk allocation is split in two integrity risks, one for the protection level and another one for the fault detection detector. A general fault tree is presented regarding SBAS context in Figure 2-3, more details are available in [RTCA, 2004] or [Roturier et al., 2001].

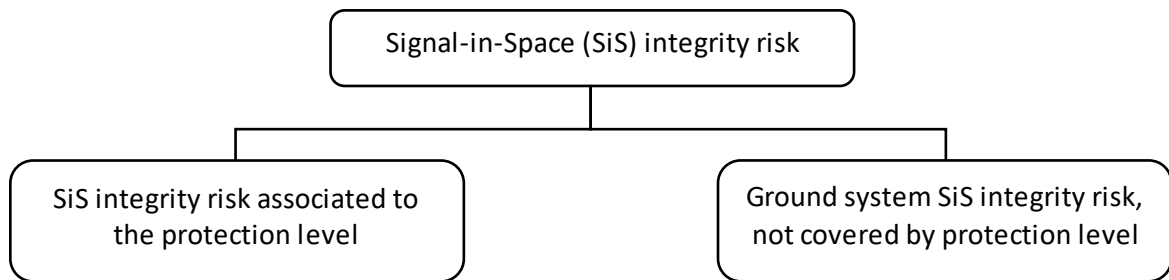


**Figure 2-3.** General SBAS fault tree, SiS integrity risk allocation.

SBAS monitors the validity of signals sent from the space segment as well as the ground segment. Current SBASs monitor only GPS signals (or GPS and GLONASS). The ground system contribution in the integrity risk corresponds to the right branch of Figure 2-3 and can be divided in three high level threats as presented for WAAS in [RTCA, 2004] and [Walter et al., 2012].

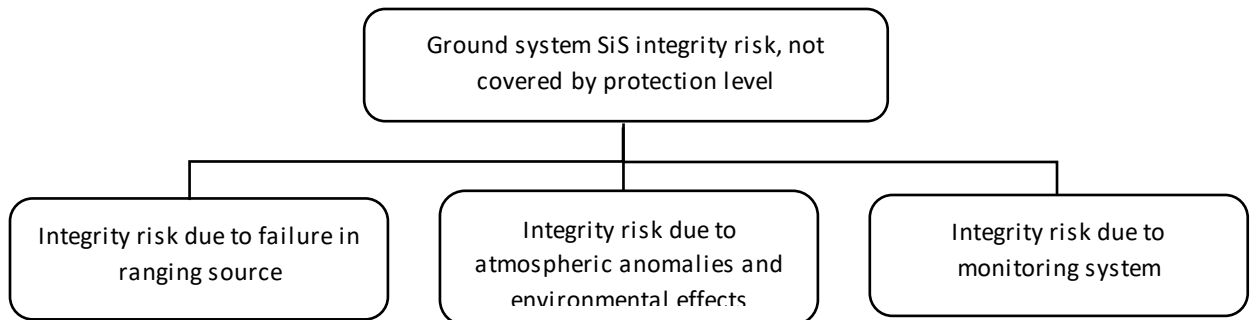


**Figure 2-4.** General fault tree, ground system SiS integrity risk allocation.

The three high level threats can be also sub-divided. The signal distortion contribution in the integrity risk allocated to Signal-in-Space (SiS) is one of the threat included in the integrity risk allocated to



failure in ranging source. Nevertheless other ranging source failures are monitored by SBAS [Fernow, 2005]:

- the clock and ephemeris inaccuracies,
- the code carrier incoherency,
- excessive acceleration (the list is not exhaustive).

#### 2.4.4 Comparison between SBAS and GBAS

In order to understand in a better way the SBAS differential concept, a brief comparison between GBAS and SBAS is given. Even if both systems are concerned by the same problem regarding signal deformations, the SBAS structure is different from the GBAS structure:

- GBAS is a system without any space segment.
- GBAS ground segment is constituted of a single ground station located at an airport, containing possibly several reference receivers with precisely known locations. SBAS relies on a network of ground stations spread over a continent.
- SBAS corrections are uploaded from the ground to the satellites and then sent to the user via SBAS satellites whereas GBAS corrections are sent by ground stations via a VHF signal.
- The GBAS user segment contains a dedicated VHF antenna and demodulator, required to decode the GBAS message. The SBAS signal is transmitted on the same band as GPS L1 C/A signals, with a similar modulation. The hardware modifications required to use the SBAS message are minor, any GNSS receiver is able to use the SBAS message with a software modification.

From an operational point of view, the two main differences between GBAS and SBAS are that:

- SBAS code pseudorange corrections are given separately for each error depending on the source of the error whereas all errors are corrected together in the GBAS approach. Mathematically, and taking back notations from 2.3.1.1.3, in GBAS all errors coming from different sources are corrected differentially in one term:  $\varepsilon_{other}^i = 0$  and  $errors_{\rho}^i = \varepsilon_{diff}^i$ .
- SBAS code corrections and integrity bounds are valid over an entire area and not only in the GBAS reference station neighborhood. To estimate corrections, many reference stations are spread over large regions. Instead of GBAS scalar correction, SBAS is based on vectorial correction. Indeed SBAS provides the user with a set of corrections values at different space locations. From this information, the user extrapolates corrections values to its own location.

GBAS integrity risk allocation is similar for GBAS and SBAS.

## 2.5 Conclusions

In this chapter, a general overview of GNSS concepts was presented. Among all GNSS, two constellations are focused on: the United State GPS constellation, as an unavoidable standard, and the European Galileo constellation, as this work is performed in a European context. In the same way, two SBASs are focused on: the United State system WAAS and the European system EGNOS.

## *2. GNSS background*

In the civil aviation framework, core constellations cannot be used in critical phases of flight (approach and landing) because accuracy, availability, continuity and integrity requirements are not all met. To mitigate these errors, improve accuracy and integrity, and meet requirements, augmentation systems were developed. In particular, this Ph.D. thesis is focused on SBASs which are DGNSS and integrity augmentation systems. To satisfy integrity requirements, SBASs have to associate probabilities allocated to different GNSS threats (these probabilities are called integrity risks). A part of the total integrity risk (it means the integrity risk considering all GNSS threats) is allocated to the SiS distortions threat. GNSS signal distortion is the particular GNSS threat that is tackled in this Ph.D. thesis in the SBAS context.

Even if GBAS is not the target of the study, its concept was introduced to illustrate the differential measurement approach and to have a comparison with SBAS. Moreover both GBAS and SBAS are concerned by the same problem of signal distortions even if slight differences exist in the strategy to monitor SiS distortions as detailed by ICAO in [ICAO, 2006].

One of the difficulties regarding the GNSS signal distortion problem is that the impact of such a threat on users depends upon two fundamental parameters: the signal modulation and the GNSS receiver processing. Both parameters are detailed in the next chapter.

### 3 GNSS signals structure and receiver processing

This chapter intends to give an overview of GNSS receiver structure. The basic architecture of a GNSS receiver is presented in a simplified way in Figure 3-1.

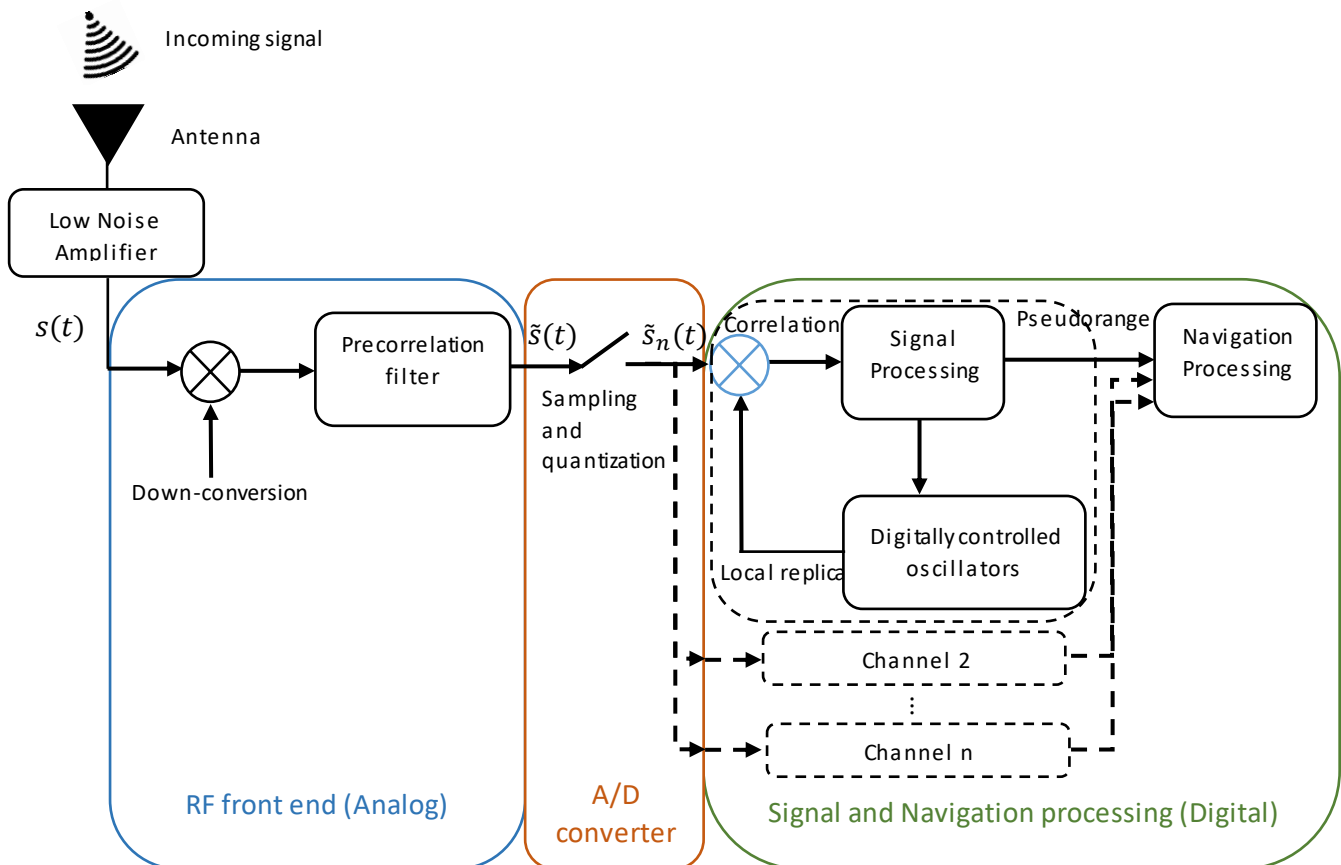


**Figure 3-1.** General structure of a GNSS receiver.

First of all, section 3.1 brings details about signals that are (or will be) used by civil aviation receivers: GPS L1 C/A, GPS L5, Galileo E5a and Galileo E1C signals. Then, section 3.2 describes briefly the antenna and the analog processing part of a GNSS receiver also called RF front-end which output consists of the input of the Analog-to-Digital Converter (ADC). Section 3.3 introduces the main digital processing steps, namely acquisition, code tracking and carrier phase tracking, which are typically implemented in GNSS receivers and that allow to have access to the pseudorange measurements. Note that the PVT computation algorithm is not described as the pseudorange measurements are the observables of interest in the present Ph.D. thesis. Information about these algorithms can be found for example in [Kaplan and Hegarty, 2006].

### 3.1 Signals of interest description

This section introduces the GPS and Galileo signals of interest for civil aviation users: GPS L1 C/A, GPS L5, Galileo E1C and Galileo E5a. For these users, stringent performances are required in terms of accuracy, availability, continuity and integrity, reflected in a need of integrity of the received signals themselves. This is why these signals are closely monitored by augmentation systems.

Satellite navigation signals are broadcasted in a frequency band allocated to the RNSS (Radio Navigation Satellite System). In the special case of GNSS signals being used by civil aviation, these signals also have to be within an ARNS frequency band (Aeronautical Radio Navigation Services). An ARNS band is specifically protected as it hosts signals used for safety-of-life applications. It is thus relatively free from interference (apart from intentional interference), except when other ARNS broadcast in the band as is the case for E5/L5 band, which is used by DMEs (Distance Measuring Equipments) for example. The frequency band allocation is provided by International Telecommunication Union (ITU).

Figure 3-2 illustrates Galileo and GPS signal frequency plans available in Galileo Interface Control Document (Galileo ICD) [GSA, 2010].

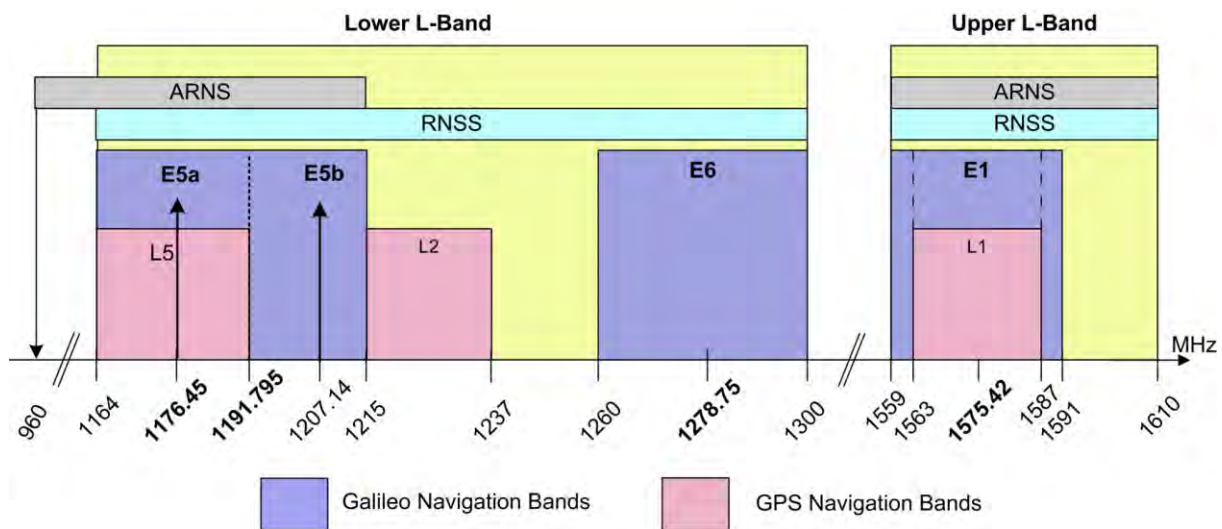


Figure 3-2. Galileo and GPS frequency plans [GSA, 2010].

#### 3.1.1 General GNSS signal structure

The modulation scheme for all the considered GPS and Galileo signals is based on Direct Sequence Spread Spectrum (DSSS). As a consequence typical GNSS signals are composed of:

- **A carrier.** To transport signals information, a suitable carrier frequency is required. It allows to choose the frequency band of the transmission, and therefore to respect the ITU frequency allocation plan. The frequency bands chosen for GNSS transmissions allow to limit the impact of the signal propagation channel (ionosphere, air, etc.) and to limit the size of antennas. The carrier frequency (noted  $f_0$ ) of L1 signals is equal to 1575.42 MHz and the carrier frequency of L5 signals is equal to 1175.45 MHz.

- **The spreading code**, which is a binary finite code composed of a large number of bits that imitates the statistical behavior of white noise. A bit of the spreading code is known as a chip. The chipping rate of a spreading code is noted  $f_c$ . The code sequence  $c(t)$  can be modeled as:

$$c(t) = \sum_{i=-\infty}^{+\infty} \left( \left( \sum_{k=1}^N c_k \cdot m(t - kT_c) \right) * \delta(t - iNT_c) \right) \quad (3-1)$$

where

- $N$  is the number of chips of the PRN code,
- $T_c = 1/f_c$  is the duration of a chip in second,
- $c_k$  are the spreading code chips,
- $m(t)$  is the shaping waveform of the chip, which can take several forms depending on the considered signal, as shown in the following paragraphs,
- $\delta(t - \tau)$  is the Dirac function centered on the delay  $\tau$ .

The spreading code name comes from the fact that the baseband signal has a wider bandwidth after modulation with the spreading code due to the high chipping rate of the spreading code with respect to the data rate. This code is also called PRN (Pseudo Random Noise) due to its statistical properties. The code period is noted  $T_{code}$ . This code allows the use of DSSS and is chosen for satellite navigation for three main reasons [Kaplan and Hegarty, 2006]:

- The frequent phase inversions in the signal introduced by the PRN waveform enable precise ranging by the receiver.
- The use of different PRN sequences from a well-designed set, enables multiple satellites to transmit signals simultaneously on the same frequency. Each satellite has its own PRN and a receiver can distinguish among these signals the signal sent by a particular satellite.
- DSSS provides significant rejection of narrowband interference.
- **A secondary code**, which is a binary finite code that modulates the signal. The secondary code generally has a bit duration equal to the code period [GSA, 2010]. Not all GNSS signals have a secondary code. The use of a secondary code can improve some signal features [Sekar et al., 2012]:
  - data symbol synchronization,
  - correlation properties,
  - narrowband interference protection.
- **The useful data**. This component contains the useful information that is meant to be passed to the user. Note that not all GNSS signals contain useful data. If they do, they are referred to as data component. If they do not, they are referred to as data-less or pilot component. Typical GNSS data component uses BPSK modulation. Data bits are sent with a rate  $f_d = 1/T_d$ , with  $T_d$  the data bit period.  $f_d$  is much smaller than the spreading code frequency  $f_c$ . The data sequence  $d(t)$  can be modeled as:

$$d(t) = \sum_{n=-\infty}^{+\infty} d_n \cdot \text{rect}_{T_d} \left( t - T_d \left( n + \frac{1}{2} \right) \right) \quad (3-2)$$

where the rectangular function is defined by:

$$rect_X(t) = \begin{cases} 0 & \text{if } |t| > \frac{X}{2} \\ 1 & \text{if } |t| \leq \frac{X}{2} \end{cases} \quad (3-3)$$

Parameters defining signals of interest are summarized in Table 3-1. Other Galileo and GPS signals are not described because they are not planned to be used by civil aviation users.

Constellation	Galileo				GPS		
Signal	E1B	E1C	E5a-I	E5a-Q	L1 C/A	L5-I	L5-Q
Navigation Data (sps)	250	Pilot	50 (25 bps)	Pilot	50	100 (50 bps)	Pilot
Secondary code length (primary code length)	No	25	20	100	No	10	20
Primary code length (chip)	4092		10230		1023	10230	
Chip rate (Mcps)	1.023		10.23		1.023	10.23	
Primary code duration (ms)	4		1		1	1	
Modulation	$CBOC(6,1,1/11)^1$		$QPSK(10)^1$		$BPSK(1)^1$	$QPSK(10)^1$	
Carrier frequency (MHz)	1575.420		1176.450		1575.420	1176.450	
Bandwidth (MHz)	24.552		20.46		20.46	24	
Polarization	Right Hand Circular Polarized (RHCP)						

<sup>1</sup>: defined in the next section

**Table 3-1.** Characteristics of Galileo and GPS signals of interest.

In the following, details are added about the structure of signals presented in Table 3-1.

### 3.1.2 GPS L1 C/A signal structure

GPS L1 C/A signal is  $BPSK(1)$ -modulated, which means:

- the PRN code chipping rate  $f_c$  is equal to  $1 \times 1.023$  MHz and
- the shaping waveform  $m(t)$  used by the PRN code is a rectangle of length the chip duration.

As a consequence, the PRN code can be modeled as:

$$c(t) = \sum_{i=-\infty}^{+\infty} \left( \left( \sum_{k=0}^N c_k \cdot \text{rect}_{T_c} \left( t - T_c \left( k + \frac{1}{2} \right) \right) \right) * \delta(t - iNT_c) \right) \quad (3-4)$$

Details about this signal can be found in a lot of documents such as in [GPS.gov, 2000] or [Gleason, 2009]. The ideal GPS L1 C/A signal at the satellite output can be modeled as:

$$s_{s\_C/A}(t) = A d(t) c(t) \cos(2\pi t f_0) \quad (3-5)$$

where  $A$  is the amplitude of the transmitted signal.

The derivation of the normalized Power Spectral Density (PSD) envelope of the GPS L1 C/A signal is given in [Avila Rodriguez, 2008] assuming an infinite PRN code:

$$G_{BPSK(1)}(f) = T_c \frac{\sin^2\left(\frac{\pi f}{f_c}\right)}{\left(\frac{\pi f}{f_c}\right)^2} \quad (3-6)$$

The inverse Fourier transform of the normalized PSD is the normalized autocorrelation function of the signal:

$$R_{BPSK(1)}(\tau) = \int_{-\infty}^{+\infty} G_{BPSK(1)}(f) e^{-2\pi i f \tau} df$$

$$R_{BPSK(1)}(\tau) = \text{tri}_{T_c}(\tau) = \begin{cases} 1 - \frac{|\tau|}{T_c} & \text{if } |\tau| < T_c \\ 0 & \text{elsewhere} \end{cases} \quad (3-7)$$

Figure 3-3 shows the normalized PSD (and not only its envelope) and the normalized autocorrelation function of the ideal GPS L1 C/A signal made of finite PRN code sequences.

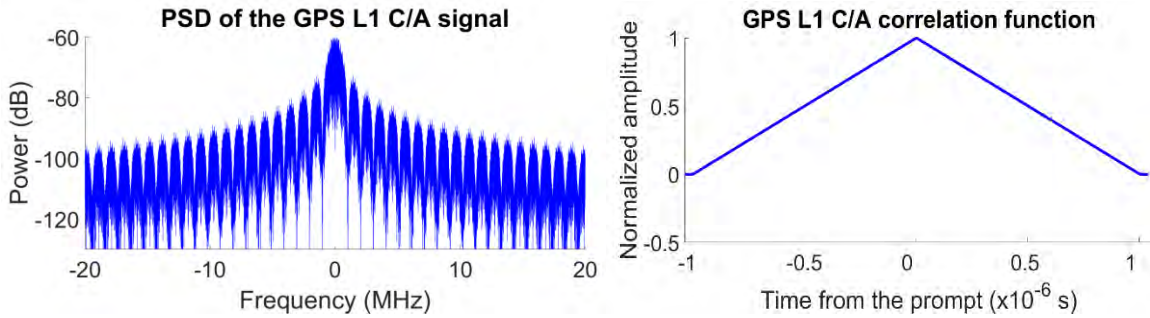


**Figure 3-3.** Normalized PSD (on the left) and normalized autocorrelation function (on the right) of the GPS L1 C/A signal.

### 3.1.3 GPS L5 signal structure

GPS L5 signal is composed of two orthogonal components. One component consists of the L5 pilot channel, on the quadrature-phase part of the signal, and the second component consists of the L5 data channel, on the in-phase part of the signal. The two channels have different PRN codes and different secondary codes (with different secondary code lengths). Both components can be considered as two independent  $BPSK(10)$ -modulated signals (the total signal is  $QPSK(10)$ -modulated). Details about

### 3. GNSS signals structure and receiver processing

GPS L5 are provided in several documents as in [GPS.gov, 2012], [Macabiau et al., 2003] or [Bastide et al., 2002].

The two GPS L5 components are  $BPSK(10)$ -modulated, which means:

- the PRN code chipping rate  $f_c$  is equal to  $10 \times 1.023$  MHz and
- the shaping waveform  $m(t)$  used by the PRN code is a rectangle of length the chip duration.

As a consequence, the PRN code can be modeled on the in-phase ( $c_I(t)$ ) and the quadrature-phase ( $c_Q(t)$ ) components as:

$$c_X(t) = \sum_{i=-\infty}^{+\infty} \left( \left( \sum_{k=0}^N c_{k,X} \cdot \text{rect}_{T_c} \left( t - T_c \left( k + \frac{1}{2} \right) \right) \right) * \delta(t - iNT_c) \right) \quad (3-8)$$

with  $X = I$  or  $Q$

where

- $X = I$  is referred to as the in-phase component and  $X = Q$  is referred to as the quadrature-phase component.
- $c_{k,X}(t)$  is the PRN chips sequence of the in-phase ( $X = I$ ) and the quadrature-phase component ( $X = Q$ ).

The ideal L5 signal,  $QPSK(10)$ -modulated, at the satellite output can be modeled as:

$$s_{s,L5}(t) = A_d(t)c_I(t)c_{2,I}(t)\cos(2\pi t f_0) + A_Q(t)c_Q(t)c_{2,Q}(t)\sin(2\pi t f_0) \quad (3-9)$$

where

- $A$  is the amplitude of the transmitted signal.
- $c_{2,I}(t)$  ( $c_{2,Q}(t)$ ) is the materialization of the secondary code on the in(quadrature)-phase component.

The pilot component is usually used essentially to improve the accuracy of the code pseudorange measurement and decrease the time necessary to acquire the signal. Moreover, the current draft SBAS Dual-Frequency Multi-Constellation (DFMC) document [Samson, 2015] seems to indicate that only the pilot channel would be used to estimate pseudorange measurements in an airborne (DFMC) receiver in SBAS mode. As a consequence, a special focus will be put on the pilot component. By consequence, the study of the GPS L5 pilot component can be seen as the study of one  $BPSK(10)$ -modulated signal.

The derivation of the normalized PSD envelope of the quadrature-phase L5 signal component ( $BPSK(10)$  modulation) is equivalent to the  $BPSK(1)$  modulation with a different chipping rate (10 times higher in the case of  $BPSK(10)$ ) and is given by:

$$G_{BPSK(10)}(f) = T_c \frac{\sin^2\left(\frac{\pi f}{f_c}\right)}{\left(\frac{\pi f}{f_c}\right)^2} \quad (3-10)$$

The inverse Fourier transform of the normalized PSD is the normalized autocorrelation function of the signal:

$$R_{BPSK(10)}(\tau) = \int_{-\infty}^{+\infty} G_{BPSK(10)}(f) e^{-2\pi i f \tau} df$$



$$R_{BPSK(10)}(\tau) = tri_{T_c}(\tau) = \begin{cases} 1 - \frac{|\tau|}{T_c} & \text{if } |\tau| < T_c \\ 0 & \text{elsewhere} \end{cases} \quad (3-11)$$

Figure 3-4 shows the normalized PSD (and not only its envelope) and the normalized autocorrelation function of the ideal GPS L5 pilot component made of finite PRN code sequences.

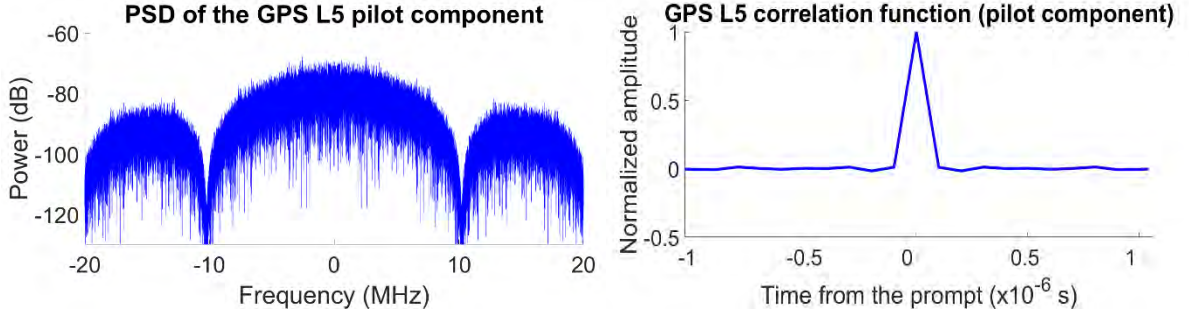


**Figure 3-4.** Normalized PSD (on the left) and normalized autocorrelation function (right) of the GPS L5 quadrature component.

### 3.1.4 Galileo E5a signal structure

The Galileo E5 band carries two sub-signals: E5a and E5b signals. These two signals have different carrier frequencies and are modulated together to form a wideband E5 signal *AltBOC*(15,10). E5a and E5b sub-signals can be considered as two *QPSK*(10)-modulated signals and can be processed independently. Each sub-signal has the same structure as the GPS L5 signal: a pilot and a data channels are sent via the in-phase and the quadrature-phase signal components. Details about Galileo E5 signals are provided in [GSA, 2010], [Bastide et al., 2002] or [Shivaramaiah and Dempster, 2009].

As only the E5a pilot channel component should be used by civil aviation to estimate pseudoranges, the E5a signal model is presented without considering the E5b signal. The ideal E5a signal, approximated by a *QPSK*(10)-modulated signal, at the satellite output can be approximated by:

$$s_{s,E5a}(t) \approx A d(t) c_I(t) c_{2,I}(t) \cos(2\pi t f_0) + A c_Q(t) c_{2,Q}(t) \sin(2\pi t f_0) \quad (3-12)$$

where

- $A$  is the amplitude of the transmitted signal.
- $c_{2,I}(t)$  ( $c_{2,Q}(t)$ ) is the materialization of the secondary code on the in(quadrature)-phase component.
- $c_I(t)$  ( $c_Q(t)$ ) is the PRN code on the in(quadrature)-phase component as defined by equation (3-8).

The normalized PSD envelope of the Galileo E5a quadrature phase component assuming an infinite PRN code can be approximated by the GPS L5 signal *BPSK*(10)-modulated PSD:

$$G_{BPSK(10)}(f) = T_c \frac{\sin^2\left(\frac{\pi f}{f_c}\right)}{\left(\frac{\pi f}{f_c}\right)^2}$$

The normalized autocorrelation function of the Galileo E5a quadrature-phased signal can be approximated by  $R_{BPSK(10)}$ :

$$R_{BPSK(10)}(\tau) = tri_{T_c}(\tau) = \begin{cases} 1 - \frac{|\tau|}{T_c} & \text{if } |\tau| < T_c \\ 0 & \text{elsewhere} \end{cases}$$

The normalized PSD and the autocorrelation function of the E5a signal pilot component are very similar to the GPS L5 signal pilot component PSD and correlation function (see Figure 3-4). In this document both signals are considered as equivalent.

### 3.1.5 Galileo E1 OS signal structure

The Galileo E1 Open Service signal is composed of two components: the E1B data component and the E1C pilot component. Both components are CBOC-modulated. The data component carries the I/NAV navigation data stream, the spreading code and is modulated with two sub-carriers whereas the pilot component is constituted of a spreading code (which includes a secondary code) and is modulated with the sub-carriers. Galileo E1 signal is  $CBOC(6,1, 1/11)$ -modulated, which means:

- the PRN code chipping rate  $f_c$  is equal to  $1 \times 1.023 \text{ MHz}$  and
- the shaping waveform  $m(t)$  used by the PRN code is a pattern with a length equal to the chip duration and defined by:

- $\alpha sc_{BOC(1,1)}(t) + \beta sc_{BOC(6,1)}(t)$  for the E1B component,
- $\alpha sc_{BOC(1,1)}(t) - \beta sc_{BOC(6,1)}(t)$  for the E1C component,

where

- $\alpha = \sqrt{\frac{10}{11}}$
- $\beta = \sqrt{\frac{1}{11}}$
- $sc_{BOC(X,1)}(t) = \begin{cases} \text{sign}(\sin(2\pi X t \times 1.023 \times 10^{-6})) & \text{if } 0 < t < T_c \\ 0 & \text{elsewhere} \end{cases}$

is the materialization of the sub-carrier.

As a consequence, the PRN code on the E1B component can be modeled as:

$$c_{E1B}(t) = \sum_{i=-\infty}^{+\infty} \left( \left( \sum_{k=0}^N c_k \cdot (\alpha sc_{BOC(1,1)}(t - kT_c) + \beta sc_{BOC(6,1)}(t - kT_c)) \right) * \delta(t - iNT_c) \right) \quad (3-13)$$

And on the E1C component as:

$$c_{E1C}(t)(t) = \sum_{i=-\infty}^{+\infty} \left( \left( \sum_{k=0}^N c_k \cdot (\alpha sc_{BOC(1,1)}(t - kT_c) - \beta sc_{BOC(6,1)}(t - kT_c)) \right) * \delta(t - iNT_c) \right) \quad (3-14)$$

It should be noted that  $c_k$  which appears in the definition of the E1B signal component is different from  $c_k$  which appears in the definition of E1C even if no distinction is made for the sake of simplicity. Details about Galileo E1 OS signal are given in [GSA, 2010] or [Julien et al., 2006]. The ideal E1 signal at the satellite output can be modeled as:

$$s_{s\_E1}(t) = Ad(t)c_{E1B}(t) \cos(2\pi t f_0) - Ac_{2,E1C}(t)c_{E1C}(t) \cos(2\pi t f_0) \quad (3-15)$$

where

- $A$  is the amplitude of the transmitted signal.
- $c_{2,E1C}(t)$  is the materialization of the secondary code on the E1C signal.

As for other signals, only the pilot component is of interest in the context of this Ph.D.: E1C. E1C modulation is defined as  $CBOC(6,1,1/11, -)$  whereas E1B as a  $CBOC(6,1,1/11, +)$ .

The PSD envelope of the transmitted Galileo E1 signal on the in-phase component is made of both E1B and E1C signals. The global E1 modulation consists in a  $CBOC(6,1,1/11)$  and its normalized PSD envelope assuming an infinite PRN code is given in [Julien et al., 2006] by:

$$G_{CBOC(6,1,1/11)}(f) = \frac{10}{11} G_{BOC(1,1)}(f) + \frac{1}{11} G_{BOC(6,1)}(f) \quad (3-16)$$

where

$$G_{BOC(X,1)}(f) = f_c \left( \frac{\sin\left(\frac{\pi f}{2Xf_c}\right) \sin\left(\frac{\pi f}{f_c}\right)}{\pi f \cos\left(\frac{\pi f}{2Xf_c}\right)} \right)^2$$

The autocorrelation of the E1C component cannot be directly estimated from the PSD of the entire E1 signal. For the E1C component, the normalized  $CBOC(6,1,1/11, -)$  autocorrelation function is defined from the convolution product as:

$$\begin{aligned} R_{CBOC(6,1,1/11,-)}(\tau) &= \left( \left( \sqrt{\frac{10}{11}} s_{CBOC(1,1)} - \sqrt{\frac{1}{11}} s_{CBOC(6,1)} \right) \right. \\ &\quad \left. * \left( \sqrt{\frac{10}{11}} s_{CBOC(1,1)} - \sqrt{\frac{1}{11}} s_{CBOC(6,1)} \right)^* \right)(\tau) \end{aligned} \quad (3-17)$$

where  $(x * y)(\tau) = \int_{-\infty}^{+\infty} (x(\tau - t) \times y(t)) dt$  is the convolution process.

From this expression, the normalized autocorrelation function definition introduced in [Julien et al., 2006] can be recovered:

$$\begin{aligned} R_{CBOC(6,1,1/11,-)}(\tau) &= \frac{10}{11} R_{BOC(1,1)}(\tau) + \frac{1}{11} R_{BOC(6,1)}(\tau) \\ &\quad - 2 \frac{\sqrt{10}}{11} R_{BOC(1,1)/BOC(6,1)}(\tau) \end{aligned} \quad (3-18)$$

with

$$R_{BOC(X,1)}(\tau) = - \sum_{k=1}^X \left( \text{tri} \left( \frac{\tau - \frac{2(k-1)}{2X}}{\frac{T_c}{2X}} \right) + \text{tri}_{\frac{T_c}{2X}} \left( \tau + \frac{2(k-1)}{2X} \right) \right)$$

$$R_{BOC(1,1)/BOC(6,1)}(\tau) = \frac{1}{12} \sum_{k=1}^{12} n_k \times \text{tri}_{\frac{T_c}{2X}} \left( \tau - \frac{2(k-1)}{2X} \right)$$

- $n_k = 1$  if  $k = 1; 2; 3; 10; 11; 12$  and  $n_k = -1$  if  $k = 4; 5; 6; 7; 8; 9$ .
- $\text{tri}_{T_c}(\tau - c)$  the triangular function centered in  $c$  with a width equal to  $2T_c$  and a magnitude equal to 1.

The three components of the correlation function are illustrated in Figure 3-5.

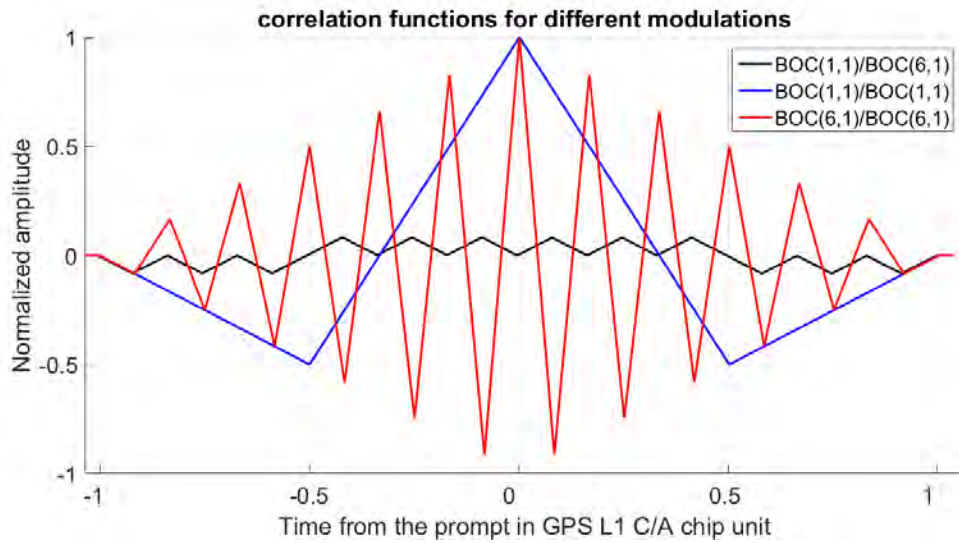


**Figure 3-5.** Correlation function terms used to defined CBOC autocorrelation function.

In the same way the normalized  $CBOC(6,1,1/11, +)$  autocorrelation function is given by:

$$R_{CBOC(6,1,1/11,+)}(\tau) = \frac{10}{11} R_{BOC(1,1)}(\tau) + \frac{1}{11} R_{BOC(6,1)}(\tau) + 2 \frac{\sqrt{10}}{11} R_{BOC(1,1)/BOC(6,1)}(\tau)$$

In the following, only the E1C component ( $CBOC(6,1,1/11, -)$  modulation) will be treated.

Figure 3-6 shows the normalized PSD (and not only its envelope) and the normalized autocorrelation function of the Galileo E1C signal made of finite PRN code sequences.

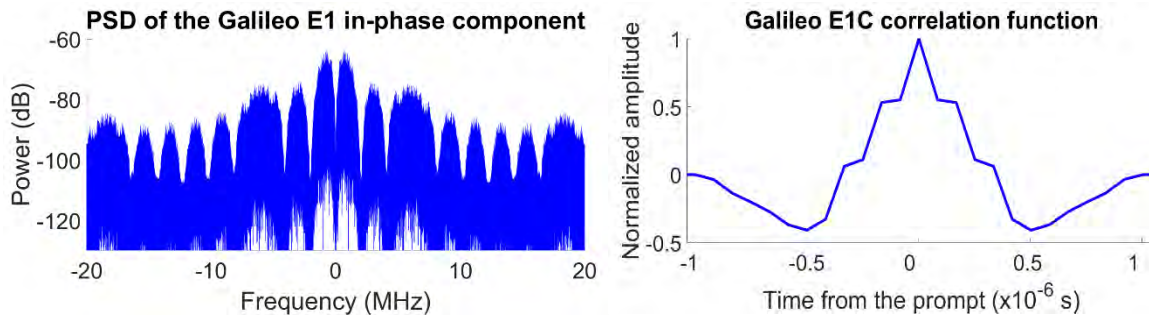


**Figure 3-6.** Normalized PSD of the Galileo E1 signal (on the left) and normalized autocorrelation function (right) of the Galileo E1C signal.

### 3.1.6 Discussion about power spectral density and correlation function

PSD expressions given for different signals have been estimated considering only the primary code materialization. This choice is equivalent to study the signal on only one spreading code chip symbol. On some signals, data and secondary code streams are also added. The consequence is that PSDs of transmitted signals are slightly different from PSDs estimated in sections 3.1.2 to 3.1.5. In the general case the mathematical definition of the PSD of a transmitted signal  $s_s(t)$  constituted of a data sequence  $d(t)$ , a spreading code sequence  $c(t)$  and a secondary spreading code sequence  $c_2(t)$  is equal to:

$$G_{s_s}(f) = G_{c_2}(f) * G_d(f) * G_c(f) \quad (3-19)$$

where

- $s_s(t) = c_2(t)d(t)c(t)$ ,
- $G_{c_2}(f)$  is the PSD of the materialized secondary code,
- $G_c(f)$  is the PSD of the materialized primary code,
- $G_d(f)$  is the PSD of the materialized data stream.

It is noteworthy that PSDs that have been presented for the different signals consist only in the  $G_c(f)$  term. Considering that the secondary code has a rate equal to  $f_{c_2}$  ( $f_{c_2} = 1/T_{c_2}$ ) and that the data rate is equal to  $f_d$  ( $f_d = 1/T_d$ ),  $G_{c_2}(f)$  and  $G_d(f)$  can be expressed as:

$$G_{c_2}(f) = T_{c_2} \frac{\sin^2\left(\frac{\pi f}{f_{c_2}}\right)}{\left(\frac{\pi f}{f_{c_2}}\right)^2}$$

$$G_d(f) = T_d \frac{\sin^2\left(\frac{\pi f}{f_d}\right)}{\left(\frac{\pi f}{f_d}\right)^2}$$

For studied signals,  $f_{c_2}$  and  $f_d$  are considerably lower than the primary code frequency  $f_c$  (at least 20 times lower as it can be seen on Table 3-1. It entails that the frequency occupation of  $G_c(f)$  is much larger than the frequency occupation of  $G_{c_2}(f)$  and  $G_d(f)$  and the consequence is that:

$$G_{s_s}(f) \approx G_c(f)$$

A second remark is that PSDs mathematical expressions established in previous sections of 3.1 are not exactly representative of transmitted signals PSD but only of the envelope of transmitted signals PSD, as discussed in [Julien, 2006]. Indeed the presence of the periodic spreading code generates PSD spectral lines separated from each other by the value of the ratio between  $f_c$  and the code length: 1 kHz for GPS L1 C/A signal, 250 Hz for Galileo E1C signal, 100 Hz for Galileo E5a and GPS L5 signals. For the sake of simplicity, only the PSD envelope is considered even if in Figure 3-3, Figure 3-4 and Figure 3-6 true PSDs are shown.

Regarding correlation functions, only models were introduced. The presence of a secondary code and/or data bits does not have a significant impact on correlation functions. Nevertheless, the primary code can slightly modify the shape of the correlation function. For instance for a GPS L1 C/A signal, depending on the PRN spreading code, the amplitude of the normalized correlation function at a

distance  $\pm T_c$  is not equal to zero but to  $\pm 1/1023$ . This phenomenon has an impact on the correlation function slope.

#### 3.1.7 Signals structures summary

The four signals that should be used by civil aviation receivers to estimate their pseudoranges and that are focused in this document are:

- the GPS L1 C/A signal, *BPSK*(1)-modulated,
- the GPS L5 quadrature-phase signal, *BPSK*(10)-modulated,
- the Galileo E5a quadrature-phase signal, *BPSK*(10)-modulated and
- the Galileo E1C signal, *CBOC*(6,1, 1/11, –)-modulated.

Signals, PSDs and correlation functions expressions were introduced for the four signals. As an approximation, PSDs were estimated from their envelopes. Secondary code and the data component were neglected in order to facilitate the analysis.

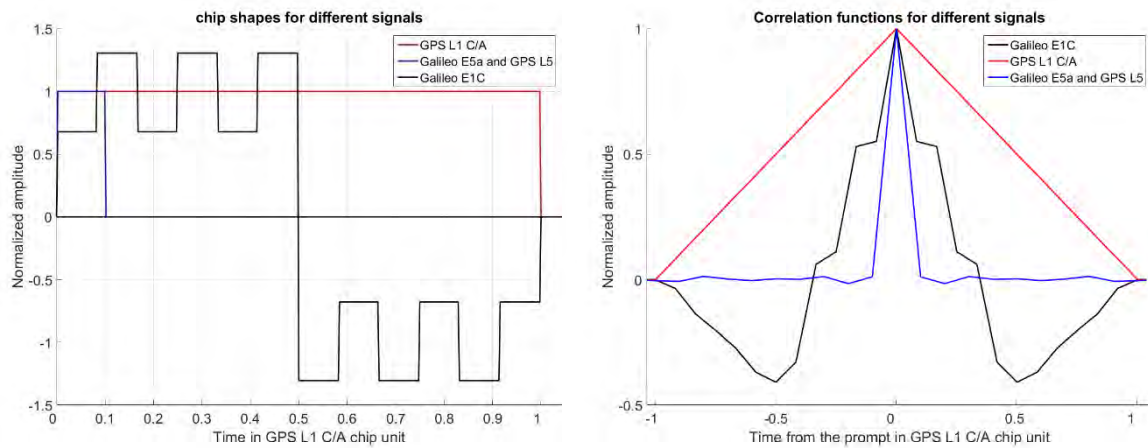


**Figure 3-7.** Chip shapes and autocorrelation functions for different signals.

Figure 3-7 illustrates the chip shape and the autocorrelation function for signals of interest. In red are presented results for the GPS L1 C/A signal, in blue results for Galileo E5a and L5 quadrature-phase signal components and in black results for Galileo E1C signal. The abscissa is given in GPS L1 C/A chip unit it means  $1.023 \times 10^{-6}$  s. The Galileo E1C correlation function corresponds to the *CBOC*(6,1,1/11, –) autocorrelation function. The Galileo E1C signal is normalized to have the *BOC*(1,1) component amplitude equal to 1 in the chip domain.

## 3.2 Analog processing of GNSS receiver

When reaching the receiver antenna, the incoming signal sent by the satellite and generated by the payload components, including the satellite antenna, has gone through the propagation channel that was described in the previous chapter (free space, ionosphere, troposphere, potential obstruction, multipath, interference). First of all this signal passes through the receiver antenna and then through the analog section of the GNSS receiver. In this section, the signal is processed as an analog signal before being digitized (sampled in time and quantified in amplitude) by the analog to digital converter.

The analog section is made of the antenna, a Low Noise Amplifier (LNA), mixers, local oscillators and filters. This receiver portion is of primary importance because it pre-conditions the signal that is then processed digitally.

### 3.2.1 Antenna

The antenna is the first component of the receiver encountered by the incoming signal. As GNSS signals are right hand circularly polarized, GNSS antennas are also right hand circularly polarized. Desired characteristics of GNSS antennas are: the frequency selectivity, a high gain towards the satellites, multipath and interference rejection capabilities, low gain in directions where no satellite is located and a stable phase and group delays.

The antenna has an impact on the signal quality. As an example, a high-gain dish antenna with a large diameter is directive and allows to amplify a signal arriving from one direction while attenuating all other. An omnidirectional antenna will have less gain in a given direction but will receive several signals with a fair  $C/N_0$ . Depending on the usage, different antennas can be selected. For the observation of tiny signal distortions, high-gain dish antennas are preferred. However, typical civil aviation users have antenna with a positive gain in the up direction and good rejection in the down direction.

### 3.2.2 RF front-end

After the antenna, the signal is passing through the RF front-end where it is amplified, down-converted and filtered. The down-conversion consists in reducing the signal carrier frequency in order to reach intermediate frequencies (IF) and filter the IF signal more selectively. The down-conversion is realized by multiplying the incoming signals by local sinusoidal waves generated by local oscillators. Several stages are usually necessary to translate the signal to IF or baseband.

The antenna and the summed effect of the different equivalent baseband filters and electronic components, part of the RF front-end, determine the so-called equivalent selective filter or pre-correlation filter of the GNSS receiver. In general, the last filter of the RF front-end (the most selective) is the one that will dominate the pre-correlation filter.

Figure 3-8 gives the chip shapes after applying a 6<sup>th</sup>-order Butterworth pre-correlation filter of 24 MHz (in red) and 12 MHz (in blue) double-sided. It is noticeable that a delay visible on the chip affects filtered measurements. The delay is higher when the filter bandwidth is lower.

At the output of the RF front-end, the GNSS signal is dominated by the noise. The next step of the signal processing which is the quantization of the signal consists essentially of a noise quantization more than a GNSS signal quantization.



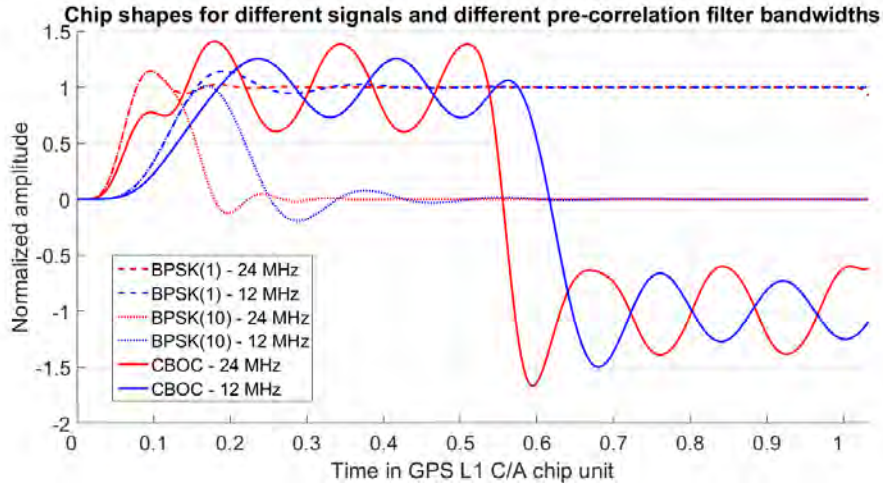


**Figure 3-8.** Influence of the filter bandwidth on chip shapes.

### 3.2.3 Analog to digital converter (ADC)

The ADC is the last step of the GNSS receiver analog processing. The purpose of this device is to digitize the analog signal. The signal is quantized in amplitude and in time. The process of time quantization is called sampling. The sampling period  $T_s$  is an important parameter because it is one of the parameters linked to the resolution with which the signal is observed. Another parameter linked to the resolution of the digitized signal is the number of bits used to quantize the amplitude of the signal. If only few quantization levels are available, the digitized signal will suffer from quantization losses. In general, to avoid these losses, the receiver can use a multi-bit ADC. In this case, an Automatic Gain Controller (AGC) is necessary to adapt the power of the received signal to the ADC quantization range and avoid signal distortions [Parkinson and Spilker, 2006].

### 3.2.4 Signal expression at the output of the analog section

Considering the ideal GNSS signal at the output of the satellite  $s_s(t)$ , the signal  $s_{input}(t)$  at the receiver antenna input can be written as a function of the propagation medium impulse response  $g_{prop}(t)$ :

$$s_{input}(t) = g_{prop}(t) * s_s(t) \quad (3-20)$$

When the signal goes through the antenna section, it is convolved with the impulse response of the antenna  $g_{ant}(t)$ . At the output of the antenna  $s(t)$ , the signal can be modeled as:

$$s(t) = g_{ant}(t) * s_{input}(t) \quad (3-21)$$

The signal at the output of the RF front-end  $\tilde{s}(t)$  can be expressed as a function of the impulse response of the RF front-end  $h_{RF}(t)$ .

$$\tilde{s}(t) = h_{RF}(t) * s(t) \quad (3-22)$$

The last step is the A/D conversion which consists in a quantization of the signal. The signal  $\tilde{s}_n$  at the output of the ADC can be modeled as:



$$\tilde{s}_n = \tilde{s}\left(\frac{n}{f_s}\right) \quad (3-23)$$

where  $f_s = 1/T_s$  is the sampling frequency in hertz.

Finally, the signal at the GNSS receiver analog section output can be written as a function of the signal at the satellite output:

$$\tilde{s}_m = (g_{tot} * s_s)\left(\frac{n}{f_s}\right) \quad (3-24)$$

Where  $g_{tot}(t) = (h_{RF} * g_{ant} * g_{prop})(t)$  is the impulse response of the propagation medium, the antenna and the RF front-end equivalent filter.  $g_{tot}(t)$  is equivalent to a delay  $\tau_c(t)$  on the code and a delay  $\tau_\varphi(t)$  on the carrier phase that are time-dependent.

Expressions of the two delays are function of parameters defined in 2.1.3 and can be expressed in seconds as:

$$\tau_c(t) = \frac{\rho_u^i(t)}{c} = \frac{R_u^i + \delta t_u + errors_{\rho,u}^i}{c} \quad (3-25)$$

and

$$\tau_\varphi(t) = \frac{\varphi_u^i(t)}{c} = \frac{R_u^i + \delta t_u + errors_{\varphi,u}^i + \lambda N^i}{c} \quad (3-26)$$

The carrier phase delay caused by the propagation of the signal is usually given in radian and is function of the carrier frequency:

$$\varphi_p(t) = 2\pi f_0 \tau_\varphi(t) \quad (3-27)$$

It is important to notice that the Doppler Effect, caused by the relative velocity between the satellite and the receiver and signals propagation effects, is included in the definition of the phase delay  $\varphi_p(t)$ .

At a given time, the Doppler frequency  $f_{dop}$  is linked to the phase delay by:

$$f_{dop} = \frac{1}{2\pi} \frac{d\varphi_p}{dt} \quad (3-28)$$

It entails that  $\varphi_p(t)$  can be written as a function of the signal initial phase  $\varphi_{p0}$ :

$$\varphi_p(t) = 2\pi t f_{dop}(t) + \varphi_{p0} \quad (3-29)$$

As an example, considering the expression of the GPS L1 C/A signal  $s_{s\_C/A}(t)$  at the satellite antenna output defined by equation (3-5):

$$s_{s\_C/A}(t) = A d(t) c(t) \cos(2\pi t f_0)$$

the signal  $\tilde{s}_{n\_C/A}$  at the output of the ADC can be modeled as:

$$\begin{aligned} \tilde{s}_{n\_C/A} = A \tilde{d}\left(\frac{n}{f_s} - \tau_c\left(\frac{n}{f_s}\right), f_{dop}\left(\frac{n}{f_s}\right)\right) \tilde{c}\left(\frac{n}{f_s} \right. \\ \left. - \tau_c\left(\frac{n}{f_s}\right), f_{dop}\left(\frac{n}{f_s}\right)\right) \cos\left(2\pi \frac{n}{f_s} f_{IF} + \varphi_p\left(\frac{n}{f_s}\right)\right) + \tilde{n}_s\left(\frac{n}{f_s}\right) \end{aligned} \quad (3-30)$$

where

- $\tilde{n}_s$  is an additive perturbation that affects the GNSS signal. It is modeled as a filtered white Gaussian noise (thermal noise).
- $\varphi_p(t)$  is the phase delay of the signal induces by the propagation, the antenna and the RF front-end in radian.
- $f_{IF}$  is the intermediate frequency after the down-conversion in hertz.
- $f_{dop}(t)$  is the Doppler frequency affecting the signal in hertz. This term is time-dependent.
- $\tilde{c}(t, f_{dop})$  is the filtered PRN chips sequence affected by a Doppler  $f_{dop}$  at time  $t$ .
- $\tilde{d}(t, f_{dop})$  is the filtered data sequence affected by a Doppler  $f_{dop}$  at time  $t$ .

The same concept can be applied to other signals.

To simplify formula without losing generality, the influence of the ADC is not taken into account in the expression of the signal at receiver digital section input. In the following, derivations are proposed considering a continuous signal.

## 3.3 Digital processing of GNSS receiver

After the digitization of the signal, the signal is processed in three main steps: the acquisition, the tracking and the data demodulation. The acquisition and the tracking aim at estimating the incoming signal parameters (code delay, carrier phase and Doppler). These parameters were defined in 3.2.4. These processes are all based on the correlation principle which is described in 3.3.1. The acquisition is introduced in 3.3.2. Then, code tracking and phase lock loops are described in 3.3.3. As introduced in this chapter, the estimation of the navigation solution is not tackled because the research about GNSS signal distortions performed in this study is limited to the pseudorange measurement domain.

### 3.3.1 Correlation process

The correlation process is at the base of the GNSS receiver processing. First of all, a correlator output model is given and some notations that are used in the continuation of this manuscript are introduced. Then, correlation functions that are derived by GNSS receivers are presented taking into account correlation function distortions induced by the analog section of the receiver. Finally, some important correlation function properties are given.

#### 3.3.1.1 Correlator output model

To extract information from the GNSS signal buried in the noisy RF front-end output, the receiver has to perform a correlation operation between the received signal and two local copies of the GNSS signal of interest (at least a copy of its PRN code and carrier, which are known by the receiver). One copy of the signal represents the in-phase component ( $s_{local_I}(t)$ ) and the other one the quadrature-phase component ( $s_{local_Q}(t)$ ).

$$s_{local_I}(t) = c(t - \hat{\tau}) \cos(2\pi t f_{IF} + \hat{\phi}(t)) \quad (3-31)$$

$$s_{local\_Q}(t) = c(t - \hat{\tau}) \sin(2\pi t f_{IF} + \hat{\phi}(t)) \quad (3-32)$$

where

- $\hat{\tau}$  is the incoming signal group delay estimated by the receiver.
- $\hat{\phi}(t)$  is the incoming signal carrier phase delay estimated by the receiver.

The correlation operation is generally performed over one or an integer multiple of the PRN code period. The resulting correlation function  $R$  (considering only the in-phase local replica) can be expressed as:

$$R(\varepsilon_\tau, \varepsilon_\phi) = \frac{1}{T_{int}} \int_0^{T_{int}} s_{local\_I}(\hat{\tau} - t) \tilde{s}^*(t) dt$$

$$R(\varepsilon_\tau, \varepsilon_\phi) = \frac{1}{T_{int}} \int_0^{T_{int}} c(\hat{\tau} - t) \cos(2\pi f_{IF}(\hat{\tau} - t) + \hat{\phi}(t)) \tilde{s}^*(t) dt \quad (3-33)$$

where

- $T_{int}$  is the coherent integration duration in second.
- $\tilde{s}^*(t)$  is the conjugate of the signal at the output of the GNSS receiver analog section.
- $\hat{\tau}$  is the delay of the local PRN code in second.
- $\hat{\phi}(t)$  is the phase of the local carrier (that can evolve over time) in radian.
- $\varepsilon_\tau$  is the difference between the incoming signal and the local code replica delay in second.
- $\varepsilon_\phi$  is the difference between the incoming signal and the local phase replica in radian.

This processing thus takes advantage of the correlation properties of the spreading codes used by GNSS signals. GNSS spreading code families have two main properties:

- Poor cross-correlation: the correlation function between any two different PRN codes is very small whatever the delay between the two signals is.
- Strong autocorrelation: the correlation between a PRN code and a local replica of itself is maximum when they are synchronised and is very low when they are not synchronized within one chip (the autocorrelation functions of the signals of interest are provided in 3.1).

In addition, the correlation process permits to accumulate the power of the data bit over the coherent integration duration, while it averages out all the other signals that are not containing the PRN code (such as the noise or interference). The consequence is such that the correlator output of the useful signal should dominate the noise (when the local replica and the incoming signal are synchronized).

A simplified model for the in-phase correlator output affected by thermal noise (assuming a constant code and carrier Doppler during the coherent integration duration and considering that the correlation is realized within one data bit) is given by [Julien, 2006]:

$$I(\varepsilon_\tau, \varepsilon_\phi, \varepsilon_f) = ADR_{\tilde{s}}(\varepsilon_\tau) \frac{\sin(\pi \varepsilon_f T_{int})}{\pi \varepsilon_f T_{int}} \cos(\varepsilon_\phi) + n_I \quad (3-34)$$

where

- $R_{\tilde{s}}$  is the correlation function between the local replica and the received signal code (which is an element of the received signal). Note that it takes into account the effect on the incoming

signal of the propagation channel, the antenna and the RF front-end equivalent filter. The expression of filtered correlation function is given in appendix A.

- $n_I$  is the noise at the in-phase correlator output. This noise is assumed Gaussian and its power is derived in appendix A taking into account the antenna and RF front-end equivalent filter.
- $A$  is the amplitude of the received signal at the receiver input.
- $D$  is the sign of the incoming signal navigation data bit (if any) during the correlation operation.
- $\varepsilon_\tau$  is the code delay difference between the local replica and the received signal in second.
- $\varepsilon_\varphi$  is the carrier phase difference between the local replica and the received signal. It corresponds to the carrier phase difference in the middle of the correlation interval in radian.
- $\varepsilon_f$  is the Doppler difference between the local replica and the received signal in hertz.

From the previous model (equation (3-34)), it can be seen that the correlator output will dominate the noise only if  $\varepsilon_\tau$ ,  $\varepsilon_\varphi$  and  $\varepsilon_f$  are close to zero. There is thus a need to synchronize the local replica generated by the receiver with the incoming signal of interest.

All GNSS receivers also use the so-called quadrature-phase correlator outputs obtained from the correlation of the incoming signal with a local replica of the signal quadrature-phased component ( $s_{local,Q}(t)$ ). The model of the quadrature-phase component is given by:

$$Q(\varepsilon_\tau, \varepsilon_\varphi, \varepsilon_f) = ADR_s(\varepsilon_\tau) \frac{\sin(\pi \varepsilon_f T_{int})}{\pi \varepsilon_f T_{int}} \sin(\varepsilon_\varphi) + n_Q \quad (3-35)$$

Where  $n_Q$  is the noise at the quadrature-phase correlator output. This noise is assumed Gaussian and is independent from  $n_I$ . It has the same power as  $n_I$ .

#### 3.3.1.2 Correlator output model function of the code delay

$I$  and  $Q$  are dependent upon the code delay error, the carrier phase error and the Doppler error. Nevertheless in signal processing, correlator outputs are also estimated for code delay errors different from zero. Assuming that  $\varepsilon_\varphi = 0$  and  $\varepsilon_f = 0$ , the following notations will be used in the continuation.

$$I_{\varepsilon_\tau} = I(\varepsilon_\tau, 0, 0) = ADR_s(\varepsilon_\tau) + n_I \quad (3-36)$$

$$Q_{\varepsilon_\tau} = Q(\varepsilon_\tau, 0, 0) = n_Q \quad (3-37)$$

Figure 3-9 gives an illustration of the normalized code correlation function on a BPSK code sequence of seven chips. It corresponds to a simplified configuration where  $\varepsilon_\varphi = 0$  and  $\varepsilon_f = 0$ . Three cases are represented, on the top the local replica is in advance compared to the incoming signal ( $\varepsilon_\tau = -T_c/2$ ). On the middle, both signals are synchronized. On the bottom, the local replica is delayed compared to the incoming signal ( $\varepsilon_\tau = T_c/2$ ). The blue point on correlation function corresponds to the correlator output given by the convolution of the two represented signals.

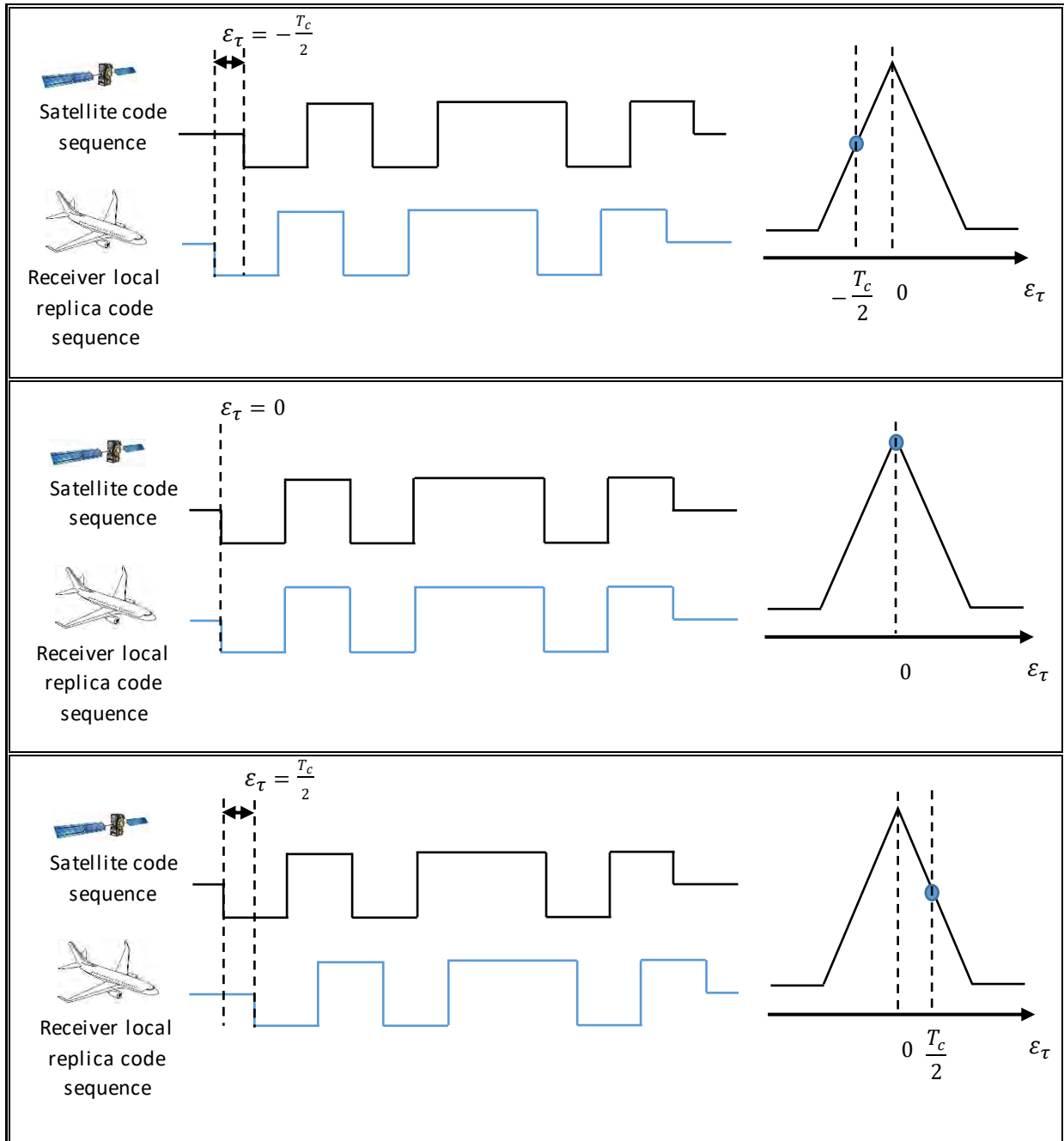


**Figure 3-9.** Illustration of the code correlation process for different code delays between the incoming signal and the local replica.

### 3.3.1.3 GNSS receiver correlation function

For GPS L1 C/A, GPS L5 and Galileo E5a signals, local replicas generated by the receiver have the same modulation as the incoming signals. By consequence, the correlation functions estimated by the GNSS receiver are defined by autocorrelation expressions presented in section 3.1. Nevertheless, in the same section, the expression of the  $CBOC(6,1,1/11,-)$  autocorrelation ( $R_{CBOC(6,1,1/11,-)}$ ) is mathematically defined while civil aviation receivers will generate a  $BOC(1,1)$  instead of a

$CBOC(6,1,1/11, -)$  local replica to simplify receiver signal generation. By consequence, civil aviation receivers will track Galileo E1C signals via a  $R_{CBOC(6,1,1/11,-)/BOC(1,1)}$  correlation function.

Even if it does not change significantly tracking performance, the difference of shape between  $R_{CBOC(6,1,1/11,-)}$  and  $R_{CBOC(6,1,1/11,-)/BOC(1,1)}$  has an influence on the impact of signal distortions on the tracking.

The correlation function of a  $BOC(1,1)$  and a  $CBOC(6,1,1/11, -)$ -modulated signals can be modeled as:

$$R_{CBOC(6,1,1/11,-)/BOC(1,1)}(\tau) = \left( \left( \sqrt{\frac{10}{11}} SC_{BOC(1,1)} - \sqrt{\frac{1}{11}} SC_{BOC(6,1)} \right) * (SC_{BOC(1,1)})^* \right)(\tau)$$

$$R_{CBOC(6,1,1/11,-)/BOC(1,1)}(\tau) = \sqrt{\frac{10}{11}} R_{BOC(1,1)}(\tau) - \sqrt{\frac{1}{11}} R_{BOC(1,1)/BOC(6,1)}(\tau) \quad (3-38)$$

The expressions of  $R_{CBOC(6,1,1/11,-)/BOC(1,1)}$  and  $R_{BOC(1,1)}$  are given in section 3.1.5.

The difference between the  $CBOC(6,1,1/11, -)$  autocorrelation function in blue and the  $CBOC(6,1,1/11, -)/BOC(1,1)$  correlation function in red is illustrated on Figure 3-10.

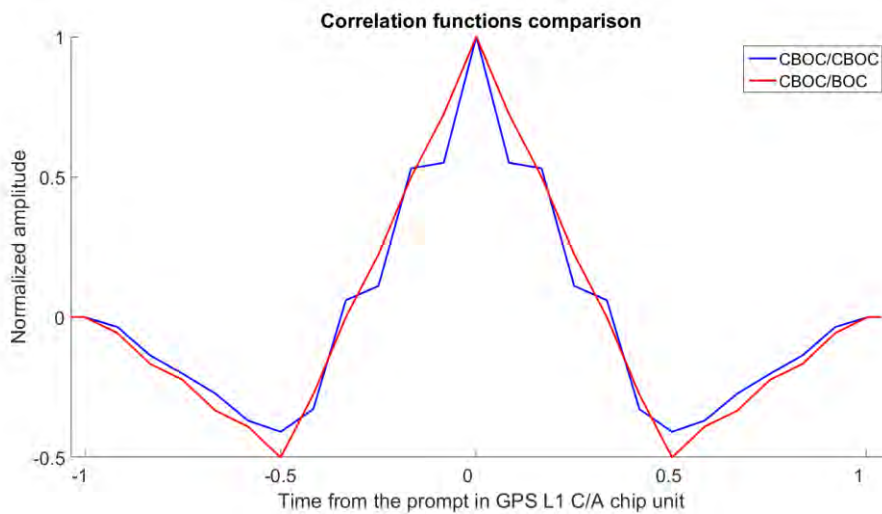


**Figure 3-10.** Correlation functions between a  $CBOC(6,1,1/11)$ -modulated signal and a  $CBOC(6,1,1/11)$ -modulated signal (blue) or a  $BOC(1,1)$ -modulated signal (red).

#### 3.3.1.4 Filtered correlation functions

When the incoming signal goes through the analog section of the receiver, its characteristics are modified as defined in section 3.2. In particular, the equivalent filter of the antenna and the RF front-end induces distortions on the signal before the correlation function process. The consequence is that correlation functions are also distorted depending on the pre-correlation function characteristics.

Figure 3-11 gives an example of correlation function shapes after applying a 6<sup>th</sup>-order Butterworth pre-correlation filter of 24 MHz (in red) and 12 MHz (in blue) double-sided. Correlation functions are delayed because of the filtering effect and the delay is higher when the filter bandwidth is lower.

Nevertheless, in Figure 3-11, the delay is not represented to underline difference that appears on the shape of the correlation function because of the filter.

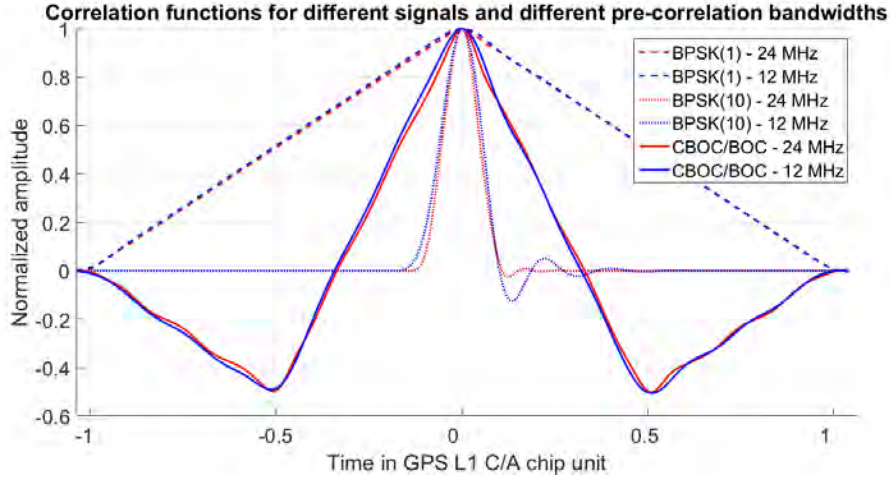


**Figure 3-11.** Correlation functions for different pre-correlation filters.

#### 3.3.1.5 Correlation function and filtering properties

Taking back notations introduced earlier in the document:

- $s(t)$  is the nominal signal at the antenna output and at the input of the RF front-end.
- $s_{local}(t)$  is the local replica.

Considering that a distortion affects the signal, new notations are introduced:

- $s_d(t) = s(t) + d(t)$  is the distorted signal at the antenna output and equivalently at the input of the RF front-end.
- $d(t)$  is the distortion affecting the temporal signal, represented as an additive component.

Due to the linearity property of the convolution product, the filtered distorted signal  $\tilde{s}_d(t)$  can be rewritten as:

$$\tilde{s}_d(t) = (h_{RF} * s_d^*)(t) = (h_{RF} * (s^* + d^*))(t) = \tilde{s}(t) + \tilde{d}(t) \quad (3-39)$$

where

- $\tilde{d}(t) = (h_{RF} * d^*)(t)$  is the signal distortion affecting the temporal signal filtered by the RF front-end.
- $\tilde{s}(t) = (h_{RF} * s^*)(t)$  is the nominal signal filtered by the RF front-end.
- $h_{RF}(t)$  is the RF front-end filter impulse response.

The linearity property of the convolution product entails that the correlation function of  $\tilde{s}_d(t)$  with the local replica is equal to:

$$R_{\tilde{s}_d}(\tau) = R_{\tilde{s}}(\tau) + R_{\tilde{d}}(\tau) \quad (3-40)$$

where

- $R_{\tilde{s}}(\tau) = (\tilde{s} * s_{local}^*)(\tau)$  is the correlation function between the filtered nominal signal and the local replica.

### 3. GNSS signals structure and receiver processing

- $R_{\tilde{d}}(\tau) = (\tilde{d} * s_{local}^*)(\tau)$  is the correlation function between the filtered distortion and the local replica.

It is noticeable that the associative property of the convolution product leads to:

$$\begin{aligned} R_{\tilde{s}}(\tau) &= (\tilde{s} * s_{local}^*)(\tau) = ((h_{RF} * s) * s_{local}^*)(\tau) = (h_{RF} * (s * s_{local}^*))(\tau) \\ &= (h_{RF} * R_s)(\tau) = \widetilde{R_s}(\tau) \end{aligned} \quad (3-41)$$

Where  $R_s(\tau) = (s * s_{local}^*)(\tau)$  is the correlation function between the unfiltered nominal signal and the local replica.

The three conclusions of these mathematical expressions are that:

- It is equivalent to apply a filter on a distorted signal or to apply the filter on the ideal signal and the distortion separately. (Equation (3-39))
- It is equivalent to apply a filter on a distorted correlation function or to apply the filter on the ideal correlation function and the distortion convolved with the local replica separately. (Equation (3-40))
- It is equivalent to apply a filter on the incoming signal or to apply it on the correlation function. (Equation (3-41))

#### 3.3.2 Acquisition

The acquisition consists in determining if a given GNSS signal is visible and can be processed by the receiver. The only way to do so is to try to see if a local replica of this signal can correlate appropriately with it. Based on the analysis of the correlator outputs, if such a correlation occurs, it should also provide the receiver with a rough estimation of the GNSS signal delay and Doppler.

The typical acquisition detector does not need a local replica synchronized in phase:

$$T = \sum_{k=0}^K (I^2(k) + Q^2(k)) \quad (3-42)$$

where  $K$  referred to as the number of non-coherent summations.

The acquisition stage is thus accomplished sequentially by testing all possible combinations of code, delay and Doppler that the incoming signal of interest can take. This is thus equivalent to use discrete bins on a grid of code delays and Doppler frequencies, all these bins representing a 2-D grid. For each bin of the so-called acquisition grid, a correlation is performed between the incoming signal and a local replica with a delay and a Doppler frequency corresponding to that bin. During acquisition, if the receiver does not have the knowledge about satellites in view, and by consequence does not know incoming signal code waveform, all possible PRN codes are tested.

The typical size for a bin is a fraction (one half) of a chip (to have a bin hitting a high part of the PRN code correlation function peak) on the code delay axis and about  $(2/3)T_{int}$  on the Doppler frequency axis [Kaplan and Hegarty, 2006].



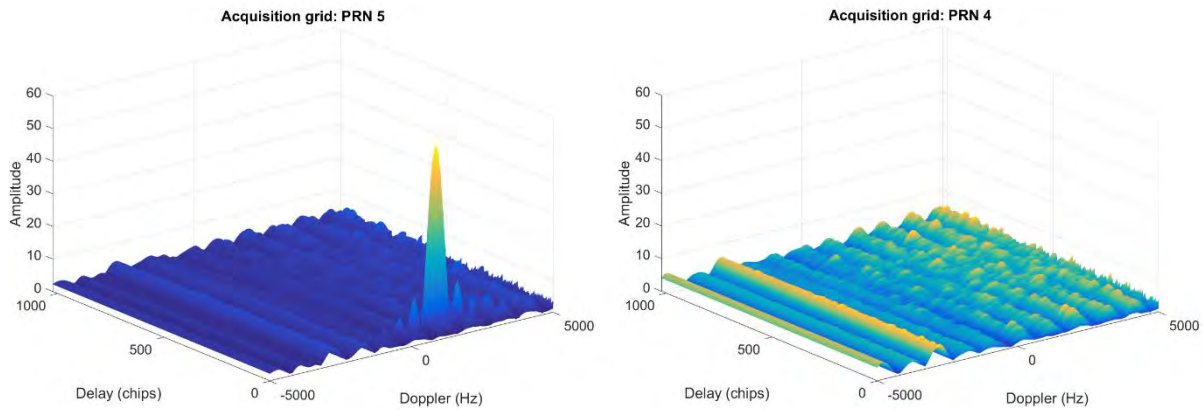


**Figure 3-12.** Example of GPS L1 C/A acquisition grids. On the left, a signal is acquired, whereas on the right no signal is found by the receiver.

Figure 3-12 gives an example of two acquisition grids for a GPS L1 C/A signal. On the left, the acquisition is successful. The estimated Doppler frequency is equal to 1500 Hz and the estimated code delay is equal to 185 chips.

It is noticeable that the code delay swept 1023 chips and 10 000 Hz of Doppler frequencies. Considering a code delay resolution of half a chip and a Doppler frequency resolution equal to 100 Hz, the number of correlations to perform for each PRN is equal to  $2046 \times 10000/100 = 204\,600$ . Acquisition is generally a relatively long and cumbersome process.

Different algorithms exist to find out the Doppler frequency and the code delay and run through the correlation grid more rapidly as described in [Kaplan and Hegarty, 2006]. Nevertheless no such technique is used in the context of this study.

### 3.3.3 Tracking

After being acquired, GNSS signals are tracked by the receiver. Tracking means that the receiver attempts to generate a local replica that follows the parameters of the incoming signal. During this phase, the code delay and the carrier phase of the incoming signal are estimated more precisely than at the output of the acquisition phase, generally using feedback loops known as Phase Lock Loop (PLL) for carrier phase tracking and Delay Lock Loop (DLL) for code delay tracking.

Also, the process of tracking is much less demanding in processing power than that of the acquisition. Both code delay and carrier phase parameters are evaluated continuously until a loss of tracking. Like the acquisition, tracking is based on the correlation process but the two approaches are different.

To understand a feedback loop, three important principles have to be introduced:

- **Discriminator functions:** discriminators use the correlator outputs to provide measurable values of code delay and carrier phase tracking errors. Different discriminators with different characteristics can be used to track the code delay and the carrier phase.
- **Numerical Controlled Oscillator (NCO):** it converts the filtered discriminator output into a frequency that drives the generation of the local replica. One NCO is used to generate the PRN code and another one to generate the carrier.

- **Loop filters:** the discriminator outputs are filtered to reduce the noise at the input of the NCO. Note that the level of filtering influences the reaction time of the loop. Note also that the filter order influences the ability of the loop to react to parameters dynamic.

In the following, delay lock loop and phase lock loop are presented separately. In GNSS receiver, both tracking loops are used jointly. Note that instead of tracking the carrier phase of the incoming signal, it is possible to track its carrier frequency using a Frequency Lock Loop (FLL). FLL concepts are not detailed but information can be found for example in [Navipedia, 2015] or [Kaplan and Hegarty, 2006].

In this section, the second order loop filter that was adopted to process some GNSS signals is described to show mathematically the impact of different tracking parameters on the NCO input.

#### 3.3.3.1 Delay lock loop (DLL)

In this part, the DLL concept is exposed. Then, performance of the DLL is assessed and parameters with an influence on this performance are listed. DLL concept and performance are of interest because it conditions GNSS receiver performance.

##### 3.3.3.1.1 DLL concept

A DLL is a feedback loop aiming to keep the code-phase of the local replica aligned with the incoming signal. The general structure of a DLL is shown in Figure 3-13.

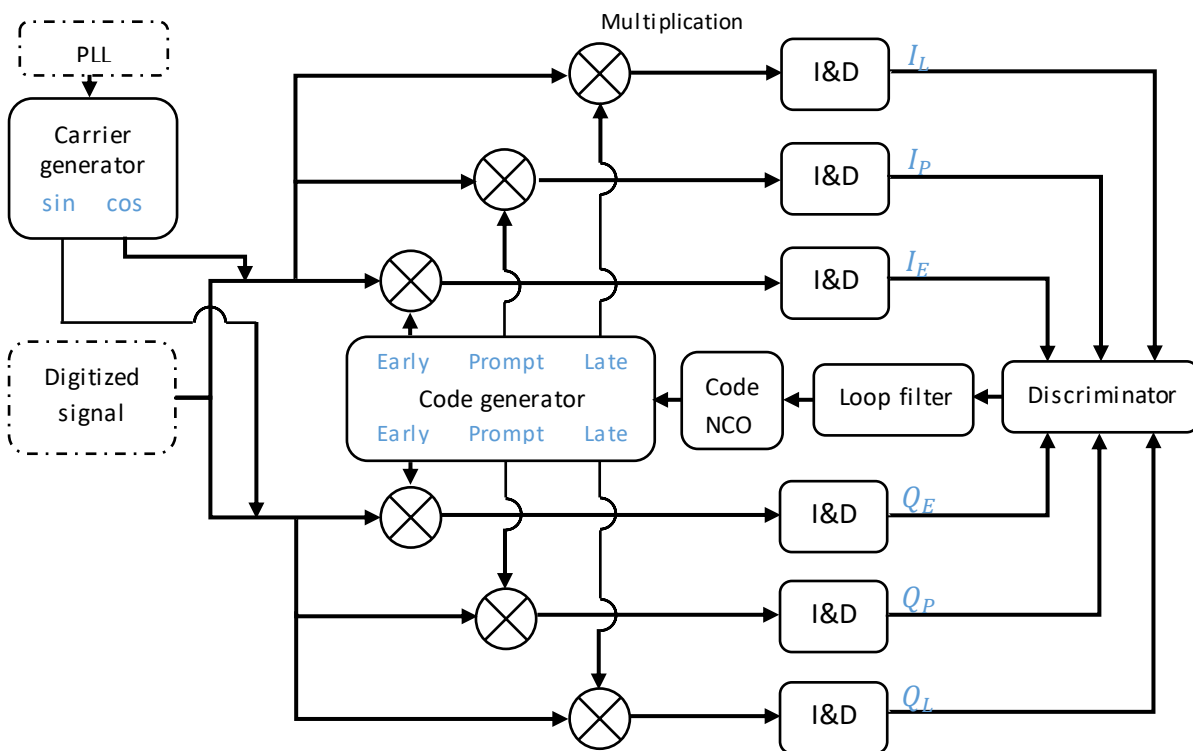


**Figure 3-13.** General structure of a DLL. Dashed block is outside the DLL.

It is important to notice that several correlator outputs are fed into the discriminator. In general, three PRN code local replicas are used by the receiver (considering one signal component): an early, a prompt, and a late replica. In ideal tracking conditions, the prompt PRN code replica is synchronized with the PRN code of the incoming signal, the early PRN code replica has an advance, noted  $C_s/2$ ,

compared to the PRN code of the incoming signal and the late PRN code replica is delayed by  $C_s/2$  compared to the PRN code of the incoming signal.  $C_s$  is known as the correlator spacing, or Early-Late spacing, and corresponds to the time delay between the two early and late PRN code local replicas used for the tracking. The mathematical definitions of replicas delivered by the code generator are function of the estimated code delay  $\hat{\tau}$  and are defined as:

- $c\left(t - \hat{\tau} + \frac{C_s}{2}\right)$  for the late replica,
- $c(t - \hat{\tau})$  for the prompt replica,
- $c\left(t - \hat{\tau} - \frac{C_s}{2}\right)$  for the early replica.

The most common discriminators are the non-coherent Early Minus Late Power (EMLP) discriminator and the quasi-coherent Dot Product (DP). The two discriminators are not considered as coherent because they are insensitive to carrier phase error, which is interesting for a tracking robustness point of view. These two discriminators are defined by:

$$D_{EMLP} = (I_E^2 + Q_E^2) - (I_L^2 + Q_L^2) \quad (3-43)$$

$$D_{DP} = (I_E - I_L)I_P + (Q_E - Q_L)Q_P \quad (3-44)$$

where

- $I_E = I_{\frac{C_s}{2}}$  ( $Q_E = Q_{\frac{C_s}{2}}$ ) is the early correlator output of the in-phase (quadrature-phase) component.
- $I_L = I_{\frac{C_s}{2}}$  ( $Q_L = Q_{\frac{C_s}{2}}$ ) is the late correlator output of the in-phase (quadrature-phase) component.
- $I_P = I_0$  ( $Q_P = Q_0$ ) is the prompt correlator output of the in-phase (quadrature-phase) component.

A DLL aims at achieving a zero code delay tracking error. The goal of the discriminator is thus to provide an unbiased estimation of the actual code delay error so that the loop can react accordingly (to do so, the aforementioned discriminators need to be normalized). In ideal condition, perfect synchronization is achieved when the Early and Late correlator outputs are levelled. Some discriminator outputs are shown in Figure 3-14 for GPS L1 C/A as a function of the code delay tracking error at the input of the discriminator. In the example given in Figure 3-14, the discriminator functions are estimated from a normalized unfiltered ideal correlation function and the correlator spacing is equal to  $C_s = 0.2$  chip. These plots are also called S-curves.

The S-curve represents the discriminator output. As a consequence, a zero-crossing of the S-curve represents a point at which the tracking loop can be locked. It is noticeable on Figure 3-14 that only a stable S-curve zero-crossing can be locked: it corresponds to a S-curve zero-crossing surrounded by a negative value on the left and a positive value on the right. On these plots, it is assumed that the carrier phase tracking error is equal to zero. As a consequence, all terms on the quadrature component are equal to zero (no distortion on the in-phase and/or the quadrature-phase signal components).

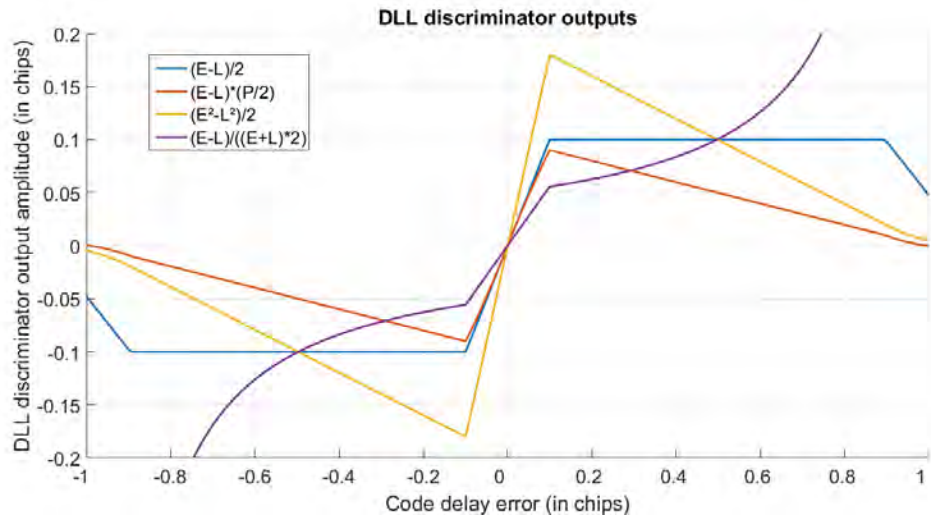


**Figure 3-14.** Examples of S-curves for an unfiltered GPS L1 C/A signal and different DLL discriminators,  $CS = 0.2$  chip. In blue is the early minus late discriminator, in orange the DP discriminator, in yellow the EMLP and in purple the early minus late normalized by the early plus late.

The important part of the DLL discriminator outputs is the linear part around the code delay error equal to zero. Indeed, if a code delay error is affecting the DLL in the discriminator linear section range, a NCO command proportional to the error will be generated by the discriminator output, and the error will be corrected in the next loop iteration.

The choice of the discriminator has an impact on the S-curve shape and on performance of the DLL that is described in the next part.

#### 3.3.3.1.2 DLL performance

Classical DLL performance is dependent upon three errors:

- the thermal noise,
- multipath and
- the dynamic stress error.

In this section, only the main source of carrier tracking error is treated: the thermal noise. It is assumed that no signal distortion and multipath affect the incoming signal. Details about other sources of errors can be found as example in [Julien, 2006]. Using a non-coherent EMLP discriminator, assuming a perfect normalization, no frequency uncertainty in the carrier wipe-off, a RF front-end filter with unity gain within  $\pm B_{fe}/2$  Hz and null elsewhere and a code delay error remaining small, the standard deviation of the DLL tracking error due to noise is given in meter by [Betz and Kolodziejski, 2000]:

$$\sigma_{EMLP} = \sqrt{\frac{B_{DLL} \int_{-B_{fe}/2}^{+B_{fe}/2} S(f) \sin^2(\pi f C_s T_c) df}{(2\pi)^2 C' / N_0 \left( \int_{-B_{fe}/2}^{+B_{fe}/2} S(f) \sin(\pi f C_s T_c) df \right)^2}} \times \sqrt{\left[ 1 + \frac{\int_{-B_{fe}/2}^{+B_{fe}/2} S(f) \sin^2(\pi f C_s T_c) df}{T_{int} C' / N_0 \left( \int_{-B_{fe}/2}^{+B_{fe}/2} S(f) \cos(\pi f C_s T_c) df \right)^2} \right]} \quad (3-45)$$

In the same way and in same conditions, the DLL tracking error standard deviation can be estimated for a DP discriminator and is equal to [Julien, 2006]:

$$\sigma_{DP} = \sqrt{\frac{B_{DLL} \int_{-B_{fe}/2}^{+B_{fe}/2} S(f) \sin^2(\pi f D T_c) df}{(2\pi)^2 C' / N_0 \left( \int_{-B_{fe}/2}^{+B_{fe}/2} f S(f) \sin(\pi f C_s T_c) df \right)^2}} \times \sqrt{\left[ 1 + \frac{1}{T_{int} C' / N_0 \left( \int_{-B_{fe}/2}^{+B_{fe}/2} S(f) df \right)^2} \right]} \quad (3-46)$$

where

- $T_c$  is the chips period in second.
- $T_{int}$  is the coherent integration time in second.
- $S$  is the power spectral density of the signal at the receiver antenna (which depends upon the modulation type), normalized to unit area over infinite bandwidth.
- $C' / N_0$  is the carrier to noise ratio in hertz.
- $B_{fe}$  is the double-sided front-end bandwidth in hertz.
- $C_s$  is the early to late correlator spacing in chip.
- $B_{DLL}$  is the code loop noise bandwidth in hertz.

It is important to notice that DLL performance is dependent upon several receiver parameters that are:

- The order of the DLL. It has an impact on the dynamic stress error. The higher the order of the loop is and the more robust the loop will be face to dynamic error. In the case of GNSS receivers, first order DLLs are generally used because the dynamic error is absorbed by the more accurate PLL and one objective of the DLL is to remove the noise on measurements.
- The coherent integration time  $T_{int}$ . To reduce the noise of the DLL, high coherent integration time can be used. In practice, on data components, because of data bit transitions, the coherent integration time is generally limited (for instance 20 ms to track GPS L1 C/A signal). On pilot components, the integration time can be increased. Nevertheless, a long coherent integration time implies that tracked parameters have a low update rate and signal conditions may vary during that period.
- The loop bandwidth  $B_{DLL}$ . To reduce the noise of the DLL, narrow bandwidth are implemented on DLL loop filters [Julien, 2006].

### 3. GNSS signals structure and receiver processing

- The RF front-end bandwidth  $B_{fe}$ . In general the wider the RF front-end filter bandwidth is, the smaller the code tracking error will be [Julien, 2006].
- The DLL discriminator including the correlator spacing  $C_s$ . In general the smaller the correlator spacing is, the smaller the code tracking error is [Julien, 2006].

As an example, Figure 3-15 gives the standard deviation of the total DLL error considering an Early Minus Late (EML) discriminator and a BPSK correlation function ([Kaplan and Hegarty, 2006]). The coherent integration time is set to 20 ms, the code loop noise bandwidth is equal to 0.2 Hz, the normalized one-sided RF front-end bandwidth is set to 17 times the chip frequency and a third order DLL is considered.

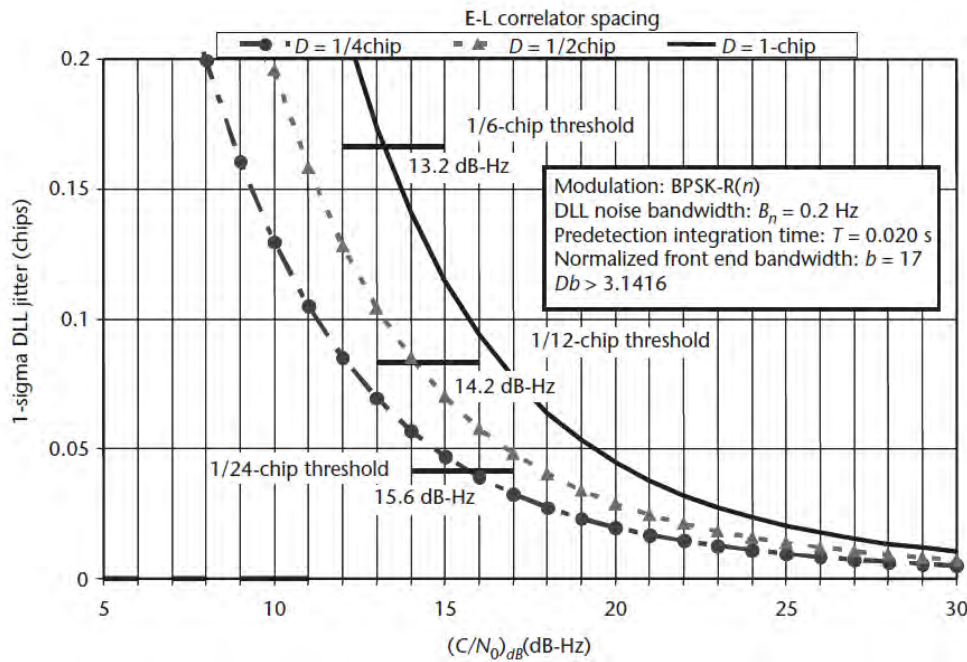


**Figure 3-15.** Example of PLL standard deviations due to all sources of errors function of the  $C/N_0$  [Kaplan and Hegarty, 2006].

#### 3.3.3.2 Phase lock loop (PLL)

In this part, the PLL concept is exposed. Then, performance of the PLL is assessed and parameters with an influence on this performance are listed. PLL concept and performance are of interest because it conditions GNSS receiver performance.

##### 3.3.3.2.1 PLL concept

The PLL is designed to keep the carrier phase of the local replica aligned with the incoming signal. The general structure of a PLL is provided in Figure 3-16.

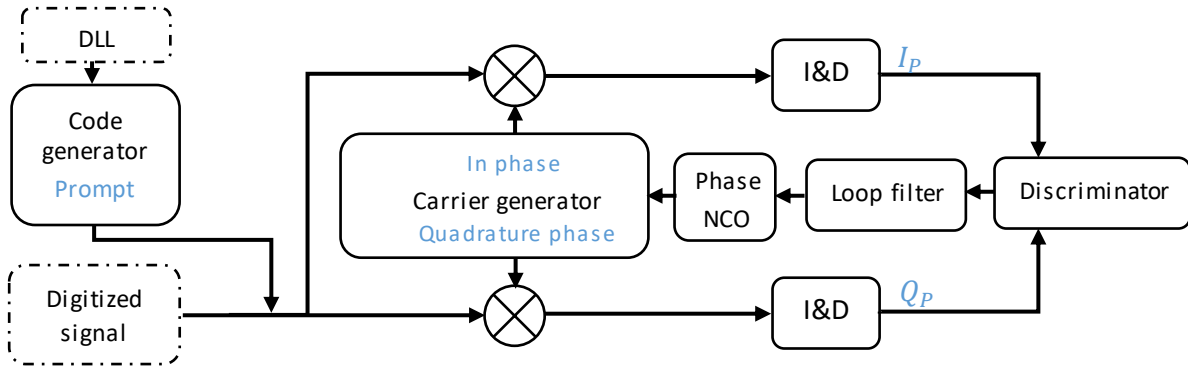


**Figure 3-16.** General structure of a PLL. Dashed block is outside the PLL.

The concept is the same as the DLL but only two local replicas (and correlator outputs) are used. The two replicas are defined mathematically by:

- $\sin(2\pi f_{IF}t - \hat{\phi})$  for the in-phase local replica,
- $\cos(2\pi f_{IF}t - \hat{\phi})$  for the quadrature-phase local replica,

where  $\hat{\phi}$  is the local carrier phase driven by the NCO.

The atan discriminator is commonly used and is defined as:

$$\text{Atan}\left(\frac{Q_P}{I_P}\right) = \varepsilon_\phi \quad (3-47)$$

The PLL aims at achieving a zero carrier phase error. PLL S-curves have several stable zero-crossings separated by  $180^\circ$ . This phenomenon is at the origin of the ambiguity in the carrier phase measurement: it is difficult to know which stable lock point is used by the loop. The atan discriminator S-curve is presented Figure 3-17.

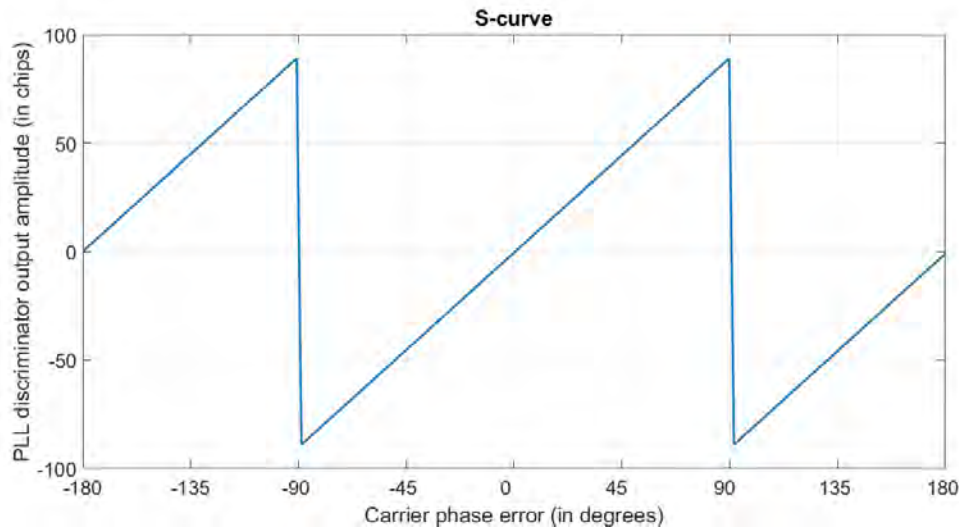


**Figure 3-17.** S-curve of the atan PLL discriminator.

### 3.3.3.2.2 PLL performance

Classical PLL performance is dependent upon four errors:

- the thermal noise,
- the oscillator frequency noise, also called the Allan deviation,

### 3. GNSS signals structure and receiver processing

- the oscillator vibration and
- the dynamic stress error.

In this section, only the main source of carrier tracking error is treated : the thermal noise. Details about other sources of errors can be found as example in [Julien, 2006].

PLL errors are also characterized by standard deviations. Assuming that the RF front-end filter is modeled by a filter with a unity gain within  $\pm B_{fe}/2$  Hz and null elsewhere, the standard deviation of the carrier tracking error due to the thermal noise for an atan PLL discriminators is given in degree by [Kaplan and Hegarty, 2006]:

$$\sigma_{n\_PLL} = \frac{360}{2\pi} \sqrt{\frac{B_{PLL}}{C'/N_0 \left( \int_{-B_{fe}/2}^{+B_{fe}/2} S(f) cdf \right)}} \left( 1 + \frac{1}{2T_{int} C'/N_0 \left( \int_{-B_{fe}/2}^{+B_{fe}/2} S(f) cdf \right)} \right) \quad (3-48)$$

where

- $C'/N_0$  is the carrier to noise ratio in hertz.
- $T_{int}$  is the coherent integration time in second.
- $S$  is the power spectral density of the signal at the receiver antenna (which depends on the modulation type), normalized to unit area over infinite bandwidth.
- $B_{PLL}$  is the code loop noise bandwidth in hertz.

It is important to notice that PLL performance is dependent upon several receiver parameters that are:

- The NCO sensitivity to vibration for some frequencies which has an impact on the oscillator vibration error.
- The NCO frequency stability (drift) regarding the noise which affects the measurement (Allan deviation). It has an impact on the oscillator frequency noise.
- The order of the PLL. It has an impact on the dynamic stress error. A second order PLL is sensitive to acceleration and a third order to the jerk. In the case of GNSS receivers, third order PLLs are generally used to account for any kind of signal dynamics.
- The integration time  $T_{int}$ . A high integration time decreases the standard deviation of the PLL thermal noise but can lead to a loss of lock if the signal dynamic is high.
- The loop bandwidth  $B_{PLL}$ . A narrow loop bandwidth decreases the standard deviation of the PLL thermal noise but can lead to loss of lock if the signal dynamic is high [Julien, 2006].
- The PLL discriminator.

As an example, Figure 3-18 gives the standard deviation of the total PLL error considering an atan discriminator ([Kaplan and Hegarty, 2006]). The integration time is set to 20 ms, the Allan deviation to  $1 \times 10^{-11}$ , the vibration sensitivity to  $1 \times 10^{-9}$  and the vibration is equal to  $0.005 \text{ g}^2/\text{Hz}$  between 20 Hz and 2000 Hz.



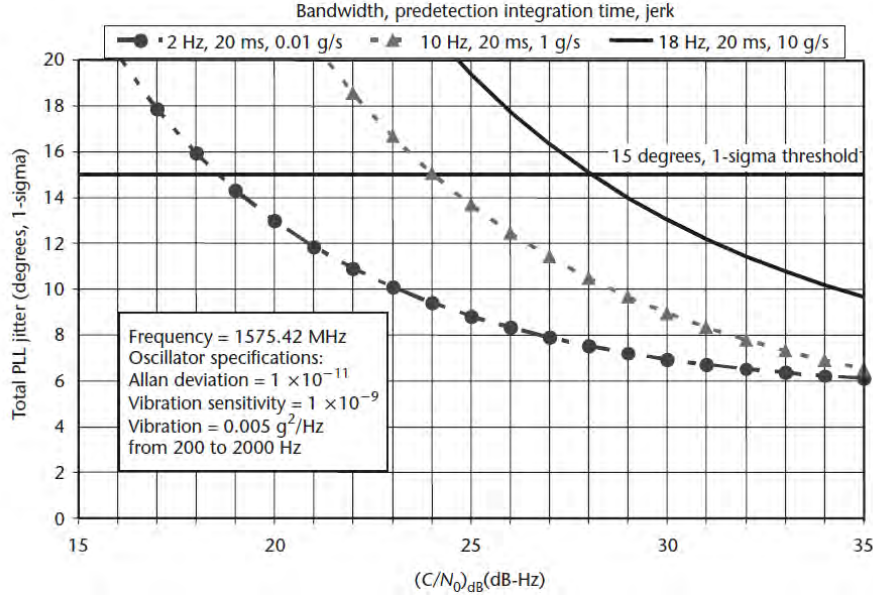


**Figure 3-18.** Example of PLL standard deviations due to all sources of errors function of the  $C/N_0$  [Kaplan and Hegarty, 2006].

### 3.3.3.3 Filtered discriminator output

It was seen that in traditional receivers, the PLL loop filter order is set to three and the DLL loop filter to one. In this part, the definition of the discriminator at the output of a second order tracking loop is mathematically defined. The second order case is treated because used in the continuation but the other cases can be found in [Kaplan and Hegarty, 2006]. The mathematical definition permits to underline the influence of the loop filter bandwidth and the integration time on the tracking.

The  $n^{th}$  filtered discriminator output is given by [Kaplan and Hegarty, 2006]:

$$\tilde{D}_X^n = (coeff_{1\_X} + T_{int} \times coeff_{2\_X}) D_X^n + (T_{int} \times coeff_{2\_X}) D_X^{n-1} \quad (3-49)$$

with

$$coeff_{1\_X} = \omega_{0\_X}^2$$

$$coeff_{2\_X} = 1.414 \times \omega_{0\_X}$$

$$\omega_{0\_X} = \frac{B_X}{0.53}$$

where

- $X = DLL$  or  $X = PLL$  makes reference to the DLL or the PLL.
- $T_{int}$  is the coherent integration time in second and corresponds also to the time between the estimation of two consecutive discriminator outputs.
- $\omega_0$  is the filter frequency in radian.
- $D_X^n$  is the  $n^{th}$  tracking loop discriminator output.
- $\tilde{D}_X^n$  is the  $n^{th}$  filtered tracking loop discriminator output.
- $B_X$  is the bandwidth of the tracking loop filter in hertz.

## 3.4 Conclusions

In this chapter, the signal processing part of a typical GNSS receiver has been presented. This chapter starts by a diagram which proposes a general overview of a GNSS receiver. A division in three steps was envisaged: the signal of interest which feeds the receiver, the analog section of the receiver and the digital section of the receiver.

The signal modulation has consequences on the signal characteristic and on the correlation function shape. The PVT computation is derived from pseudorange measurements estimated from the correlation function. It entails that the modulation has an impact on the receiver processing and the PVT estimation. This is the reason why signals of interest for this study are presented in 3.1. These are GNSS signals that are or will be used by civil aviation receivers for positioning and navigation. Four signal structures are described: GPS L1 C/A, GPS L5, Galileo E5a and Galileo E1C. For each signal, modulation, PSD and correlation function are defined.

In addition to the signal structure, the analog section of the GNSS receiver has an influence on the correlation function, the pseudorange measurement and the PVT estimation in that sense that it pre-conditions the signal before its processing in the digital section. The analog section is introduced in 3.2 and the three main components are briefly presented: the antenna, the RF front-end and the ADC.

Finally, in 3.3 the digital section is described. The correlation process is introduced in 3.3.1 before the presentation of acquisition (3.3.2) and tracking phases (3.3.3). A particular care is taken to define DLL and PLL principles because tracking loops are of primary importance for the study of GNSS signal distortions. Indeed, signal distortions impact straightforwardly the shape of the signal and by consequences receiver processing and pseudorange measurements. The derivation of the position (navigation processing) from pseudorange measurements is not detailed in this document because the impact of GNSS signal distortions is traditionally looked at the pseudorange level and not at the position level.

In the next chapter, the influence of GNSS signal distortions on the receiver processing is tackled.

## 4 Impact of GNSS signal distortions on signal processing

In the previous chapter, principles of GNSS receiver processing were detailed. In this chapter, the consequences of GNSS Signal-in-Space (SiS) distortions on the signals of interest and on the receiver processing presented in chapter 3 are investigated.

In section 4.1, the two types of distortions that can be generated by the payload and that can affect a GNSS signal are defined. Firstly, nominal distortions that are present on signals in fault-free conditions (healthy satellite) are introduced. Secondly non-nominal distortions are investigated. It corresponds to signal distortions induced by a payload failure. Both distortion types are defined based on observations made in former studies.

To illustrate concepts developed in this chapter, and before introducing the general distortion models that will be the core of the chapter 6, one example of representative distortion is introduced in section 4.2.

In section 4.3, the relation between signal distortions and the antenna/RF front-end equivalent filter is exposed. The impact of these distortions on tracking loops (PLL and DLL) is then investigated. It is seen that depending on the receiver configurations (antenna, RF front-end equivalent filter and tracking technique) the impact of a given signal distortion on the pseudorange measurement can be different. Parameters with an influence on the pseudorange measurement bias are highlighted with a primary interest to DGNSS applications.

In section 4.5, two techniques which permit to observe GNSS signal distortions are described. The first method consists of looking at the signal in the temporal domain and is called in this manuscript the Chip Domain Observable (CDO) whereas the second method consists of looking at the correlation function between the incoming signal and the local replica.

A conclusion ends the chapter in section 4.6.

### 4.1 Category of GNSS signal distortions

SiS signal distortions are, by definition, generated at satellite level because visible to all users and are divided into two categories:

- nominal distortions which affect the signal in fault-free condition and
- non-nominal distortions or Evil WaveForm (EWF) which affect a signal in satellite failure condition.

In this section, nominal distortions are introduced based on previous studies (4.1.1). Then, the impact of the first and largest observed non-nominal distortion is described in details (4.1.2). An overview of GPS signal distortions reported in the past is also given. The part ends on speculations about the origin of nominal and non-nominal distortions (4.1.3).

### 4.1.1 Nominal distortions

Even in fault-free condition (also called nominal case), signals transmitted by GNSS satellites are affected by small distortions. These distortions are generated by the nominal payload, coming from the signal generation unit and the antenna. They generally appear as distortions of the PRN chips. Previous works put forward characteristics of these distortions:

- oscillations after each chip transitions (analog distortion) and
- delay (lead or lag) between rising and falling edges of PRN chips (digital distortion).

This phenomenon impacts the receiver processing and can introduce unwanted errors at different levels of the signal processing. This kind of problem was already tackled by different laboratories: Stanford ([Phelts et al., 2009], [Wong et al., 2010], [Wong et al., 2011], etc.), Air Force Institute of Technology and Ohio University ([Gunawardena and van Graas, 2012a], [Gunawardena and van Graas, 2013], [Gunawardena, 2015], etc.), DLR ([Thoelert et al., 2014], etc.) and CNES ([Lestarquit et al., 2012]). This section introduces some results already obtained about nominal distortions in order to show consequences of such distortions on GNSS receiver.

#### 4.1.1.1 Objective of studies on GNSS signal nominal distortions

The two main objectives of nominal distortions studies are:

- Increase GNSS performance (in terms of integrity and continuity). The detection of threatening distortions requires a detailed understanding of satellites performance when satellites are operating in nominal conditions. Indeed, the detection of distortion is based on a comparison between the nominal and the current signal behavior. An accurate definition of the nominal case improves the probability allocation for faulty modes. The impact of nominal distortions are traditionally looked at the correlation function level or/and pseudorange level. A precise understanding of nominal distortions is also a first step in the mitigation of these distortions and the increase of GNSS performance as discussed in [Wong, 2014].
- Quantify their impact on GNSS users. The impact of nominal distortions is dependent upon the receiver as it will be seen in this chapter. Most of the time, the impact of nominal distortions is assessed on the pseudorange measurement.

As the causes of these small perturbations find their origin on the disturbance of the temporal signal, the chip domain observation was used in previous studies. The aim was to characterize nominal distortions generated by the payload at chip level. From this characterization and with a precise knowledge of receiver processing, the two main objectives defined above can be reached, it means that nominal distortions (including the effect of the antenna and the RF front-end) that affect final pseudorange measurements can be assessed.

The characterization of nominal distortions that affect the pseudorange measurements can be difficult as it depends upon many parameters: the receiver configuration has an impact on the resulting tracking error, the satellite type (for instance satellites from different GPS blocks, potentially using different technologies) can create different magnitudes of error. The modeling of the distortion can be complex although simple models based on a limited number of parameters are generally used [Phelts et al., 2009], etc.

## 4.1.1.2 Different techniques to isolate nominal distortions

Two ways to estimate nominal distortions consists in 1) observing them directly at the signal level or 2) visualizing their effect at different stages of the receiver processing (correlation function, S-curve, pseudorange, etc.). However, specific equipment and/or processing are required to observe these distortions: high-gain antennas [Wong et al., 2010], [Thoelert et al., 2014], [Lestarquit et al., 2012] multicorrelator receivers [Phelts, 2001], long integration time [Lestarquit et al., 2012], etc. To isolate nominal signal distortions generated by the payload (and that entail the so-called natural biases) from distortions caused by the receiver, the 3 dB bandwidth of pre-correlation equivalent filters has to be chosen large enough (typically larger than 50 MHz) and the reception channel has to be calibrated.

High-gain parabolic dish measurements are traditionally used for the study of nominal distortions because of their high gain and their robustness against noise, interference and multipath. This type of antenna can only observe one satellite at a time. It was shown in [Wong, 2014] that without any calibration, *short term and long term errors in this measurements process cannot be distinguished from the satellite signal distortion range biases*. The problem is that the calibration of such antenna is a difficult task as exposed in [Thoelert et al., 2009].

On the other side, omnidirectional antennas are able to collect and process several signals simultaneously and can be calibrated easily. But measurements are more affected by multipath and the  $C/N_0$  of signals at the output of the antenna are lower than  $C/N_0$  of measurements collected from a high-gain dish antenna. The latter drawback is that signals collected with omnidirectional antennas are generally filtered by RF front-ends with 3 dB bandwidth lower than 25 MHz. In this condition, the RF front-end has a strong influence on observed distortions. Such measurements were processed for instance in [Liu et al., 2006].

Results obtained from measurements collected with the two types of antennas are provided for instance in [Wong, 2014]. In this manuscript, high-gain dish and omnidirectional measurements are studied but no hybrid algorithm using both measurements together is envisaged.

## 4.1.1.3 Nominal distortions on the signal

Nominal distortions are generally classified into analog (ringing phenomenon) and digital (delay between rising and falling transitions zero-crossings) distortions. To characterize these two types of nominal distortions a way is to estimate distortions parameters that are able to represent these distortions. Analog parameters are difficult to estimate because no model is perfectly representing the observed ringing effects whereas the digital distortion characterization is easier to asses with only one parameter.

## 4.1.1.3.1 Digital distortion

Digital distortions are characterized by the parameter  $\Delta$ .

This parameter corresponds to the difference existing in the zero-crossing between rising and falling transitions. Figure 4-1 is a zoom on transitions for the GPS satellite 34 (Block II-A, PRN 4) obtained with real data from the chip domain, it means observing directly the signal. The processing technique to obtain such observable is presented in 4.5.2. It is noticeable that the two curves (falling transitions in blue and rising transitions in red) are not crossing the zero value at the same time. Indeed, a lag of approximately 1.5 ns exists on the falling edge zero-crossing compared to the rising one.

#### 4. Impact of GNSS signal distortions on signal processing

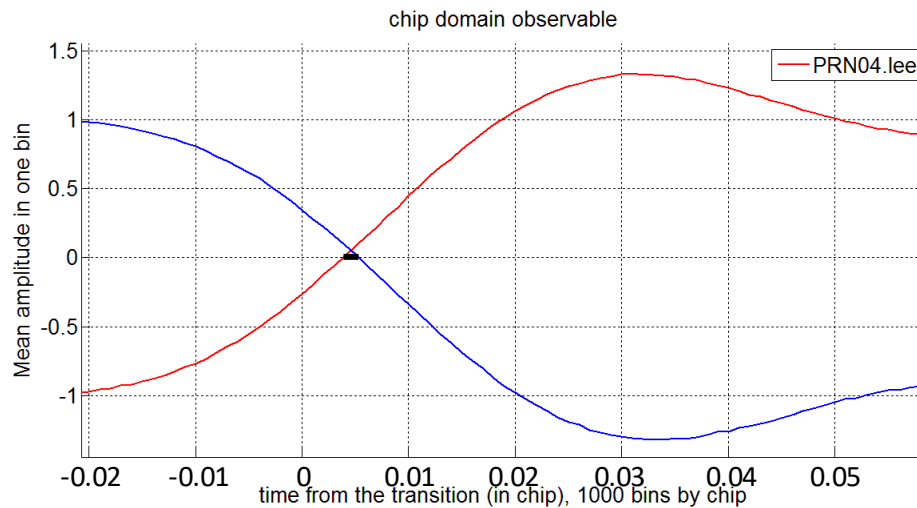


**Figure 4-1.** Example of delay between rising and falling transitions zero-crossings (GPS L1 C/A, PRN 4).

The value of the delay was estimated for signals generated by different satellites. Results on GPS L1 C/A and GPS L5 obtained by Stanford University from measurements collected with a high-gain dish antenna [Wong et al., 2010] are summarized in Figure 4-2. Information about the setup is available in [Wong et al., 2010].

It can be seen that the delay is satellite-dependent and that the payload technology has an influence on the parameter. The second important result is that the maximum value of the delay is lower than 5 ns for GPS L1 C/A signals and around 5 ns for the GPS L5 signal sent by the Block II-F satellite (SVN 62).

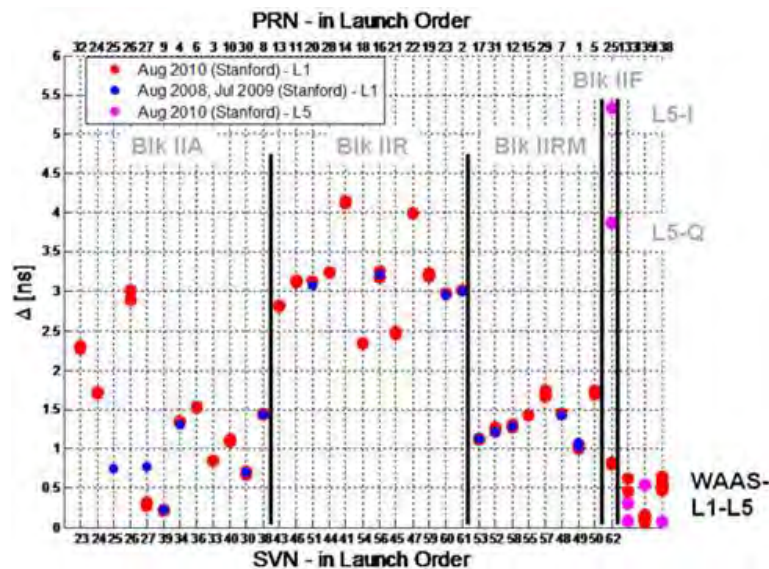


**Figure 4-2.** Results about delay between rising and falling transitions zero-crossings for different signals (GPS L1 C/A and one GPS L5) [Wong et al., 2010].

Some results on GPS II-F4 L5 (SVN 66, PRN 27) and Galileo PFM E1/E5a are also given in [Thoelet et al., 2014]. Information about the setup is available in [Thoelet et al., 2014]. Table 4-1 gives a summary of results provided in this publication.



Signal	Mean digital distortion (ns)
L5 data	4.6
L5 pilot	3.7
E1 OS data	$\approx 0$
E1 OS pilot	$\approx 0$
E5a-I	$\approx 0$
E5a-Q	$\approx 0$
E5b-I	$\approx 0$
E5b-Q	$\approx 0$

**Table 4-1.** Results about delay between rising and falling transitions zero-crossings for different signals (GPS L5, Galileo E5a and Galileo E1 OS) [Thoele et al., 2014].

Values estimated on GPS II-F4 L5 are consistent in [Wong et al., 2010] and in [Thoele et al., 2014]. Results on Table 4-1 show that chip symmetry is better with Galileo E1 OS and E5 signals than with GPS L1 C/A and L5 signals. The low delay values between zero-crossings of rising and falling transitions on Galileo E1 was also noticed in [Gunawardena et al., 2015].

#### 4.1.1.3.2 Analog distortion

Analog distortions can be recognized by the ringing effects affecting the temporal signal. Observations of these distortions were realized on the temporal signal in [Wong et al., 2010] and are shown in Figure 4-3. In red are represented the distorted chip rising transitions on all SVNs for the L1 C/A signal and in blue the in-phase and the quadrature-phase of the GPS II-F1 L5 (SVN 62, PRN 25). The step response represented for L5 signals was averaged considering a transition followed by five consecutive positive L5 chips to be compared to the L1 C/A step response on one L1 C/A chips.

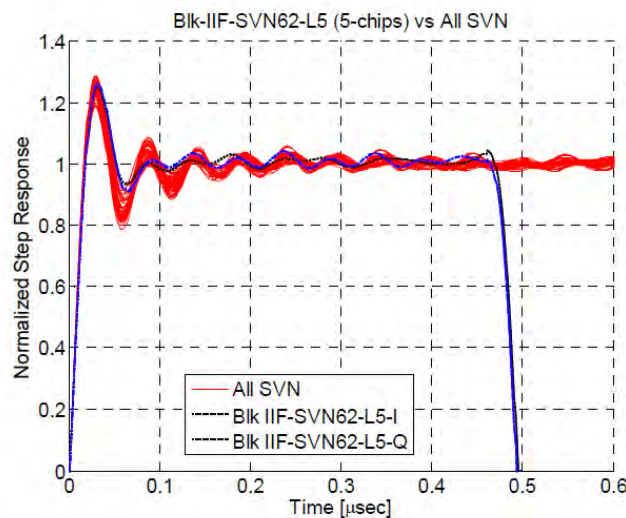


**Figure 4-3.** Results about analog nominal distortions (GPS L1 C/A in red and one GPS L5 in blue) [Wong et al., 2010].

#### 4. Impact of GNSS signal distortions on signal processing

From this plot, it can be seen that a ringing phenomenon is visible on signals sent by healthy GPS satellites. Frequency of the ringing phenomenon is approximately equal to 20 MHz whatever the signal is (L5 or L1 C/A). It is noticeable that the ringing effect is attenuated at the beginning of chips but remains at a visible level all along the chip.

Instead of characterizing the analog nominal distortion by a frequency and a damping factor, other characterizations can be preferred as in [Phelts et al., 2009]. It was proposed to characterize analog distortions by their equivalent step response using four parameters. For each parameter, definition and associated overbound value obtained in [Phelts et al., 2009] by high resolution measurements are given in brackets.

- *Rise time/Fall time* (25 ns): It is the time it takes for the rising (falling) edge of the signal to increase from the preceding zero-crossing to the ideal amplitude.
- *Peak time* (45 ns): It is the time it takes for the rising edge of the signal to increase from the preceding zero-crossing to the first peak value.
- *Settling time* (180 ns (at 10 % convergence)): It is the time measured from the zero-crossing preceding a positive (or negative) chip to when the signal response first enters and then remains within a band whose width is computed as a percentage of amplitude for the remaining duration of the chip width.
- *Peak overshoot ratio* (35 %): It is the difference of the amplitude of the first peak and the ideal amplitude, divided by the ideal amplitude.

Chip shape of Galileo E1 signals is investigated in [Gunawardena et al., 2015]. Nevertheless, to reproduce GNSS receiver conditions, an equivalent RF filter bandwidth equal to 24 MHz was implemented. The consequence is that nominal distortions ringing effect cannot be distinguished from ringing effect caused by the receiver equivalent RF filtering.

In several publications, such as in [Phelts et al., 2009] or [Thoelert et al., 2014], equivalent filters that are able to reproduce analog distortions behavior are proposed.

##### 4.1.1.3.3 Other distortions: observation of the quadrature-phase channel

In addition to analog and digital nominal distortions principally studied in various publications, two other nominal distortions were reported on GPS L1 C/A into [Gunawardena and van Graas, 2012b]: in-phase and quadrature-phase of the signal are imbalanced (they are not perfectly orthogonal) and a ringing phenomenon with a frequency equal to 10 times the GPS L1 C/A chip frequency is affecting the signal. Both nominal distortions are well visible on the average quadrature channel as presented in Figure 4-4. Different colors represent the chip observable for different chips sequences. In green is plotted the average of chips sequences corresponding to -1;-1;-1, in pink the chips sequence +1;+1;+1, in red the chips sequence -1;+1;-1, and in blue the chips sequence +1;-1;+1.

It can be seen that whatever the chip sequence is, even when the signal is tracked, the average of the quadrature signal component is not null. This phenomenon is typically entailed by an imbalance between the in-phase and the quadrature-phase of the signal which leads to a residual of the in-phase signal on the quadrature-phase signal. In addition, the 10 MHz ringing, is clearly visible on the quadrature component of the signal.



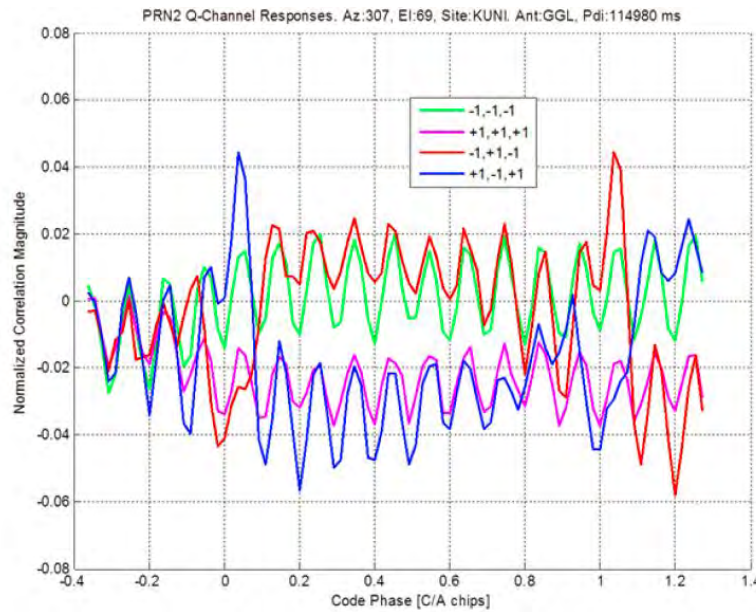


**Figure 4-4.** Imbalance between I and Q channels and 10 MHz ringing [Gunawardena and van Graas, 2012b].

#### 4.1.2 Non-nominal distortions

GNSS signal distortions in nominal conditions are problematic for GNSS users with high requirements in terms of integrity, accuracy, continuity and availability because they induce errors difficult to quantify and they impact receiver measurements not negligibly. Naturally, GNSS signal distortions in a faulty condition are burning issues for these particular GNSS users. In this section are introduced non-nominal GNSS signal distortions, also called Evil WaveForm (EWF).

The EWF matter is based on the initial problem raised by the first GNSS signal non-nominal distortion observed in 1993 on the SV 19 (block II). This anomaly was the first real incident regarding GNSS signal distortions. Consequently, it was the first *example of something that could cause a large error in landing an aircraft* [Adams, 1999]. The investigation of this new problem led the FAA (Federal Aviation Administration) to consider a new GNSS threat. *The primary objective was to study the problem and look at the entire class of signal anomalies that could have similar effects. The agency wanted assurance that next-generation navigation systems will be protected, not only against SV 19 like anomalies, but against any other possible EWF* [Adams, 1999].

In 4.1.2.1, the SV 19 anomaly is detailed. Observations made in 1993 and already published are presented. In 4.1.2.2, an overview of other recorded GNSS signal distortions generated at payload level is given.

##### 4.1.2.1 Origin of the problem: the SV 19 anomaly

The first threatening GNSS signal anomaly was reported in 1993. Several measurements were collected from the anomalous signal emitted by the faulty satellite. The different impacts of the failure were reported as in [Mitelman, 2004] or in [Edgar et al., 1999]. A summary of these impacts is proposed:

#### 4. Impact of GNSS signal distortions on signal processing

- *Impact on the position domain.* Tests made in July 1993 confirmed the presence of severe positioning error experienced by GPS users under certain conditions. Specifically, these tests indicated differentially corrected vertical position errors up to 8 m when SV 19 was included in the PVT solution set, compared with errors on the order of 50 cm when the satellite was not in view.

An important point is that different receivers were affected differently by this error. By consequence, the receiver configuration is fundamentally linked to the impact of the error on the receiver PVT and the failure was a threat for differential users.

- *Impact on the frequency domain.* The University of Leeds has noticed a difference between the spectrum of the unhealthy SV 19 (Block II) and the spectrum of the healthy SV 31 (Block II-A). These differences were observed using a 3 m dish antenna, the same RF chain and the same elevation (25°) and azimuth (165°) for both signal measurements.

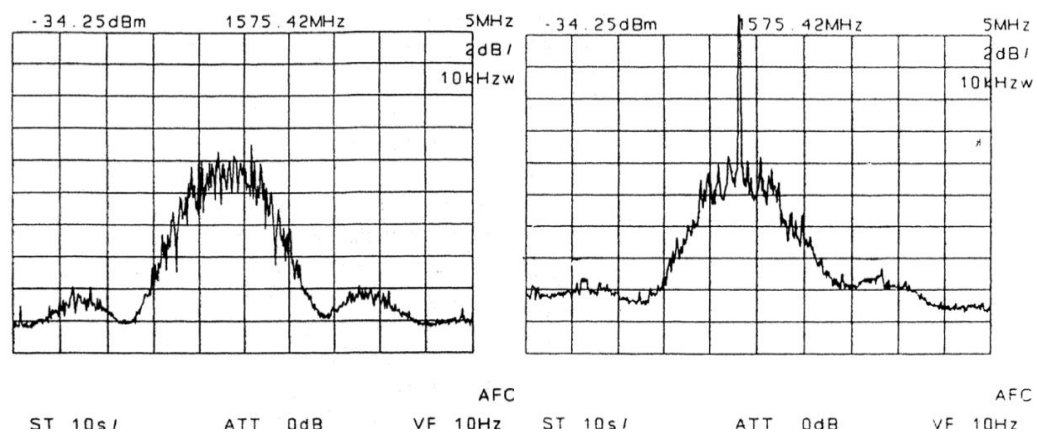


**Figure 4-5.** Spectrum of signals transmitted by a healthy satellite (left) and SV 19 during its failure (right).

Figure 4-5 shows the L1 power spectra for the SV 31 (on the right) and the SV 19 (on the left). Two important points have to be noticed:

- a 11 dB spike at the center of the main lobe of the SV 19 spectrum and
  - a slight asymmetry at the edges of the main lobe and first side lobes.
- *Impact on the time domain.* Measurements were done with a 20 m high-gain antenna by the Aerospace Corporation to estimate the signal behavior in the chip domain for the L1 C/A (on the top) and for the P(Y) (on the bottom) signals. Figure 4-6 provides results for the unhealthy SV 19 (Block II) on the right and the healthy SV 26 (Block II-A) on the left.

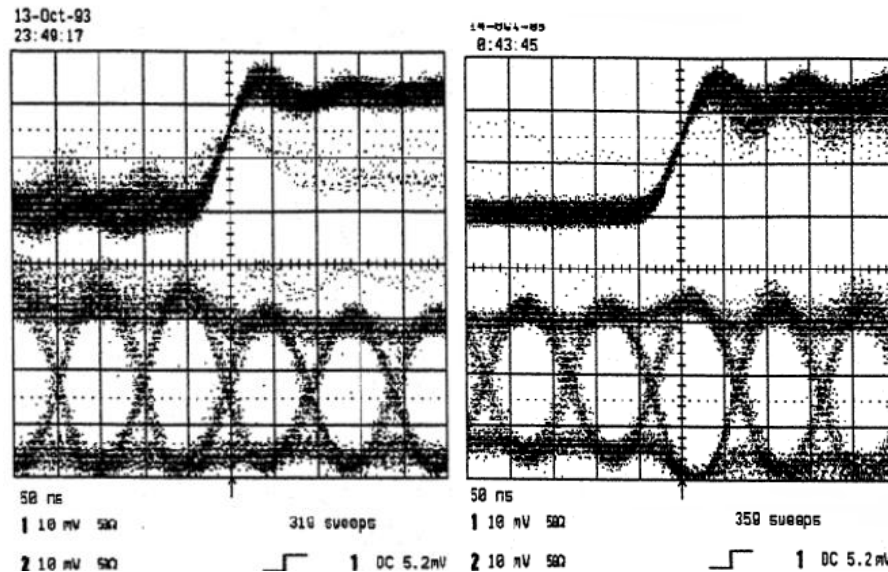


**Figure 4-6.** Chip domain representation of signals transmitted by a healthy satellite (left) and the SV 19 during the failure (right).

In the chip domain several key features were worth noting:

- The zero-crossings of the C/A and P(Y) codes on the healthy SV are aligned within few nanoseconds, while those of SV 19 are misaligned by approximately 30 ns. (in-phase and quadrature-phase components are not synchronized)
- More ringing is visible after the transition on SV 19.

An important result underlined in [Mitelman, 2004] is that the error was not detected in real time. The consequence is that the satellite failure was an integrity threat for GNSS users estimating a PVT solution with a pseudorange measurement derived from the faulty satellite without being warned.

To summarize, *an EWF was initially a distortion of the GNSS signal which could entail a “large error” using DGPS without being detected* (thus the notion of “Evil”).

The notion of a SBAS user is thus closely linked to EWFs:

- The anomaly was observed in a DGNSS configuration.
- SBAS systems are high integrity systems that are using DGNSS principles, but that are also meant at detecting all SiS threats. The EWF is an integrity threat that thus has to be taken into account in the SBAS integrity scheme. It does not mean that non-SBAS users are not affected by the EWF threat, just that they have to take it into account in a different way.
- Observations shown that different receivers have reported different errors depending on the receiver configuration. It entails that SBAS users, affected by these configuration dependencies, have to be taken care of cautiously. By consequence, it is a necessity for the SBAS to monitor and detect this kind of distortion.

#### 4.1.2.2 Other satellite anomalies

The SV 19 anomaly is not the only example of reported GNSS signal distortion. In this section, an overview of other EWF threats is given:

#### 4. Impact of GNSS signal distortions on signal processing

- *SV 49 (PRN 1, Block II-RM) anomaly.* Since the emission of the GPS L1 signal in mid-April 2009, an anomaly was announced on that signal. Nowadays, the signal is still unusable until further notice. Today, the cause of the anomaly is recognized as a reflection of the L1 signal when reaching the filtering stage at payload level which affects the transmitted signal [Suard, 2010]. The distortion is an EWF in that sense that it corresponds to a signal distortion which affects pseudorange measurements of all users processing the signal in a non-nominal way. In addition, the impact of the distortion is different depending on the GNSS receiver configuration and is by consequence a threat for all DGNSS users.
- *SV 61 (PRN 2, Block II-R) anomaly.* SV 61 experienced a degraded signal quality starting on 10/31/13 and ending with maintenance on 11/3/13. The anomaly was not a threat in the sense that pseudorange measurements were within the normal range. Nevertheless the signal was affected by more noise than usually and slight distortions were observed on the correlation function. Correlation function distortions were not high enough to be considered as threatening and trigger an alarm [FAA, 2016b].
- *SV 54 (PRN 18, Block II-R) anomaly.* A first distortion was observed, starting on 7/26/09 and ending on 8/7/09 and a second distortion starting on 3/8/2016 still continues. In both cases, the distortion consists in a correlation function distortion. In 2016, some GBASs have detected the signal distortion causing PRN 18 to be unused which was not the case in 2009 [FAA, 2016b].

It is noticeable that some other signals broadcasted by GPS satellites are affected by distortions that could be considered as non-nominal distortions depending on the limit between nominal and non-nominal distortions. To avoid availability issues, these distortions are considered as nominal but it is noticeable that they could be classified as anomalies depending on the application. In [Brenner et al., 2009], natural signal distortions are divided in two categories:

- SV 49-like distortion, satellite elevation-dependent. With an amplitude lower than what was observed on SV 49, the reflection of the signal at payload level induces a distortion which depends upon the satellite elevation. This phenomenon is visible on SV 41 (PRN 14, Block II-R), SV 44 (PRN 28, Block II-R), SV 58 (PRN 12, Block II-RM), SV 59 (PRN 19, Block II-R), SV 60 (PRN 23, Block II-R) and SV 61 (PRN 2, Block II-R). In another publication [Springer and Dilssner, 2009], similar behaviors were reported on SV 43 (PRN 13, Block II-R) and SV 55 (PRN 15, Block II-RM).
- Signal distortion that entails large bias. The phenomenon particularly visible on SV 60 (PRN 23, Block II-R) also affects, with a lower impact, some other signals. This phenomenon is visible on SV 41 (PRN 14), SV 45 (PRN 24), SV 46 (PRN 11), SV 47 (PRN 22), SV 51 (PRN 20), SV 54 (PRN 18) and SV 56 (PRN 16), all from the Block II-R.

##### 4.1.3 Origin of GNSS signal distortions

Distortions focused in this Ph.D. thesis are distortions generated at satellite level. They can be induced by the satellite payload or by the reflection of a signal at satellite level. A knowledge about payload components is necessary to understand what could be the cause of such distortions. Nevertheless, it will be seen that the lack of information available on payload components makes possible only some speculations about the origin of nominal as well as non-nominal distortions.

#### 4.1.3.1 GPS payload components

The GPS satellite signal generation unit can be divided in three main processing blocks [Parkinson and Spilker, 2006]:

- The Mission Data Unit (MDU): baseband signals are synthesized. The signal at this stage consists of the multiplication of the spreading code with the square wave sub-carrier (if any) and the navigation message (if any).
- Up-conversion to L frequencies: L-band carriers are generated by frequency multipliers followed by intermediate amplifiers. Carriers are then BPSK-modulated with baseband signals. Separate balanced mixers are used for each modulated waveform to split in-phase and quadrature-phase components.
- Combiner and Radio frequency Antenna Beam Forming (RABF): modulated carriers are summed to obtain a signal with a constant envelope. The signal is then amplified with High-gain solid-state Power Amplifier (HPA).

The time of a GPS satellite is managed by three Atomic Frequency Standards (AFS). AFS are used to tune a Voltage Control Oscillator (VCO) which provides the clock signal with the correct output frequency. Three clocks are used for redundancy.

Several payload technologies are implemented on different GPS satellites. Among new technologies, MDU are upgraded in new GPS satellites to generate new signals such as L2C and M-code (Block II-RM) or also L5 (Block II-F). Moreover, high precision L1 and L2 modulators are implemented in new GNSS generations (Block II-RM, Block II-F). Intermediate and high power amplifiers are upgraded to high frequency GaAs technology and incorporate signal power and code power ratio flexibilities for Block II-RM and Block II-F generations [Rajan and Irvine, 2005].

More details about GPS satellite payloads are available in [Marquis and Shaw, 2011], [Fan et al., 2008] or [Rajan and Irvine, 2005].

#### 4.1.3.2 Galileo payload components

By analogy, Galileo satellite signal generation unit can be divided in three main processing blocks [OHB System, 2012], [Rebeyrol, 2007]:

- The Navigation Signal Generation Unit (NSGU): it generates the navigation message. As in GPS satellite, it consists of the multiplication of the spreading code with the square wave sub-carrier (if any) and the navigation message (if any). The main difference with GPS technology is that the NSGU includes a navigation signal modulator which generates three *digital* modulated baseband signals: one for each frequency band (E1, E5, E6). The E5 digital modulated baseband signal is generated from a look-up table [GSA, 2010]. According to the signal bandwidth, the modulator puts the baseband signals around a *digital* intermediate frequency and keeps the signals in-phase and quadrature-phase components separated. After being modulated, signals are filtered by *digital* filters.
- The Frequency Generation and Up-conversion Unit (FGUU): it delivers the sampling frequency to the NSGU, achieves the digital to analog conversion and performs the signals up-conversion to their respective frequency bands before broadcasting to users. Different frequencies are generated by independent frequency synthesizers which include two oscillators (a reference and a VCO), a phase detector, a loop filter and a frequency divider.

#### 4. Impact of GNSS signal distortions on signal processing

- Combiner and Radio frequency Antenna Beam Forming (RABF): different L-band signals are amplified. The two types of power amplifiers that may be used on navigation satellites are the Traveling Wave Tube Amplifier (TWTA) and the Solid State Power Amplifier (SSPA). At the payload output, before the antenna subsystem, the Output MultipleX unit (OMUX) combines amplified signals.

The time of Galileo satellites is managed by four atomic clocks. The clock unit is supported by a Clock Monitoring and Control Unit (CMCU). One atomic clock is chosen by the CMCU to provide the reference time to the FGU.

The main difference between GPS and Galileo signal generations is that in Galileo satellites, all modulations of a given L-band are digitally synthesized in one navigation signal baseband component. Then the composite digital waveform is converted into an analog signal before being up-converted. In GPS, different modulations are mixed in an analog way during the signal up-conversion.

##### 4.1.3.3 Speculation about SiS distortions origins

This section aims at finding the origins of SiS signal distortions. The strategy consists of studying what could be the cause of nominal distortions at payload level. Then it is possible to investigate which payload component could lead to a signal distortion if operating in a faulty condition.

The starting point of this approach is observation made on nominal signals especially observation based on chip domain. Possible explanation of all nominal distortions listed earlier are given.

- Post-transition damped ringing effect. This phenomenon is typically entailed by bandlimited transfer function processes that can occur in the signal generation unit or in the transmission sub-system.
- Delay between rising and falling transitions. In [ICAO, 2006] is said that this distortion *is associated with a failure in the navigation data unit (NDU), the digital partition of a GPS satellite*.
- Imbalanced in-phase and quadrature-phase components. The in-phase and the quadrature-phase components are split during the up-conversion. A slight error in balance mixers could explain such a distortion as presented in [Gunawardena and van Graas, 2012b].
- 10.23 MHz spectral components. This distortion can be explained by the imbalance between the in-phase and the quadrature-phase components of the signal. Indeed, the quadrature-phase channel carries the P(Y) code with a frequency 10 times higher than the C/A signal carried by the in-phase channel. If both channels are not exactly orthogonal, the P(Y) code is visible on the C/A code in-phase component [Gunawardena and van Graas, 2012b].
- Transition time (at rising and falling transitions). In theory, the passage from a positive chip to a negative chip (or reciprocally) is instantaneous. Nevertheless, as discussed in [Gunawardena and van Graas, 2012b] the modulator Schottky diodes have finite switching time (between one hundred picoseconds to a few nanoseconds).
- Elevation dependence. In [Gunawardena and van Graas, 2013] it was observed that signal distortions were dependent upon the elevation of the satellite. This phenomenon is different from other listed distortions in that sense that it is a time varying effect. It could be expected to have nominal distortions which are constant in time for a given satellite but the elevation dependency shows that in nominal conditions, distortions can be time-dependent. An explanation of this phenomenon is proposed in [Gunawardena and van Graas, 2012b]:



multipath reflections and phase variations at satellite level can entail such nominal distortions elevation dependency. In addition, it was noticed, for example in [Haines et al., 2012], that there is a variation of the satellite antenna group delay with the nadir angle due to the antenna pattern.

It is more difficult to speculate about the cause of non-nominal distortions, nevertheless some conclusions can be established from the past:

- SV 19 (1993). Two corrective actions were undertaken to solve the problem on SV 19 [Mitelman, 2004]. The first one was to switchover the modulator and initial power amplifier taking place in the RABF from the primary unit to the on-board backup. It had the consequence to reduce the spectral asymmetry and the height of the central spectral spike. The second corrective action consisted of the switchover of the digital component known as navigation data unit (NDU) from the primary unit to the on-board backup. This second action totally restored the signal sent by the SV 19. To conclude the NDU was at the origin of the problem. It is not possible to estimate if the RABF was another origin of the problem or if it just enhanced the distortion generated by the NDU.
- SV 49 (2009). As already discussed, it was suggested that the signal distortion observed from SV 49 was induced by a reflection at satellite level.

## 4.2 Example of signal distortion

For the sake of illustration, the same example of distortion will be assumed on the three different modulations ( $BPSK(1)$ ,  $BPSK(10)$ ,  $CBOC(6,1,1/11)$ ) till the end of this chapter. Filtered distorted signals (blue) are compared to nominal signals (orange): on Figure 4-7 for a  $BPSK(1)$ -modulated signal, on Figure 4-8 for a  $CBOC(6,1,1/11)$ -modulated signal and on Figure 4-9 for a  $BPSK(10)$ -modulated signal. Ten chips are shown.

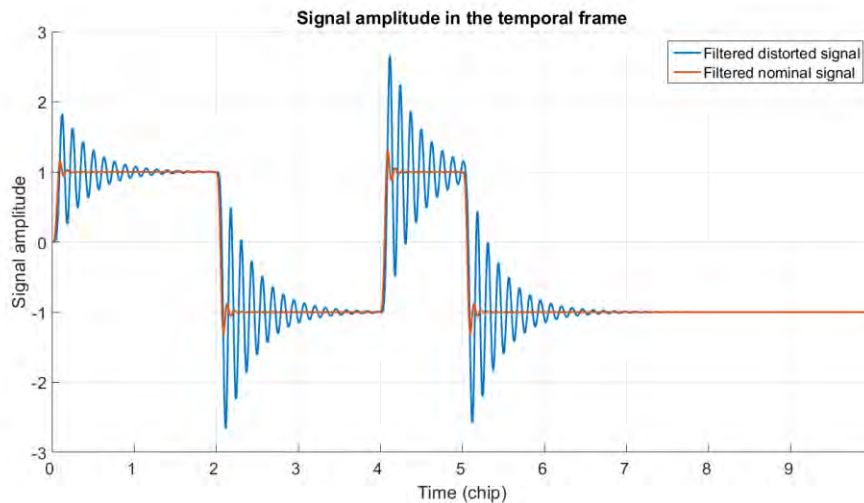


**Figure 4-7.** Nominal (orange) and distorted (blue)  $BPSK(1)$ -modulated signals on ten chips.

#### 4. Impact of GNSS signal distortions on signal processing

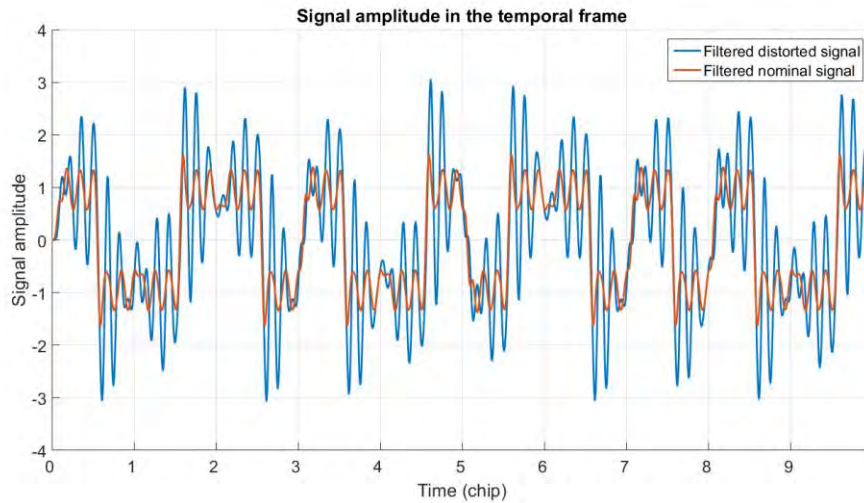


**Figure 4-8.** Nominal (orange) and distorted (blue) CBOC(6,1,1/11,-)-modulated signals on ten chips.

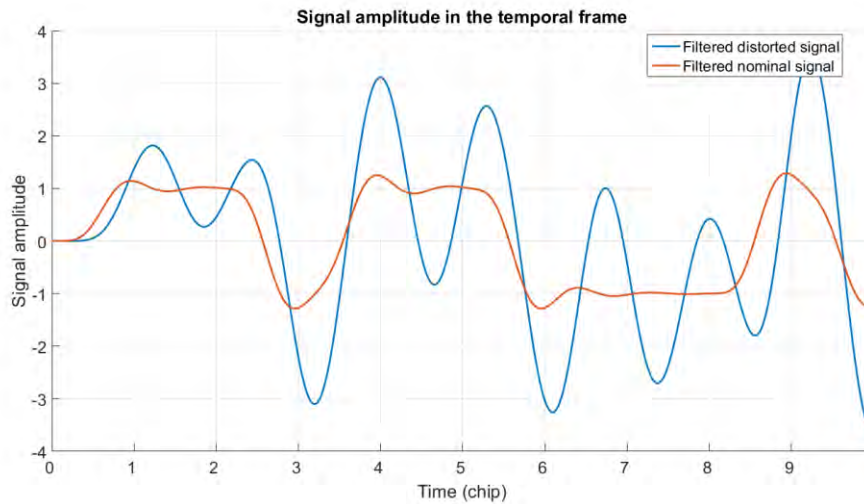


**Figure 4-9.** Nominal (orange) and distorted (blue) BPSK(10)-modulated signals on ten chips.

The distortion consists in a second order ringing distortion with a ringing frequency equal to 8 MHz and a damping factor equal to 2.8 Mnepers/s. A 6<sup>th</sup>-order Butterworth filter with a 24 MHz bandwidth is applied to model the pre-correlation filter.

Nominal and distorted filtered signals shown on figures above will be used to illustrate the impact of signal distortions on a GNSS receiver.

### 4.3 Impact of GNSS signal distortions on the receiver

After the description of GNSS signal distortions (nominal and non-nominal) reported in previous studies, in this section impacts of GNSS signal distortions on the user are listed and some illustrations are proposed. The impact of a distortion on the pseudorange measurement is logically dependent upon the distortion affecting the SiS. Nevertheless, the impact is also dependent upon several parameters that are receiver-dependent and that are function of:



- the antenna and RF front-end equivalent filter and
- the tracking technique.

The difference of receiver configurations is one of the main problems in differential systems. Indeed, if the reference receiver configuration is different from the user receiver configuration, both receivers, processing the same signal affected by the same distortion, might be affected by different errors on the pseudorange. As differential corrections are based on pseudorange measurements, corrections estimated at reference level could be not adapted to a user with another configuration.

In this section, illustrations show the impact of the distortion on the DLL and on pseudorange measurements. The pseudorange measurement error is of primary interest because official requirements on GNSS signal distortions aim at limiting the impact of these distortions at pseudorange level. As a consequence, the impact of a distortion has finally to be assessed on pseudorange measurements to know if a receiver meets requirements regarding the considered distortion.

#### 4.3.1 RF front-end and antenna equivalent filters

The antenna and the RF front-end were presented in sections 3.2.1 and 3.2.2. The influence of the antenna and the RF front-end is visible on the sampled signal and consequently on all the downstream receiver processing. Specifically, the equivalent pre-correlation filter model, dependent upon the antenna and the RF front-end, has an impact on the pseudorange measurement error. More precisely, three parameters of the antenna and the RF front-end equivalent filter have an influence on the signal before its digitization:

- The technology of the antenna (and RF front-end) which has an influence on the filter pattern and the “filtered signal shape”. It can introduce distortions on the signal.
- The 3 dB bandwidth of the antenna and RF front-end equivalent filter. Figure 3-8, shown in 3.2.2, already illustrates the rounding of the correlation function peaks entailed by the pre-correlation equivalent filter bandwidth.
- The maximum group delay variation of the equivalent filter which has an influence on the “signal shape”. It can introduce distortions on the signal.

This last parameter is also called the maximum differential group delay and is defined in [ICAO, 2006] by:

$$\left| \frac{d\phi}{d\omega}(f_{center}) - \frac{d\phi}{d\omega}(f) \right| \quad (4-1)$$

where

- $f_{center}$  is the pre-correlation band pass filter center frequency in hertz,
- $f$  is any frequency within the 3 dB bandwidth of the pre-correlation filter in hertz,
- $\phi$  is the combined phase response of pre-correlation band pass filter and antenna in radian,
- $\omega$  is equal to  $2\pi f$ .

#### 4.3.2 Impact on tracking loops

In this part, the impact of distortions on the tracking and more precisely on the DLL and PLL is tackled.

#### 4. Impact of GNSS signal distortions on signal processing

It is assumed that the distortion affects only the in-phase signal component or the quadrature-phase signal component. This assumption is important to simplify the study of GNSS signal distortions. Instead of having a two dimensional distortion, the problem is reduced to one dimension. It is noteworthy that distortions on both components can affect GNSS signals. Nevertheless, the correlation process is performed between the incoming signal and a local replica that reproduces the PRN code of only one channel of the incoming signal (in-phase or quadrature-phase). For this reason, models which represent threatening distortions define the distortion only on one component of the signal.

##### 4.3.2.1 Impact on the DLL

The DLL design has a major influence on the final pseudorange measurement and more precisely, three parameters of the DLL which are:

- the receiver local replica,
- the discriminator type and
- the correlator spacing used to perform the tracking.

The local replica has an impact on the correlation function and consequently on the S-curve whereas the discriminator type and the correlator spacing only have an impact on the S-curve.

##### 4.3.2.1.1 DLL parameters with an influence on the distortion that affects the pseudorange measurement

Regarding the influence of the *local replica*, the problem is raised especially for the  $CBOC(6,1,1/11)$  modulation on E1C signal. Indeed, for BPSK modulations, same BPSK-modulated replicas are always used for the tracking. However, civil aviation decided to choose Galileo E1C receivers that are able to generate  $BOC(1,1)$  modulated local replicas instead of  $CBOC(6,1,1/11)$  for simplicity reasons. An illustration of the  $R_{CBOC(6,1,1/11,-)}(\tau)$  and  $R_{CBOC(6,1,1/11,-)/BOC(1,1)}(\tau)$  correlation functions is given in Figure 3-10.

The impact of the *local replica* used to derive correlator outputs was introduced in 3.3.1.3. It shows that depending on the receiver local replica modulation, correlation functions are different, and are by consequence impacted differently by a distortion. It entails that a signal distortion will have a different impact on two GNSS receivers with different local replicas. Therefore, the tracking error and the pseudorange measurement estimated from a distorted signal are dependent upon the receiver local replica.

The impact of the *discriminator type* on the S-curve was introduced in 3.3.3.1. In the same way, the discriminator type changes the shape of the S-curve and by consequence its shape when affected by a distortion. For that reason, the tracking error and the pseudorange measurement estimated from a distorted signal are dependent upon the discriminator.

The impact of the *correlator spacing* is shown on Figure 4-10. The comparison is made considering a filtered GPS L1 C/A signal and an Early Minus Late (EML) discriminator on a normalized correlation function (prompt equal to one). Both nominal (dashed line) and distorted (continuous line) S-curves are plotted for correlator spacing's equal to 0.2 chip (in red) and 0.35 chip (in blue).

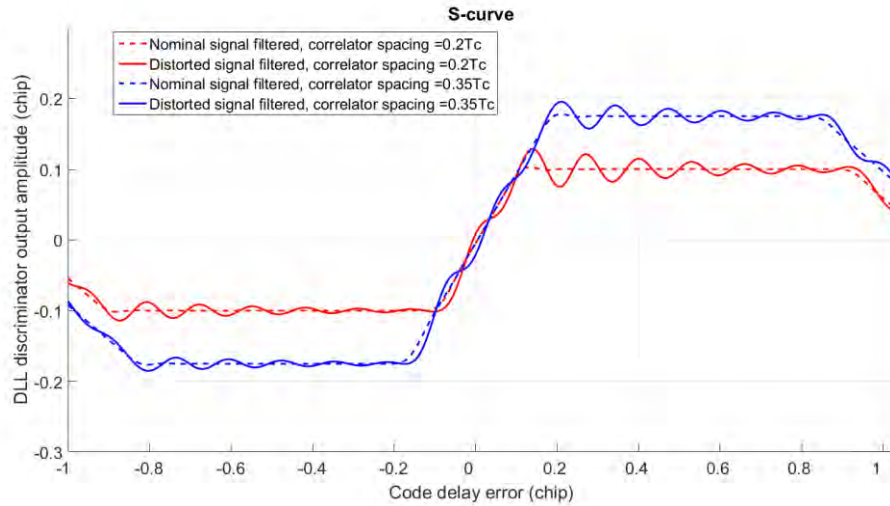


**Figure 4-10.** EML S-curves for a nominal signal (dashed plots) and a distorted signal (continuous plots) BPSK(1) modulated and different correlator spacing's: 0.2 chip (red), 0.35 chip (blue).

The fact is that the aim of the DLL is to reach a steady-state corresponding to a stable zero-crossing of the S-curve. Any bias in the stable zero-crossing of the S-curve would thus result in a bias on the DLL synchronization, and thus in a bias on the corresponding pseudorange. In other words, if the zero-crossing of the S-curve is not obtained for a code delay error equal to zero (perfect synchronization with the received signal), the DLL loop will converge towards a code delay tracking error that is representative of a synchronization bias.

From Figure 4-10 it can be seen that the two S-curves are different in the nominal and the distorted cases. It is also remarkable that the zero-crossings of distorted S-curves are different depending on the correlator spacing, by consequence, pseudorange measurements estimate for various correlator spacing's will be different.

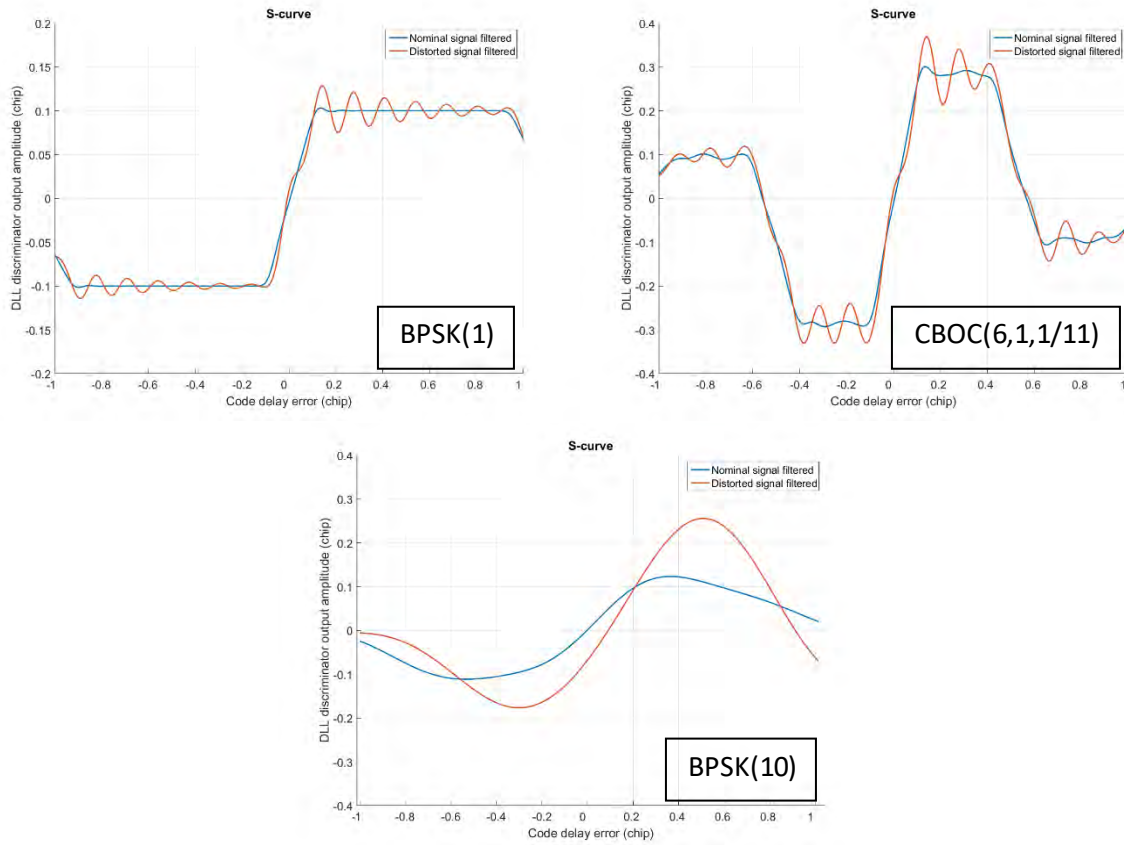
#### 4.3.2.1.2 Impact of a distortion on the S-curve for different modulations

Figure 4-11 illustrates the impact of the considered distortion on the EML discriminator  $(I_E - I_L)/2$ . Plots represent the S-curves of that discriminator on a normalized correlation function (prompt equal to one). For all modulations, the correlator spacing is equal to 0.2 chip of the studied modulation. In blue are shown nominal S-curves (filtered by a 6<sup>th</sup>-order Butterworth filter) and in orange S-curves obtained from distorted correlation functions.

It is noticeable from Figure 4-11 that the distortion has a direct impact on the S-curve. The zero-crossing translation is more visible with the BPSK(10) modulation and a tracking error of 0.1 chip ( $\sim 3$  m) is expected for a receiver tracking the distorted signal compared to a receiver tracking the nominal signal. The code pseudorange measurement error is equal to the code delay error made by the DLL, converted in meter.

For the BPSK(1) and CBOC(6,1,1/11) modulations the S-curve zero-crossing bias is approximatively equal to 0.007 chip ( $\sim 2.1$  m).

#### 4. Impact of GNSS signal distortions on signal processing



**Figure 4-11.** Nominal (orange) and distorted (blue) EML S-curves for BPSK(1) (top left), for CBOC(6,1,1/11) (top right) and BPSK(10) (bottom) modulations.

##### 4.3.2.2 Impact on the PLL

It is assumed that the carrier phase error of the PLL is only affected by the noise and can be neglected. This assumption is equivalent to presume steady state tracking conditions. In this thesis, this hypothesis is kept valid because transient problem is not investigated in this manuscript.

A carrier phase error can affect the PLL if the in-phase and the quadrature-phase components are not orthogonal because of a distortion. In this condition, the same phenomenon as on the DLL discriminator will affect the PLL: the PLL S-curve zero-crossing will be shifted due to the distortion and a bias will appear on the carrier phase measurement. Nonetheless, due to the fact that carrier phase errors have a smaller order of magnitude in terms of impact on the pseudorange measurement ( $\sim 1000$  for a BPSK(1) modulation and  $\sim 100$  for a BPSK(10) modulation), the bias induced by a delay of PLL S-curve zero-crossing can be neglected.

##### 4.3.3 Effect of nominal distortions on the tracking bias

It was seen by looking at S-curve zero-crossing that distortions can entail biases on pseudorange measurements. Nominal signal distortions are presented in 4.1.1.3 on the temporal signal. Nevertheless, as introduced, the main objective of nominal distortions studies is to quantify the impact of such distortions on the pseudorange measurement. This part provides some results about the impact of nominal distortions on the tracking error, in 4.3.3.1 obtained from high-gain dish antennas,

and in 4.3.3.2 obtained from omnidirectional antennas. Finally, 4.3.3.3 introduces methods that permit to limit the impact of nominal distortions on the tracking error.

#### 4.3.3.1 Tracking bias error observed from high-gain dish antenna

As discussed in 4.3.1 and in 4.3.2, the impact of a signal distortion on the pseudorange measurement is dependent upon the pre-correlation equivalent filter and the tracking technique. In the context of nominal distortions research, the pre-correlation equivalent filter should not have any influence on the signal and by consequence on the pseudorange measurement. In this condition, so-called nominal natural biases can be estimated. This case cannot be reached but can be approached using a large dish antenna, a 3 dB bandwidth of the pre-correlation equivalent filter large enough (larger than 50 MHz) and a constant gain inside the band.

In Figure 4-12, tracking bias curves are given considering an EML discriminator and relatively to a correlator spacing equal to 0.1 chip. The figure comes from [Wong et al., 2011] and each curve corresponds to the tracking error observed on a different PRN. Data were collected from a high-gain dish antenna.

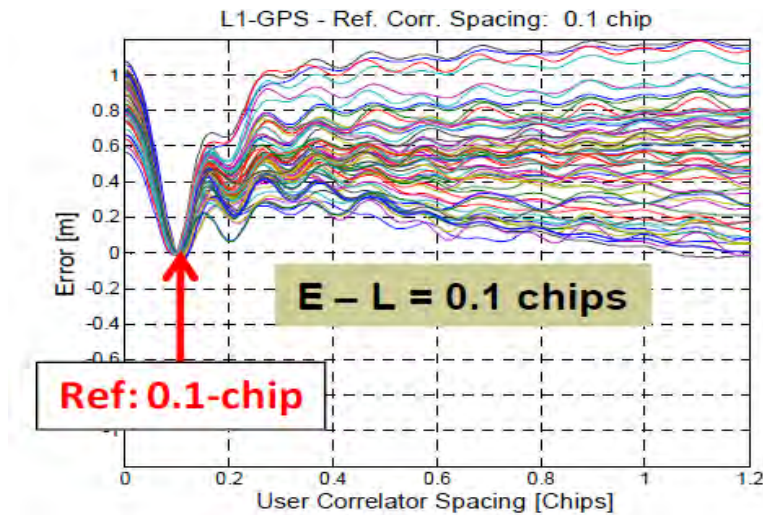


**Figure 4-12.** Tracking error induced by different GPS L1 C/A signals at different correlator spacing's [Wong, 2014]. One curve corresponds to one PRN.

Measurements collected from a high-gain dish antenna are dependent upon the time of the day and the temperature of the antenna [Wong, 2014]. It means that a part of the bias observed on these curves is induced by the antenna and RF front-end. In order to remove the time varying bias induced by the high-gain antenna and which affects results shown in Figure 4-12, a solution is proposed in [Wong, 2014]. The mitigation is performed by estimating biases that affect signals collected close in time. After the subtraction of these biases to the different curves, residual nominal biases still affect pseudorange measurements but with less amplitude and can be seen as the natural biases.

#### 4.3.3.2 Tracking bias on a commercial GNSS receiver

The impact of nominal distortions can also be estimated from omnidirectional antennas and commercial wideband receivers as in [Wong, 2014], [Gunawardena and van Graas, 2012a] or [Liu et al., 2006]. In these conditions, the pre-correlation equivalent filter has a larger impact on the

#### *4. Impact of GNSS signal distortions on signal processing*

pseudorange measurement that cannot be distinguished from the impact of nominal distortions. In every cases, a particular care is taken to mitigate the multipath (environment free of obstacle, multipath-limiting antenna, tracking techniques, etc.) Results can be presented using the same representation as in Figure 4-12 [Gunawardena and van Graas, 2013]. Important conclusions obtained from omnidirectional antenna measurements about the impact of nominal distortions on a user are listed:

- Impact of nominal distortions on a user is dependent upon the satellite elevation [Gunawardena and van Graas, 2013].
- Impact of nominal distortions on a user is dependent upon the RF front-end filter technology and bandwidth [Gunawardena, 2015], [Gunawardena and Van Graas, 2014] and more generally, upon the antenna and the analog section of a GNSS receiver.
- Impact of nominal distortions on a user is dependent upon the receiver discriminator and its correlator spacing.
- Nominal distortions are dependent upon the satellite.
- As an order of magnitude, for single frequency GPS L1C/A users, the differential error induced by the natural bias can be as large as  $\pm 0.12$  m considering a reference with an EMLP discriminator and a correlator spacing equal to 0.1 chip and a user with an EMLP and a correlator spacing equal to 0.2 chip. This differential bias can be as large as  $\pm 0.25$  m considering a reference with a EMLP discriminator and a correlator spacing equal to 0.1 chip and a user with an EMLP and a correlator spacing equal to 1 chip [Wong, 2014].

##### **4.3.3.3 Nominal distortions characterization and mitigation**

The impact of nominal distortions has to be taken into account in the nominal error model in order to be able to make the difference between nominal and non-nominal distortions. By consequence, it is important to quantify the impact of such distortions on civil aviation GNSS users. Moreover, it is also possible to mitigate the impact of nominal distortions.

A strategy to mitigate nominal distortions can be envisaged: the characterization of the nominal distortions and the application of a correction on pseudorange measurements depending on the feature of the nominal distortions. The “Measure-and-Correct” method is described in [Wong, 2014]. It is noteworthy that this method can be applied only on nominal distortions because these distortions can be measured.

This method has one main drawback: nominal distortions are difficult to characterize accurately. One of the reasons is that as presented in 4.3.3.1 and 4.3.3.2, nominal distortions vary in time (depending on the receiver temperature, satellite elevation, etc.). Moreover, as the impact of nominal distortions is receiver-dependent, each receiver has to assess the impact of nominal distortions on itself. Nevertheless, this strategy is studied in ARAIM (Advanced RAIM) discussions as presented in [GPS.gov, 2016]. ARAIM is a solution proposed by the GNSS Evolutionary Architecture Study (GEAS) in the civil aviation context in order to guarantee LPV-200 operation worldwide in the future.



#### 4.3.4 Conclusions about the impact of distortions on a user and differential considerations

It is seen in section 4.3.1, 4.3.2 and 4.3.3 how standalone GNSS users are affected by signal distortions. To study the impact of GNSS signal distortions, several receiver parameters have to be specified and are listed in Figure 4-13. Without these specifications results that are provided relatively to the impact of signal distortions lost their interest, because the domain of applicability of results is not known.

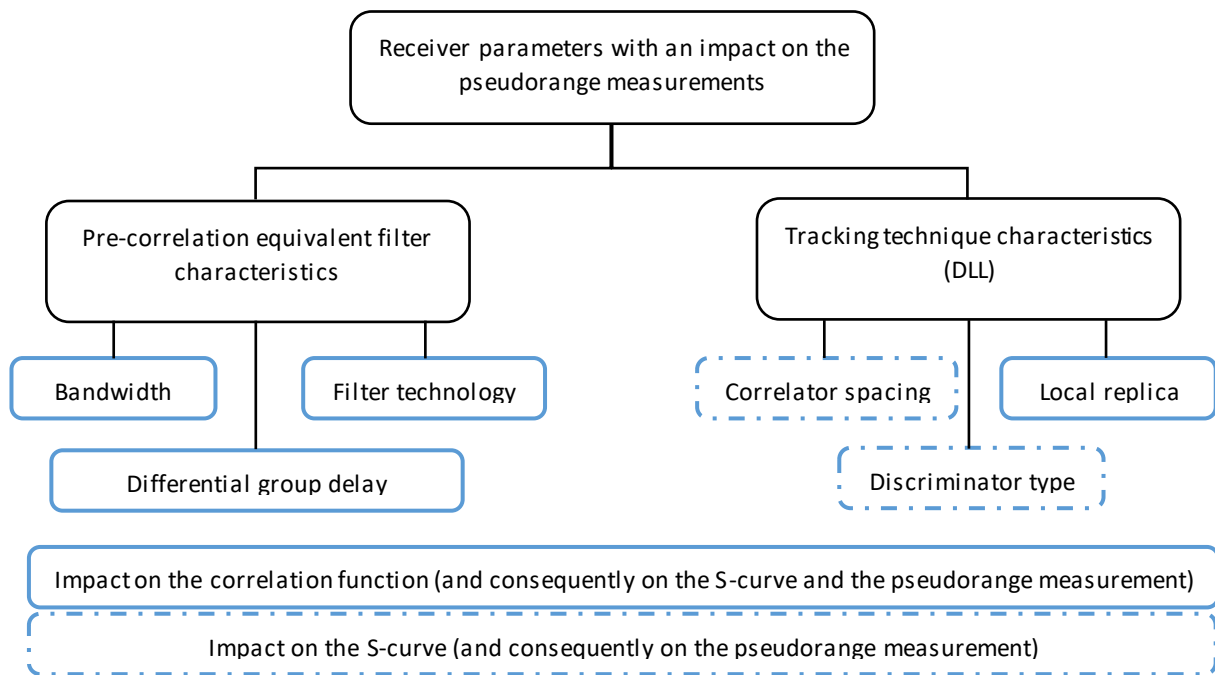


**Figure 4-13.** Receiver parameters having an influence on the impact of GNSS signal distortions on pseudorange measurements.

As a matter of fact, signal distortions also have an impact on differential users because of their different impacts on receivers with different configurations.

As presented in 2.3.1.1, differential corrections are estimated by the reference receiver from its estimated pseudorange measurements and the knowledge of its accurate location. The impact of the tropospheric error, ionospheric error and clock and ephemeris inaccuracies is not dependent upon the receiver and can be differentially corrected (at least partially). On the contrary, signal distortion impact which is dependent upon the receiver configuration cannot be corrected precisely if user and reference receivers configurations are too different.

To conclude, signal distortions and especially non-nominal signal distortions are one of the main threats for differential users. More precisely, differential users with high requirements in terms of accuracy, integrity, continuity and availability have to be protected against signal distortions that induce large differential bias.

If a distortion induces a too large error on pseudorange measurement estimated from the distorted signal, a strategy is to detect and exclude from the PVT computation the affected signal. In this approach the difficulty is to define a bound above which a signal is considered as haz ardously distorted and must be excluded. The method is difficult to adopt in the nominal distortion context. Indeed, as

underlined in [Wong, 2014], it is challenging to achieve good availability performance excluding signals based on their nominal distortions. Nevertheless, this is the strategy used to detect non-nominal distortions.

### 4.4 Non-nominal signal distortions and SBAS

It was seen in the previous section that GNSS signal distortions are a threat for differential users that have to meet stringent requirements. This is the reason why SBAS users (that use mono-frequency or DFMC measurements) must deal with the signal distortions issue carefully.

Even if the failure observed on SV 19 was corrected in January 1994, the problem of EWF was still under discussion after 1994. Indeed, one important issue raised by the distortion is about the integrity risk induced by signal distortions generated at payload level on users with stringent integrity requirement as SBAS users. The three main questions about non-nominal distortions are:

- 1) What kind of distortion can affect a GNSS signal?
- 2) How to detect a GNSS signal distortion in a given Time-To-Alert (TTA) and with a given probability of false alarm (also called probability of fault-free detection)  $P_{ffd}$  and a given probability of missed detection  $P_{md}$ ?
- 3) What is the maximum differential error induced by an undetected GNSS signal distortion?

Solutions proposed in the past to answer to these three questions are detailed in this section.

#### 4.4.1 Necessity to model threatening distortions

The first question (What kind of distortion can affect a GNSS signal?) is the most difficult to answer because GNSS signal distortions are seldom and are difficult to characterize. With current knowledge, it is not possible to be sure that if a GNSS signal distortion occurs, the distortion will have the same signature that what was already observed.

Two answers of this question were proposed and are detailed in the following:

- the Most EWF concept and
- the ICAO Threat Model (TM) concept.

##### 4.4.1.1 Most EWF concept

The Most EWF was defined in [Mitelman, 2004] by: *The most evil waveform (MEWF) is the waveform that will produce the largest differential pseudorange error (PRE) for a particular user, while appearing completely benign (undetectable) to the reference station monitor receiver.*

The Most EWF concept answers to the first question (What kind of distortion can affect a GNSS signal?) only by fixing the maximum energy of the distortion. It means that the threat space is infinite and constrained by only one parameter. The second question (about the detection of distortion) is answered by fixing the design of the Signal Quality Monitor (SQM) implemented at the reference station. The answer to the third question (impact of undetected distortions) requires more mathematical tools. The concept is to find the maximum differential error (among considered users)



entailed by a GNSS signal distortion not detected by the SQM. The term Maximum Undetected Differential Error (MUDE) is used in the following and is referred to as this quantity. In [Mitelman et al., 1999], a mathematical model based on the orthogonally property (Gram-Schmidt orthogonalization) between the distortion and the SQM is detailed and gives the possibility to estimate the MUDE.

This method has the advantage to find the worst differential error without making strong assumption on the distortion which is important due to uncertainties of what could happen in a faulty case.

Nevertheless, the Most EWF concept was put aside because of four main limitations:

- MEWFs are not necessarily causal (it does not respect law of physics),
- an assumed *signal-to-evil ratio* has to be defined to limit the threat space and no method was found to limit this parameter,
- MEWFs are dependent upon the SQM design and
- the Most EWF is dependent upon the user and the reference configurations (SQM design, equivalent RF front-end filter and correlator spacing).

#### 4.4.1.2 Proposition of a threat model: example of the ICAO TM

Another way, adopted by ICAO, to deal with the problem of non-nominal distortions is to define a TM. The difficulty of this approach is to answer to the question one (What kind of distortion can affect a GNSS signal?). Then, a SQM can be designed to detect threatening distortions among distortions of the TM. Finally, the MUDE entailed by undetected distortions can be assessed. If MUDE values do not meet requirements, other implementations of the SQM can be undertaken until its performance meets the requirements.

Due to the difficulties to characterize all non-nominal distortions which could affect a GNSS signal and because of the lack of observations of GNSS signal distortions (in the non-nominal case), a method is to propose TMs. These models are based on modeling possible phenomenon that could occur at the satellite level. They do not necessarily represent the reality but are approaching expected signal distortions which could appear on a GPS L1 C/A signal. In fact, these TMs, and their associated parameters range, referred to as Threat Space (TS), are powerful and necessary tools to design and test performance of SQM.

The approach adopted by ICAO to define TMs for the GPS L1 C/A signal is given in the following and consists in two steps:

- the definition of correlation function threats and
- the limitation of the problem to a characterized TM defined by few parameters and a limited TS.

##### Definition of correlation function threats

For the sake of simplification, ICAO proposed to study only three threatening effects (also called “problematical effects”) on the correlation function:

- *Dead zones: If the correlation function loses its peak, the receiver’s discriminator function will include a flat spot or dead zone. If the reference receiver and aircraft receiver settle in different portions of this dead zone, MI (Misleading Information) can result.*
- *False peaks: If the reference receiver and aircraft receiver lock to different peaks, MI could exist.*

#### 4. Impact of GNSS signal distortions on signal processing

- *Distortions: If the correlation peak is misshapen, an aircraft that uses a correlator spacing other than the one used by the reference may experience MI.*

These signal effects were selected because they *might cause a GBAS or SBAS to output Misleading Information* [ICAO, 2006]. The threat is defined on the correlation function because the pseudorange is estimated from correlator outputs via tracking loop processing.

##### Limitation to a threat model

The ICAO TM includes all GNSS signal distortions with the two following properties:

- distortions have to entail at least one of the three threats (dead zones, false peaks, distortions) on the correlation function and
- distortions must be physically feasible.

ICAO defines two kinds of distortions that satisfy the two properties: a delay on the falling edge of each chip, and a second order oscillation at each chip transition. (Details about the ICAO TM definitions are defined in 6.1.1).

Following the first property, the three correlation function threatening effects can be generated by these TMs to address all threatening distortions. The limitation to distortions covered by the TM is the consequence of the second property that a distortion has to satisfy (physically feasible). Indeed, a delay and a second order oscillation are “natural” in that sense that they could be easily produced by a malfunction of a filter or a digital to analog convertor. Even if no information is given about the link between the proposed distortions included in the TM and a payload failure, it seems reasonable to assume that payload components can provoke it. Moreover, these distortions exist with less amplitude in the nominal case as shown in 4.1.1.3.

With the TM approach, the problem of EWF is reduced to a simple model.

#### 4.4.2 Necessity to detect non-nominal distortions

To meet stringent requirements that are defined by ICAO, augmented systems were developed as presented in section 2.3. As the Ph.D. thesis focuses SBAS application, only the strategy used by SBAS to detect non-nominal distortions is detailed.

The goal of SBAS regarding non-nominal deformations is to detect threatening distortions for differential users, it means distortions which entail differential tracking error higher than a so-called MERR (Maximum allowable ERRor) with a probability  $P_{ffd}$  and  $P_{md}$  in a given TTA equal to 6 s. The TTA notion is important in the sense that GPS Signal Performance Standard (SPS) only guarantee to provide in the navigation message an information about the quality of the signal within 6 hours.

In SBAS, the detection of non-nominal distortion is performed by the SQM defined by ICAO as [ICAO, 2006]:

*The objective of the signal quality monitor (SQM) is to detect satellite signal anomalies in order to prevent aircraft receivers from using misleading information (MI). MI is an undetected aircraft pseudo-range differential error greater than the maximum error (MERR) that can be tolerated. These large pseudo-range errors are due to C/A code correlation peak distortion caused by satellite payload failures. If the reference receiver used to create the differential corrections and the aircraft receiver*

*have different measurement mechanizations (i.e. receiver bandwidth and tracking loop correlator spacing), the signal distortion affects them differently. The SQM must protect the aircraft receiver in cases when mechanizations are not similar. SQM performance is defined by the probability of detecting a satellite failure and the probability of incorrectly announcing a satellite failure.*

In EGNOS, the SQM function is implemented in dedicated ground stations, the RIMS-Cs, whereas in WAAS, the SQM is implemented in the World Reference Stations (WRS). For the two SBASs, the SQM is based on the observation of the receiver correlation function between the incoming signal and the local replica. Details about SQM are provided in chapter 7.

In EGNOS, each RIMS-C provides individual satellite warning flags to the CPF (Central Processing Facility). The CPF then performs majority voting in order to secure the diagnostic. *RIMS-C channels are installed in fifteen of the thirty-three RIMS sites. This allows each EGNOS monitored satellite to be observed by at least three stations equipped with RIMS-C and make the CPF voting diagnostic robust in terms of missed detection and false alarm rate* [Brocard et al., 2000]. As a majority voting is adopted, two RIMS-Cs over three have to flag the same satellite to consider that a signal distortion affect that satellite.

#### 4.4.3 Estimation of the Maximum Undetected Differential Error (MUDE)

With the definition of a TM and a SQM, it is possible by simulations to test the capacity of the SQM to detect signal distortions included in the TM.

The main difficulty to assess performance of one SQM when the TM is defined and finite, is to take into account all receiver configurations that have to be protected. Indeed, the impact of signal distortions on different receivers depends upon the receiver configurations. By consequence, for a given distortion, the MUDE has to be estimated considering the user receiver configuration and the associated reference receiver configuration leading to the worst differential error (the highest MUDE) for that distortion. The closer the user configuration is from the reference station configuration, the more adapted the differential correction is (with the effect to decrease the MUDE). In an extreme case where user and reference station receivers are identical, GNSS signal distortions are not a threat anymore for differential users because fully compensated by the differential correction.

To limit the issue of various receiver configurations, in the civil aviation context, airborne receiver configurations are limited as defined by ICAO [ICAO, 2006]. ICAO defines constraints on parameters presented in Figure 4-13 for aircraft tracking GPS L1 C/A signals: the pre-correlation equivalent filter bandwidth, the local replica, the correlator spacing and the differential group delay at airborne level is limited. The local replica is BPSK-modulated. Two discriminators can be used by civil aviation users: the EML and the double delta discriminators. For receivers with an implemented EML discriminator, the three remaining receiver parameters with an influence on pseudorange measurements are defined in Table 4-2 and are given for four different regions. Regions are represented by blue rectangles in Figure 4-14.

#### 4. Impact of GNSS signal distortions on signal processing

Region	3 dB pre-correlation double-sided bandwidth (BW) (MHz)	Correlator spacing (CS) (chip)	Differential group delay (ns)
1	$2 < BW \leq 7$	$0.04 \leq CS \leq 1.2$	$\leq 600$
2	$7 < BW \leq 16$	$0.04 \leq CS \leq 0.235$	$\leq 150$
3	$16 < BW \leq 20$	$0.04 \leq CS \leq 0.15$	$\leq 150$
4	$20 < BW \leq 24$	$0.07 \leq CS \leq 0.13$	$\leq 150$

**Table 4-2.** Characteristics of GPS L1 C/A civil aviation receivers parameters with an influence on code pseudorange measurements defined by ICAO [ICAO, 2006].

The restriction of user receiver configurations is deeply studied in [Wong, 2014] and more stringent limits are nowadays proposed to limit airborne receiver configurations in a Dual-frequency Multi Constellation (DFMC) SBAS context.

A summary of expected configurations allowed to DFMC SBAS civil aviation users that are focused in this thesis is given in Table 4-3 and are represented by red rectangles in Figure 4-14.

	GPS L1 C/A	Galileo E1C	Galileo E5a GPS L5
Local replica modulation	<i>BPSK</i> (1)	<i>BOC</i> (1,1)	<i>BPSK</i> (10)
Correlator spacing (CS) (chip)	$0.08 \leq CS \leq 0.12$	$0.08 \leq CS \leq 0.12$	Narrow area around $CS = 1$
Differential group delay (ns)	$\leq 150$		
Discriminator type	EML		
3 dB pre-correlation double-sided bandwidth (BW) (MHz)	$12 \leq BW \leq 24$		
Filter technology	Manufacturer freedom		

**Table 4-3.** Characteristics of expected civil aviation receivers parameters with an influence on code pseudorange measurements for different signals.

In civil aviation application, the filter technology choice is let free to the receiver manufacturer but generally the equivalent pre-correlation filter is modeled by a 6<sup>th</sup>-order Butterworth [Mitelman, 2004], [Phelts, 2001], [Macabiau and Chatre, 2000].

The drawback of limiting receiver configurations is that it reduces freedom of the manufacturer in terms of receiver design and possible innovation for competitive market sharing.

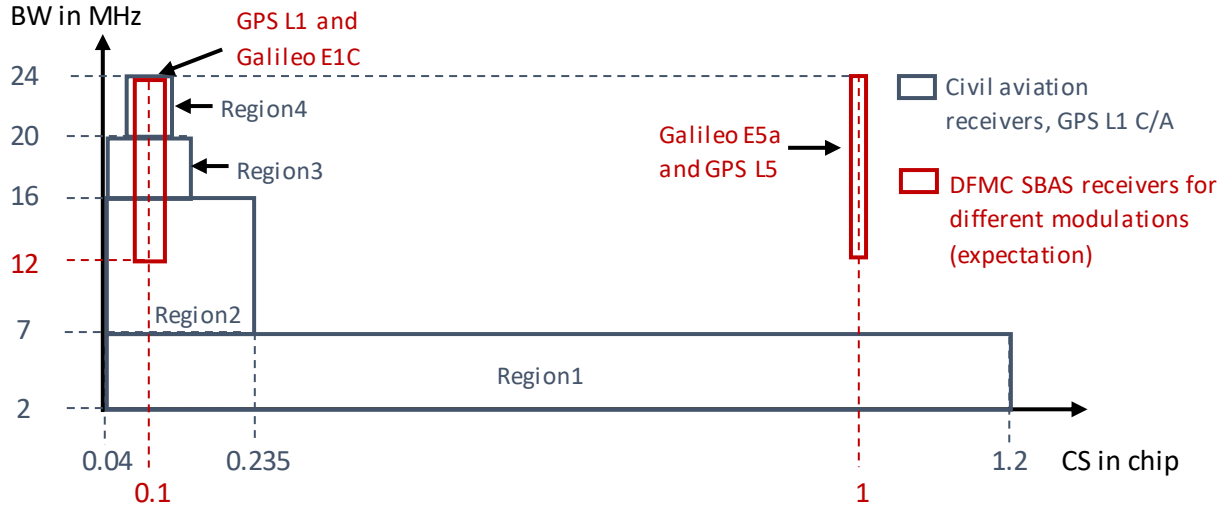


**Figure 4-14.** Summary of civil aviation and DFMC SBAS receivers configurations in terms of bandwidth and correlator spacing.

## 4.5 Visualization of GNSS signal distortions

To understand the impact of a given distortion on the GNSS signal processing, it is important to be able to visualize how this distortion affects some specific critical functions of the signal processing. Two different observables can be reported for the study of GNSS signal distortions:

- The Chip Domain Observable (CDO) which is a way to extract the shape of distortions directly from the digitized signal samples using the PRN code periodicity. It gives information about  $\tilde{s}(t)$ , the incoming signal filtered by the antenna and the RF front-end as shown in section 4.5.2.  $\tilde{s}(t)$  can be affected by a distortion.
- The correlation function defined in section 4.5.3. It gives information about  $R_{\tilde{s}}(\tau)$ , the correlation function of the local replica with the incoming signal filtered by the antenna and the RF front-end. The signal and by consequence the correlation function can be affected by a distortion.

Both observations are located after the A/D section of the receiver. In the following the two methods are described and compared.

### 4.5.1 Standard deviation and general considerations

One way to compare the two observables is by analyzing their standard deviation: the standard deviation of the noise affecting the CDO ( $\sigma_{CDO}$ ) and correlator outputs ( $\sigma_{Corr}$ ) are derived in this part. It is noticeable that the same principle can be used to estimate the two standard deviations. Considering that a noise with a standard deviation  $\sigma_n$  affects the digitized signal and neglecting the impact of the antenna and the RF front-end, the following general relation can be written:

$$\sigma_X = \frac{\sigma_n}{\sqrt{N_X P_s}} \quad (4-2)$$

where

#### 4. Impact of GNSS signal distortions on signal processing

- X indicates the processing technique: CDO or correlation,
- $N_X$  is the number of samples involved in the processing X and
- $P_s$  is the power of the received GNSS signal in decibel.

The computation of  $\sigma_n$  is possible considering that the noise is an averaged white Gaussian noise [Thevenon et al., 2014]:

$$\sigma_n = \sqrt{P_n} = \sqrt{\frac{1}{2} \cdot P_s * \frac{F_s}{C'/N_0}} \quad (4-3)$$

where  $C'/N_0$  is the carrier to noise density ratio expressed in hertz (natural scale) and  $F_s$  is the sampling frequency in hertz. The factor 1/2 comes from that only the noise affecting one component of the signal (in-phase or quadrature-phase component) is considered. This value of signal power does not take into account possible filtering of the noise at the antenna and RF-front end. In appendix A, the filter effect on the noise is taken into account for the estimation of  $\sigma_{CDO}$  and  $\sigma_{Corr}$ .

##### 4.5.2 Chip domain observable method

GNSS signals distortions find their origin on the disturbance of the temporal signal. Then, the first approach is to directly observe the impact of the signal distortion in the temporal domain as it is done using the CDO. The CDO observations are realized on the filtered signal  $\tilde{s}(t)$  in ideal conditions and in non-nominal conditions, and are compared.

This method is also known as the Vision Correlator (NovAtel) [Fenton and Jones, 2005]. Several studies were performed using this processing technique especially regarding the study of nominal distortions as in [Mitelman, 2004], [Wong, 2014], [Pini and Akos, 2007] or [Phelts et al., 2009]. Nevertheless this method can also be used for the study of non-nominal distortions as in [Thevenon et al., 2014]. It is also possible to find, in open access, a software receiver toolbox that is able to generate the CDO from GNSS signal samples [Gunawardena, 2014].

###### 4.5.2.1 Chip Domain Observable concept

The Chip Domain Observable is a processing of the digitized GNSS signal that permits to observe an average GNSS signal on a section of the signal. The section can be chosen depending on the part of the signal that has to be observed and is also called in the following the observed section. In most of studies, chip transitions are focused because signal distortions are enhanced by the chip transition. An “average” chip transition is obtained by superimposing every spreading code transitions (rising transitions are added and falling transitions are subtracted) during a chosen time window called the observation time, in order to average out the noise affecting the temporal samples of the GNSS signal. Superimposing only rising (or falling) transitions gives another observable (if rising and falling transitions need to be distinguished). The CDO can be applied on chip (superimposing only positive, only negative, or all chips) or on parts of the entire code period. This method is based on the periodicity of the PRN code.

The actual CDO observation is done in a discrete way and thus each discrete observation is associated to the notion of bin in which the signal is observed.

Figure 4-15 illustrates the CDO concept. It is considered that only rising transitions are observed on an ideal normalized BPSK signal. The observable is centered on the transition and is built from  $N_{bin} = 10$  values. Different notations that are used on the figure are defined below

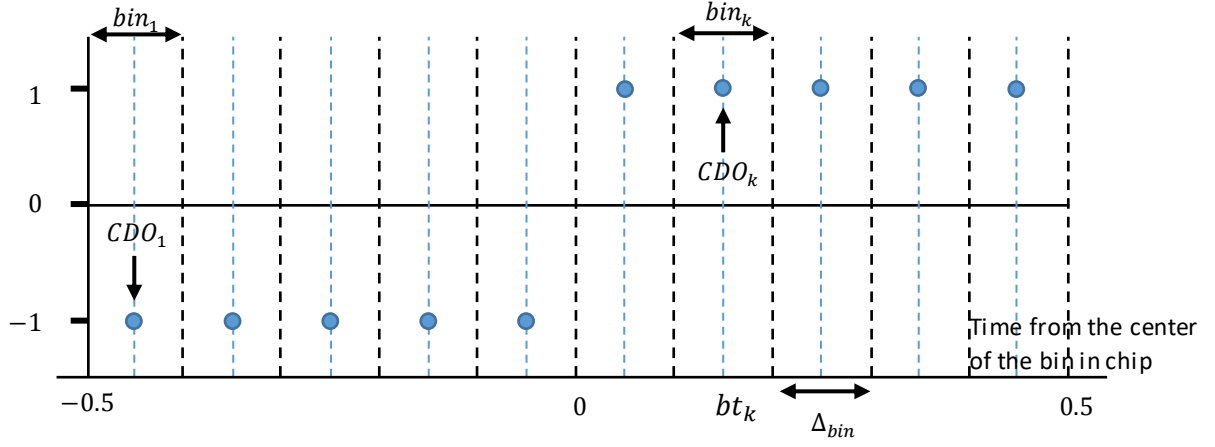


**Figure 4-15.** Illustration of the CDO concept.

Parameters that are used in Figure 4-15 are presented with their notation:

- $CDO_k$  is the  $k^{th}$  value of the averaged signal amplitude in a given delay bin.
- $bt_k$  is the instant of the  $k^{th}$  bin center of the observed section, expressed in chip. In this example  $bt_1 = 0.5 - \Delta_{bin} / 2$  corresponds to the instant of the first bin center.
- $\Delta_{bin}$  is the length of the bin in chip. It corresponds to the time resolution with which the observed section is looked at. This delay is considered constant for all bins if bins are uniformly distributed.
- $N_{bin}$  is the number of delay bins on which the CDO is computed. The relation between  $\Delta_{bin}$  and  $N_{bins}$  is given by:  $\Delta_{bin} = T_c / N_{bins}$  where  $T_c$  is the chip period if the observed section is one chip long and if bins are uniformly distributed along the observed section.
- $T_{obs}$  the observation time in second. It consists of the time during which the signal is averaged.

From the introduced notations, the CDO consists in a vector of  $N_{bin}$  values grouped in  $CDO_k$  where  $CDO_k$  is the average on  $T_{obs}$  of the signal amplitude in the  $k^{th}$  delay bin of length  $\Delta_{bin}$  at a distance  $bt_k$  from the beginning of the observed section.

In the following, it is assumed that bins are uniformly distributed along the observed section if no information is provided about bins distribution. Nevertheless, bins could be arbitrarily placed along the observed part and could have different lengths.

In the CDO context, the expression of the average number of samples in one bin is:

$$N_{CDO} = F_s \Delta_{bin} T_c \frac{T_{obs}}{T_{code}} N_{observed\_part\_code} \quad (4-4)$$

with

- $F_s$  is the sampling frequency in hertz,
- $T_{obs}$  is the observation time in second,
- $T_{code}$  is the code period in second,
- $N_{observed\_part\_code}$  is the number of the wanted observed sections per code period,
- $\Delta_{bin}$  is the size of the bin in chip and
- $T_c$  is the chip period in second.



#### 4. Impact of GNSS signal distortions on signal processing

Consequently, assuming that the noise distribution is Gaussian, neglecting the effect of the antenna and the RF front-end and considering that tracking errors are negligible, the noise standard deviation in a bin can be modeled as:

$$\sigma_{CDO} = \frac{\sigma_n}{\sqrt{N_{CDO}P_s}} \quad (4-5)$$

In appendix A, the standard deviation of chip domain observables taking into account the pre-correlation filtering is derived. Figure 4-16 shows an example of CDO based on one hundred bins and reusing distortions presented in section 4.2. Nominal (blue) and distorted (orange) signals for the *BPSK(1)* (top left), the *CBOC(6,1,1/11)* (top right), and the *BPSK(10)* (bottom) modulations are represented. The observed section is centered on the middle of chips.

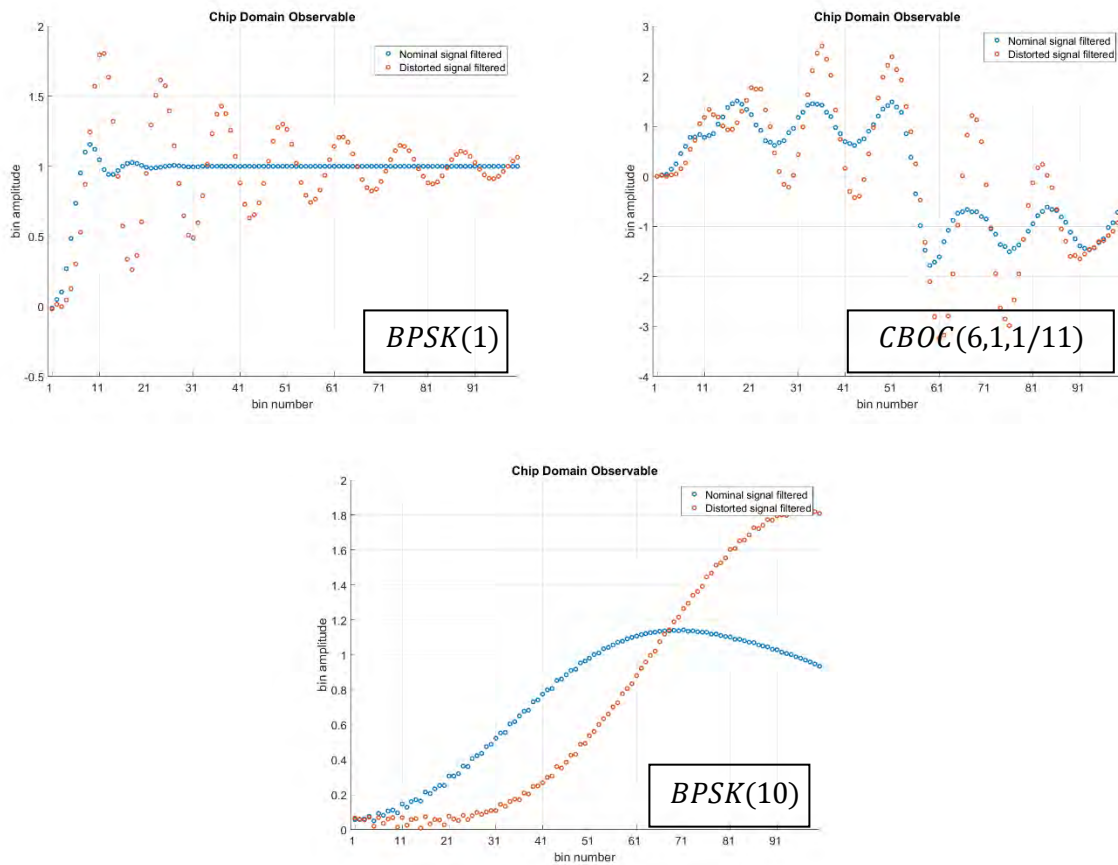


**Figure 4-16.** Example of nominal (blue) and distorted (orange) CDO for *BPSK(1)* (top left), *CBOC(6,1,1/11)* (top right) and *BPSK(10)* (bottom) modulations.

From Figure 4-16, the impact of the signal distortion on the CDO is clearly visible for all modulations.

##### 4.5.2.2 Chip Domain Observable algorithm

The CDO processing is summarized in Figure 4-17 and is based on [Thevenon et al., 2014].



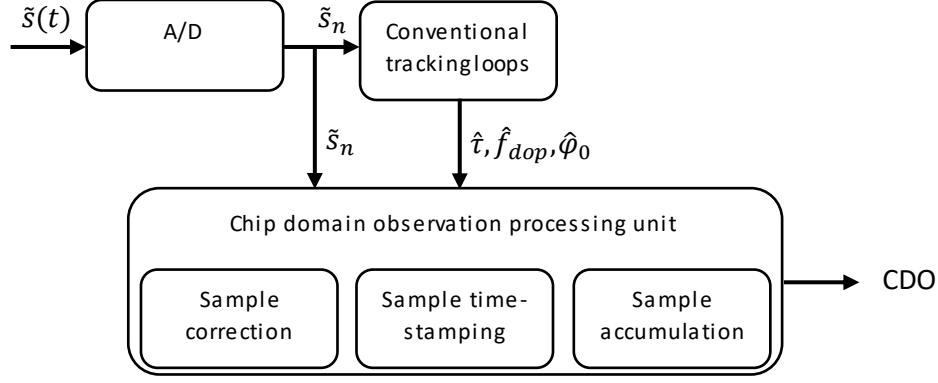


**Figure 4-17.** Block scheme summarizing CDO algorithm.

The CDO is built from digital samples  $\tilde{s}_n$  of the incoming signal after it went through the RF front-end. The expression of the digital signal is given in section 3.2.3. Digitized samples are processed by conventional tracking loops as described in section 3.3.3. This step is necessary to estimate the code delay  $\hat{t}$ , the Doppler frequency  $\hat{f}_{dop}$ , and the phase  $\hat{\phi}$  of the signal to observe. Indeed, to average signal samples in an observed section, their position in the observed section has to be precisely known to avoid averaging samples that are at different locations on the observed section. Moreover, the phase offset due to the Doppler or residual phase that affect the received signal has to be removed. The three estimated parameters are used to process signal samples before averaging them.

The **sample correction** is necessary to remove the phase, the Doppler and the intermediate frequency  $f_{IF}$  which affect the signal carrier. Corrected samples  $s_n^{corr}(t)$  can be written as:

$$s_n^{corr} = s_n \times \cos\left(-\frac{2\pi n}{f_s}(f_{IF} + f_{dop}) - \hat{\phi}_0\right) \quad (4-6)$$

The **sample time-stamping** is necessary to express the time of samples in the emitter reference frame. In the receiver time frame each sample is temporally distant from the previous sample by  $T_s$ . Nevertheless, because of the Doppler Effect which affects the signal, it does not correspond to the distance between two samples in the emitter frame. The adjusted Doppler-corrected sampling interval in the emitter time is function of the carrier frequency ( $f_0$ ) and is equal to  $T'_s = T_s/(1 - f_{dop}/f_0)$ . Translated into a Doppler corrected frequency it leads to:

$$f'_s = f_s(1 - f_{dop}/f_0) \quad (4-7)$$

Moreover, in the receiver time frame, samples are affected by a delay  $\hat{t}$  compared to samples time at the instant of their transmission. Finally, the time-stamp  $\tau_n$  attached to each sample, taking into account  $f_{dop}$  and  $\hat{t}$  is equal to:

$$\tau_n = \frac{n}{f'_s} - \hat{t} = \frac{n}{f_s(1 - \hat{f}_{dop}/f_0)} - \hat{t} \quad (4-8)$$

The **sample accumulation** is the last step of the CDO estimation. Each corrected sample is associated to a given bin based on its time-stamp  $\tau_n$  and its location in the PRN sequence. Only samples from the chosen observed section are accumulated in the bins.

Each time-stamp can be expressed relatively to the theoretical delay from the center of the  $k^{th}$  bin of the  $l^{th}$  occurrence of the observed section ( $bt_k^l$ ), by subtracting  $bt_k^l$  to  $\tau_n$ .  $bt_k$  can only takes values smaller than the length in chip of the observed section whereas  $bt_k^l$  can take any value as it

#### 4. Impact of GNSS signal distortions on signal processing

corresponds to the time-stamp of the  $k^{th}$  bin of the  $l^{th}$  occurrence of the observed section. Then, a sample is allocated to a delay bin if the relative time-stamp to  $bt_k^l$  delay falls into a delay bin.

Samples associated to the  $k^{th}$  bin of the CDO are noted  $s_k^{bin}$  and have a time-stamp  $\tau_n$  which satisfies:

$$\tau_n - bt_k^l \in \left[ -\frac{\Delta bin}{2}, \frac{\Delta bin}{2} \right]$$

All observed sections  $l$  must be treated.

The CDO can be obtained by averaging in the  $k^{th}$  bin all samples  $s_k^{bin}$  associated to this bin:

$$CDO_k = \text{mean}(s_k^{bin}) \quad (4-9)$$

##### 4.5.3 Correlation function observable

Another way to observe the impact of a signal distortion is to look at its influence on the PRN code correlation function which is an observable closely related to the pseudorange estimation as shown in section 3.3. The observation is made on the filtered correlation function  $\tilde{R}_s(\tau)$  that can be affected by distortions.

One correlation function output is obtained by the correlation of the incoming signal on a time period called observation time  $T_{obs}$  with a local replica generated over the same observation time. To obtain  $N_{corr}$  correlator outputs,  $N_{corr}$  correlations must be computed with  $N_{corr}$  delayed versions of the local replica. The complexity of the generation of the correlation function observable is thus dependent upon the number of correlator outputs that have to be observed.

As it was done for the CDO, Figure 4-18 illustrates the concept of correlation function observable considering an ideal normalized BPSK signal. The observable is built from  $N_{corr\_out} = 5$  values.

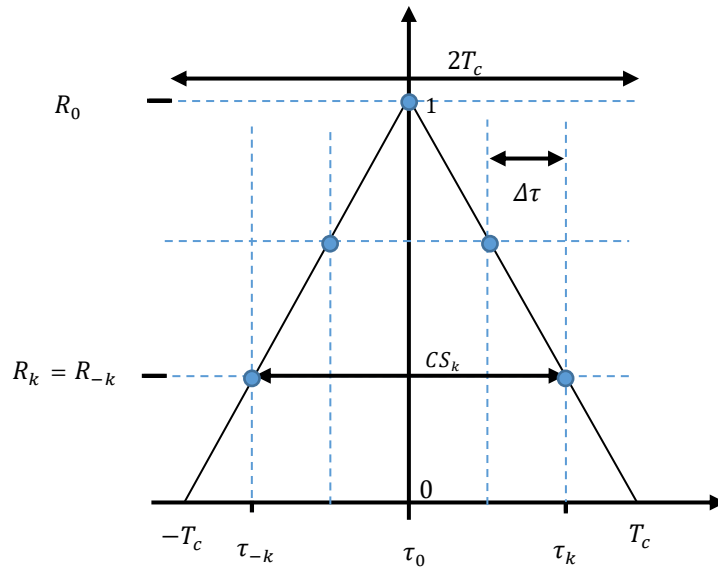


**Figure 4-18.** Illustration of the correlation function observable concept.

Several notations are introduced to define the correlation function observable presented in Figure 4-18:

- $R_k$  is the  $k^{th}$  value of the normalized correlation function amplitude at a given point of the function.  $k = 0$  at the correlation function prompt.
- $\tau_k$  is the value of the  $k^{th}$  correlator output delay in chip. ( $\tau_0 = 0$  corresponding to the prompt output).
- $\Delta\tau_k$  is the distance along the time axis between two outputs of the correlation function, expressed in chip. It corresponds to the resolution with which the correlation function is observed. In the following it is assumed that the distribution of correlator outputs is uniform if no information is provided about the distribution of correlator outputs. With this assumption  $\forall k, \Delta\tau_k = \tau_{k+1} - \tau_k = \Delta\tau$ .
- $N_{corr\_out}$  is the number of correlator outputs at which the correlation function is estimated. For simplicity reasons, it is considered that  $N_{corr\_out}$  is an odd number. The following relation can be written:  $\Delta\tau = 2 \times T_c / (N_{corr\_out} - 1)$  (if the entire correlation function is observed and is  $2 \times T_c$  large).
- $CS_k$  represents the correlator spacing of the  $k^{th}$  correlator pair.  $CS_k = \tau_k - \tau_{-k} = 2 \times k \times \Delta\tau$ .

In the context of correlation function, one correlator output is computed according to a number of signal samples equal to:

$$N_{Corr} = F_s T_{obs} \quad (4-10)$$

where

- $F_s$  is the sampling frequency in hertz,
- $T_{obs}$  is the observation time in second.

Assuming that the distribution of the noise at a correlator output is Gaussian, neglecting the impact of the antenna and the RF front-end and considering that the tracking errors are negligible, the standard deviation of a correlator output can be modeled as:

$$\sigma_{Corr} = \frac{\sigma_n}{\sqrt{F_s T_{obs} P_s}} \quad (4-11)$$

In appendix A, the standard deviation of correlator outputs taking into account the pre-correlation filtering is derived. Figure 4-19 shows examples of correlation function observables using one hundred correlator outputs and reusing distortions presented in section 4.2. Nominal (blue) and distorted (orange) signals for the *BPSK*(1) (top left), the *CBOC*(6,1,1/11) (top right), and the *BPSK*(10) (bottom) modulations are represented.

From Figure 4-19, the impact of the signal distortion on the correlation function is clearly visible for all modulations. It can also be seen that a single distortion has different signature depending on the modulation.

#### 4. Impact of GNSS signal distortions on signal processing

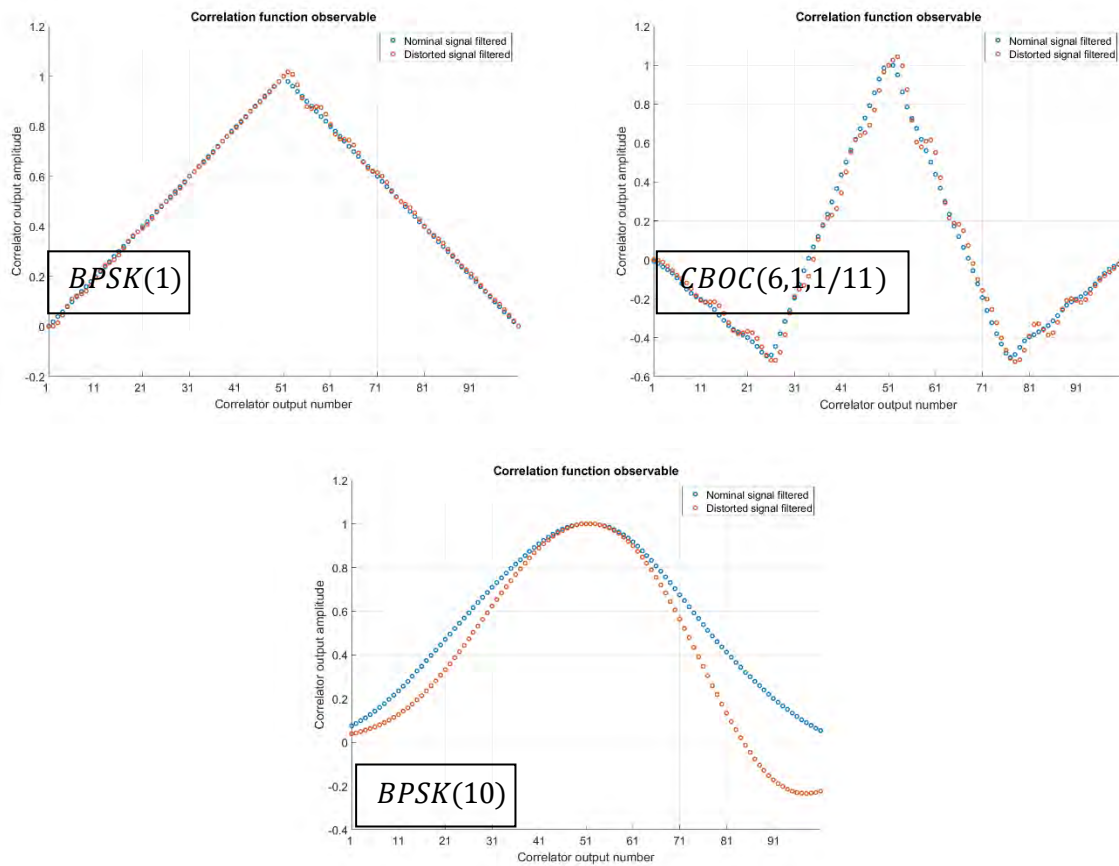


**Figure 4-19.** Nominal (blue) and distorted (orange) correlation function observables for BPSK(1) (top left), CBOC(6,1,1/11) (top right) and BPSK(10) (bottom) modulations.

#### 4.5.4 Comparison of chip domain and correlation function domain observables

Advantages and drawbacks of both techniques are detailed in [Thevenon et al., 2014]. A summary is presented in the following.

The advantages of the CDO are:

- Inputs of the CDO (IF signal samples) are given directly by the RF front-end while multi-correlator outputs have to be computed specifically for a given code delay.
- The noise affecting the CDO is an uncorrelated white noise (or weakly correlated by the RF front-end filter), while the noise affecting a correlator output is correlated through the multiplication with the local replica.
- The resolution of the CDO can be increased beyond the sampling frequency of the signal based on a principle called dithered sampling. [Pini and Akos, 2007]
- The CDO permits to observe independently different types of signal sections. An important consequence is that falling and rising edges can be visualized separately whereas it is not possible on the correlation function.

However, correlation function observables have also advantages compared to the CDO because of the place of the correlation operation in the tracking processing. Then:

- The tracking is directly dependent upon the correlation function. As a consequence, the distortion visible on the correlation function is directly related to the pseudorange error. In that sense, the distortion on the correlation function appears more representative of the potential problems on the pseudoranges. A corollary of this is that some of the distortions visible on the CDO could be filtered/transformed by the correlation process which is based on the entire PRN code. Consequently, some signal distortions visible on the CDO could not influence the correlation function and by consequence the tracking process.
- Correlation processing is already available in conventional receivers, although multi-correlator outputs are not yet widely available.
- Correlator outputs are much less noisy than IF samples.

The last point is illustrated by the comparison of estimated standard deviation for the two observables. From (4-4) and (4-10), the ratio of the two standard deviations can be estimated:

$$\frac{\sigma_{CDO}}{\sigma_{Corr}} = \sqrt{\frac{N_{Corr}}{N_{CDO}}} = \sqrt{\frac{T_{code}}{N_{observed\_part\_code} \Delta_{bin}}} \quad (4-12)$$

(4-12) is a general equation that can be used on all signals with different observable parameters. As an example a particular GPS L1 C/A case is considered. Only rising transitions are superimposed to estimate the CDO. The observed part is chosen with a  $T_c$  length and bins uniformly distributed along this time interval. It entails that:

- $N_{observed\_part\_code} = N_{trans}$  where  $N_{trans} \approx 250$  is the number of rising or falling transitions in one GPS L1 C/A spreading code period.
- $\Delta_{bin} = T_c / N_{bins}$  where  $N_{bins}$  is the number of bins in the observed section.

In this particular case, (4-12) becomes:

$$\frac{\sigma_{CDO}}{\sigma_{Corr}} = \sqrt{\frac{N_{Corr}}{N_{CDO}}} = \sqrt{\frac{N_{bin} T_{code}}{N_{trans} T_c}} \approx \sqrt{4 \times N_{bin}} \quad (4-13)$$

And the ratio between the two standard deviations is only dependent upon the number of bins  $N_{bin}$  computed for the CDO.

It is demonstrated in [Pagot et al., 2015] that the correlation and the chip domain observables, estimated from the average of all chips of the spreading code and convolved by a rectangular shape, have the same expression assuming that:

- the correlation function is null outside the peak (for delay smaller than  $-T_c$  and higher than  $T_c$  around the prompt),
- all chips are used to estimate the CDO (positive and negative chips, after a transition or not).

In any case, for GPS L1 C/A, a triangular shape (code correlation function-like) can be obtained by the convolution of the CDO on one chip with an ideal rectangle. Some receivers use this property and derive “correlation functions-like” from the CDO [NovAtel Inc., 2012] to estimate if GNSS signals are distorted from CDO observables.

### 4.6 Conclusions

The aim of this chapter is to present the different problematics linked to GNSS signal distortions and more precisely GNSS signal distortions generated by the payload that are a problem for all GNSS users and particularly for SBAS users.

In section 4.1 nominal and non-nominal distortions that can affect a GNSS signal are described. As nominal distortions affect continuously GNSS signals, they can be observed precisely using particular setups to collect signals at every time. Results from previous studies about nominal distortions are introduced. A ringing effect after each transition and a lead/lag between zero-crossings of rising and falling edges of code transitions is observed even on signals generated by healthy satellites. It has been seen that nominal distortions generated at payload level are challenging to characterize especially because they are time varying and they are difficult to dissociate from distortions induced by the receiver. The concept of signal distortion also appears in faulty conditions (these distortions are also called EWF) and is different from the study about nominal distortions. Indeed, due to the lack of examples about signal distortions generated in faulty conditions, it is difficult to characterize the kind of distortion that could appear in a case of a satellite failure.

In section 4.2 an example of signal distortion is considered on a  $BPSK(1)$ -modulated signal (GPS L1 C/A), a  $BPSK(10)$ -modulated signal (GPS L5 and Galileo E5a) and a  $CBOC(6,1,1/11, -)$ -modulated signal (Galileo E1C). This signal distortion is used in section 4.3 and 4.5 to illustrate the impact of signal distortions at different levels of the GNSS receiver signal processing.

The main issue with GNSS signal distortions is that their consequences on different user's receivers are dependent upon several characteristics of receivers presented in section 4.3: the technology and the bandwidth of the antenna and RF front-end filter, the discriminator and the correlator spacing used for the tracking. In particular, in part 4.3.2 the impact of the signal distortion on tracking loops is tackled.

In section 4.4, the issue entailed by non-nominal deformation is exposed. Even if EWF are not frequent, GNSS users with stringent performance, as civil aviation users, have to be protected from such threats. To deal with the EWF issue, the Most EWF concept was introduced in a previous study but the preferred solution was the definition of a TM. Nowadays a TM is adopted by ICAO to represent distortions expected on the GPS L1 C/A signal.

In section 4.5, the impact of the distortion is looked at in the chip and in the correlation function domains. The technique to generate the CDO is detailed and will be reused in the following.

From this chapter, it can be seen that the study of GNSS signal distortions is made difficult because the characterization of these distortions is complicated and because the impact of GNSS distortions are dependent upon several features of the receiver. This chapter introduces all important notions linked to GNSS signal distortions and can be viewed as an introduction to the following chapters (chapter 5 and chapter 6), where a deepened study about nominal and non-nominal distortions is undertaken.

## 5 Nominal distortions

The first GNSS signal distortions that are tackled in details are distortions that affect the signal in fault-free conditions. Even if these distortions have a limited impact on GNSS receivers, they can be a problem for users with high requirements. Real data were collected to observe nominal distortions on real GNSS signals. Two types of data collections were performed:

- using high-gain dish antennas and
- using omnidirectional antenna.

Nominal distortions that affect GNSS signals recorded with the two types of antennas are estimated and results are presented and compared to the state-of-the-art (chapter 4). The aim of this chapter is to confirm results already available in the state-of-the-art relatively to the study and the characterization of nominal distortions and to present new results on Galileo E1C signal. More precisely, in this chapter different results are provided:

- A characterization of GPS L1 C/A nominal deformations that affect high-gain dish antennas collected signals. This characterization is based on [Phelts et al., 2009].
- A visualization of nominal distortions that affect Galileo E1C signals collected with high-gain dish antennas.
- A visualization of nominal distortions that affect GPS L1 C/A and Galileo E1C correlation functions.
- A description of advantages and drawbacks between the study of nominal distortions using a high-gain dish antenna and using an omnidirectional antenna.
- A characterization of GPS L1 C/A tracking biases that affect signals collected with an omnidirectional antenna. This characterization is based on [Wong, 2014].

Even if one of the purposes of the nominal distortions study is to establish a limit between the nominal case and the non-nominal case, because of the lack of measurements and the difficulties to characterize nominal distortions in an absolute way, this task is not developed in this chapter.

In section 5.1, the setup that was used to collect GNSS signals with high-gain dish antennas is presented. Indeed, the antenna, the digitizer and the software used to process signals have an influence on the observed nominal distortions and have to be defined.

In sections 5.2 and 5.3, results obtained from high-gain dish antennas are presented. The first section introduces nominal distortions visualized on the Chip domain Observable (CDO), and the second section nominal distortions visualized on the correlation function domain and the S-curve zero-crossing plot. It is seen in 5.4 that some distortions generated by the receiver cannot be distinguished from nominal distortions when the setup is not calibrated.

Distortions generated by the receiver have the particularity to affect all received signals. Therefore, to remove the main part of the distortion induced by the receiver, omnidirectional measurements were collected and processed. Results are provided in section 5.5. The common bias that affects all PRNs measurements collected at the same time are subtracted from pseudorange measurements error to estimate inter-PRN biases which effectively affect a GNSS user.

In section 5.6, inter-PRN biases estimated from the omnidirectional antenna data collection and from one calibrated high-gain antenna data collection are compared to the state-of-the-art.

Finally, section 5.7 makes a conclusion about all results provided in this chapter.

### 5.1 Setups definition and high-gain dish antenna measurements

First in this section, different antennas and receivers that were used to collect high-gain dish antenna measurements are described. Three different setups are presented in this part. Then, an overview of the software which was implemented to process the collected data is given. Finally, the strategy to obtain CDO and correlation function outputs is defined. These outputs are of interest to study GNSS signal distortions as discussed in 4.5.

#### 5.1.1 Data collections from high-gain dish antennas

A high-gain antenna is useful to obtain a sufficiently good signal observation. Indeed, after traveling the distance which separates the satellite and an antenna located on Earth, the GNSS signals are below the noise floor of usual measurement devices. It is therefore advantageous to amplify the received signal in order to better observe it. In our case, this was performed thanks to three directive antennas with the features described in Table 5-1. More details about the ESA antenna can be found in [Gisbert et al., 2012].

The signals collected by CNES and DLR were digitized by a dedicated signal digitizer, called BitGrabber2 and developed by CNES [Ries and Perello Gisbert, 2006] with a sampling frequency of 125 MHz (the sampling is done in complex), a 8-bits quantization and a 3 dB bandwidth of 70 MHz. The data collected by the DLR were obtained from an antenna owned by the German administration.

The signals collected at ESA were digitized using a FSQ from Rohde & Schwarz® [Rohde and Schwarz, 2014]. The sampling frequency was set to 125 MHz (the sampling is done in complex), the digitizer 3 dB bandwidth was equal to 120 MHz.

Antenna holder	German administration	CNES	ESA
Antenna site	Leeheim (Germany)	Toulouse (France)	Noordwijk (the Netherlands)
Antenna diameter	7 m	2.4 m	3 m
Antenna bandwidth	1000 – 2000 MHz	1100 – 1650 MHz	1100 – 1650 MHz
Collection period	Mars 2012	May-July 2014	September 2015
Digitizer	BitGrabber2	BitGrabber2	FSQ

**Table 5-1. Antennas and digitizers features.**

Because of the antenna directivity, it can be considered that multipath are not perturbing the signals. The received  $C/N_0$  is typically between 70 and 80 dB-Hz.



The list of collected signals is given in appendix C.

### 5.1.2 Software overview

A Matlab® software is used to post-process digitized signals and observe nominal distortions. The digital processing is inspired from real GNSS receivers design and is based on concepts defined in section 3.3. The acquisition and a first coarse tracking are performed before the precise PLL/DLL tracking. During the PLL/DLL tracking, the CDO and the correlation function outputs are estimated.

#### 5.1.2.1 Acquisition and coarse tracking

The first step of the Matlab® software processing is the acquisition introduced in section 3.3.2. The advantage of high-gain dish antenna measurements compared to traditional GNSS receiver measurements is that only one signal from one satellite is collected by a directional antenna at a given time. Knowing the PRN associated to the satellite, it is not necessary to test the thirty-two PRNs. It simplifies and accelerates the acquisition process.

After the acquisition, an initial tracking process is implemented to have a better estimation of the Doppler and the delay affecting the signal. A DLL and a FLL are used together. Even if the FLL is not as precise as a PLL, it permits to converge faster toward the steady state. No detail is provided in this document about the FLL implementation because the initial tracking stage has no impact on the observation of nominal distortions. At the end of the DLL/FLL tracking process, a data bit synchronization is performed on signals which carry data information.

#### 5.1.2.2 Fine tracking parameters

After the FLL and DLL coarse tracking, a more precise tracking is implemented based on a PLL and a DLL. During this second tracking phase, the DLL discriminator and the PLL discriminator are given by:

$$D_{DLL} = \frac{(I_E^2 + Q_E^2) - (I_L^2 + Q_L^2)}{(I_E^2 + Q_E^2) + (I_L^2 + Q_L^2)} \quad (5-1)$$

and

$$D_{PLL} = \text{Atan}\left(\frac{Q_P}{I_P}\right) \quad (5-2)$$

It is noticeable that the  $D_{DLL}$  corresponds to a normalized EMLP discriminator. Both discriminators feed a second order loop filter.

A list of parameters of interest that are used for the precise tracking is given in Table 5-2. Parameters values are different from values of typical receivers. More specifically, in typical receivers:

- correlator spacing's are smaller to limit the impact of the multipath and track the signal with high amplitude correlator outputs,
- $B_{DLL}$  are close to 1 Hz and
- $B_{PLL}$  are close to 10 Hz.

Because of the use of high-gain antennas and the observation of signals with high  $C/N_0$ , tracking parameters were adapted to collected signals.

## 5. Nominal distortions

	GPS L1 C/A	GPS L5 Q	Galileo E1C
$T_{int}$	1 ms	1 ms	4 ms
Correlator spacing	$1 T_c$	$1 T_c$	$0.5 T_c$
$B_{DLL}$	5 Hz	10 Hz	2 Hz
$B_{PLL}$	20 Hz	30 Hz	10 Hz

**Table 5-2.** Tracking parameters used in the setup.

### 5.1.2.3 CDO and correlator outputs estimation

The CDO and correlator outputs are estimated in parallel to the PLL/DLL signal tracking. Algorithms to estimate both observables are described in section 4.5.2 and in section 4.5.3. To avoid too long simulations, the strategy is to save CDO and correlation function observables and to post-process outputs to evaluate nominal distortions that affect signals. In results presented in the following, the CDO is built on one thousand delay bins, and eight hundred and one correlator outputs are derived.

A particular care was taken to estimate and save CDO and correlator outputs after the convergence of the PLL and DLL tracking processes (steady state).

## 5.2 Chip observation from high-gain dish measurements

The CDO is described in section 4.5.2 and is used in this section to assess nominal distortions which affect signals collected from high-gain dish antennas presented in the previous section. GPS L1 C/A and Galileo E1C signals are processed and results are compared to the state-of-the-art (when available).

### 5.2.1 GPS L1 C/A

Two types of nominal distortions were observed on GPS L1 C/A signals in previous studies (as described in 4.1.1.3). Nominal distortions are generally classified into analog (ringing phenomenon) and digital distortions (delay between rising and falling transitions zero-crossings). Results provided in this part were obtained with a 4-second observation time.

#### 5.2.1.1 Ringing phenomenon

Figure 5-1 illustrates the average on 4-second of rising and falling PRN transitions for several PRNs collected by antennas located at Leeheim (DLR) and Toulouse (CNES).

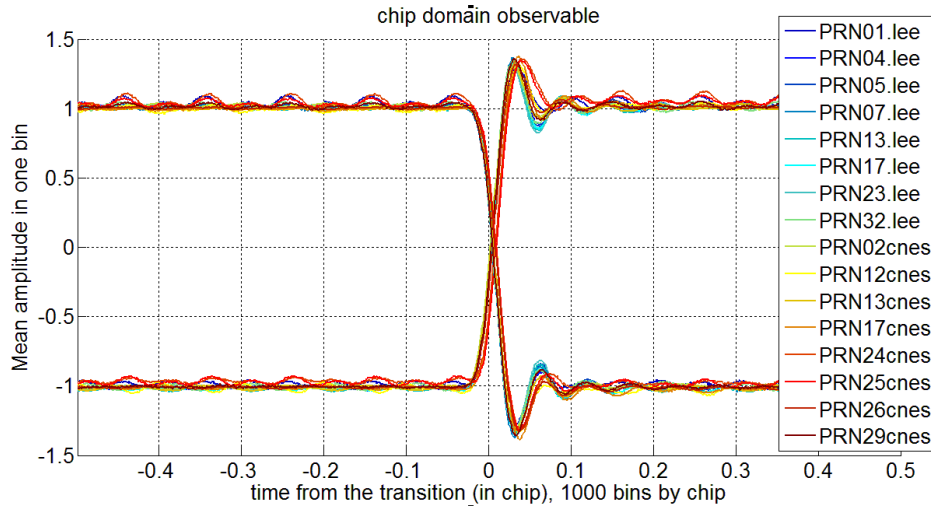


**Figure 5-1.** Chip domain observable of rising and falling transitions, 1000 bins/chip, GPS L1 C/A.

Analog parameters are difficult to estimate because no model is perfectly representing the observed ringing effects. Nevertheless, same ringing distortion features as in Figure 4-3 or in [Phelts et al., 2009] are visible. Especially, it is noticeable that the ringing frequency is approximately equal to 20 MHz.

Table 5-3 gives results obtained from the collected data considering the four parameters defined in 4.1.1.3.2 to characterize nominal distortions.

	State-of-the-art (overbound)	Obtained results
Maximum first peak overshoot ratio (chip amplitude)	35 %	39 %
Maximum rise time (ns)	25	16
Maximum peak time (ns)	45	33
Maximum settling time (ns)	180	85

**Table 5-3.** Comparison of nominal distortion parameters for GPS L1 C/A signal.

In appendix D, values of these four parameters are given for each PRN.

The values of three over the four parameters that were estimated in [Phelts et al., 2009] (column state-of-the-art of Table 5-3), are higher than values obtained in this study. It is consistent with the fact that in [Phelts et al., 2009], an overbound for the four parameters was looked for, and a margin was taken to ensure that all nominal distortions are enclosed within the overbounds. Only the first peak overshoot ratio exceeds the limit of 35 %.

It is noticeable that the data collection setup (different antennas, digitizers, signals, etc.) also has an impact on the four estimated parameters.

#### 5.2.1.2 Delay between rising and falling transitions

The digital parameter is easier to evaluate than ringing phenomenon parameters. Moreover, the digital parameter can be easily assessed from the CDO. As defined in 4.1.1.3.1, this parameter corresponds to the difference existing between the zero-crossing of rising and falling transitions. The estimation of

this delay was performed for several satellites and compared with Stanford University's outcomes [Wong et al., 2010].

Figure 5-2 shows that obtained delays are consistent with Stanford University's results [Wong et al., 2010]. These similarities are observed with the data from CNES and DLR. Therefore, it shows that digital nominal distortions are relatively constant over time and that these characteristics are not dependent upon the receiver. It tends to confirm that the satellite is at the origin of such a distortion.

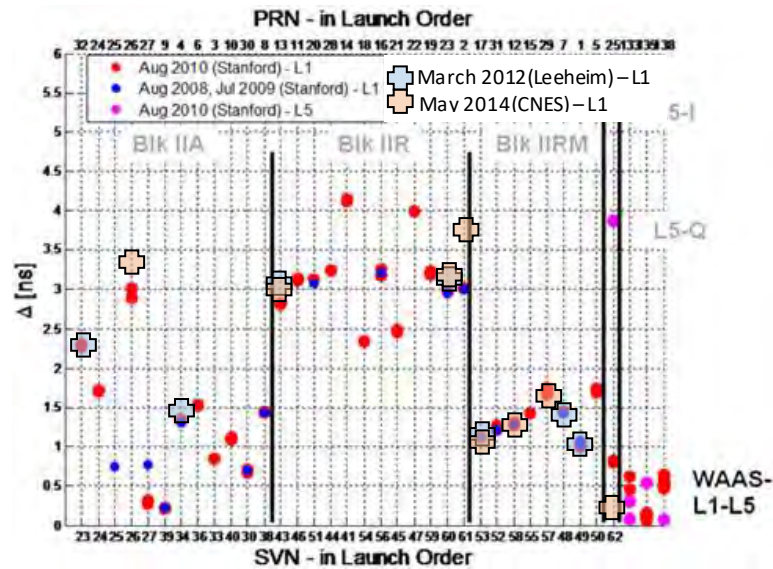


**Figure 5-2.** Superposition of results from Stanford University [Wong et al., 2010] with results obtained by another set of collected data (Leeheim and CNES). Visualization of the delay between rising and falling transitions.

### 5.2.2 Galileo E1C

No specific SiS distortions were observed on Galileo E1C signals until now. The delay between rising and falling transitions is relatively small (see 4.1.1.3.2) and no chip domain observables estimated from Galileo E1C signals collected with high-gain dish antenna are available in the literature.

Figure 5-3 shows the chip shape estimated with the data collected from the ESA's antenna. The CDO is assessed for three different PRNs: PRN 18 (FOC-FM1), PRN 14 (FOC-FM2) and PRN 22 (FOC-FM4). Continuous lines correspond to the mean (on 800 ms) of positive chips and dashed lines to the mean of negative chips. The PRN 18 was collected in March 2015 whereas PRN 14 and PRN 22 were collected the same day in September 2015. Several results can be noticed:

- Distortions on PRN 14 and PRN 22 are similar whereas distortions on PRN 18 are different from the two others. The origin of these differences is unknown. It could come from the satellite payload but more likely from the acquisition setup. Even if the same instruments were used for the three data collections, a difference in the experimental setup parametrization (antenna, acquisition chain, digitizer, temperature) could explain the differences between the collections.
- Even if it is not possible from these plots to distinguish distortions caused by the satellite and distortions caused by the receiver, a ringing effect approximately equal to 24 MHz is observed on all signals.

- A “pre-ringing” phenomenon is visible before transitions (on the  $BOC(6,1)$  as well as on the  $BOC(1,1)$  component). This kind of phenomenon has already been observed on high-gain dish antenna collected data or/and on data collected by receivers with RF front-end equipped with a SAW filter [Gunawardena and Van Graas, 2014]. More likely, the “pre-ringing” phenomenon is induced by the receiver.
- On PRN 18,  $BOC(6,1)$  component is not centered on the amplitude of  $\pm 1.5$ . The phenomenon is especially visible on the second half of the chip and corresponds to a  $BOC(1,1)$  component distortion signature. The source of this distortion is unknown. Even if it is doubtful, it cannot be excluded that this distortion is generated at satellite level.

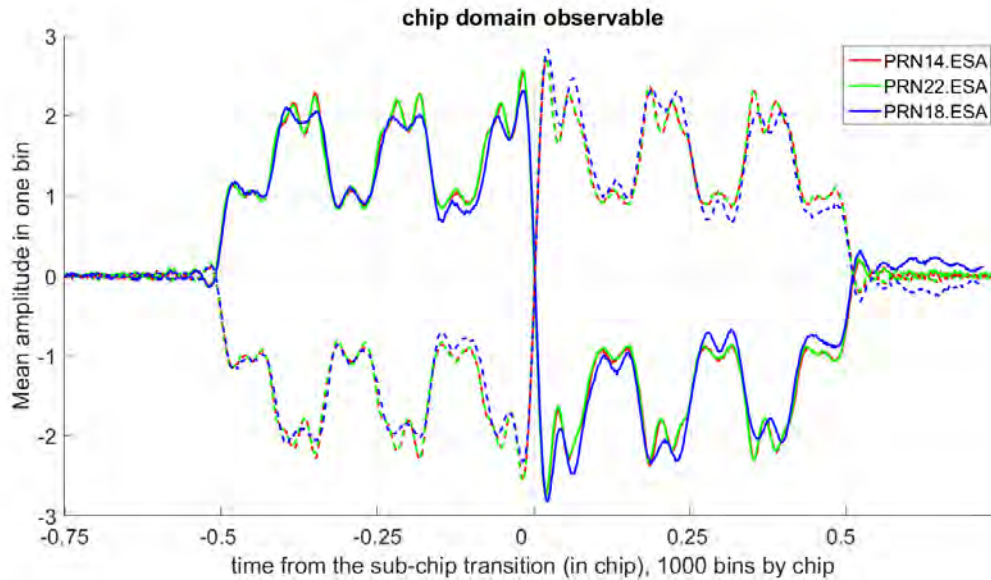


**Figure 5-3.** Chip domain observable on positive and negative chips, 1000 bins/chip, Galileo E1C.

The zero-crossing difference between rising and falling edges is smaller than 0.1 ns for the three collected signals which is consistent compared to the state-of-the-art ([Thoelert et al., 2014] and [Gunawardena et al., 2015]).

### 5.3 Correlation function observable from high-gain dish measurements

After looking at nominal distortions that affect high-gain dish measurements using the CDO, the impact of these distortions at a different receiver processing level is envisaged. The correlation function observable is described in 4.5.3 and is used in this section to assess nominal distortions which affect the collected signals. The S-curve zero-crossing observable, estimated from the correlation function is also introduced. GPS L1 C/A and Galileo E1C signals are processed and results on GPS L1 C/A are compared to the state-of-the-art. The advantage of the correlation function and the S-curve observables is that they are the last processing step before estimating pseudorange.

To reduce the standard deviation of the noise affecting the observable, the received signal is correlated with a local replica over a long observation time (including non-coherent summations).

### 5.3.1 GPS L1 C/A

Correlator outputs shown in this part were obtained with a 4-second observation time.

#### 5.3.1.1 Impact on the correlation function

As nominal distortions have a small amplitude, they cannot be observed in a straightforward manner on the correlation function. It is necessary to subtract the ideal correlation function to the distorted one. The normalization of the ideal correlation function is of primary importance when looking at distortions affecting the correlation function observable. The definition of the ideal correlation function that is used in this manuscript is exposed below.

For GPS L1 C/A signals eight hundred and one correlator outputs are visualized and are described as:

$$corr\_out_{L1\_C/A}(k) \text{ with } k = 1:1:801$$

The maximum of the correlation function is equal to one and is reached for  $k_{max}$  which is not necessarily equal to four hundred and one because slight tracking errors (entailed by correlation function distortions) can affect measurements.

The slopes of the rising and the falling edges are estimated by:

$$slope_{rise} = \frac{corr\_out_{L1\_C/A}(k_{max} - 100) - corr\_out_{L1\_C/A}(100)}{(k_{max} - 200)} \quad (5-3)$$

$$slope_{fall} = \frac{corr\_out_{L1\_C/A}(k_{max} + 100) - corr\_out_{L1\_C/A}(700)}{(600 - k_{max})} \quad (5-4)$$

Correlator outputs located near the prompt and at  $\pm 1 T_c$  of the prompt of the correlation function are not considered to normalize slopes of the ideal correlation function. Indeed, it allows not to take into account in the normalization areas where the correlation function is strongly distorted (typically rounded by the RF front-end).

Then, two indexes  $k_1$  and  $k_2$  are defined as follows:

$$k_1 = first_k(corr\_out(k) > 0.5) \quad (5-5)$$

$$k_2 = last_k(corr\_out(k) > 0.5) \quad (5-6)$$

Finally the ideal correlation function is defined in two segments:

$$\begin{aligned} & corr\_ideal\_L1\_C/A(k) \\ &= \begin{cases} slope_{rise} \times (k - k_1) + corr\_out_{L1\_C/A}(k_1) & \text{for } k = 1:1:k_{max} \\ slope_{fall} \times (k - k_2) + corr\_out_{L1\_C/A}(k_2) & \text{for } k = k_{max}:1:801 \end{cases} \quad (5-7) \end{aligned}$$

The ideal correlation function is not filtered.

Figure 5-4 shows the real part of the difference between the ideal correlation function and the one affected by nominal distortions for the different GPS L1 C/A collected signals.

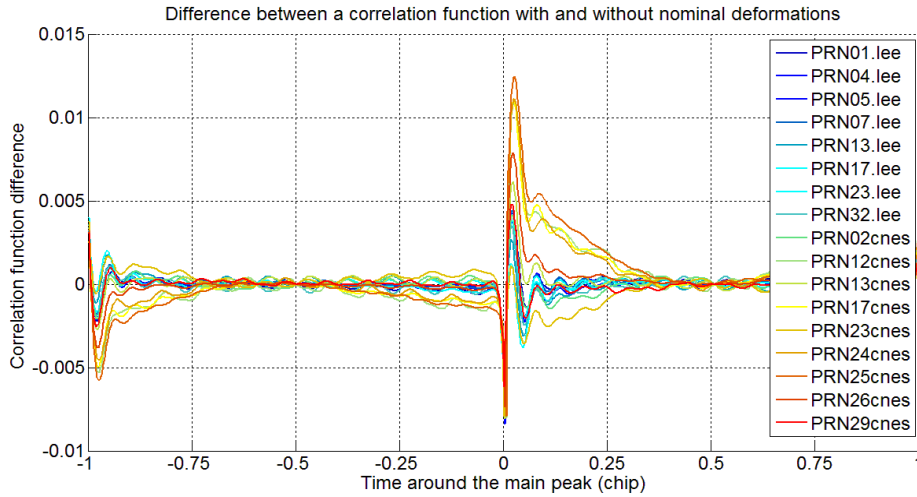


**Figure 5-4.** Difference between correlation functions affected by nominal distortions and the ideal unfiltered correlation function. GPS L1 C/A.

It is noticeable that these distortions cannot be considered or even approached by second order oscillations contrary to results established in the chip domain (see 4.1.1.3.2). Moreover, for some plots obtained from the CNES data, in addition to the ringing effect, a low frequency bending of the correlation function is strongly visible. This phenomenon is discussed later.

This kind of plot cannot be used directly to estimate tracking biases affecting a user. Indeed, depending on the normalization of the ideal correlation function involved in the computation of the correlation distortion difference, the plot will change. Here, the normalization is realized at  $-0.5$  and  $0.5$  chip (it explains that correlation function differences are equal to zero at  $-0.5$  and  $0.5$  chip from the prompt) and no filtering is applied on the ideal function. Therefore, Figure 5-4 only gives an idea of the distortion pattern. These results match with the study performed in 2012 by CNES [Lestarquit et al., 2012].

#### 5.3.1.2 Impacts on the S-curve and the tracking error

S-curves were obtained considering an EMLP discriminator. The analysis of the S-curve zero-crossing function of the correlator spacing is a second approach to visualize the correlation function distortion from a measurement point of view. Indeed, assuming that the DLL has time to converge, the zero-crossing of the S-curve translates directly into a pseudorange bias. It is recalled that on a S-curve the tracking error is given as a function of the correlator spacing  $CS_k$ .

In the present case, the tracking error is expressed relatively to a reference tracking error. This makes sense as it is difficult to assess the tracking bias due to a signal distortion directly (the actual tracking bias is also affected by other RF front-end characteristics, such as the group delay). This computed differential tracking bias is directly convertible into a differential pseudorange error by multiplying it by the speed of light (because an EMLP discriminator is used). The EGNOS and WAAS reference receiver characteristics are close. In particular, these reference receivers use an Early-Late spacing of  $0.1$  chip which is used as a reference to plot the S-curve zero-crossing.

Figure 5-5 shows the differential tracking bias induced by nominal distortions for each correlator spacing between  $0$  and  $1T_c$  with respect to the reference tracking configuration for the data collected at Leeheim and the data collected by CNES. These results can be compared to Stanford University's



outcomes presented in [Wong et al., 2011] with one difference. Indeed the technique introduced in [Wong et al., 2011] is slightly different from the strategy used in this document to estimate the S-curve zero-crossing function.

Here, we compute the differential tracking error observed by a correlator pair  $k$  considering that the tracking is performed by these correlator outputs (it means  $I_k - I_{-k} = 0$  for each  $k$ ). The differential tracking error is then the difference between the tracking error obtained for the reference correlator pair and the tracking error obtained for the correlator pair  $k$ .  $k$  tracking processes have to be repeated.

In the study of Stanford University, the differential tracking error observed by a correlator pair  $k$  is deduced from the difference of height between the two correlator outputs of the pair  $k$  ( $I_k - I_{-k} = \varepsilon_{CS_k}$ ) on a correlation function tracked by the reference tracking pair (only the reference tracking pair satisfies  $I_k - I_{-k} = 0$ ). One tracking process is sufficient and has to be performed considering only the reference tracking pair.

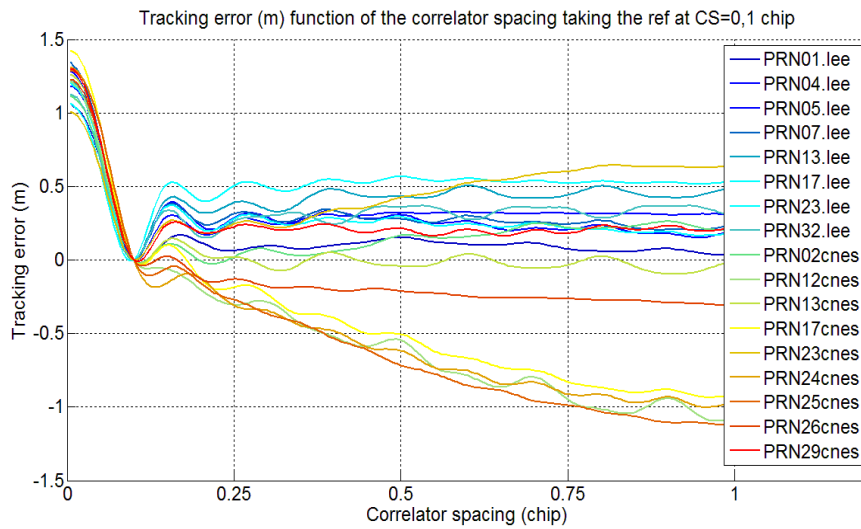


**Figure 5-5.** Tracking error function of the correlator spacing for different GPS L1 C/A PRNs (reference at  $CS = 0.1$  chip).

Looking at the results obtained from the data collected at Leeheim, Figure 5-5 complies with differential tracking bias plots that have been published in [Lestarquit et al., 2012]. However, important negative slopes can be observed on these plots for some data from CNES. A deeper comparison of results obtained from both antennas (CNES and DLR) is introduced later.

Differences between plots are noticeable regarding some CNES data with opposite low frequency bending (deviation of the tracking error toward negative values rather than positive values). Nevertheless, the data from Leeheim lead to similar shape of differential tracking bias curves to the results presented in the Stanford University's study [Wong et al., 2011] and recalled in Figure 4-12. It is noticeable, that differential tracking biases reported by Stanford University are going from 0 m to 1.2 m compared to values going from 0 m up to 0.5 m obtained with the data from Leeheim.

The difference between the CNES and DLR's data sets does not come from:

- *The satellite PRN:* three PRNs (13, 17 and 23) were recorded by both antennas and for the same PRN, results are different depending on the antenna.
- *The day period:* the data collected at Leeheim were recorded at different periods of the day but similar behaviors are observed whatever the data collection is.



- *The signal post-processing*: the same software was used to process all signals and obtain correlation function outputs.

The difference between the CNES and DLR's data sets can comes from:

- *The antenna*: a different antenna was used at Toulouse (CNES) and at Leeheim (DLR).
- *The digitizer*: even if the same digitizer was utilized for both collections, it cannot be excluded that an experimental setup parametrization difference between both collection sets leads to different signal distortions on the correlation function. Indeed, from the CDO on Galileo E1C signals, using the same antenna and the same digitizer, differences were observed between different collections.
- *The location of the antenna and the period of the data collection*: it cannot be excluded from these plots that differences are caused by the period of the data collection and the location of the antenna. Indeed, signals were collected in 2012 at Leeheim and in 2014 at Toulouse. The signal distortion and by consequence the correlation function distortion could vary depending on the time and the location of the data collection. Nevertheless it is important to look at the consistency of results obtained from the data collection performed at Leeheim compared to differences that affect results obtained from the data collection made at Toulouse. The period of the data sets and the location of the antenna could justify different results obtained from the two data collections but cannot entirely justify differences that are observed among data collected at the same location, at Toulouse. It is seen later that the main contribution of the reported low frequency bending of the S-curve zero-crossing plots affecting differently signals collected by the CNES is caused by the antenna and/or the digitizer as it was already noticed in [Wong, 2014].

A part of the difference of signal distortions that affects signals collected by CNES are necessarily caused by the antenna and/or the digitizer. Most probably, a problem in the antenna and/or digitizer calibration is at the origin of these differences, already obtained in the state-of-the-art, as exposed in [Wong, 2014]. It can explain the fact that at ESA, different signal distortions were observed on Galileo E1C signals while the same antenna and digitizer configurations were used.

#### 5.3.2 Galileo E1C pilot component

After observing nominal distortions on GPS L1C/A signals collected with high-gain dish antennas, the same approach is used on Galileo E1C signals. Results proposed in this part were obtained with a 1-second observation time. Results on PRN 18 are not presented because from the CDO, the data collection on PRN 18 cannot be trusted.

##### 5.3.2.1 Impact on the correlation function

For Galileo E1C signal, the ideal correlation function that is subtracted to the nominal one is normalized differently than for GPS L1 C/A. The presence of the  $BOC(6,1)$  component makes more difficult the slope normalization. As for GPS L1 C/A, eight hundred and one correlator outputs are visualized and are described as:

$$corr\_out_{E1C}(k) \text{ with } k = 1:1:801$$

## 5. Nominal distortions

The ideal correlation function is simply an ideal unfiltered  $CBOC(6,1, 1/11)$  /  $BOC(1,1)$  correlation function built from eight hundred and one points and with its maximum obtained for  $k_{max}$ .

The maximum of the correlation function is reached for  $k_{max}$  which is not necessarily equal to four hundred and one.

Figure 5-6 shows the real part of the difference between the ideal unfiltered correlation function ( $corr\_out_{E1C}$ ) and the one affected by nominal distortions.

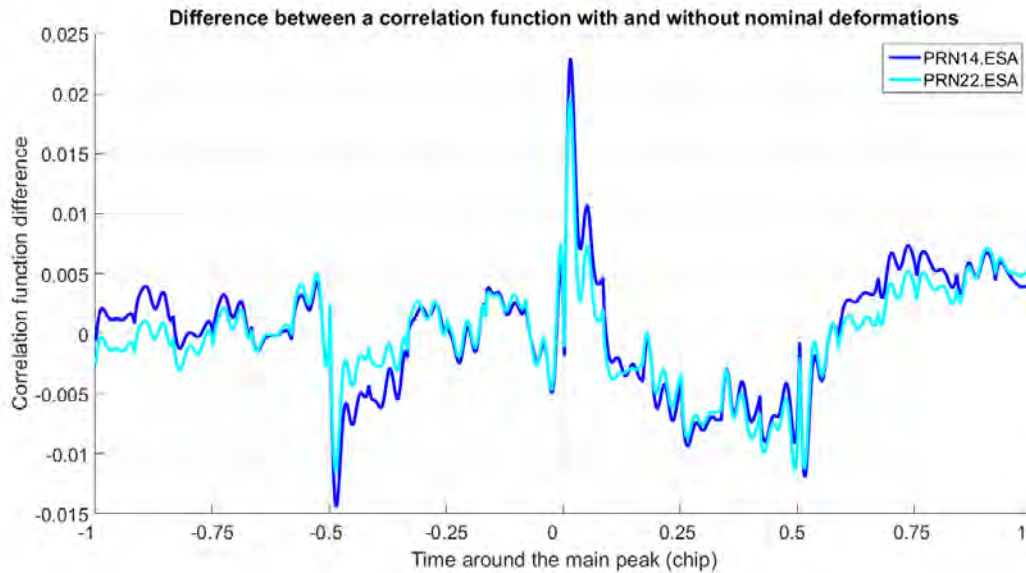


**Figure 5-6.** Difference between correlation functions affected by nominal distortions and an ideal unfiltered correlation function. Galileo E1C.

From Figure 5-6 three main results are noticeable:

- Ringing phenomenon affects the correlation function and the frequency of the oscillation is approximatively equal to 24 MHz as seen with the CDO.
- At  $-0.5$ ,  $0$  and  $0.5 T_c$  from the prompt, steps are present. This phenomenon is linked to the fact that the ideal correlation function is not exactly normalized as the distorted correlation function. Such distortions can be induced by the filtering of the  $BOC(1,1)$  component on the signal affected by nominal distortions.
- A high slope affects the correlation function between  $0$  and  $0.25 T_c$ .
- Discontinuities appear at “ $BOC(6,1)$  correlation function peaks”, it means for delays from the prompt equal to  $\pm 0.08$ ;  $\pm 0.17$ ;  $\pm 0.25$ ;  $\pm 0.33$ ;  $\pm 0.42$ ;  $\pm 0.58$ ;  $\pm 0.67$ ;  $\pm 0.75$ ;  $\pm 0.83$  and  $\pm 0.92 T_c$ . Discontinuities are more or less visible and are caused by a change of the correlation function slope and/or a slight error in the normalization of the ideal correlation function that does not match the distorted correlation function. Such distortions can be induced by the filtering of the  $BOC(6,1)$  component on the signal affected by nominal distortions.

It was seen from some GPS L1 C/A collected signals that a distortion can be induced by the receiver in addition to nominal distortions generated by the satellite. The drawback of high-gain antenna measurements is that the distortions induced by the receiver cannot be distinguished from the distortions generated by the satellite because only one signal can be collected at a given time. One advantage of Galileo E1 signals collected with high-gain dish antenna is that two components are available: E1C and E1B. Since antenna and/or digitizer effects will distort both components in the same

way, making the difference between distortions that affect the E1C component and distortions that affect the E1B component will remove the common distortions due to the receiver front-end. The problem is that with this approach, a distortion generated at payload level with a similar impact on both components is also removed.

Figure 5-7 gives difference between the ideal and the distorted correlation functions for Galileo E1C and Galileo E1B for one signal (PRN 14).

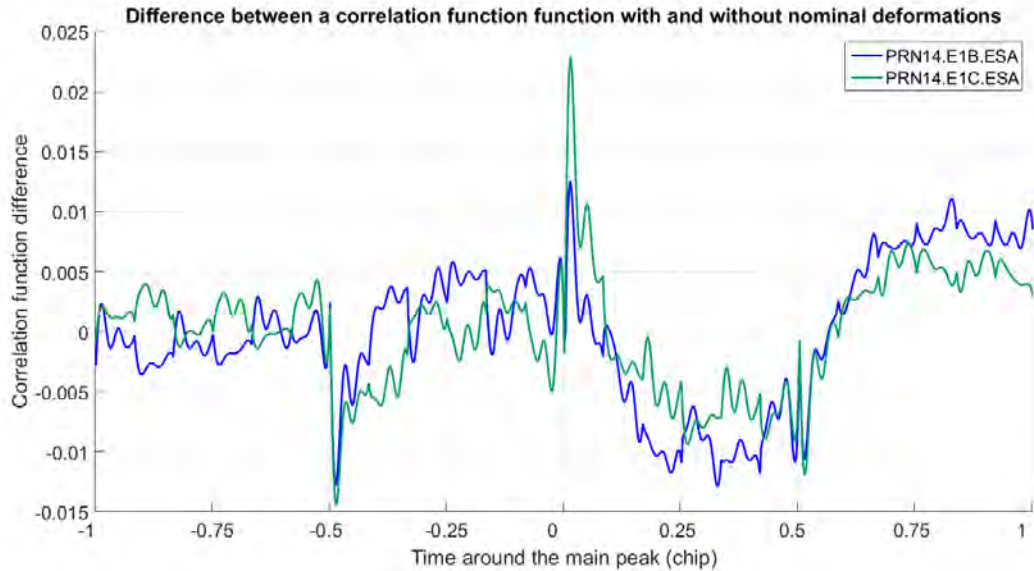


**Figure 5-7.** Difference between correlation functions affected by nominal distortions and an ideal unfiltered correlation function. Galileo E1C and E1B. (PRN 14 only)

Figure 5-8 shows the difference between the correlation function distortion on the E1B component and on the E1C component. Compare to nominal distortions visible on Figure 5-6, on Figure 5-8 it is noticeable that:

- High slope which affects the correlation function between 0 and  $0.25 T_c$  is removed. More generally the amplitude of the distortion is lower because distortions that affect in the same way both components are removed.
- Discontinuities caused by the  $BOC(6,1)$  are enhanced because E1C modulation consists in the subtraction of the  $BOC(6,1)$  component whereas E1B modulation consists in the addition of the  $BOC(6,1)$  component.
- A low frequency phenomenon of 1 MHz is clearly visible and corresponds to a distortion which affects in different way the E1B and the E1C components.

Using the two E1 components to estimate distortions that affect a Galileo E1 signal permits to remove distortions that have the same effect on Galileo E1C and Galileo E1B components. In particular it permits to reduce the amplitude of nominal distortions. Nevertheless, two problems remain with this strategy:

## 5. Nominal distortions

- Distortions induced by the satellite and having the same effect on E1B and E1C components are removed (if they exist).
- Distortions induced by the receiver and having different effects on E1B and E1C components are still present (if they exist). By consequence, it is not possible to distinguish distortions introduced by the satellite and by the receiver.

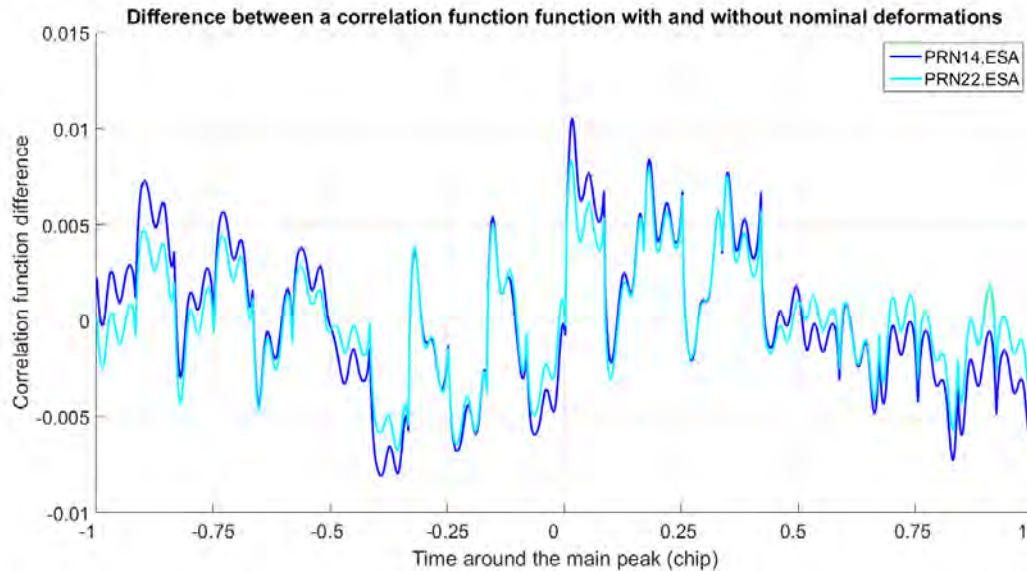


**Figure 5-8.** Difference between nominal distortions on the correlation functions of the E1C and the E1B components.

### 5.3.2.2 Impacts on the S-curve and the tracking error

Figure 5-9 shows the differential tracking bias generated by nominal distortions for each correlator spacing between 0 and  $0.75 T_c$  with respect to the reference tracking configuration for the data collected at ESA. The correlator spacing of the reference is fixed to  $0.25 T_c$ .

From Figure 5-9 it can be seen that around the prompt the differential tracking error varies rapidly for correlator spacing's smaller than  $0.25 T_c$ . For instance, a user who tracks the Galileo E1C PRN 14 with a correlator spacing equal to  $0.1 T_c$  will be affected by a differential error equal to 0.8 m relatively to a user who tracks the same signal with a correlator spacing equal to  $0.15 T_c$ . The phenomenon is also visible with less amplitude on GPS L1 C/A signal. It means that around the correlation function peak, the correlation function is slightly asymmetric. The signal distortion which entails the asymmetry can come as well from the satellite as from the receiver (antenna, digitizer, etc.). From proposed results, it is not possible to isolate the distortion induced by the satellite and the one induced by the receiver.

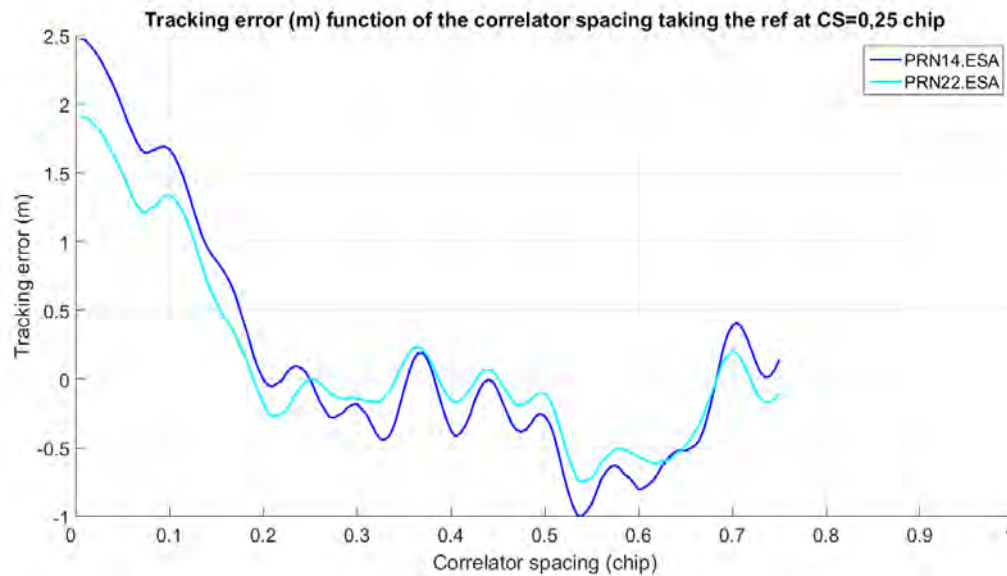


**Figure 5-9.** Tracking error function of the correlator spacing for different Galileo E1C PRNs (reference at  $CS = 0.25$  chip).

As a matter of fact the S-curve zero-crossing is closely related to the distortion which affects the correlation function on Figure 5-6. By comparing carefully Figure 5-6 and Figure 5-9, plots have similar behaviors but a factor approximatively equal to one hundred has to be applied. By analogy, high differential error variations observed for reference receivers with a tight correlator spacing (below  $0.25 T_c$ ) are induced by the distortion visible between 0 and  $0.25 T_c$  on the correlation function. It can be expected that if this distortion, close to the prompt, is removed from the measurement (better calibration of the antenna, use of a measurement based on E1B and E1C, etc.), the differential error should not be so high for differential Galileo E1C users with tight correlator spacing.

## 5.4 Conclusions and problems related to the observation of nominal distortions with high-gain dish antennas

Three powerful tools were used to observe nominal distortions from high-gain dish antenna data collections:

- the CDO,
- the correlation function and
- the S-curve zero-crossing.

Results presented in sections 5.2 and 5.3 were obtained from data collected with high-gain dish antennas. One problem of these data collections and that has already been discussed in 4.1.1.2 is that the calibration of the measurements is difficult. The consequence is that it is not possible to isolate the nominal signal distortion generated by the satellite and the distortion induced by the receiver. When looking at Figure 5-4 and Figure 5-6 it is clearly visible that an additive low frequency bending affects the correlation function and the S-curve zero-crossing plot for some collected GPS L1 C/A and Galileo E1C PRNs. The phenomenon is observed with the data collected at ESA and the data collected by the CNES whereas nothing is visible on data collected at Leeheim. By consequence, it seems that the general bending of the correlation function is caused by the receiver (antenna and/or digitizer).

## 5. Nominal distortions

To explain the difference between correlation functions obtained from the data collected by CNES, it has been shown in the literature that the correlation function distortion can be different depending on the period of the day of the data collection if the antenna is not perfectly calibrated [Wong, 2014]. Consequently, a possible explanation of the consistency between data collected with the German administration antenna is that a better calibration was put in place on this antenna to collect measurements.

To explain the difference between results obtained from data collected by CNES and by the German administration antenna, a comparison is proposed to visualize in a better way the difference between data collected by the two antennas at two different epochs and at two different locations. Results obtained from one PRN (PRN 13) collected by the DLR (March 2012) and by the CNES (May 2014) are shown together.

Figure 5-10 puts forward the comparison at the correlation function level of nominal distortions that affect signals from the two data collections.

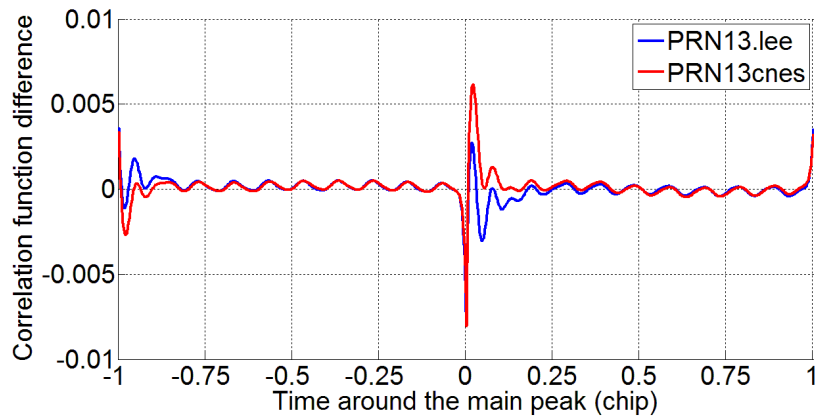


**Figure 5-10.** Comparison of nominal distortions for the same PRN making the difference of correlation functions with and without nominal distortions. In red, data were collected by the CNES, in blue, by the DLR.

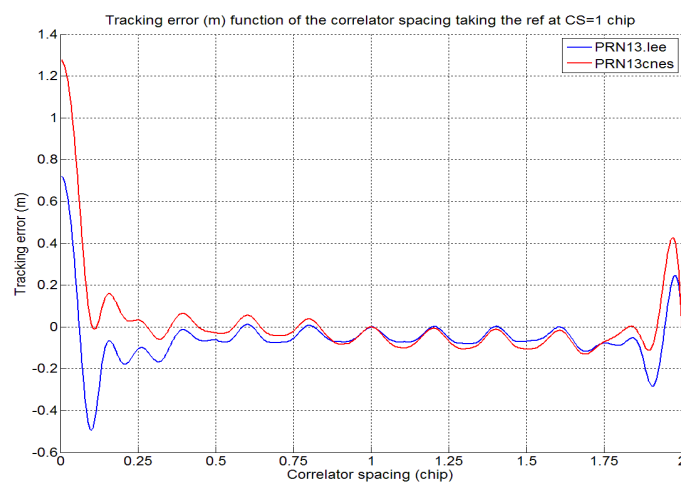


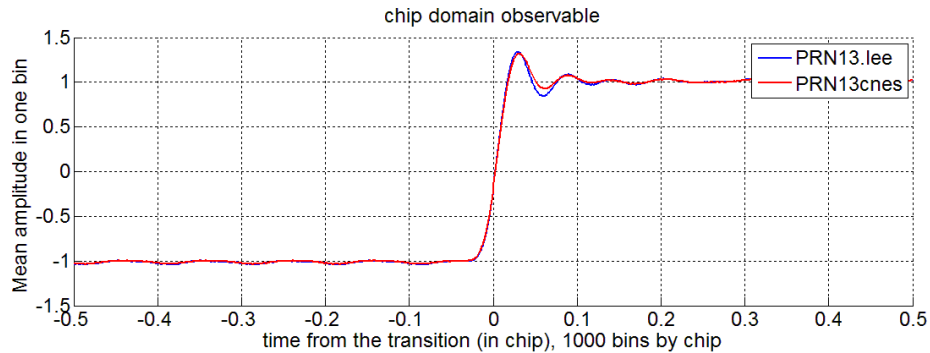
**Figure 5-11.** Comparison of differential tracking biases entailed by nominal distortions for the same PRN (reference at  $CS = 1$  chip).



### 5.5 Nominal differential tracking errors studied from an omnidirectional antenna and inter-PRN biases

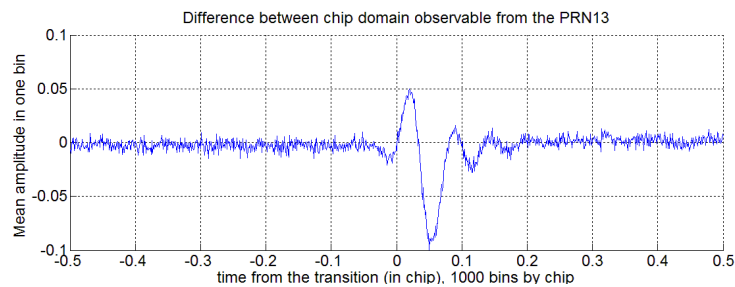
It is interesting to notice that nominal distortion ringing effects look very similar for both scenarios at a distance higher than  $0.25 T_c$  from the prompt (especially from the Figure 5-10). However, from the Figure 5-11 which shows the S-curve zero-crossing obtained from the two data collections, it appears that the general low frequency bending of the two differential tracking bias plots is slightly different.

Figure 5-12 illustrates the impact of nominal distortions on the CDO.



**Figure 5-12.** Chip domain comparison of nominal distortions for the same PRN.

In order to visualize differences between these two curves estimated in the chip domain, Figure 5-13 represents the difference between them.



**Figure 5-13.** Difference between chip domain observables obtained from the same PRN.

The only remarkable difference appears at the transition level. This variation could be the signature of a filtering phenomenon. The origin of such filtering can come from the satellite filter, the time of the data collection, the location of the antenna but more likely from the receiver antenna.

To conclude, results obtained from high-gain dish antenna measurements are useful to understand nominal distortions but have to be interpreted carefully, especially because of antenna calibration problems. To solve the calibration issue, a second way to look at the impact of nominal distortions is to analyse data collected from an omnidirectional antenna.

## 5.5 Nominal differential tracking errors studied from an omnidirectional antenna and inter-PRN biases

It was seen that the distortion and more precisely the general low frequency bending of the correlation function and the S-curve zero-crossing plot may varies depending on the collected signal. This phenomenon makes the characterization of nominal distortions difficult, especially the signal distortion component generated at payload level.

Nevertheless, this section shows that even if the bending is time-dependent, all PRNs are affected by the same bending at the same time. This phenomenon is difficult to see with a directional antenna when only one signal is collected at a given time. However, with measurements obtained from an omnidirectional antenna, several signals can be processed at a given time and the common (low frequency bending) distortion which affects all measurements can be isolated. The inter-PRN bias is defined in this document as the difference between the tracking error affecting a PRN for a given correlator spacing and the average among PRNs of tracking errors for that correlator spacing.

The inter-PRN bias corresponds to the parameter which is effectively threatening for a receiver. Indeed the common bias to all measurements is absorbed by the clock bias.

In this section, results about the differential tracking error obtained with an omnidirectional antenna are presented.

### 5.5.1 Omnidirectional antenna measurements setup

The concept used in this dissertation to process omnidirectional antenna measurements is different from the one to process high-gain dish antenna measurements. Signals collected by the omnidirectional antenna are already partially processed and thirteen correlator outputs are provided instead of raw signals. The data were collected by Capgemini at Bayonne (France) with an Aero-Antenna AT2775 - 100 patch antenna with a choke-ring to limit the multipath and a radome. The antenna is 13.75 cm high (including the radome) and 14 cm large (including the choke-ring). The antenna bandwidth is equal to 28 MHz centered on the L1 frequency. Correlator outputs were obtained from a WAAS Novatel G-III reference receiver with an equivalent RF front-end bandwidth equal to 24 MHz. In our case, the thirteen correlator outputs are available. They are estimated based on a 1 s integration time over a 1 h period.

Three sets of data were collected at different times in order to check the repeatability of the observed distortion according to the time of the day:

- **Data set 1** TOW: 322217 s, the 18/02/2015 (from 18h30 to 19h30)
- **Data set 2** TOW: 235816 s, the 17/02/2015 (from 18h30 to 19h30)
- **Data set 3** TOW: 135139 s, the 09/02/2015 (from 14h30 to 15h30)

The fact to have access to a few number of correlator outputs makes harder the visualization of distortions which affect the correlation function. In addition, some chip domain outputs are provided by the Novatel G-III receiver, but because of the limited number of outputs (thirteen), the signal distortion at chip level is not investigated. Only the S-curve tracking error plots are estimated.

### 5.5.2 Data set 1 results and introduction of the inter-PRN bias

Plots in Figure 5-14 are similar to results obtained from the high-gain dish antenna for GPS L1 C/A signals on Figure 5-5 but only few points are available and the concept to estimate these points is slightly different. Indeed, Figure 5-14 does not strictly represent the S-curves zero-crossing. The nuance is the same as described in section 5.3.2.1 and, on Figure 5-14, the concept used in [Wong et al., 2011] is applied.



### 5.5 Nominal differential tracking errors studied from an omnidirectional antenna and inter-PRN biases

The tracking is performed one time considering a reference correlator spacing equal to  $0.1 Tc$  and an EML discriminator ( $D_{EML} = (I_E - I_L)/2$ ). Points plotted for different  $CS_k$  which are shown in Figure 5-14 correspond to the EML discriminator outputs obtained from correlator outputs of the pairs  $k$ . It means that it corresponds to the delay error estimated by a receiver with a correlator spacing  $CS_k$  in the particular configuration of a correlation function tracked by the reference correlator spacing  $CS = 0.1$  chip. Nevertheless, if the amplitude of the distortion is small compared to the correlation function amplitude, the EML output amplitude, multiplied by  $c$  (the speed of light), is approximatively equal to the differential tracking error between a receiver using  $CS_k$  and a receiver using  $CS = 0.1$  chip. In this chapter about nominal distortions, the value of  $D_{EML} \times c$  estimated for different  $CS_k$  is considered as the differential tracking error that affects a correlator output pair  $k$  compared to the reference tracking pair.

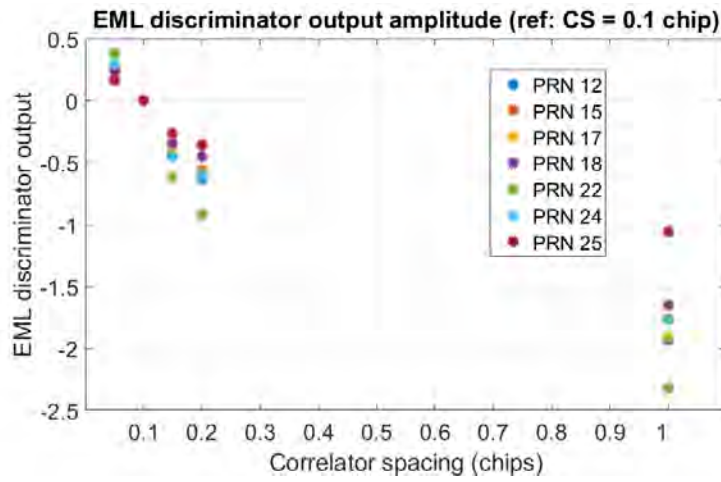


**Figure 5-14.** EML discriminator outputs multiplied by  $c$  (reference  $CS$  at  $0.1$  chip) recorded with an omnidirectional antenna and process by a NovAtel GIII receiver.

A strong low frequency bending is observed on the differential tracking error plots. The tracking error behavior is similar to results obtained from data collected by the CNES with the high-gain dish antenna. The advantage of omnidirectional measurements is that several signals are observed at the same time and a general behavior appears on all PRNs.

To underline the fact that all PRNs are affected by a common bias, another representation is given in Figure 5-15. Considering that the user operates with a correlator spacing equal to  $1 Tc$ , the differential tracking error is estimated during one hour from correlator outputs averaged over one minute.

Even if the differential errors are around  $-2$  m, the inter-PRN biases which affect the user are smaller.

Table 5-4 gives the averaged inter-PRN bias for the different PRNs, considering a user who tracks signals with a correlator spacing equal to  $1 Tc$  and a reference with a correlator spacing equal to  $0.1 Tc$ . Satellites elevations are also provided because it is noticeable that a link exists between the inter-PRN bias and the satellite elevation.

Two sky-plots are also shown in Figure 5-16. On the left it corresponds to the sky-plot at the beginning of the data collection and on the right to the sky-plot at the end of the data collection.

## 5. Nominal distortions

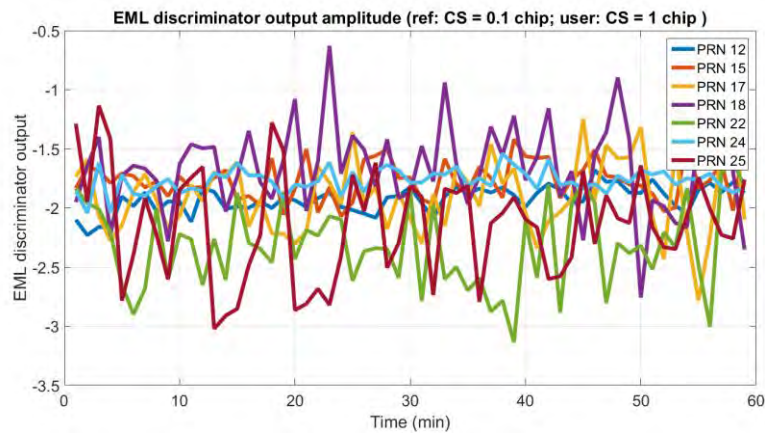


**Figure 5-15.** Differential tracking errors (reference at 0.1 chip and user at 1 chip) recorded with an omnidirectional antenna and processed by the NovAtel GIII.

PRN	Satellite elevation (18h30)	Satellite elevation (19h30)	Inter-PRN bias (cm)
25	9	33	−19,3
24	67	76	15,3
12	47	74	−0,9
22	15	17	−39,4
15	65	36	15,5
17	29	18	1,8
18	28	16	26,9

**Table 5-4.** Inter-PRN biases for different PRNs with associated satellite elevations at the beginning and at the end of the data collection. (data set 1)

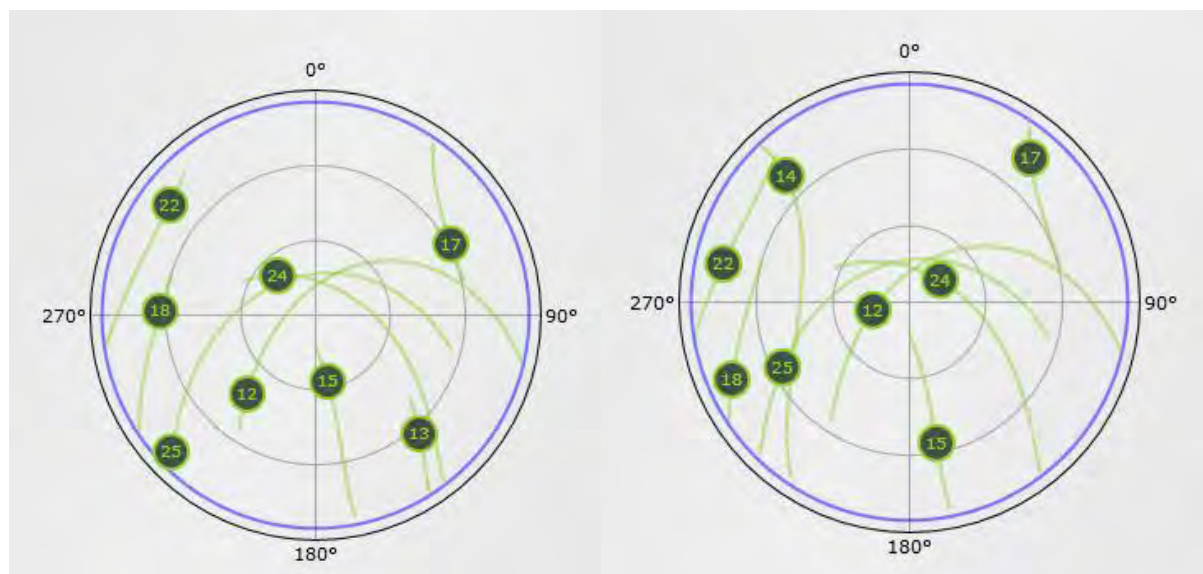


**Figure 5-16.** Sky-plots at the beginning of the data set 1 collection (left) and at the end of the data set 1 collection, 1 h after (right).

Three major results can be established from the processing of the data set 1:

- A strong common bending is observed on the S-curve zero-crossing plots. Considering a reference station operating with a correlator spacing equal to  $0.1 T_c$  and a user with a correlator spacing equal to  $1 T_c$  the average differential tracking error among all PRNs is equal to  $-1.92$  m.
- If the common bias component which affects all PRNs is removed, the remaining inter-PRN biases which effectively impact the user (because the common bias is removed in the estimated clock bias) is smaller. The inter-PRN bias runs from  $-39.5$  cm to  $26.9$  cm which is equivalent to a difference equal to  $66.3$  cm between extreme inter-PRN bias values.
- The satellite elevation seems to have an impact on the inter-PRN bias even if some exceptions are noticeable. The three highest absolute values of inter-PRN bias are obtained for the two satellites with the lowest elevation (PRN 18, PRN 22 and PRN 25). It cannot be deduced that the satellite elevation explains by itself difference of inter-PRN biases. Indeed, PRN 18 and PRN 22 are in the list of PRNs affected by strong nominal distortions. Nevertheless, it was shown in [Gunawardena, 2015] or [Haines et al., 2012] that the satellite elevation has an influence on the pseudorange natural biases (biases induced only by the distortion generated at payload level). Moreover, the increase of the inter-PRN bias measured from satellites with a low elevation can also be explained by multipath or by the GNSS receiver antenna phase delay variation and group delay variation function of the observation angle as discussed for example in [Murphy et al., 2007].

### 5.5.3 Comparison of results obtained from the three different data sets

Table 5-5 gives the inter-PRN biases obtained from the three different data sets. As for Table 5-4, it is considered that the user is operating with a correlator spacing equal to  $1 T_c$  whereas the reference station with a correlator spacing equal to  $0.1 T_c$ . Three parameters are introduced to make a comparison between results established from the three different sets:

- *The common bias*: this is the average bias that is subtracted to all PRN biases in order to only obtain the inter-PRN bias.
- *The amplitude*: this is the difference between the maximum and the minimum inter-PRN biases.

The maximum absolute inter-PRN bias for a set is underlined in red.

From Table 5-5 it can be seen that inter-PRN biases and the common bias are stable when fixing the period of the day, but for two distinct periods of the day, results are different.

Differences obtained between the two distinct periods of the day can have several origins:

- The difference of satellites sets. Even if sets were chosen randomly and seven satellites were in view during the entire period of 1 h, the presence of highly distorted signals can explain the difference. It is remarkable that PRN 18, PRN 22 and PRN 24 are in the list of signals strongly affected by nominal distortions (see section 4.1.2.2) whereas other satellites are not.
- The temperature of the antenna and the receiver at the time of the data collect.
- The consideration that the inter-PRN bias depends upon the elevation (especially because of antennas pattern).

## 5. Nominal distortions

- The multipath. Rather than the satellite elevation, the multipath is related to the state of the constellation and the position of satellites in the sky relatively to the user together with the user environment.

Most likely, the difference of satellite sets has the highest influence on the difference that is observed between set 1/set 2 and set 3 results. Nevertheless, other options cannot be excluded.

PRN	Satellite elevation (18h30)	Satellite elevation (19h30)	Inter-PRN bias (cm) data set 1	Inter-PRN bias (cm) data set 2	Inter-PRN bias (cm) data set 3
25	9	33	-19,3	-21.8	
24	67	76	15,3	16.8	
12	47	74	-0,9	3.1	
22	15	17	-39,4	-42.0	
15	65	36	15,5	19.1	
17	29	18	1,8	1.6	
18	28	16	26,9	23.2	
13	35	51			10,6
5	60	75			5,1
28	17	40			-9,4
7	46	22			-10,2
2	30	14			2,5
30	73	51			4,1
10	52	25			-6,7
Common bias (cm)			-192,2	-195,7	-237,8
Amplitude (cm)			66.3	65.2	20.8

**Table 5-5.** Inter-PRN biases for different PRNs with associated satellite elevations at the beginning and at the end of the data collection. (data sets 1, 2 and 3).

### 5.5.4 Conclusions about the observation of nominal distortions with an omnidirectional antenna

The main advantage of processing measurements collected from an omnidirectional antenna is that several signals can be observed simultaneously. A general low frequency bending affects S-curve zero-crossing plots established with data collected by Capgemini. The same phenomenon is observed on data collected by CNES with high-gain dish antenna. Nonetheless, it has been shown that the low frequency bending of the S-curve zero-crossing plots is not a signal distortion generated by the satellite but by the antenna and the receiver. With omnidirectional measurements, the bias component introduced by the antenna and the receiver can be removed by subtracting the mean value of the differential errors for a given correlator spacing to estimate the inter-PRN biases. For instance, data set 1 is considered and it is assumed that the user and the reference track the same correlation function. Considering a  $0.1 T_c$  correlator spacing at the reference level and a  $1 T_c$  correlator spacing at the user level, the maximum averaged differential error (over one hour) is equal to 2.3 m. Knowing that the distortion that is looked at is entailed in nominal conditions, the value of 2.3 m is high compared to values provided by the literature. Removing the common distortion (low frequency bending) affecting the differential tracking error across all visible satellites, the inter-PRN biases are

assessed with a maximum value equal to 0.4 m. The value of 0.4 m is closer to the expected impact of nominal distortion on a differential user.

The main drawback of omnidirectional data collections is that multipath can affect some measurements. By consequence, the inter-PRN bias is not directly equal to the so-called natural bias, induced by the satellite. The mitigation of the multipath (a choke-ring antenna was used in this case to collect signals) permits to estimate in a better way the natural biases as done in [Gunawardena and van Graas, 2012a].

Results provided in this section must be carefully interpreted because based on only three data sets that were collected with a given setup and in a given environment. It shows order of magnitude of nominal distortions on users but also the difficulty to characterize such distortions.

## 5.6 Comparison between estimated inter-PRN biases and the state-of-the-art

Other inter-PRN biases estimated in previous works are available in the literature. For instance, inter-PRN biases reported from data collected with a mini-dish antenna and with a choke-ring hemispherical antenna are presented in [Wong, 2014]. Inter-PRN biases were estimated considering a  $0.1 T_c$  correlator spacing at the reference, a  $1 T_c$  correlator spacing at the user and a front-end filter bandwidth equal to 16 MHz. Information about the setup can be found in [Wong, 2014]. Results provided by [Wong, 2014] show inter-PRN biases and their associated standard deviation.

Results obtained from Leeheim (high-gain dish antenna) data collection and Bayonne (omnidirectional antenna) data collection are compared with results provided in [Wong, 2014].

### 5.6.1 High-gain dish antenna inter-PRN biases (Leeheim)

The comparison is proposed in Figure 5-17 only for signals collected with the German administration's high-gain dish antenna: in blue inter-PRN biases estimated from the mini-dish antenna, in red from the choke-ring antenna used in [Wong, 2014] and in green from the high-gain dish antenna.

Inter-PRN biases estimated in this document from the German administration's antenna measurements are consistent with the state-of-the-art. Only PRN 23 collected at Leeheim is slightly above the limit estimated in the literature and represented by the standard deviation ( $1\sigma$ ).

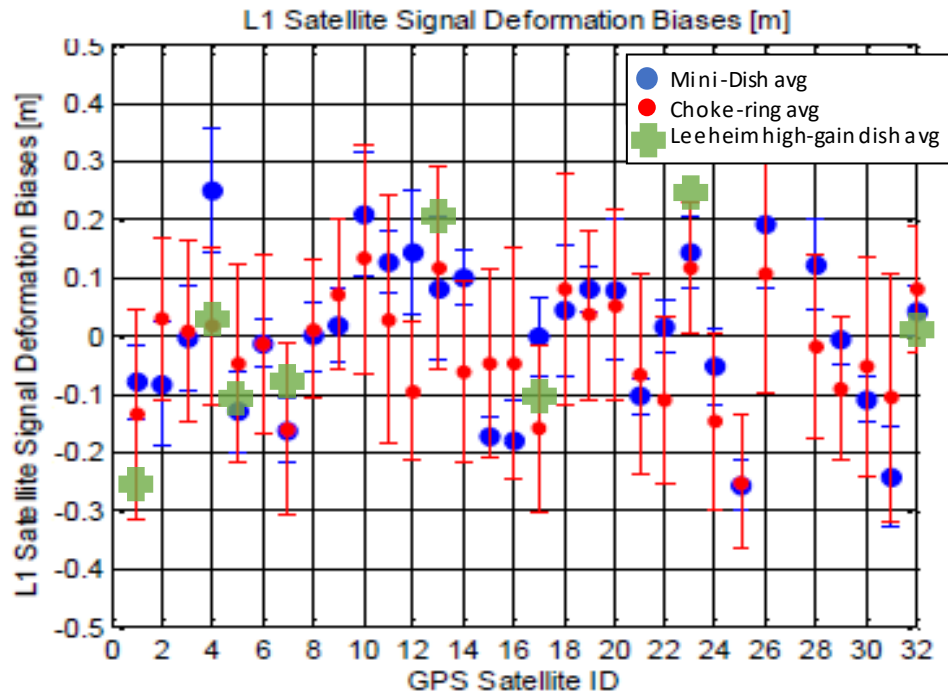


**Figure 5-17.** Superposition of inter-PRN biases estimated from high-gain dish antenna measurements with results obtained in [Wong, 2014]. (reference at 0.1 chip and user at 1 chip)

### 5.6.2 Omnidirectional antenna inter-PRN biases

In Figure 5-18, inter-PRN biases estimated from the omnidirectional antenna are compared to the state-of-the-art: in blue inter-PRN biases estimated from the mini-dish antenna, in red from the choke-ring antenna used in [Wong, 2014] and in green from the Capgemini omnidirectional antenna (also choke-ring). Inter-PRN biases from set 1 and set 2 are averaged but the two measurements estimated from the two satellites at low elevation (PRN 22 and PRN 25) are not shown and are removed from the average which is subtracted to estimate the inter-PRN biases. Results from the set 3 are also given.

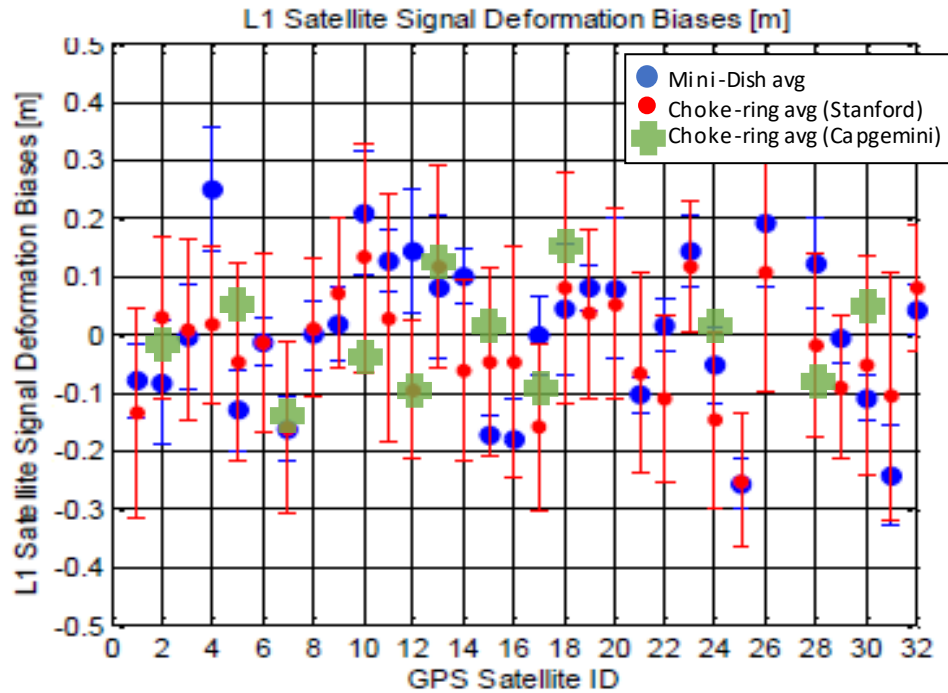


**Figure 5-18.** Superposition of inter-PRN biases estimated from omnidirectional antenna measurements with results obtained in [Wong, 2014]. (reference at 0.1 chip and user at 1 chip)

### 5.6.3 Conclusion about the estimation of inter-PRN biases

An important conclusion established in [Wong, 2014] is that: *the high degree of consistency between the two sets of measurements (Mini-dish and Choke-ring antenna) strongly demonstrates that the observed biases are due to satellite signal distortion and not to measurement errors.*

Without speaking about a demonstration in this document because of the low number of observations, inter-PRN biases estimated from the high-gain dish antenna and the omnidirectional antenna are consistent with the state-of-the-art. These results are of primary importance because despite of difficulties to characterize the impact of nominal distortions on users, the inter-PRN bias parameter is consistent over different data collections recorded at different periods and with different devices. It is noteworthy that results from [Wong, 2014] were obtained with a 16 MHz RF front-end bandwidth whereas results provided from collected signals were obtained with larger RF front-end bandwidths. By consequence, it appears an interesting alternative to characterize nominal distortions.

## 5.7 Conclusions

In this section, nominal distortions affecting GPS L1 C/A and Galileo E1C signals were observed on different signals collected in different conditions. The study was divided in two steps:

- the impact of nominal distortions on signals collected from high-gain dish antennas and
- the impact of nominal distortions on signals collected from one omnidirectional antenna.



Several results were established from the different data collections. Not enough data collections were available on GPS L5 and Galileo E5a signals to be presented in this manuscript.

### **High-gain dish antenna data collections**

Three observables were used to observe nominal distortions:

- *The Chip Domain observable (CDO).*
  - On GPS L1 C/A, results are consistent with results already published: a damped ringing effect is visible on the chip, and rising and falling transitions zero-crossings are delayed. Based on one characterization found in the state-of-the-art, four parameters were estimated from observed nominal distortions. Although, the rise time, the settling time and the peak time are overbounded by the maximum values that are reached by nominal distortions in [Phelts et al., 2009], the first peak overshoot ratio is slightly higher than the limit defined in [Phelts et al., 2009]. This can be explained by a difference in signal processing (antenna, digitizer, processing of sampling signals). Regarding the delay which affects zero-crossing of rising transitions compared to falling transitions, results show the stability of this parameter independently from the signal processing and the period of the measurement.
  - On Galileo E1C, only the estimation of the delay between rising and falling transitions can be compared to the state-of-the-art and results are consistent: the delay is negligible. The visualization of the analog distortion shows that the same damped ringing phenomenon as on GPS L1 C/A is visible but with a frequency slightly higher (24 MHz instead of 20 MHz). This result is directly linked to the bandwidth of the satellite equal to 20.46 MHz for GPS L1 C/A and 24.552 MHz for Galileo E1C. Additional distortions were visible on one of the collected signals (obtained with the ESA antenna) raising a question about origin of such distortions. Is the distortion induced by the satellite or by the receiver? Without more measurements the question cannot be answered.
- *The correlation function.* It gives another representation of the distortion. From this representation, it is clear that the receiver has an influence on distortions observed on the signal. A low frequency bending (1 MHz) is visible on signals collected from two (CNES and ESA) over three (CNES, ESA and German administration) high-gain dish antennas. The additive distortion already noticed in [Wong, 2014] is mainly caused by a problem that affect all collected signals. It puts forward the main drawback of high-gain dish antennas measurements: having only one signal from one satellite at a given time, it is not possible to isolate and quantify the impact of the receiver on the observed distortion. One advantage of Galileo E1 signals is that two components are received on the Galileo E1 band: E1C and E1B. Making the difference between the two components, all distortions that affect both components in the same way are removed whereas all distortions that affect both components differently are mixed. It cannot be concluded that the distortion induced by the receiver is removed making the difference between E1C and E1B correlation functions, but it is noticeable that it reduces the low frequency distortion.
- *The S-curve zero-crossing plot.* The low frequency phenomenon visible on the correlation function - called low frequency bending in this chapter - is enhanced by the S-curve zero-crossing plot and is visible on signals collected at CNES and ESA. S-curve zero-crossing plots obtained from the data collected with the German Administration's antenna are consistent with the state-of-the-art while S-curve zero-crossing plots obtained from the data collected



with the CNES antenna differ from the state-of-the-art because of a low frequency phenomenon introduced by the receiver on collected signals.

### **Omnidirectional antenna**

Only S-curve zero-crossing plots are estimated from data collected by Capgemini with an omnidirectional antenna. It was shown that S-curve zero-crossing plots are distorted in the same way if data are collected with a high-gain dish antenna without proper calibration and if data are collected with an omnidirectional antenna: a general curvature affects these plots (low frequency bending). The advantage is that with an omnidirectional antenna, several measurements can be recorded simultaneously and it is clearly visible that the general low frequency bending of the S-curve zero-crossing plots affects all collected signals in the same way. The low frequency distortion will be by consequence absorbed in the receiver clock bias. The bias which effectively affects pseudorange measurements, also called inter-PRN bias can be estimated by removing the common bias to all collected PRNs.

It appears that the inter-PRN bias is constant over different data collections (for directional as for omnidirectional antennas measurements) and is by consequence an interesting parameter to characterize the impact of nominal distortions on a user.

To summarize, the characterization of nominal distortions is an arduous task because if receivers are not calibrated, it is not possible to isolate distortions induced by the receiver and distortions induced at by the satellite. Nevertheless, results provided in this section show that analog and digital distortions visualized from CDO are highly consistent with outcomes from the state-of-the-art. In this chapter, new CDO results are proposed for Galileo E1C signals. Results on Galileo E1C have to be carefully interpreted because of the lack of measurements.

In spite of the fact that the characterization of nominal distortions is difficult, the inter-PRN bias reveals itself as a good parameter to quantify the impact of nominal distortions on a user. Indeed, the inter-PRN bias is constant independently from the antenna, the digitizer, the period of the day, etc. used during the data collection.



## 6 Non-nominal distortions

Threat Models (TMs) are based on modeling possible phenomenon occurring at the satellite level in faulty conditions and inducing non-nominal distortions on the GNSS signals. They are meant at representing the reality, although they might only be an approximation of signal distortions which could appear on a transmitted signal. These TMs, and their associated parameters range, referred to as Threat Space (TS), are also necessary to design and test performance of Signal Quality Monitor (SQM), which is in charge of detecting the threatening distortions represented by the TM. This signal monitoring is necessary to protect users with high requirements in terms of integrity, accuracy, availability, and continuity such as civil aviation users. Nowadays, this monitoring task is performed in SBAS and GBAS systems.

A proposition of signal distortions types was made in 1999 for GPS L1 C/A signal [Enge et al., 1999]. This proposition has been adopted by ICAO with the definition of three TMs [ICAO, 2006] that are defined in section 6.1: TM-A, TM-B and TM-C. When the term “ICAO Threat Model” is used in this Ph.D. thesis, it actually corresponds to three sub-threat models (TM-A, TM-B and TM-C).

Section 6.2 describes a general concept to define TMs for GPS L1 C/A, Galileo E1C, Galileo E5a and GPS L5 GNSS signals. This concept can also be used to design TMs on other signals. The challenge of defining a TM for new signals is making harder due to the fact that no non-nominal distortion has been observed on Galileo signals and that information about payload components are not available. This is the reason why, in this manuscript, the definition of TMs for new signals is based on the current ICAO GPS L1 C/A TM. Even if Galileo and GPS satellite payloads are different, it is assumed that the retained TM on the GPS L1 C/A signal is able to characterize signal distortions that could affect a Galileo signal which aim is also to provide measurements to estimate a PVT.

The strategy is to adapt the distortion models characterized by TM-A, TM-B and TM-C to new signals (with new correlation functions). It could thus be referred to as ICAO-like TM, as the new TM uses the same category of distortions as the current ICAO TMs. The concept is also used to propose an update to the TS for a GPS L1 C/A signal and to compare it with the ICAO TS.

In section 6.3, 6.4, and 6.5, a proposition of TM-A, TM-B and TM-C respectively are given for the four signals of interest.

Section 6.6 ends the chapter by summarizing results provided about TM-A, TM-B and TM-C for new signals and bring a critical point of view on the proposed solution.

### 6.1 GPS L1 C/A Threat Model

In this section, the definitions of the GPS L1 C/A TM delivered by ICAO are reminded. Definitions provide a characterization of distortions that could affect a signal. The characterization is given in the chip domain and on the correlation function. To illustrate the fact that these distortions are a threat for DGNSS users, the impact on the differential tracking error induced by distortions included in the ICAO TM is assessed for particular reference receiver configurations and user receiver configurations.

### 6.1.1 ICAO Threat Model definition

As it was seen in section 4.4.1.2, ICAO proposed to consider only three threatening effects (also called “problematical effects”) on the correlation function:

- Dead zones
- False peaks
- Distortions

The ICAO TM is defined for GPS L1 C/A signal and consists of three TMs that are described in this section: the TM-A, the TM-B and the TM-C. Definitions that are provided in this section are taken from [ICAO, 2006].

#### 6.1.1.1 TM-A

*Threat Model A (TM-A) consists of the normal C/A code signal except that all the positive chips have a falling edge that leads or lags relative to the correct end-time for that chip. This TM is associated with a failure in the navigation data unit (NDU), the digital partition of a GPS or GLONASS satellite.*

*TM-A for GPS has a single parameter  $\Delta$ , which is the lead ( $\Delta < 0$ ) or lag ( $\Delta > 0$ ) expressed in fractions of a chip. The range for this parameter is  $-0.12 \leq \Delta \leq 0.12$ .*

Within this range, TM-A generates the dead zones. Negative values of  $\Delta$  do not have to be tested because their effects on the correlation function are simply to advance the correlation function compared to positive values of  $\Delta$  which delay by the same amount the correlation function. By consequence threats entailed by positive and negative values are identical. This property can be theoretically demonstrated taking into account the correlation function mathematical expression as done in [Phelts, 2001].

Figure 6-1 illustrates chip and correlation deformations induced by the TM-A.

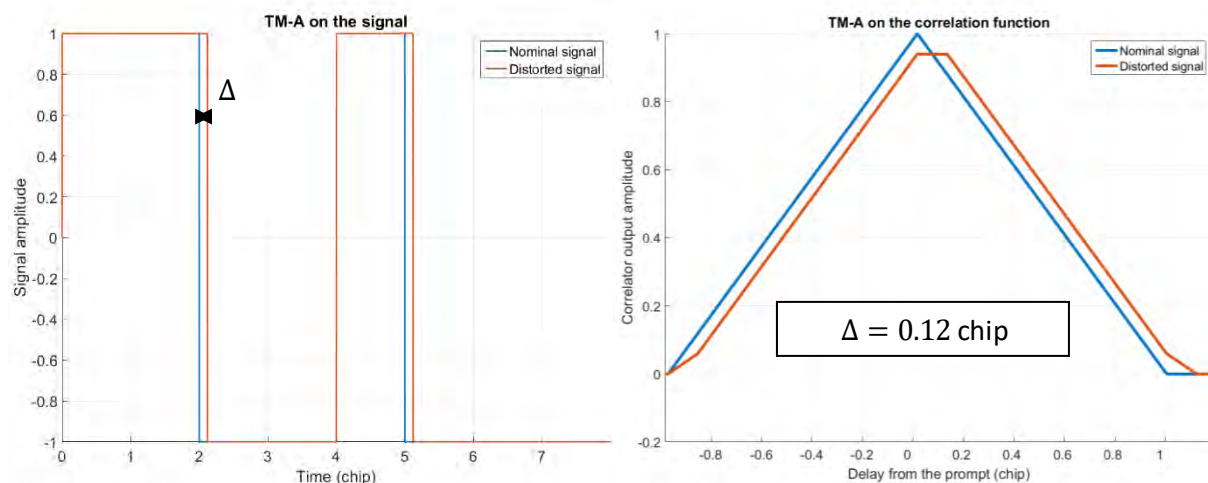


**Figure 6-1.** Illustration of the ICAO TM-A impact on the signal (left) and on the correlation function (right). The nominal signal is in blue, the distorted one in orange.

## 6.1.1.2 TM-B

*Threat Model B (TM-B) introduces amplitude modulation and models degradations in the analog section of the GPS or GLONASS satellite. More specifically, it consists of the output from a second order system when the nominal C/A code baseband signal is the input. TM-B assumes that the degraded satellite subsystem can be described as a linear system dominated by a pair of complex conjugate poles. These poles are located at  $\sigma \pm j2\pi f_d$ , where  $\sigma$  is the damping factor in  $10^6$  nepers/s and  $f_d$  is the resonant frequency with units of  $10^6$  cycles/s.*

The unit step response of a second order system is given by:

$$e(t) = \begin{cases} 0 & t < 0 \\ 1 - e^{-\sigma t} \left[ \cos(\omega_d t) + \frac{\sigma}{\omega_d} \sin(\omega_d t) \right] & t > 0 \end{cases} \quad (6-1)$$

where  $\omega_d = 2\pi f_d$ .

TM-B for GPS corresponding to second order anomalies uses the following ranges for the parameters  $\Delta$ ,  $f_d$  and  $\sigma$ :

$$\Delta = 0; 4 \leq f_d \leq 17; \text{ and } 0.8 \leq \sigma \leq 8.8$$

Within these parameter ranges, TM-B generates distortions of the correlation peak as well as false peaks.

The analog distortion is modeled as a second order linear filter with a Laplace transfer function:

$$G(s) = \frac{(2\pi f_{d\_bis})^2}{s^2 + 2\sigma s + (2\pi f_{d\_bis})^2} \quad (6-2)$$

With

$$f_{d\_bis} = \frac{1}{2\pi} \sqrt{\sigma^2 + (2\pi f_d)^2}$$

Figure 6-2 illustrates chip and correlation deformations induced by a TM-B distortion.

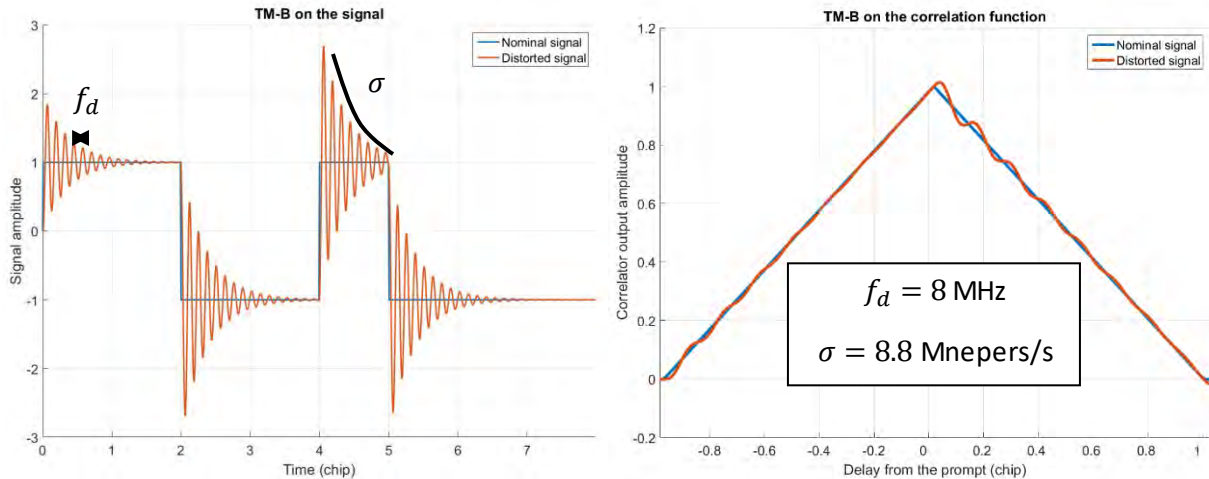


**Figure 6-2.** Illustration of the ICAO TM-B impact on the signal (left) and on the correlation function (right). The nominal signal is in blue, the distorted one in orange.

## 6. Non-nominal distortions

### 6.1.1.3 TM-C

TM-C introduces both lead/lag and amplitude modulation. Specifically, it consists of outputs from a second order system when the C/A code signal at the input suffers from lead or lag. This waveform is a combination of the two effects described above.

TM-C for GPS includes parameters  $\Delta$ ,  $f_d$  and  $\sigma$  with the following ranges:

$$-0.12 \leq \Delta \leq 0.12; 7.3 \leq f_d \leq 13; \text{ and } 0.8 \leq \sigma \leq 8.8$$

Within these parameters ranges, TM-C generates dead zones, distortions of the correlation peak and false peaks.

Figure 6-3 illustrates chip and correlation distortions induced by the TM-C.

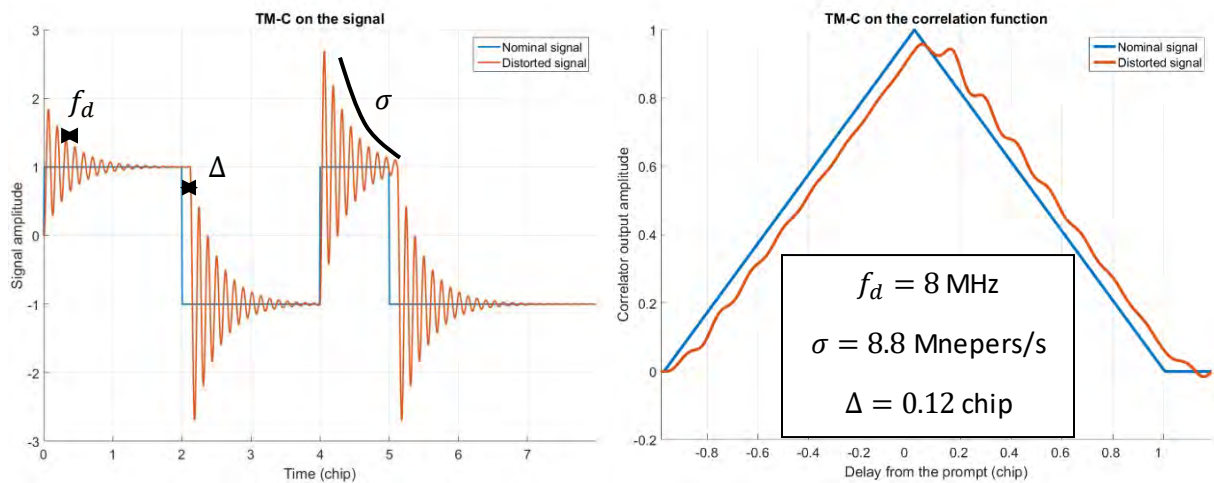


**Figure 6-3.** Illustration of the ICAO TM-C impact on the signal (left) and on the correlation function (right). The nominal signal is in blue, the distorted one in orange.

### 6.1.1.4 Justifications about the ICAO GPS L1 C/A TM

#### Characterization of the TM

The characterization of the ICAO TM is based on three parameters:  $\Delta$ ,  $\sigma$  and  $f_d$ . The choice of the three parameters is justified by the fact that in nominal conditions, distortions that affect the signal can be approximatively characterized by these three parameters. Indeed, a delay between rising and falling transitions zero-crossing average and a damped ringing phenomenon can be observed on GPS L1 C/A signals in nominal conditions (see chapter 5). By consequence, it seems reasonable to assume that payload components can provoke the same kind of distortion with a larger amplitude in non-nominal conditions.

Moreover, the ICAO TM satisfies two other important criteria: it is easy to implement and it is capable of generating the three correlation peak pathologies (dead zone, false peak and asymmetry).

#### Limitation of the TS

Criteria used to define the TS for GPS L1 C/A signal, (i.e. the possible values of the TM parameters ( $\Delta$ ,  $\sigma$  and  $f_d$ )) are described in [Phelts, 2001].

Considering TM-A:

- For  $\Delta$ , the range of the parameter is limited to  $\pm 0.12$  of the chip duration, because larger values are easily detectable by SQMs based on multi-correlator techniques.

Considering TM-B:

- [Phelts, 2001] mentions that the upper bound for  $f_d$  (17 MHz) has been chosen because higher frequency ringing effects would be filtered out by the satellite RF output filter, which is 20.46 MHz for GPS L1.
- The lower bound for  $f_d$  (4 MHz) is justified by the fact that lower frequency ringing will affect the L1 P(Y) code, that is “closely monitored” by military users.
- For  $\sigma$ , lower values ( $\sigma < 0.8$  Mnepers/s) are not realistic since they would introduce unrealistic instability of the ringing. Distortions with larger values ( $\sigma > 8.8$  Mnepers/s) shall not be threatening for users protected against TM-B distortions.

Considering TM-C no justification about the TS is proposed in the literature.

#### 6.1.1.5 GPS L1 C/A ICAO TM summary

This part gives a summary about the three sub-TMs defined by ICAO for the GPS L1 C/A signal. Table 6-1 gives the limit values that the three TMs parameters can take as defined by ICAO.

	$\Delta$	$\sigma$	$f_d$
TM A	$[-0.12 ; 0.12]$ chip or $[-117.3 ; 117.3]$ ns	-	-
TM B	-	$[0.8 ; 8.8]$ Mnepers/s	$[4 ; 17]$ MHz
TM C	$[-0.12 ; 0.12]$ chip or $[-117.3 ; 117.3]$ ns	$[0.8 ; 8.8]$ Mnepers/s	$[7.3 ; 13]$ MHz

**Table 6-1.** ICAO TS defined for GPS L1 C/A signals.

#### 6.1.2 Impact on differential users

In this section differential tracking errors induced by the TM-A, TM-B and TM-C are estimated. The differential tracking error induced by a given distortion is dependent upon the user and reference station configurations as discussed in section 4.3, and notably upon the following parameters:

- the tracking technique (including the local replica and the discriminator),
- the correlator spacing,
- the antenna and the RF front-end (technology, bandwidth, maximum group delay variation).

In section 6.1.2.1, parameters that are defined in this chapter at reference and at user levels to estimate differential tracking errors are given considering a GPS L1 C/A signal. Then in section 6.1.2.2, the impact of the three TMs on the differential tracking error is assessed to put forward that distortions defined by ICAO are effectively leading to threatening differential errors.

### 6.1.2.1 Tested configurations and worst differential tracking error

Values and information about receiver parameters that are used in this chapter to estimate differential errors estimated for GPS L1 C/A signal are given in Table 6-2. The allowable range that these parameters can take was provided in chapter 5 and is referred to as the User Design Space (UDS). These parameters are representative of expected standardized DFMC civil aviation configurations [Samson, 2015]. Note that different types of filters are used to account for the wide variety of filters encountered across multiple receiver manufacturers. All these filters satisfy the ICAO requirement on the maximal differential group delay which must be lower than 150 ns:

- Filter1: 6<sup>th</sup>-order Butterworth.
- Filter2: resonator filter type with a constant group delay equal to zero.
- Filter3: resonator filter type with a concave group delay and a 150 ns differential group delay.
- Filter4: 6<sup>th</sup>-order Butterworth for the amplitude and the smallest order Butterworth filter leading to a differential group delay higher than 150 ns for the phase.

A detailed description of the four filters (amplitude, phase and differential group delay) is provided in appendix E. When designing TMs, to be as conservative as possible, the four filters are also tested at reference level even if, in the literature, 6<sup>th</sup>-order Butterworth is usually used to model the pre-correlation filters (at reference as well as at user levels).

Only an EML discriminator ( $D_{EML} = (I_E - I_L)/2$ ) is used to perform the tracking as this is the discriminator retained by civil aviation for both reference and airborne receivers [Samson, 2015]. The tracking bias is estimated by simply finding the discriminator stable lock point. The use of an EMLP, an EML or a DP discriminator do not change provided results.

	reference	user
Tracking technique	EML	EML
Correlator spacing	0.1 chip	0.08 and 0.12 chip
Pre-correlation bandwidth (double-sided)	24 MHz	12, 14, 16, 18, 20, 22, 24 MHz
Equivalent reception filter	4 filters are tested (6 <sup>th</sup> -order Butterworth, 0-group delay resonator, 150 ns differential group delay resonator, 150 ns differential group delay 6 <sup>th</sup> -order Butterworth) to estimate differential tracking error. Only the 6 <sup>th</sup> -order Butterworth filter is applied to the reference to estimate the absolute tracking error.	

**Table 6-2.** Reference receiver and user receiver configurations used to estimate tracking errors and differential tracking errors in chapter 6 for GPS L1 C/A signal.

To estimate the worst (or maximal) differential tracking error entailed by a distortion, the differential tracking error entailed by that distortion on each reference/user receiver configuration combination is assessed. 4 (reference filters) + 4 (user filters) x 2 (correlator spacing's at user level) x 7 (bandwidths at user level) = 60 differential tracking errors are derived per tested distortion. Then, the highest differential tracking error estimated from tested reference/user receiver configurations is kept and is considered as the worst (or maximal) differential tracking error entailed by that distortion.



## 6.1.2.2 Results

Figure 6-4 gives the worst differential tracking error induced by ICAO TM-A, TM-B and TM-C on a GPS L1 C/A signal considering user receiver configurations presented in Table 6-2 and a reference station with an equivalent 6<sup>th</sup>-order Butterworth reception filter. To plot results provided by Figure 6-4:

- 12 distortions are tested regarding TM-A:  
 $\Delta = 0: 0.01: 0.12$  chip.
- 126 distortions are tested regarding TM-B:  
 $f_d = 4: 1: 17$  MHz and  $\sigma = 0.8: 1: 8.8$  Mnepers/s.
- 99 distortions are tested regarding TM-C:  
 $f_d = 7.3: 0.57: 13$  MHz and  $\sigma = 0.8: 1: 8.8$  Mnepers/s.  $\Delta$  is set to 0.12 chip for the sake of illustration even if it is not necessarily the  $\Delta$  value that entails the largest differential tracking errors.

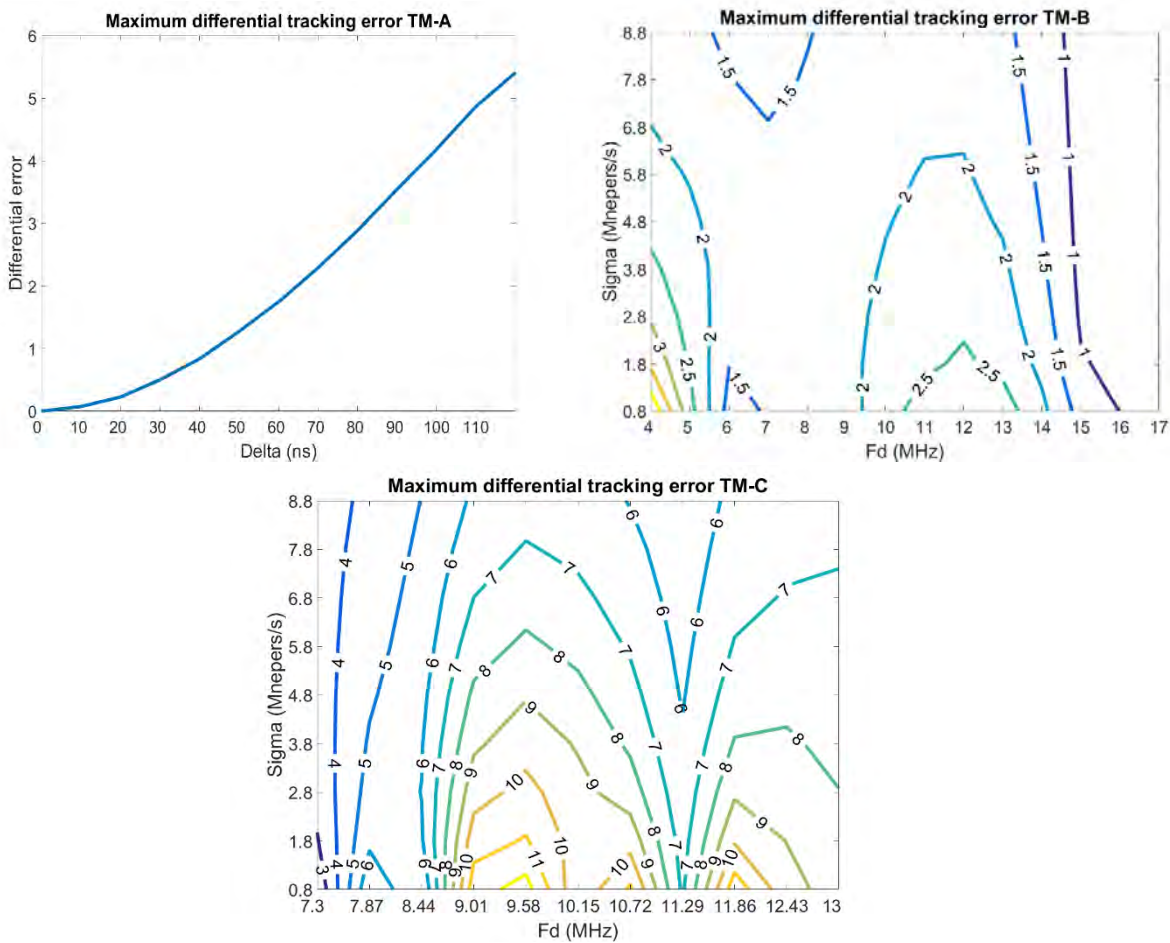


**Figure 6-4.** Impact of the TM-A (at top on the left), the TM-B (at top on the right), and the TM-C (at bottom) on the worst differential tracking error.

From Figure 6-4, it can be seen that the worst differential error induced by distortions from the TM-A, TM-B and TM-C on a GPS L1 C/A signal pseudorange measurement can reach 12 m. By consequence, it is necessary to warn a user that has to meet stringent requirements if such distortions affect a signal. The definition of the limit between threatening and nominal differential pseudorange measurement errors, referred to as MERR, is given in the next chapter (see section 7.1.1).

### 6.2 Generalization to other modulations

It was seen that some signal distortions can introduce high differential tracking errors. Even if several strategies were investigated to deal with this problem (see section 4.4.1), the adopted strategy was to design a TM to characterize distortions that could affect in a hazardous way a GPS L1 C/A signal. With the definition of new GNSS signals that will be used by civil aviation users, it is necessary to adopt the strategy that was developed for GPS L1 C/A: define representative distortions TM for new signals. The issue is that the adaptation to new signals of the ICAO TM developed for GPS L1 C/A signal is not elementary. Indeed, new signals and/or new tracking methods change the conception of hazardous signal distortions. The problem was already studied in [Phelts et al., 2006], [Fontanella et al., 2010] and [Thevenon et al., 2014] but the idea was more about replicating the GPS L1 C/A TM on new signals and on new correlation functions. The justification of using such models with the same TS as GPS L1 C/A was not clear. In this section, justifications of the TM design for new signals are given and a method to define a TM for different GNSS signals is exposed.

An important remark is that, on GPS L5, the use of the ICAO TM defined for GPS L1 C/A is taken for granted [Phelts et al., 2013]. The logic behind is that the same hardware and same satellites are used to generate both signals.

#### 6.2.1 Difficulties to translate GPS L1 C/A case to other modulations

To define a TM, two questions have to be answered:

- How are the distortions from the TM characterized? The answer consists in finding relevant parameters necessary to generate these distortions.
- How can the TS be limited? The answer consists in finding the limit values that the TM parameters can reasonably take.

The answer to both questions can be found in the literature in a GPS L1 C/A context ([Phelts, 2001]) as summarized in section 6.1.1.4. Nevertheless it appears that the answer cannot be applied in a straightforward manner for new modulations as discussed in this part.

The first step regarding the design of the ICAO TM was to define correlation peak pathologies that can be threatening for a DGNSS user (dead zone, false peak and asymmetry). However, it was seen that the impact of distortions is dependent upon the tracking technique and the correlation function shape. By consequence, threatening distortions on a given modulated signal and for a given receiver (with a given tracking technique) are not necessarily threatening on another signal (with another modulation) and for a different receiver.

For the studied modulations and signals (Galileo E1C, Galileo E5a and GPS L5), it is assumed that only EML discriminators will be used by future reference and airborne receivers (as it was the case to define the three GPS L1 C/A correlation peak pathologies). Note that this includes EML, EMLP and Dot Product discriminators. Moreover, the shape of the correlation function on the tracked area can be approximated by a triangular shape. By consequence, it is decided in this Ph.D. thesis to consider that whatever the signal is, the three threatening correlation peak pathologies remain dead zone, false peak and asymmetry.

Therefore, the first strategy to define a TM on new GNSS signals is to apply concepts used to define the GPS L1 C/A TM and to adapt them to new modulations.

#### Characterization of the TM

From the observation of nominal deformations (state-of-the-art), it can be deduced that the same types of nominal distortions exist on GPS L5 and GPS L1 C/A. It justifies that the same characterization can be applied to define distortions on GPS L5 signal as on GPS L1 C/A signal (it is indicative of similar payload architecture that could thus lead to similar failures).

Regarding Galileo E1C and Galileo E5a signals, it appears that no digital distortion seems to affect the signal in nominal conditions. This might be due to a very well calibrated payload, or a different generation scheme. Observations of Galileo E1C signals show, however, the same ringing phenomenon as on GPS L1 C/A, visible from the CDO.

From the observation of nominal distortions and because of the lack of knowledge about payload architecture and behavior in a faulty condition, it is assumed in this manuscript, to be conservative, that the distortion model is the same for GPS L5, Galileo E1C and Galileo E5a as for GPS L1 C/A. It means that the analog failure consists in the output of a second order system (TM-B) whereas a lead/lag on falling signal transitions (whether chip or sub-chip) characterizes a digital failure (TM-A), or a combination of both failures (TM-C).

#### Limitation of the TS

Even if it seems reasonable to adapt the ICAO's strategy to estimate parameters that are chosen to define distortions, it seems more difficult to use this strategy to limit the TS. Indeed:

- $\Delta$  cannot be limited a-priori by SQM capabilities because new modulations require new SQM designs and new SQM performance assessment.
- The satellite RF output filter bandwidth is larger for Galileo E1 than for GPS L1. It entails that the higher bound for  $f_d$  has to be redefined.
- No description of a "close monitoring checking" on other component of a signal is available to limit  $f_d$ .
- Since chips have a length (or a shape) which depends upon the modulation, the instability of distortions at low  $\sigma$  must be reconsidered.
- The impact on differential users of highly attenuated distortions has to be estimated in a new modulations context.

These are the reasons why another strategy is developed in this manuscript to limit the TS associated to TM on new modulations.

### 6.2.2 Proposition of a new methodology to define the TS

Due to difficulties to adapt the method that was used in the past to define the ICAO TS for GPS L1 C/A signal, a new approach is envisaged to limit the TS for other signals. The proposed TS for new modulations is based on two quantities that are defined in section 6.2.2.1:

- the impact of a distortion on a GNSS receiver and
- the impact of a distortion on a reference station receiver.

These two quantities are dependent upon two parameters:

## 6. Non-nominal distortions

- reference receiver and user receiver configurations that are considered (presented in section 6.2.2.2) and
- the value of the maximum tolerable differential error (defined in section 6.2.2.3).

### 6.2.2.1 Introduction to the proposed TS definition methodology

To establish all parameters limits (for TM-A and TM-B), it is proposed to evaluate two quantities in order to limit the TS:

**The impact of a distortion on a receiver working with differential corrections.** More precisely, a parameters limitation is established based on the consequence of a distortion on the corrected pseudorange measurement of a differential user. If a distortion can only lead to small differential biases that will not create a hazardous situation (bias smaller than a specified maximum differential error:  $\Delta_{err\_max}$ ) for all considered user/reference configurations, the corresponding TM parameters values can be removed from the TS. To determine the worst differential bias, all possible civil aviation airborne receiver and reference station receiver configurations (essentially different correlator spacing's, RF front-end filter bandwidths and RF front-end filter types) are used.

**The impact of a distortion on a reference receiver.** If a signal distortion induces a tracking bias on the reference station higher than a specified limit, the distortion is not included in the TS because is assumed to be detected by the ground segment (with a given false alarm and missed detection probabilities). Today, no such requirement on the tracking error detection at the reference level is defined for SBAS. However, such strong hypothesis is useful to limit the TS. It is presumed in this manuscript that the SBAS reference station is able to detect, in steady state, an absolute tracking bias higher than 20 m with another process than the SQM. Nowadays, no algorithm is implemented to perform this task but it is assumed in this document that in the future such detectors will be provided. These detectors would permit to detect translation of the correlation function that cannot be detected by the SQM, only capable of detecting a correlation function distortion. Such detectors could be based on same principles as RAIM algorithm detecting large residual biases on faulty pseudorange measurements. The value of 20 m is chosen to be reachable and conservative.

### 6.2.2.2 Tested configurations

As it was the case for GPS L1 C/A, the impact of a distortion is dependent upon the reference receiver and user receiver configurations. The consequence is that the TS limits are dependent upon the reference receiver and user receiver configurations that are considered.

Values and information about receiver parameters that are defined in this chapter to estimate differential tracking errors and tracking errors estimated for new signals are given in Table 6-3. These parameters represent expected civil aviation configurations [Phelts et al., 2014]. The four tested filters were introduced in 6.1.2.1 and are detailed in appendix E. The four filters are also used to account for the wide variety of filters encountered across multiple receiver manufacturers.

	Galileo E1C signal ( <i>CBOC</i> (6.1))		Galileo E5a and GPS L5 signal ( <i>BPSK</i> (10))	
	reference	user	reference	user
Tracking technique	EML ( <i>BOC</i> (1.1) local replica)	EML ( <i>BOC</i> (1.1) local replica)	EML ( <i>BPSK</i> (10) local replica)	EML ( <i>BPSK</i> (10) local replica)
Correlator spacing	0.1 chip	0.08 and 0.12 chip	1 chip	0.8, 1.2 chip
Pre-correlation bandwidth (double-sided)	24 MHz	12, 14, 16, 18, 20, 22, 24 MHz	24 MHz	12, 14, 16, 18, 20, 22, 24 MHz
Equivalent reception filter	4 filters are tested (6 <sup>th</sup> -order Butterworth, 0-group delay resonator, 150 ns differential group delay resonator, 150 ns differential group delay 6 <sup>th</sup> -order Butterworth) to estimate differential tracking error. Only the 6 <sup>th</sup> -order Butterworth filter is applied to the reference to estimate the absolute tracking error.			

**Table 6-3.** Reference receiver and user receiver configurations used to estimate tracking error and differential tracking error in chapter 6 for new signals.

#### 6.2.2.3 Limitation of $\Delta_{err\_max}$

$\Delta_{err\_max}$  is of primary importance because it represents the limit of the acceptable differential error in presence of a distortion. Signal distortions which entail smaller differential errors than this limit do not need to be included in the TS. The smaller  $\Delta_{err\_max}$  is, the wider the TS is.  $\Delta_{err\_max}$  thus has to be quantified to ensure that a bias smaller than  $\Delta_{err\_max}$  would not lead to a hazardous situation.

The notion of hazardous situation is related to targeted SQM performance. The current SBAS L1 requirement regarding SBAS SQM is provided by [ICAO, 2006] and states that the ground segment should be able to detect any EWF-induced differential bias greater than a given Maximum Error Range Residual (MERR), also known as maximum tolerable error, with a  $P_{md}$  and a  $P_{ffd}$ .

MERR values are derived in 7.1.1 and are summarized hereafter. In the context of DFMC receiver, assuming that an EWF can only occur on one frequency at a time, the SQM performance will be limited to the detection (with appropriate required  $P_{md}$  and  $P_{ffd}$ ) of any EWF that would create:

- a differential bias on a Galileo E1 OS measurement greater than MERR equal to 1.55 m or
- a differential bias on a Galileo E5a measurement greater than MERR equal to 2.78 m.

In the context of mono-frequency L1 receiver the MERR is equal to 3.5 m.

To be conservative, in this document,  $\Delta_{err\_max}$  is fixed to 1 m, a value lower than any MERR value, thus providing some margin with respect to the computation of the worst differential bias. It means that the TM includes all signal distortions following the ICAO-like TM leading to a worst-case differential error higher than 1 m.

### 6.3 TM-A like propositions for new signals

In this section, the TM-A of GPS L1 C/A is extended to Galileo E5a, GPS L5 and Galileo E1C signals. It is recalled that the reasoning developed in this manuscript is based on the assumption that the same kind of failure appears on GPS L1 C/A, Galileo E1C, Galileo E5a and GPS L5 signals.

The extension to the  $BPSK(10)$  (Galileo E5a and GPS L5) is fairly straightforward. However, it is more difficult for Galileo E1C signal because of the presence of sub-carriers on the CBOC signal. That is why in part 6.3.2 two digital TMs are proposed for the CBOC modulation: one conservative TM and one simplified TM.

#### 6.3.1 Galileo E5a and GPS L5 TM-A

To be in line with the current TM-A defined for GPS L1 C/A and to be conservative, the lower bound of  $\Delta$  is taken equal to zero for  $BPSK(10)$ -modulated signals. For this signal it is not possible to use the proposed technique to limit the upper bound of the TS (selection in the TS of a distortion based on its impact on the tracking error and differential tracking error) as shown in 6.3.1.1. By consequence, another method copying the ICAO TM-A developed for GPS L1 C/A signal is proposed.

##### 6.3.1.1 Use of the proposed methodology

Figure 6-5 shows on the left the tracking error observed by the reference station when tracking a signal affected by a TM-A with different values of  $\Delta$  running from 0 to 117 ns. On the right, is shown the worst differential error seen among all reference/user receiver configurations combinations.

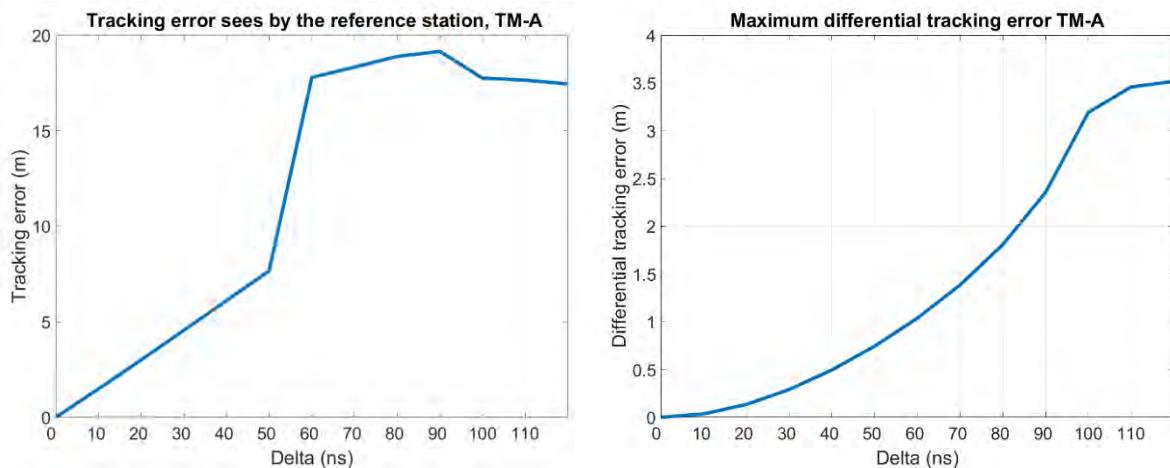


**Figure 6-5.** Impact of the TM-A for GPS L5 and Galileo E5a signals for different  $\Delta$ . On the left, impact on the reference station tracking error. On the right, impact on the worst differential tracking error.

From Figure 6-5 (left), the tracking error seen by the reference station is always lower than 20 m whatever the value of  $\Delta$  is. As a consequence, it is not possible to use the criterion about the impact of a distortion on the reference station tracking error to limit the TS.

From Figure 6-5 (right), the worst tracking error entailed by a TM-A distortion increases when  $\Delta$  increases. Consequently, it is not possible to apply the criterion about the impact of a distortion on the



differential tracking error to estimate the upper bound of  $\Delta$ . It is noticeable that for  $\Delta$  values lower than or equal to 50 ns, the differential tracking errors are lower than 1 m and are by consequence not a threat for the considered DGNSS users. Nevertheless, to be in line with GPS L1 C/A TM it is decided to keep small  $\Delta$  values in the TS.

To conclude, the strategy to estimate the  $\Delta$  upper bound from the two proposed criteria (tracking error observed by reference and worst differential tracking error that affect DGNSS users) does not allow the reduction of the TS.

### 6.3.1.2 Proposition of a TM-A

Based on the above results, it is proposed to keep the range of  $\Delta$  (in second) of GPS L1 C/A TM-A:

$$-1.2 E5a (L5) \text{ chips} \leq \Delta \leq 1.2 E5a (L5) \text{ chips}$$

Figure 6-6 illustrates correlation functions affected by TM-A distortions with different  $\Delta$  values.

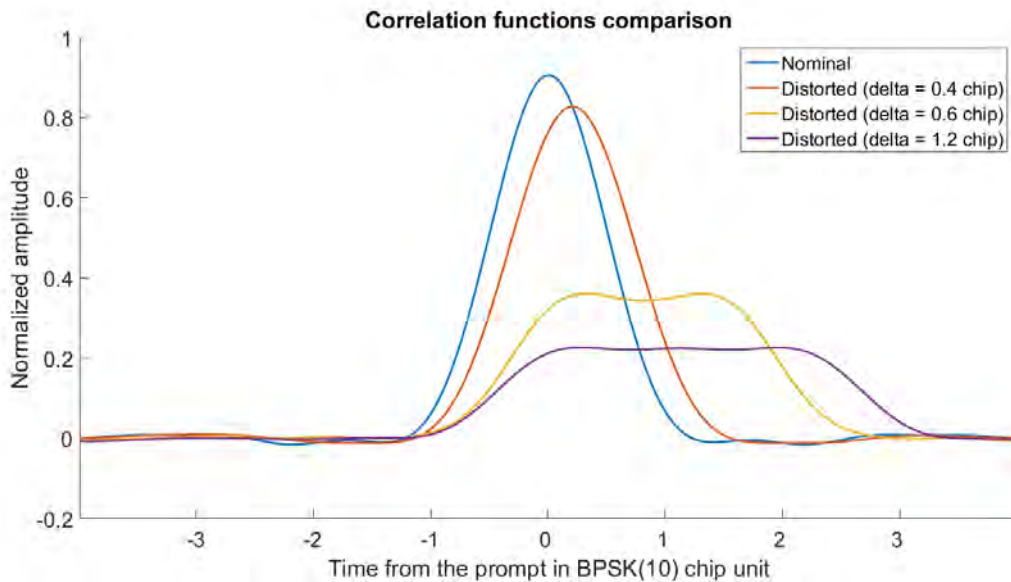


**Figure 6-6.** Distorted GPS L5/Galileo E5a correlation functions for different values of  $\Delta$  filtered by a 6<sup>th</sup>-order Butterworth (24 MHz).

From Figure 6-6, it can be seen that the correlation peak is still visible for high  $\Delta$  values even if strongly flattened. The legitimacy of distortions with high  $\Delta$  values could be discussed. Indeed, if the distorted signal cannot be tracked by any considered receiver, it is not necessary to include this distortion in the TM. Two distorted signal features that could prevent the tracking can be defined:

- *A too low amplitude of the correlation function at tracking correlator outputs level.* The worst case is considered: a user's receiver tracks a TM-A distorted signal ( $\Delta = 1.2$  chips) with a correlator spacing equal to 1.2 chip. From Figure 6-6, the amplitudes of the correlation function at tracking correlator outputs are equal to 0.67 in nominal conditions and 0.23 on the distorted correlation function which represents a factor of 3. It means that the receiver will observe a 4.7 dB Signal-to-Noise Ratio (SNR) loss when tracking the distorted signal compared to a nominal one. A 4.7 dB difference between two GNSS signals received by the same antenna/receiver is a typical order of magnitude in nominal conditions, for example

between a low elevation satellite and one at high elevation. The consequence is that the loss of correlation function amplitude entailed by the distortion does not prevent the tracking.

- *A flat zone which includes the two tracking correlator outputs.* From Figure 6-6, it is noticeable that the two tracking correlator outputs are on the flat zone when the signal is affected by a  $\Delta$  higher than 0.6 chip. Nevertheless, depending on the implementation of the discriminator, the behavior of the DLL when both correlator outputs used for the tracking are on a flat zone will be different. This difference in the receiver behavior can become a threat for DGNSS users. By consequence, it is important to take into account even distortions with high  $\Delta$  values.

### 6.3.2 Galileo E1C TM-A

As introduced previously, the digital failure of  $CBOC(6,1,1/11)$ -modulated signal is more difficult to design because of the presence of sub-carriers. The presence of several components in the signal entails a multiplication of distortion threats.

#### 6.3.2.1 Proposition of digital distortions

No occurrence of EWF has been observed on Galileo signals. Payload knowledge could help to make choices among the large number of conceivable digital failures. However, the lack of information about a payload miss-functioning prevents the selection. In this section, only the two most likely digital distortions that could affect a Galileo E1C signal are presented and are called digital distortion 1 and digital distortion 2.

The scheme on Figure 6-7 presents the Galileo E1 signal generation [Navipedia, 2015]. Only the bottom part (highlighted green box) is of interest in the E1C component generation.

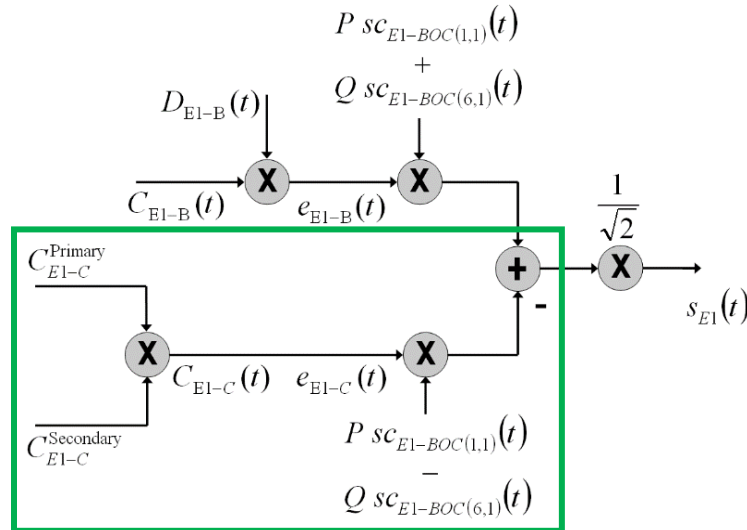


**Figure 6-7.** Galileo E1 signal generation block scheme [Navipedia, 2015].

**Digital distortion 1:** A lead/lag on the falling transitions of all signal components after modulation. It is possible to imagine that only  $BOC(6,1)$  or  $BOC(1,1)$  transitions are affected by this lead/lag but because the distortion occurs after modulation, it is most likely that a delay will appear on every transitions.



The impact on the signal and on the correlation function, of such a signal distortion is shown in Figure 6-8 on the left and on the right respectively for  $\Delta = 0.05$  chip (in blue the undistorted signal, in red the distorted signal).

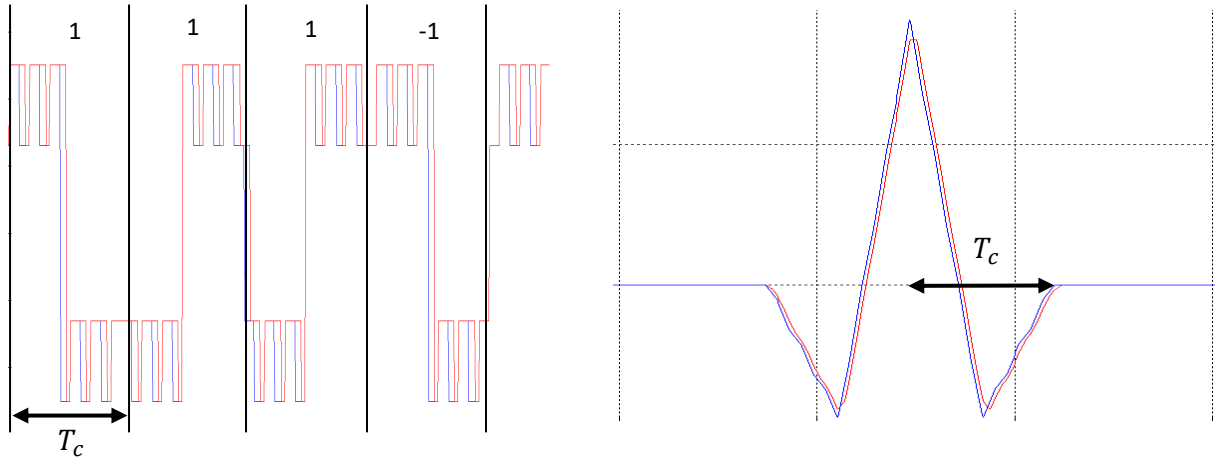


**Figure 6-8.** Impact of digital distortion 1 on the signal (left), and on the correlation function (right).

**Digital distortion 2:** A lead/lag on the  $BOC(1,1)$  sub-carrier or/and on the  $BOC(6,1)$  sub-carrier falling transitions at the signal square wave generator level (before modulation). This distortion was introduced in [Phelts et al., 2006] for  $BOC(1,1)$  signal. In Figure 6-9, the lag on  $BOC(1,1)$  and  $BOC(6,1)$  transitions is similar. To be conservative and take into account most of possible cases, two independent parameters are defined:

- $\Delta_{11}$  : the lead/lag parameter on  $BOC(1,1)$  sub-carrier component (before modulation).
- $\Delta_{61}$  : the lead/lag parameter on  $BOC(6,1)$  sub-carrier component (before modulation).

The impact on the signal and on the correlation function of such a signal distortion is shown in Figure 6-9 on the left and on the right respectively for  $\Delta_{11} = \Delta_{61} = 0.05$  chip (in blue the undistorted signal, in red the distorted signal).

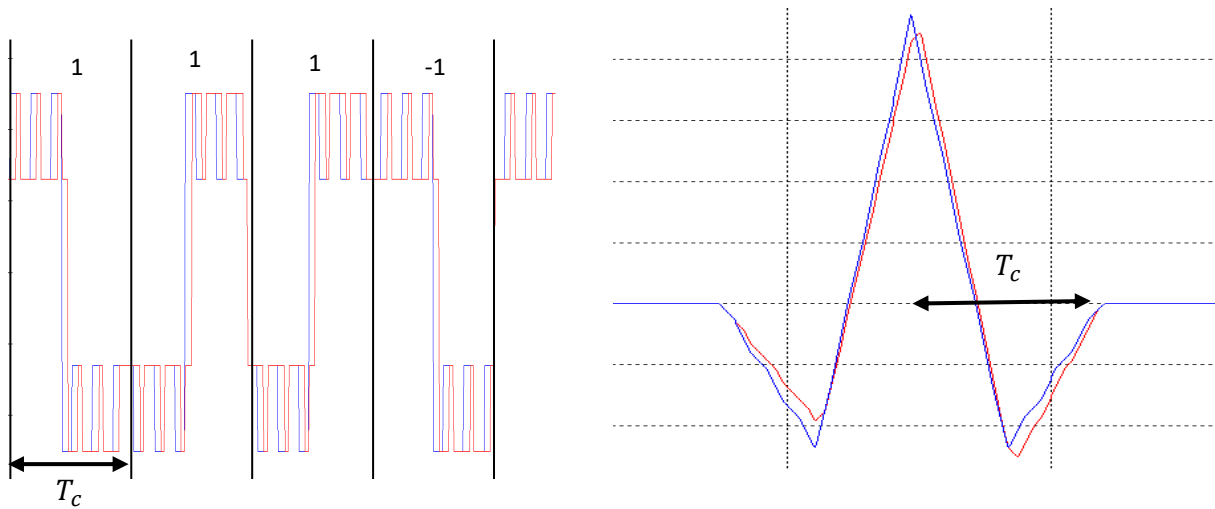


**Figure 6-9.** Impact of digital distortion 2 on the signal (left), and on the correlation function (right).

In Figure 6-10 is represented in red the Galileo E1C signal generation level where the digital distortion 1 appears and in green where digital distortion 2 appears.

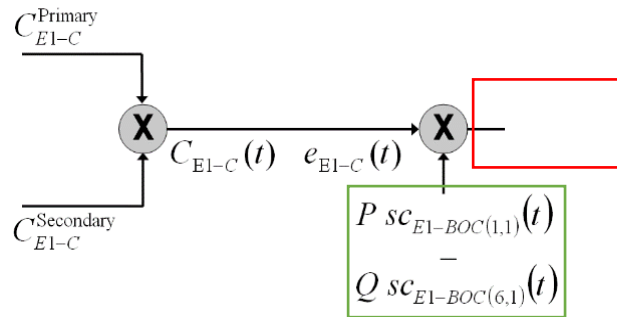


**Figure 6-10.** Galileo E1C signal generation unit and digital distortions.

#### 6.3.2.2 First TM-ATS limitation based on physical considerations

Two TM-A are proposed to take into account each proposed digital distortion for the new Galileo E1C signal:

- TM-A1: A lead/lag ( $\Delta$ ) on every signal falling transitions after modulation. Only one parameter is necessary (digital distortion 1).
- TM-A2: A lead/lag on the  $BOC(6,1)$  ( $\Delta_{61}$ ) and on the  $BOC(1,1)$  ( $\Delta_{11}$ ) sub-carrier falling transitions at signal square wave generator level (before modulation). Two parameters are necessary (digital distortion 2).

$\Delta$ ,  $\Delta_{61}$  and  $\Delta_{11}$  parameters range can be fixed observing the shape of signals distorted by the different digital distortions:

- From a certain value of  $\Delta$ , the distorted signal keeps the same shape because a chip is composed of one positive and one negative sub-chip. It entails that from a certain value of  $\Delta$  ( $\Delta = 1.08$  chips), increasing the value of  $\Delta$  (above 1.08 chips) does not change the shape of the signal and the correlation function. From this value of  $\Delta$ , chips are disappearing and the signal is constant.
- From a certain value of  $\Delta_{11}$ , the signal keeps the same shape because a chip is composed of one positive and one negative sub-chip. It entails that from a certain value of  $\Delta_{11}$  ( $\Delta_{11} = 0.5$  chip), sub-chips (of the  $BOC(1,1)$ ) are disappearing. Increasing the value of  $\Delta_{11}$  above 0.5 chip does not change the shape of the signal and the correlation function.
- From a certain value of  $\Delta_{61}$ , the signal keeps the same shape because  $BOC(6,1)$  signal is composed of alternative positive and negative values with the same amplitude. It entails that from a certain value of  $\Delta_{61}$  ( $\Delta_{61} = 0.08$  chip), sub-chips (of the  $BOC(6,1)$ ) are disappearing.

Illustrations presented in Figure 6-11 show this concept for different distortions:

- 1) TM-A1 with  $\Delta = 1.08$  chips
- 2) TM-A2 with  $\Delta_{11} = 0.5$  chip ( $\Delta_{61}$  not considered)
- 3) TM-A2 with  $\Delta_{61} = 0.08$  chip ( $\Delta_{11}$  not considered)

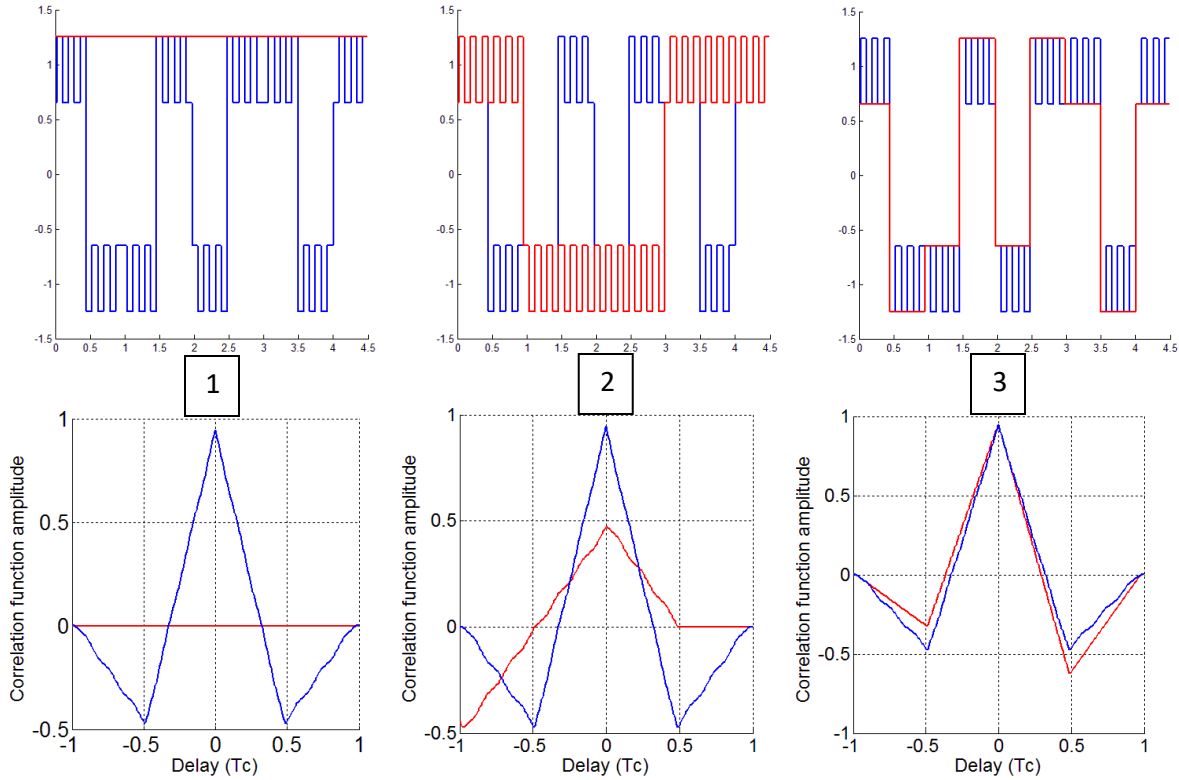


**Figure 6-11.** CBOC signals affected by different digital distortions on the top and associated correlation functions on the bottom.

In the three cases, choosing higher values of  $\Delta$ ,  $\Delta_{61}$  and  $\Delta_{11}$  does not bring any change on the signal. These limits can be considered as  $\Delta$ ,  $\Delta_{61}$  and  $\Delta_{11}$  values that entail a saturation of the distortion. By consequence it is not necessary to take into account higher values of  $\Delta$ ,  $\Delta_{61}$  and  $\Delta_{11}$ .

### 6.3.2.3 Limitation of the TM-A TS based on the detection capability of the reference station

It is noticeable that some of the distortions with high values of  $\Delta$  should be easily detected. The range of  $\Delta$  could be limited by the assumed capability of the reference to detect tracking bias larger than 20 meters.

Using this condition,  $\Delta$  and  $\Delta_{11}$  can be decreased to 0.12 chip and 0.10 chip respectively, as represented in Figure 6-12. Reference configuration was applied to establish these plots.

By consequence, for TM-A1, the following parameter values are envisaged:

$$-0.12 \text{ chip} \leq \Delta \leq 0.12 \text{ chip}$$

and for TM-A2,

$$-0.1 \text{ chip} \leq \Delta_{11} \leq 0.1 \text{ chip}$$

$$-0.08 \text{ chip} \leq \Delta_{61} \leq 0.08 \text{ chip}$$

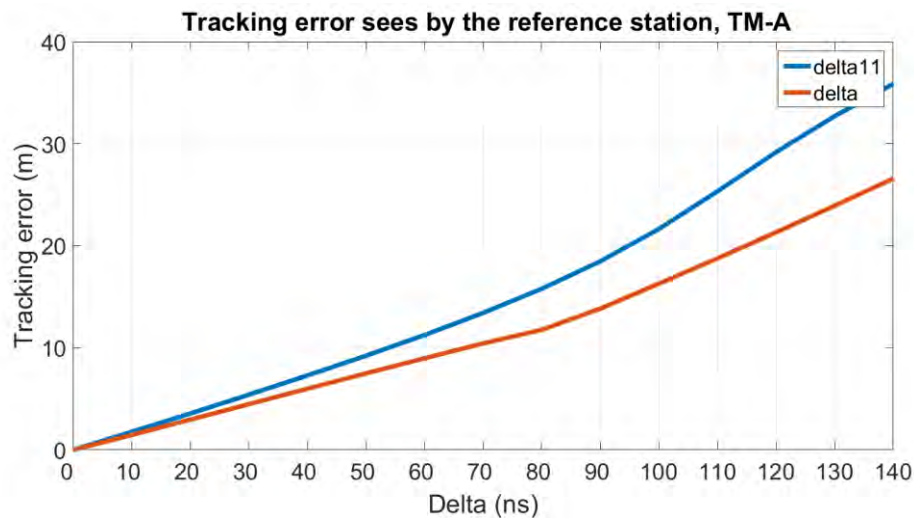


**Figure 6-12.** Tracking error for TM-A1 and TM-A2 and different delta values ( $\Delta$  and  $\Delta_{11}$  ).

#### 6.3.2.4 Proposition of a simplified TM-A

Considering the current GPS L1 C/A digital TM, it is clear that it is assumed that the distortion occurs on the signal after its modulation with the PRN code. However, no information about the Galileo E1C signal generation on-board the payload is available in the literature. Knowing if the three signal components ( $BOC(1,1)$ ,  $BOC(6,1)$ , PRN) are generated independently (TM-A2) or as the product of the components (TM-A1) could help to choose between TM-A1 or TM-A2 or both.

Assuming that the digital signal is directly generated as the components product would entails that only TM-A1 should be preserved. It is noteworthy that no digital distortion was observed on Galileo nominal signals. It means that the TM-A1 already takes into account distortions that are not generated by Galileo satellites payload in nominal conditions. Based on these assumptions a simplified TM-A is proposed and consists only in TM-A1.

#### 6.3.3 Summary of the proposed TM-A for new signals

It is proposed to consider as a signal distortion threat for Galileo E5a, GPS L5 and Galileo E1C, digital distortions that replicate the type of threat of the current ICAO GPS L1 C/A TM.

- For Galileo E5a and GPS L5,  $BPSK(10)$ -modulated, it is decided to reuse the TM-A defined for GPS L1 C/A because of similarities between modulations.
- For Galileo E1C, a larger number of digital distortions could be considered due to the presence of sub-carriers in the signal. Without prior knowledge about the satellite payload, two digital distortions for Galileo E1C signals are proposed: TM-A1 and TM-A2 that consider potential separation of the origin of the distortions related to the sub-carriers. TM-A2 results in the definition of two new TM parameters.

The TS for Galileo E1C has firstly been limited by physical considerations and then using one of the two criteria proposed to select threatening distortions: distortion which entails a tracking error on the reference station larger than 20 m are removed from the TS.

As a conclusion, the proposed parameters for the TM-A of GPS L5, Galileo E5a and Galileo E1 C are given in Table 6-4.

	Conservative TM	Simplified TM
Galileo E1C	$-117 \text{ ns} \leq \Delta \leq 117 \text{ ns}$	$-117 \text{ ns} \leq \Delta \leq 117 \text{ ns}$
	$-97 \text{ ns} \leq \Delta_{11} \leq 97 \text{ ns}$	/
	$-78 \text{ ns} \leq \Delta_{61} \leq 78 \text{ ns}$	/
Galileo E5a and GPS L5	$-117 \text{ ns} \leq \Delta \leq 117 \text{ ns}$	$-117 \text{ ns} \leq \Delta \leq 117 \text{ ns}$

**Table 6-4.** Digital parameters proposed range for Galileo E1C, Galileo E5a and GPS L5.

It is noteworthy to remind that all these limits can be reduced if the reference station is able to detect bias smaller than 20 m.

## 6.4 TM-B like proposition for new signals

As presented at the beginning of this chapter, ICAO TM-B consists of a damped ringing phenomenon induced at chip transitions and can be modeled by a second order low pass filter characterized by two parameters:  $f_d$  and  $\sigma$ . It is proposed to also apply the same second order ICAO TM-B filter to represent analog signal distortions on the investigated GNSS signals. The remaining difficulty is to define the TS. The same methodology as the one introduced in section 6.2.2 is used to limit the TS:

### 6.4.1 Lower limit for $\sigma$ and $f_d$ parameters

In this section, the lower TS bounds are defined: firstly the ringing frequency  $f_d$  and then the damping factor  $\sigma$ .

#### 6.4.1.1 Ringing frequency $f_d$

Figure 6-13 presents the influence of distortions with low  $f_d$  (1, 2, 3 and 4 MHz) on the reference receiver as a function of the damping factor for Galileo E5a, GPS L5, GPS L1 C/A and Galileo E1C signals. It reads as follows:

- Results for Galileo E1C are in red, for Galileo E5a and GPS L5 in blue and for GPS L1 C/A in green.
- In black is represented the 20 m tracking error limit over which distortions are considered as detected by the ground.
- For one given signal, dotted curves represent the lowest  $f_d$  that induces a tracking error on the reference receiver lower than 20 m for at least one  $\sigma$  value. This  $f_d$  must thus be included in the TS.
- For one given signal, continuous curves represent the lowest  $f_d$  that induces a tracking error on the reference receiver higher than 20 m for all  $\sigma$  values.

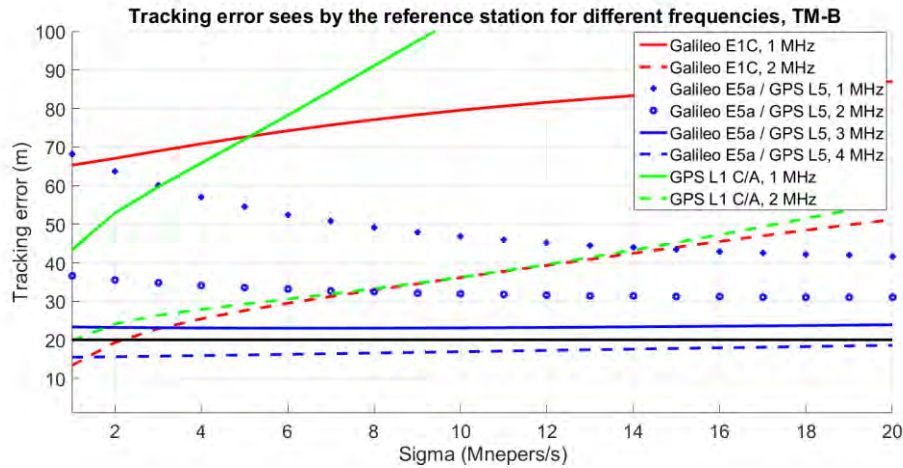


**Figure 6-13.** Tracking errors entail by low  $f_d$  distortions on a reference station for different signals.

Curves represented by circles and crosses for Galileo E5a and GPS L5 show that analog distortions with  $f_d$  lower than 3 MHz are detected by the reference and do not have to be included in the TS.

As a consequence, all  $f_d$  lower than 1 MHz for Galileo E1C and GPS L1 C/A and 3 MHz for Galileo E5a and GPS L5 should be detected at the reference station level by the complementary monitor on the absolute bias. Therefore, it seems legitimate to remove these low  $f_d$  from the TS.

#### 6.4.1.2 Damping factor $\sigma$

Without any consideration, the lowest value of  $\sigma$  should be taken equal to zero. To be conservative, this value is also adopted for GPS L1 C/A signal even if nowadays the lowest value of  $\sigma$  is fixed to 0.8 Mnepers/s by ICAO. For simulation reasons, the lowest tested value of  $\sigma$  is not taken equal to zero but equal to 0.05 Mnepers/s as discussed in 6.4.3.

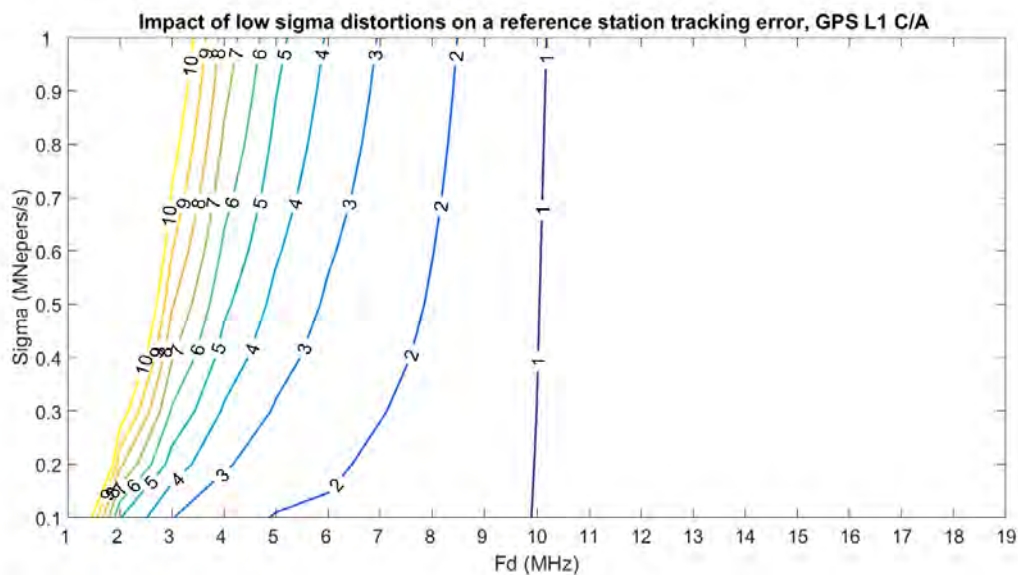


**Figure 6-14.** Tracking error entails by low  $\sigma$  distortions on a reference station, GPS L1 C/A.



It can be seen from Figure 6-14 that distortions with low  $\sigma$  values ( $\sigma$  between 0.1 Mnepers/s and 1 Mnepers/s) are physically conceivable and can be assumed undetected by the reference station because inducing tracking errors on that reference station lower than 20 m.

#### 6.4.2 Upper limit for $\sigma$ and $f_d$ parameters

##### 6.4.2.1 Maximum differential tracking errors entailed by second order distortions

The following plots represent the worst differential tracking error for all considered reference configurations. Results are presented for Galileo E1C in Figure 6-15, for Galileo E5a and GPS L5 signals in Figure 6-16 and for GPS L1 C/A in Figure 6-17.

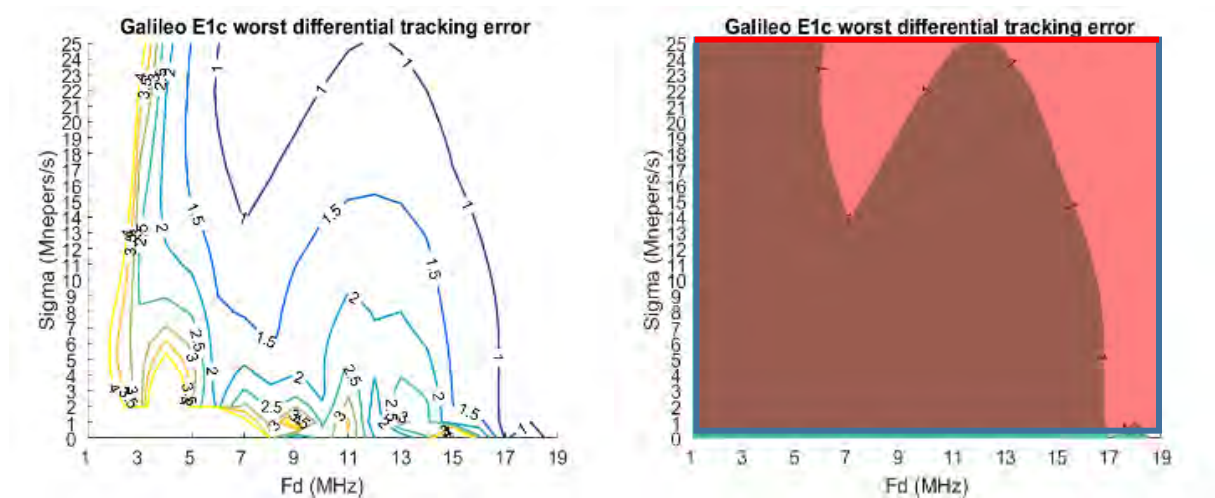


**Figure 6-15.** Worst differential tracking error for different signal distortion parameters. On the right, only the 1 m limit is shown. Blue limits give the remaining conservative TM. Red limit underlines that the TM cannot be bounded for high  $\sigma$  values. Galileo E1C.

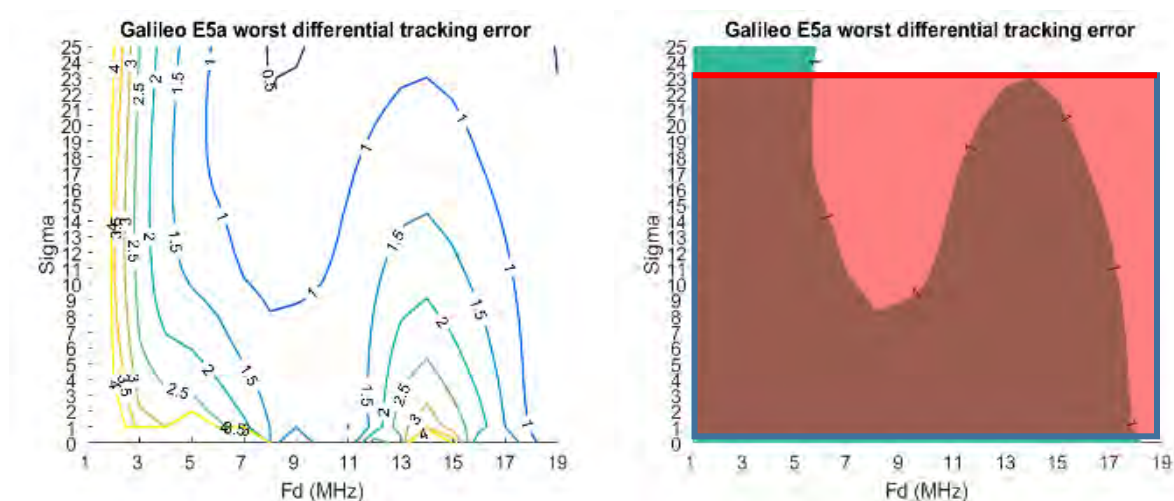


**Figure 6-16.** Worst differential tracking error for different signal distortion parameters. On the right, only the 1 m limit is shown. Blue limits give the remaining conservative TM. Red limit underlines that the TM cannot be bounded for high  $\sigma$  values. Galileo E5a and GPS L5.

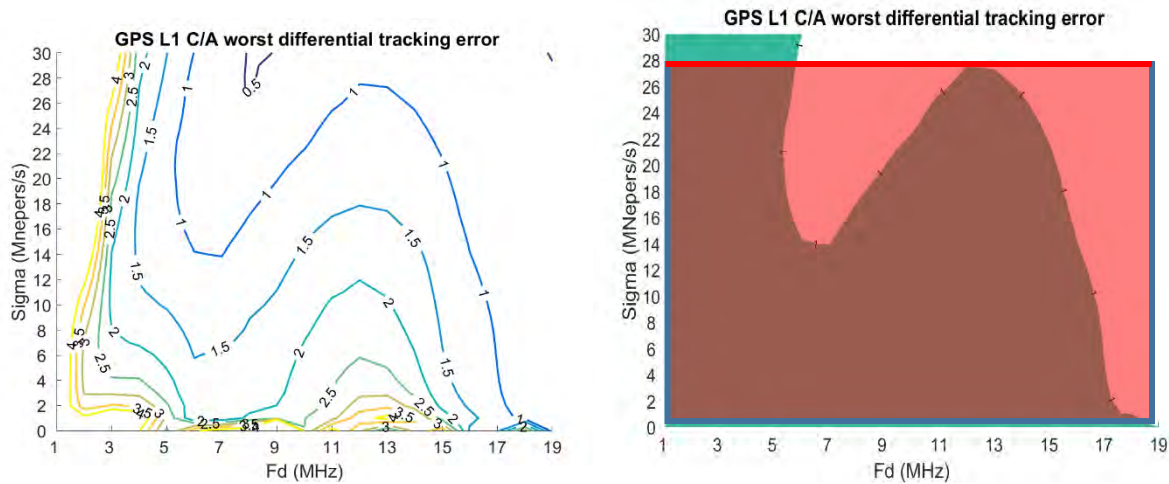


**Figure 6-17.** Worst differential tracking error for different signal distortion parameters. On the right, only the 1 m limit is shown. Blue limits give the remaining conservative TM. Red limit underline that the TM cannot be bounded for high  $\sigma$  values. GPS L1 C/A.

As a reminder, the withheld TS is the parameters range leading to a worst case differential error higher than  $\Delta_{err\_max} = 1$  m (dark colored area on right plots).

To have a simple TM definition, it is decided to adopt a rectangular TS. Table 6-5 represents the TM limits (also representing with blue and red lines in the above figures) for  $f_d$  and low  $\sigma$  that can be chosen from differential tracking error considerations or that have been fixed in the previous section 6.4.1. This rectangle is referred to as TM-B “area 1”.

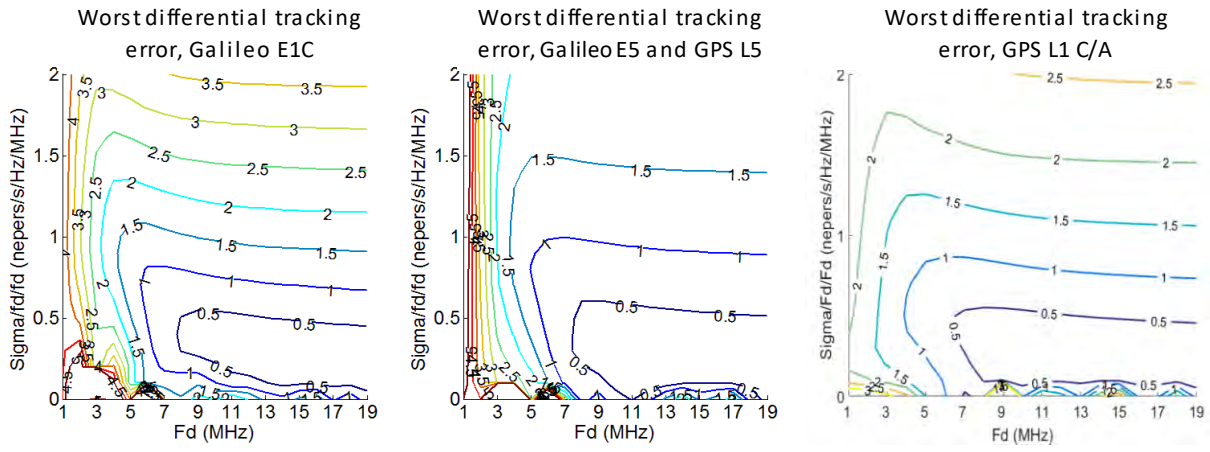
	Galileo E1C	Galileo E5a and GPS L5	GPS L1 C/A
$f_d$ (MHz)	1 to 19	3 to 19	1 to 19
$\sigma$ (Mnepers/s)	0 to 26	0 to 24	0 to 28

**Table 6-5.** Analog parameters proposed range for different signals on area 1.

It is however noticeable that the rectangular area does not include large differential tracking errors generated by high  $\sigma$  distortions when  $f_d$  is low. There is thus a need to define a complementary area to the area 1 to define the TS.

To define this second area, another representation to observe the impact of high  $\sigma$  on the tracking error is used. It consists in plotting the tracking error for signal distortions with  $(\frac{\sigma}{f_d})^2; f_d$  axis as shown in Figure 6-18. As an example, this figure gives the differential tracking error after applying filter 3 (150 ns differential group delay resonator) on the user receiver (and taking the worst case among the two different correlator spacing values and the seven different bandwidths) and filter 1 (6<sup>th</sup>-order Butterworth) on the reference for the four signals of interest. It is noteworthy to mention that differential errors can also be large (i.e. larger than the considered  $\Delta_{err\_max} = 1$  m limit) for high  $\sigma$  values. Galileo E1C results are presented on the left, Galileo E5a and GPS L5 results on the middle and GPS L1 C/A results on the right.

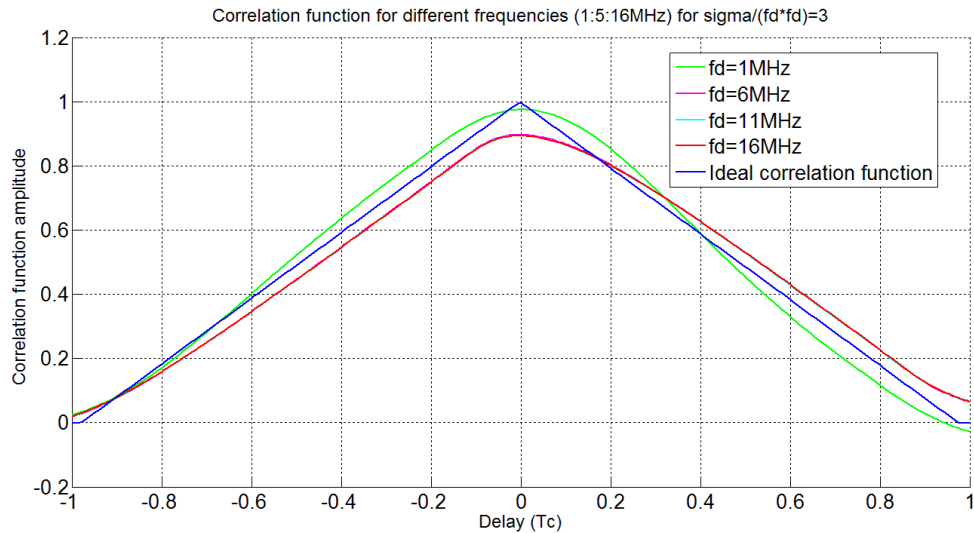




**Figure 6-18.** Differential tracking errors in meter generated by a TM-B distortion, function of  $\frac{\sigma}{(f_d)^2}$  and  $f_d$  for signals of interest.

This new  $(\frac{\sigma}{(f_d)^2}; f_d)$  representation has a lot of interest because it illustrates that:

- even strongly attenuated distortions can lead to high differential tracking errors. This phenomenon can be explained by the fact that the correlation function is strongly rounded and distorted in an asymmetric way for high  $\sigma$  values (as illustrated in Figure 6-19) for an unfiltered GPS L1 C/A signal. In this figure, the ratio  $\sigma/(f_d)^2$  is set to 3 and four different  $f_d$  values are tested. It is noticeable that curves obtained for  $f_d = 6$  MHz ( $\sigma = 36$  Mnepers/s),  $f_d = 11$  MHz ( $\sigma = 121$  Mnepers/s) and  $f_d = 16$  MHz ( $\sigma = 256$  Mnepers/s) are superimposed.
- the tracking error is (almost) constant for a given  $\sigma/(f_d)^2$  and high frequencies. More details about this property is given in appendix G.



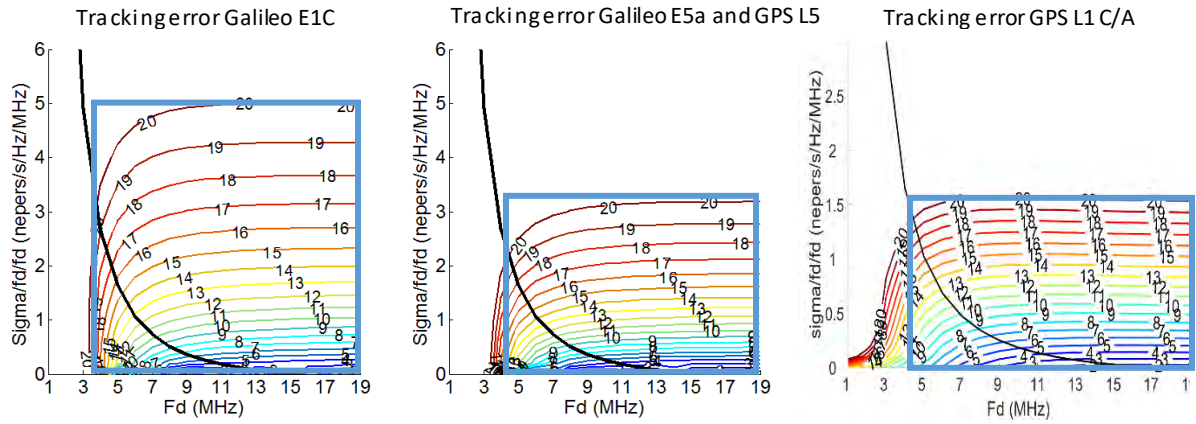
**Figure 6-19.** Impact of highly attenuated TM-B distortions on the correlation function.

Figure 6-20 represents the tracking errors observed by a reference station with the considered configurations for a Galileo E1C (left), a Galileo E5a and GPS L5 (middle), and a GPS L1 C/A signal (right).

An advantage of the  $\sigma/(f_d)^2$  representation is that high values of  $\sigma/(f_d)^2$  can be easily bounded using the condition related to the reference capability to detect large absolute tracking bias. Consequently,

## 6. Non-nominal distortions

it is decided to establish a TM-B “area 2” upper limit in the  $\sigma/(f_d)^2$  representation based on this reference capability. It is reminded that in this document the reference minimum detectable bias is assumed equal to 20 m.



**Figure 6-20.** Tracking errors affecting the reference in meter generated by TM-B distortions, function of  $\frac{\sigma}{(f_d)^2}$  and  $f_d$ . Blue rectangles represent area 2 limits, black lines area 1 upper limits.

The “area 2” lower limit is based on its complementarity with “area 1”. To be conservative, the lower limit for

- Galileo E1C is given by:

$$\left(\frac{\sigma}{(f_d)^2}\right)_{\min} = \frac{26}{19^2} \approx 0.07 \text{ nepers/s/Hz/MHz}$$

- Galileo E5a and GPS L5 is given by:

$$\left(\frac{\sigma}{(f_d)^2}\right)_{\min} = \frac{24}{19^2} \approx 0.06 \text{ nepers/s/Hz/MHz}$$

- GPS L1 C/A is given:

$$\left(\frac{\sigma}{(f_d)^2}\right)_{\min} = \frac{28}{19^2} \approx 0.07 \text{ nepers/s/Hz/MHz}$$

One important point is that distortions with  $\sigma/(f_d)^2$  value higher than  $(\sigma/(f_d)^2)_{\min}$ , can be studied in the  $\sigma/(f_d)^2$  representation. Indeed, from this  $(\sigma/(f_d)^2)_{\min}$  the new representation is able to take into account most of the different threatening distortions even for high  $f_d$  where less  $\sigma$  are tested. This is supported by the fact that above this limit, distortions vary slowly as intuited on Figure 6-20 and as it will be demonstrated in the next part.

TM-B “area 2” could be reduced to the area between the 20 m absolute tracking error upper limit and the black line representing the “area 1” upper limit in the  $\sigma/(f_d)^2$  representation (Figure 6-20). Nonetheless, to be conservative and simplify the TMs definition, it is decided to limit “area 2” to the blue rectangles. Finally, the proposed “area 2” limits are given in Table 6-6 for all considered signals.

	Galileo E1C	Galileo E5a and GPS L5	GPS L1 C/A
$f_d$ (MHz)	3 to 19	4 to 19	4 to 19
$\frac{\sigma}{(f_d)^2}$ (nepers/s/Hz/MHz)	0.07 to 5	0.06 to 3.5	0.07 to 1.8
$\sigma$ (Mnepers/s) For the minimum $f_d$ value	0.6 to 45	1 to 56	1 to 29
$\sigma$ (Mnepers/s) for $f_d = 19$ MHz	25 to 1805	22 to 1266	25 to 650

**Table 6-6.** Analog parameters proposed range for different signals on area 2.

### 6.4.3 Number of tests to cover the entire proposed TM

It is noticeable that the proposed TS for TM-B, composed of both areas 1 and 2, is wider (by a factor 100) than the GPS L1 C/A TS defined by ICAO. The purpose of this part is to compare the TS in terms of number of tests to consider to take into account all threatening distortions with a fair resolution. In this part, the term resolution is used to represent the capacity of a set of tests to get the largest variety of different distortions as possible in a given TS.

#### 6.4.3.1 Tested distortions in the $\sigma/(f_d)^2$ and in the $\sigma$ representation

The new  $\sigma/(f_d)^2$  representation is equivalent to a y-axis scale change compared to the traditional  $\sigma$  representation used to define the TM-B and TM-C TSs.  $\sigma/(f_d)^2$  and  $\sigma$  scales have advantages and drawbacks that are exposed in this part.

- **$\sigma$  representation:** the  $\sigma$  resolution is identical for low and high  $f_d$ . Indeed, if the resolution on the y-axis ( $\sigma$ ) is 1 Mnepers/s, tested distortions will have  $\sigma$  values equal to 0, 1, 2, 3 Mnepers/s etc. whatever  $f_d$  is, as illustrated in Figure 6-21.

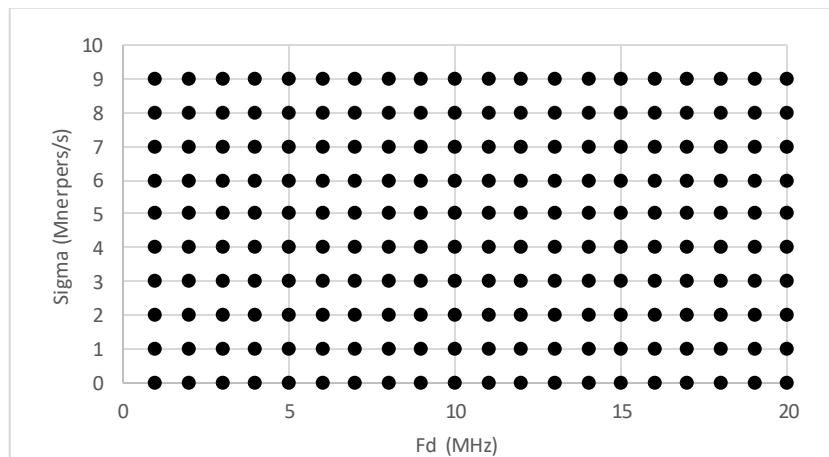


**Figure 6-21.**  $\sigma = 1$  Mnepers/s increment in the traditional  $\sigma$  TM representation. Points represent tested distortions.

## 6. Non-nominal distortions

- $\sigma/(f_d)^2$  representation: the  $\sigma$  resolution is  $f_d$ -dependent. Indeed, if the resolution on the x-axis ( $\sigma/(f_d)^2$ ) is 1 nepers/s/Hz/MHz, the tested distortions will have  $\sigma$  values equal to 0, 1, 2, 3 Mnepers/s etc. for a frequency equal to 1 MHz and 0, 400, 800, 1200 Mnepers/s etc. for a frequency equal to 20 MHz. This allow to run through  $\sigma$  values faster, as illustrated in Figure 6-22, but an explanation is necessary to justify that this resolution is applicable.

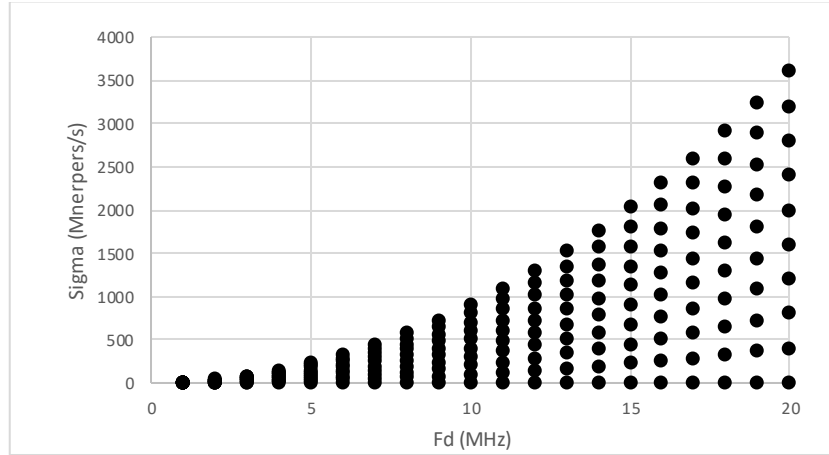


**Figure 6-22.**  $\frac{\sigma}{(f_d)^2} = 1$  nepers/s/Hz/MHz increment in the traditional  $\sigma$  TM representation. Points represent tested distortions.

The problem is that for high frequencies, the tested distortions resolution could not be high enough in the  $\sigma/(f_d)^2$  representation. A proposition to estimate the resolution with which a TS has to be studied is presented in the next part.

### 6.4.3.2 Strategy to limit the number of distortions to test in the proposed TM

It is not possible to test all threatening distortions because there is an infinity of distortions in a TS. It is thus required to sample the TS so that it is representative of all distortions without missing any potential hazardous ones.

Let us define the spacing between two consecutive tested distortions as the spacing between two distortions with the same  $f_d$  but two consecutive  $\sigma$  values, or with the same  $\sigma$  but two consecutive  $f_d$ . To measure the appropriate spacing between consecutive tested distortions, let us introduce the parameter  $\Delta_{err\_dist}$ , representative of the tracking error difference observed between the two tested distortions. To be sure that the filter does not have any impact and to extract only the impact of the distortion on the shape of the correlation function,  $\Delta_{err\_dist}$  is estimated from unfiltered distorted correlation functions.

The methodology to define an appropriate spacing between two consecutive distortions is to consider that only low enough  $\Delta_{err\_dist}$  values are tolerable. Indeed, if these values are too large, it means that the sampling of the TS is too loose and that the correlation function shape varies significantly between two consecutive tested distortions. The consequence is that some threatening distortions could be omitted. It is important to note that  $\Delta_{err\_dist}$  does not reflect directly the difference of correlation function shape between two tested distortions. To be rigorous, a metric based on all correlation function points could be evaluated. Nevertheless, for the present purpose, only a general idea of the correlation function behavior is sufficient.

The lower the value of  $\Delta_{err\_dist}$  is, the better the resolution is. The  $\Delta_{err\_dist}$  used to decide if the test grid is well designed for the propose TM is assumed to have the same order of magnitude than the  $\Delta_{err\_dist}$  resulting from the ICAO GPS L1 C/A test methodology. As an example, it is decided to introduce the grid of tested distortions presented in Figure 6-23 for the GPS L1 C/A ICAO TS:  $f_d = 4: 1: 17$  MHz,  $\sigma = 0.8: 1: 8.8$  Mnepers/s. In this case, one hundred and twenty-six tests are performed to cover the GPS L1 C/A ICAO TS. A significantly coarser grid is used in this section for GPS L1 C/A than was used for WAAS. Indeed, for WAAS, the increment on  $f_d$  is equal to 0.1 MHz and the increment on  $\sigma$  is equal to 0.5 Mnerpers/s [Phelts et al., 2003]. Nevertheless, the aim of this section is only to give orders of magnitude of the number of distortions to test on proposed TMs compared to the number of distortions to test on the ICAO one. For this particular case,  $\Delta_{err\_dist}$  values are given Figure 6-24. Different curves correspond to the fourteen tested  $f_d$ . The x-axis gives the mean value of  $\sigma$  between the two consecutive tested values of  $\sigma$ .

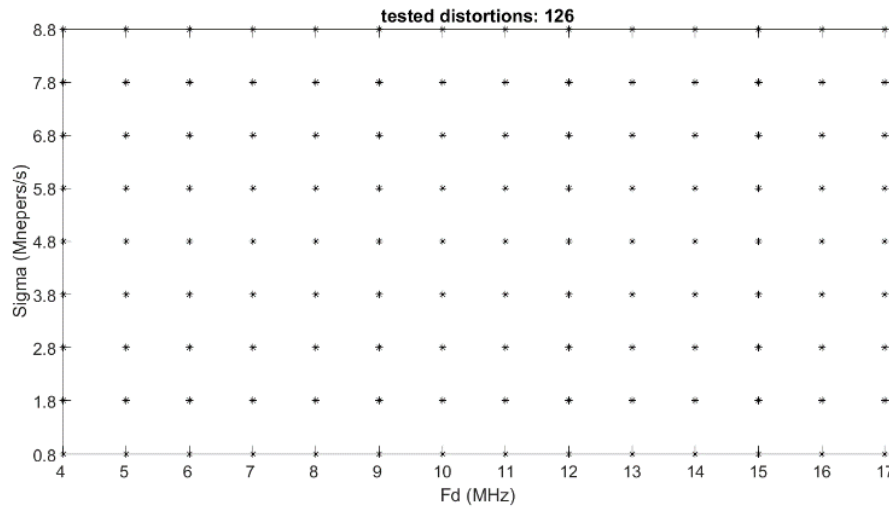


**Figure 6-23.** Example of a TS grid (GPS L1 C/A ICAO TM).

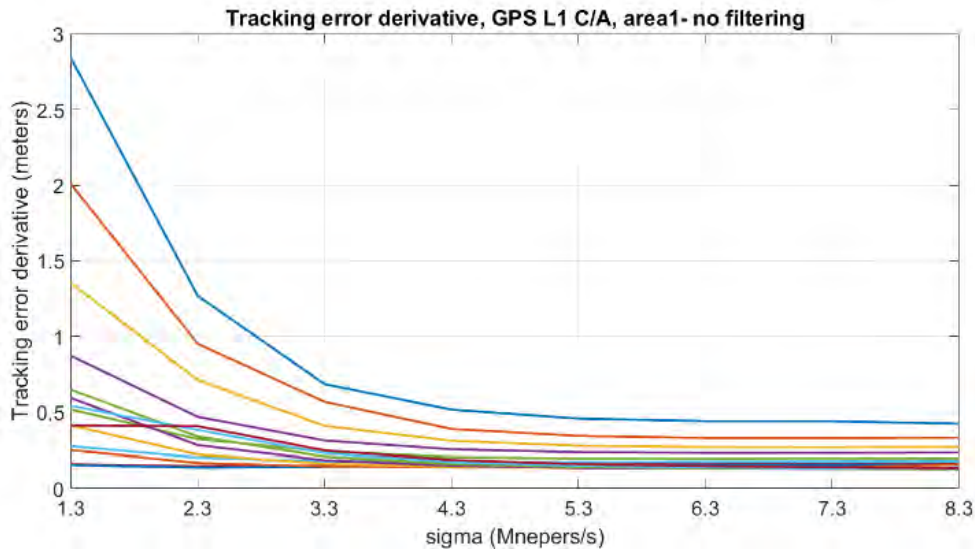


**Figure 6-24.**  $\Delta_{err\_dist}$  as a function of  $\sigma$  associated to the TS grid from Figure 6-23 (GPS L1 C/A ICAO TM).

From Figure 6-24, the maximum  $\Delta_{err\_dist}$  obtained with this sampling of the L1 C/A current TS is 2.8 m. This is the approximate upper limit of  $\Delta_{err\_dist}$  that has to be targeted when sampling the TS of

the proposed new GNSS signals TM. Note that the value of 2.8 m might appear relatively high and could be decreased by choosing a thinner grid to test the TS.

### 6.4.3.3 Number of tests: example of TM-B area 1 on Galileo E1C

The methodology introduced above is used in this part to estimate the number of distortions to test on area 1 for Galileo E1C. Results for Galileo E5a, GPS L5 signals and GPS L1 C/A on TM-B area 1 and TM-B area 2 are provided in appendix F as well as results for Galileo E1C on TM-B area 2.

#### 6.4.3.3.1 Galileo E1C area 1

To find the same  $\Delta_{err\_dist}$  as on the ICAO GPS L1 C/A TM-B, for the area 1 of the Galileo E1C TM-B, one thousand and three tests are necessary to cover the whole area. This augmentation (compared to the one hundred and twenty-six for GPS L1 C/A) is due to the fact that higher values of  $\sigma$  and more values of  $f_d$  are considered in area 1 of the proposed TM. Moreover, for low  $f_d$  and  $\sigma$  values, a thinner grid has to be designed to reach the same  $\Delta_{err\_dist}$  order of magnitude as on the GPS L1 C/A TM-B. The proposed grid is presented in Figure 6-25.

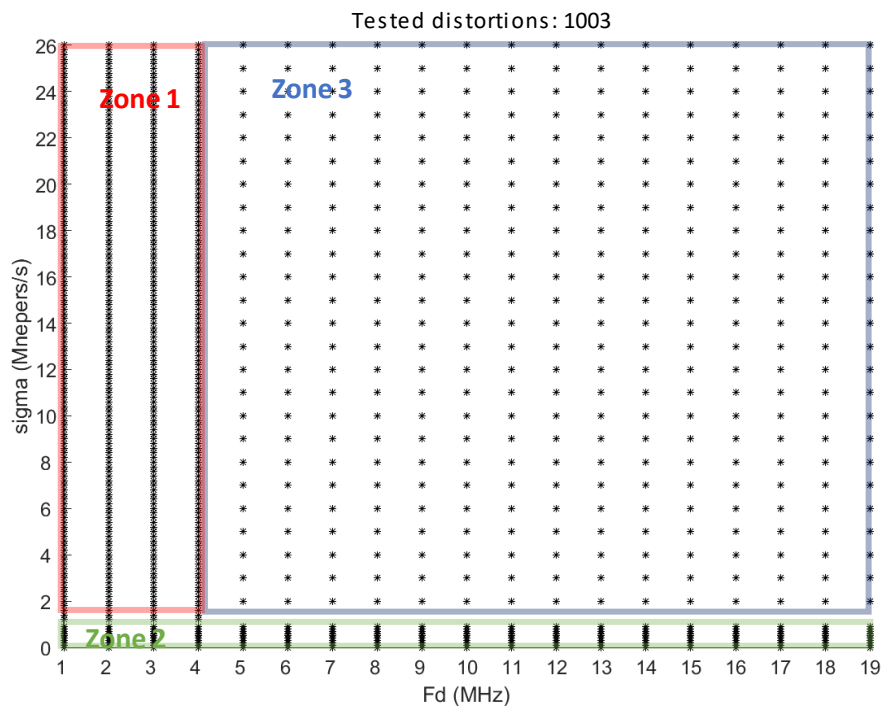


**Figure 6-25.** Example of TS grid (Galileo E1C, area 1 of the proposed TM-B).

The area 1 can be decomposed in three tested zones:

- Zone 1 to study low  $f_d$ . The grid consists of  $f_d = 1:1:4$  MHz,  $\sigma = 1:0.2:26$  Mnepers/s. This zone is included in the red square on Figure 6-25.
- Zone 2 to study low  $\sigma$ . The grid consists of  $f_d = 1:1:19$  MHz,  $\sigma = 0.05:0.1:1$  Mnepers/s. It is noticeable that distortions with  $\sigma$  lower than 0.05 Mnepers/s cannot be studied without increasing dramatically the number of tests. This is why this lower bound of 0.05 Mnepers/s is set. This zone is included in the green square on Figure 6-25.

- Zone 3 to study the rest of the TS. The grid consists of  $f_d = 4:1:19 \text{ MHz}$ ,  $\sigma = 1:1:26 \text{ Mnepers/s}$ . This zone is included in the blue square on Figure 6-25.

$\Delta_{err\_dist}$  associated to zone 1 are presented Figure 6-26.  $\Delta_{err\_dist}$  associated to zone 2 are presented Figure 6-27.  $\Delta_{err\_dist}$  associated to zone 3 are presented Figure 6-28. It is recalled that one curve corresponds to one  $f_d$ . The blue curve corresponds to the lowest tested  $f_d$  (1 MHz), the orange to the second one, the yellow to the third one and the purple to the fourth one.

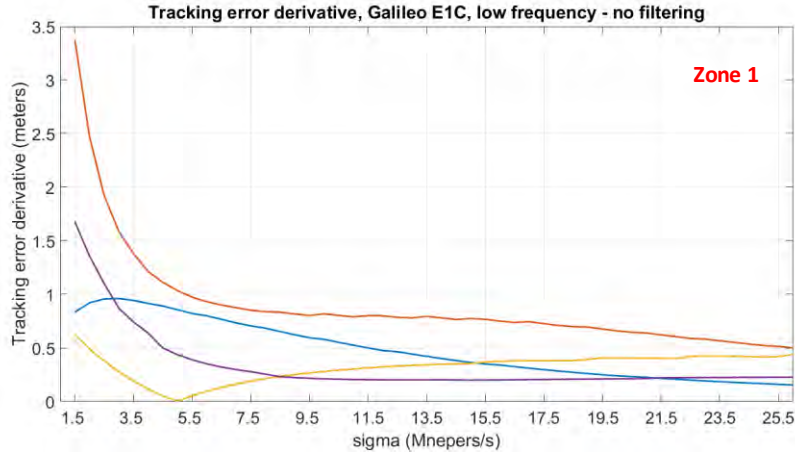


**Figure 6-26.**  $\Delta_{err\_dist}$  as a function of  $\sigma$  associated to the zone 1 of the selected TS grid (Galileo E1C, area 1 of the proposed TM-B).

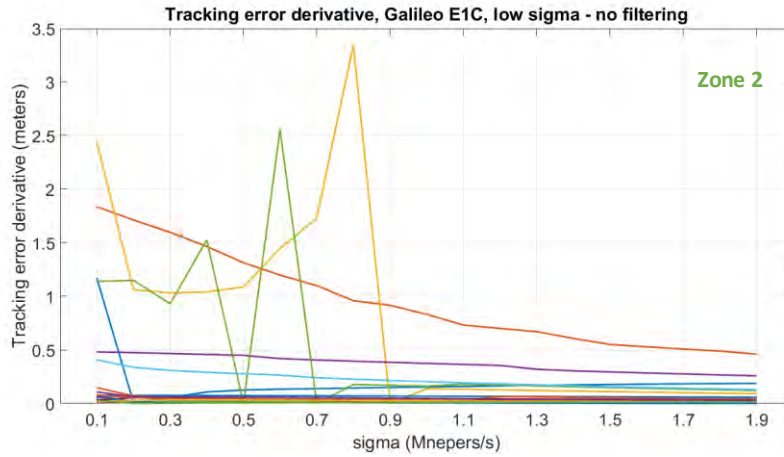


**Figure 6-27.**  $\Delta_{err\_dist}$  as a function of  $\sigma$  associated to the zone 2 of the selected TS grid (Galileo E1C, area 1 of the proposed TM-B).



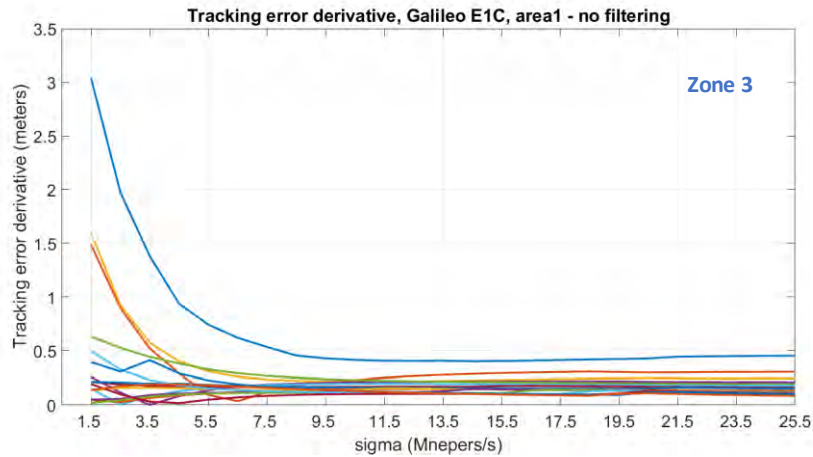


**Figure 6-28.**  $\Delta_{err\_dist}$  as a function of  $\sigma$  associated to the zone 3 of the selected TS grid (Galileo E1C, area 1 of the proposed TM-B).

With the grid proposed for the area 1 of the Galileo E1C signal TM-B, the maximum value of  $\Delta_{err\_dist}$ , equal to 3.4 m, has same order of magnitude as the maximum value of 2.8 m obtained with the GPS L1 C/A ICAO TM (see Figure 6-23). Even if the value is slightly higher, it can be noticed that only three cases entail  $\Delta_{err\_dist}$  higher than 2.6 m. Another zone could be defined around cases which entail  $\Delta_{err\_dist}$  higher than 2.6 m, nevertheless for simplicity reasons on Galileo E1C area 1, this new grid can be adopted to obtain approximatively the same resolution. In this condition, the number of tested values is multiplied by a factor 8 ( $\approx 1003/126$ ).

#### 6.4.3.3.2 Conclusions about the number of distortions to test

To conclude, it has been seen in this section how to estimate the number of distortions to test on the proposed TMs. It is clear that more tests are required to cover the proposed TS as shown in appendix F. However, to obtain approximatively the resolution with which the TS is examined in the GPS L1 C/A ICAO TM case, the number of simulations can be limited to:

- $13.4 + 8 = 21.4$  times the number of simulations compared to the current ICAO TM for Galileo E1C.
- $6.7 + 1 = 7.7$  times the number of simulations compared to the ICAO current TM for Galileo E5a and GPS L5.
- $8.3 + 2.7 = 11$  times the number of simulations compared to the ICAO current TM for GPS L1 C/A because more distortions are considered in the proposed TS.

These three values are reasonable considering GNSS signal distortions context.

#### 6.4.4 Summary on the proposed TM-B for new signals

In this part, a proposition of ICAO TM-B like has been given for Galileo E1C, Galileo E5a, GPS L5 and GPS L1 C/A based on a new methodology. The GPS L1 C/A case has also been looked at in order to fairly compare the proposed TS for the considered signals obtained with the proposed methodology.

The proposed TM is purposely conservative because it includes all dangerous signal distortions, meaning that it also includes very high  $\sigma$  values. This differs from the current ICAO TM for GPS L1 C/A.



A solution is proposed to limit the number of distortions to test. This solution consists in the separation of the TS in two areas:

- Area 1: This representation is equivalent to the classical ICAO TM-B distortion representation. This area is necessary to take into account low  $\sigma$  signal distortion behaviors.
- Area 2: This area resides on  $\sigma/(f_d)^2$  on the y-axis and  $f_d$  on the x-axis. This area is the complementary of area 1.

Two criteria were used to limit the TS of each TM based on the impact of distortions on:

- the differential tracking error which has to be higher than 1 m to be considered as a threat and
- the reference ground station tracking error which has to be lower than 20 m to be considered as a threat not detected by the ground.

These criteria led to the following TS restrictions that are summarized in Figure 6-29:

- Low  $f_d$  are detected by the ground station.
- High  $f_d$  do not have a threatening impact on DGNSS users.
- Low  $\sigma$  lead to divergent signals.
- High  $\sigma$  are detected by the ground station.

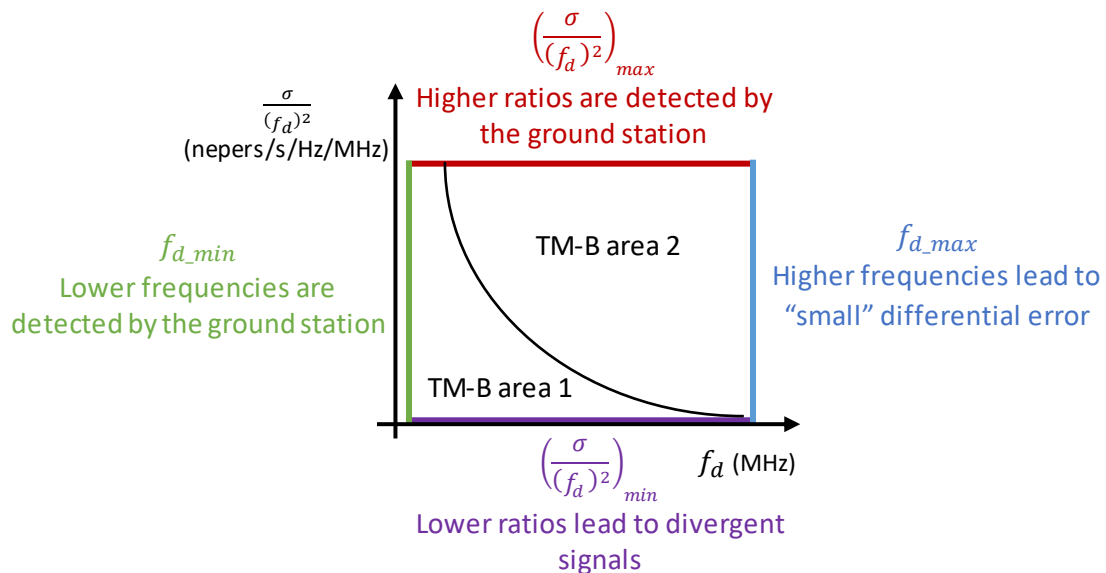


**Figure 6-29.** Summary of reasons that are considered to limit TSs.

An important remark is that the TS is dependent upon the reference station capability to detect a large tracking bias. Such bias detectors are not specified in current requirements but could be envisaged. Results given in this document are established making the assumption that the reference is able to detect minimum detectable bias on any pseudorange equal to 20 m. If performance of the reference station is better, the TS could be smaller.

Proposed TS parameters presented in Table 6-7 are fairly conservative. It is noticeable that more signal distortions have to be tested on new signals in comparison to the current ICAO GPS L1 C/A TM. Indeed, to run through the proposed TM, the number of tests have to be increased by a factor 8 for Galileo E5a and GPS L5 and a factor 21 for Galileo E1C.

		Galileo E1C	Galileo E5a and GPS L5	GPS L1 C/A
Area 1	$f_{d\_min}$ (MHz)	1	3	1
	$f_{d\_max}$ (MHz)	19	19	19
	$\sigma_{min}$ (Mnepers/s)	0	0	0
	$\sigma_{max}$ (Mnepers/s)	26	24	28
Area2	$f_{d\_min}$ (MHz)	3	4	4
	$f_{d\_max}$ (MHz)	19	19	19
	$\left(\frac{\sigma}{(f_d)^2}\right)_{min}$ (nepers/s/Hz/MHz)	0.07	0.06	0.07
	$\left(\frac{\sigma}{(f_d)^2}\right)_{max}$ (nepers/s/Hz/MHz)	5	3.5	1.8

**Table 6-7.** Proposed TM-B parameters range for different signals using two representations.

Figure 6-30 gives, as an example, the two areas in the  $\sigma$  (left plot) and in the  $\sigma/(f_d)^2$  (right plot) representations for Galileo E5a and GPS L5 signals.

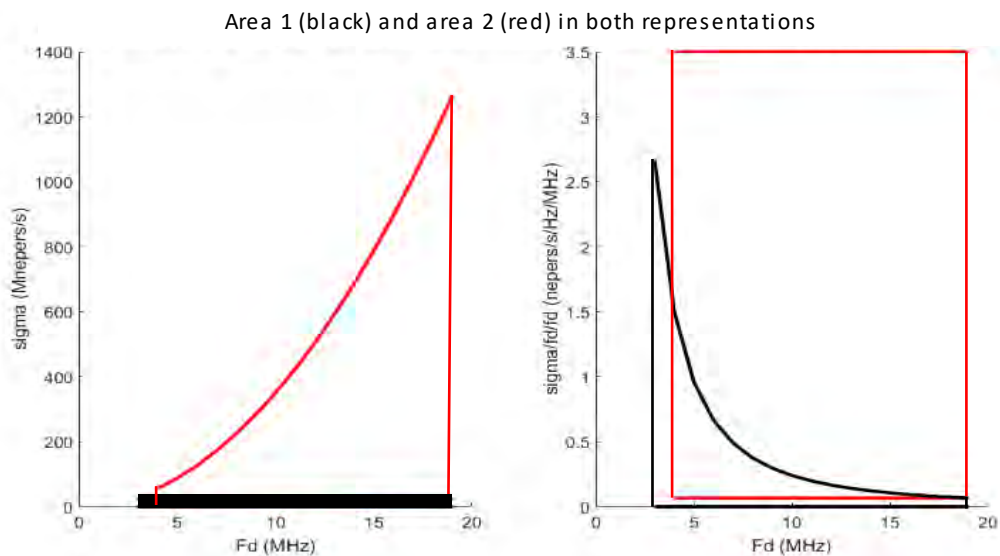


**Figure 6-30.** Area 1 (black) and area 2 (red) in the  $\frac{\sigma}{(f_d)^2}$  representation (left) and in the  $\sigma$  representation (right) for Galileo E5a and GPS L5 signals.

## 6.5 TM-C like propositions for new signals

In the current ICAO TM, the TM-C is a TM-A and TM-B combination. Parameters range chooses for TM-C is smaller than individual parameters range for TM-A and TM-B.

To be conservative and without more knowledge, the TS of the proposed TM-C takes parameters range established for the TM-A and the TM-B. A simplified TM-A was envisaged for Galileo E1C. As a consequence, a simplified TM-C is also envisaged and consists of a combination of the TM-B with the simplified TM-A. It was seen that the simplified TM is based on the assumption that the signal is

generated as the product of signal components and that if this assumption cannot be verified, the conservative TM-A (and TM-C) has to be adopted. Nevertheless, it is also noteworthy to highlight that no digital distortion was observed on Galileo E1C signal. For this reason, the TM-A on Galileo E1C signal could be considered as irrelevant. To be conservative, the TM-C based on the TM-A1 is exposed but to make the study of the TM-C easier, the simplified TM-C is adopted in the following (TM-A2 distortions are not tested conjointly with TM-B distortions).

Proposed parameters ranges are summarized in Table 6-8:

		Galileo E1C	Galileo E5a and GPS L5	GPS L1 C/A
Area 1	$f_d$ ( MHz )	1: 19	1: 19	1: 19
	$\sigma$ ( Mnepers/s )	0: 26	0: 24	0: 28
Area 2	$f_d$ ( MHz )	3: 19	4 : 19	4 : 19
	$\frac{\sigma}{(f_d)^2}$ ( nepers/s/Hz/MHz )	0.07 : 5	0.06 : 3.5	0.07 : 1.8
	$\Delta_{min} =$ $-\Delta_{max}$ ( chips )	0.12	1.2	0.12
Not in the simplified TM-C	$\Delta_{11min} =$ $-\Delta_{11max}$ ( chips )	0.1	/	/
	$\Delta_{61min} =$ $-\Delta_{61max}$ ( chips )	0.08	/	/

**Table 6-8.** Proposed TM-C parameters range for different signals.

## 6.6 Conclusions

A TM is of primary importance regarding GNSS applications with stringent requirements. It permits to characterize expected distortions that could occur on a GNSS signal. The definition of the TM is necessary to estimate what could be the influence of GNSS signal distortions on users and how to deal with such GNSS threats. Indeed, with a given TM, the threat is known and an adapted SQM can be designed.

This chapter proposes three TMs that are all based on the same types of distortions as the ones used current by ICAO for GPS L1 C/A: one for Galileo E5a and GPS L5, one for Galileo E1C and one for GPS L1 C/A signals. The case of GPS L1 C/A is treated to compare a TS obtained from the proposed methodology with the original ICAO TS.

It is clear that the ICAO TM main drawbacks are still present in this approach: only a model is considered with its imperfections, its assumption of the type of payload failure that could occur and the assumption that what was observed in 1993 with a given payload is representative of what could happen with a current payload. Moreover, applying it directly to Galileo signals means that there is an acknowledgement that the Galileo payload would not provide different distortions, which is very unsure. This question of TM legitimacy is raised for example in [Pullen, 2009] but the present work was aiming at providing a first set of TM for new signals that could be justified based on previous work.

## 6. Non-nominal distortions

The approach to limit the TS of the proposed TM-A and TM-B is based on keeping only signal distortions that generate:

- a differential bias higher than  $\Delta_{err\_max} = 1$  m in a specific receiver worst case configuration, which is assumed to be problematic for dual-frequency users,
- a bias at the reference station smaller than 20 m, which is assumed to be a value that can be easily detected by a separate monitor.

These new TMs, with limits summarized in Table 6-9, are interesting because they take into account all possible threats for reference/user configurations considered in this chapter.

Simplified TM-C							
Conservative TM-C							
TM-B				TM-A			
Area 1		Area 2		TM-A1	TM-A2		
$f_d$ (MHz)	$\sigma$ (Mnepers/s)	$f_d$ (MHz)	$\frac{\sigma}{(f_d)^2}$ (nepers/s/ Hz/MHz)	$\Delta_{min} =$ $-\Delta_{max}$ (chip)	$\Delta_{11min} =$ $-\Delta_{11max}$ (chip)	$\Delta_{61min} =$ $-\Delta_{61max}$ (chip)	
Galileo E1C	1: 1: 4	3: 1: 19	0.07: 0.05: 5	0: 0.01: 0.12	0: 0.01: 0.1	0: 0.01: 0.08	
	1: 1: 19						
	4: 1: 19						
Galileo E5a and GPS L5	3: 1: 19	4: 1: 19	0.06: 0.075: 3.5	0: 0.1: 1.2	/	/	
GPS L1 C/A	1: 1: 4	4: 1: 19	0.07: 0.1: 1.8	0: 0.01: 0.12	/	/	
	3: 1: 19						
	1: 1: 3						
	4: 1: 19						

**Table 6-9.** Summary of proposed TM parameters range for different signals.

In Table 6-9, the resolution with which TMs are tested are given for information and can be increased or reduced depending on the application.

Compare to the ICAO TS defined for the GPS L1 C/A signal, proposed TSs are larger because highly attenuated distortions (high values of  $\sigma$ ) are considered.

Note that the proposed methodology could be applied to other signal modulations (modernized GPS, GLONASS, Beidou, etc.).

Once the TM is established, new SQM algorithms can be studied to protect a civil aviation users from the defined threats. This is the subject of the next chapter.

## 7 Signal quality monitoring of new signals

After proposing an EWF TM for Galileo E1C, Galileo E5a and GPS L5 signals in the previous chapter, it is necessary to make sure that the distortions that are part of the TM will not generate hazardous effects on an airborne receiver. In particular, for stringent phases of flight (typically the ones with vertical guidance), it is necessary to detect the occurrence of such distortions and timely inform the user. This is thus one of the roles of augmentation systems such as SBAS or GBAS.

In this chapter, the SQM adapted to the proposed TM and the new GNSS signals is presented. A representation to assess the performance of the SQM is exposed and is used to design a simplified SQM for new signals modulations.

In section 7.1, principles and definitions linked to SQM are given. It is seen that current SQM is based on measurements estimated from correlator outputs that are combined to form metrics that are compared to their nominal values.

In section 7.2, parameters with an influence on the SQM are listed and values of parameters used in this chapter to estimate the SQM performance are given. The definition of these parameters is of primary interest because changing their values also modify the performance of the SQM.

In section 7.3, an innovative representation inspired from [Phelts et al., 2013] is proposed to assess the SQM performance based on the theoretical metrics standard deviation. A reference SQM based on three different metrics (simple ratio, difference ratio and sum ratio metrics) and a high number of available correlator outputs (fifty one outputs) spaced by 0.01 chip is first tested on GPS L1 C/A signal. GPS L1 C/A signal will be taken as an example to illustrate the concept of the innovative representation to assess SQM performance. As a conclusion of this section, a method to adapt theoretical results to operating reference station conditions is suggested.

Section 7.4 compares performance of different SQMs regarding Galileo E1C, Galileo E5a and GPS L5 signal distortions. A compromise will be found between SQM complexity and its performance.

Finally, Section 7.5 concludes this chapter.

### 7.1 SQM requirements and performance assessment

The official definition of the SQM provided in [ICAO, 2006] has been presented in section 4.4.2 and is not reminded in this section.

To summarize, the objective of the SQM is to detect signal distortions generated by a satellite payload failure that can be hazardous for a certified airborne user. It has been seen that a given distortion can affect differently receivers with different configurations: RF front-end technology, group delay, bandwidth and tracking technique (including the local replica and the correlator spacing).

More precisely, the SQM has to ensure that all distortions inducing threatening events are detected with a given  $P_{ffd}$  (probability of fault-free detection, also called probability of false alarm) and a given

$P_{md}$  (probability of missed detection) within a given TTA (Time-To-Alert). These probabilities are actual requirements that are derived from an integrity analysis. It means that the SQM has to ensure that the maximum differential bias induced by an undetected distortion (also called **MUDE** for Maximum Undetected Differential Error) is below a Maximum tolerable ERRor (**MERR**) with a required  $P_{ffd}$ ,  $P_{md}$  and TTA. To meet this objective, **metrics values** based on correlator outputs are assessed and compared to **thresholds**. Theoretically, to estimate if a distortion is detected meeting the proper requirements, the value of the metric without noise can be compared to a Minimum Detectable Error (**MDE**).

By consequence SQM performance is based on six important notions: the MUDE, requirements, the MERR, metrics, thresholds and MDE. The definition of the MUDE is already given in 4.4.3 and is not re-defined in this section. The notion of MERR is tackled in 7.1.1 and the notion of metrics and tests in 7.1.2. Then MDE and requirements are presented in 7.1.3 and 7.1.4, and principles of MDE and thresholds estimation are exposed in 7.1.5.

### 7.1.1 Maximum tolerable ERRor (MERR)

Even if results provided in this chapter can be adapted to different MERR values, this parameter is of primary importance to estimate if SQM performance fulfils requirements. A mathematical expression to estimate the MERR is defined by ICAO and is presented in this part. Nevertheless it appears that in the literature, other expressions and methodologies are used to derive the MERR. In this part, different approaches to derive the MERR are presented and MERR values that will be targeted in this chapter are given.

#### 7.1.1.1 ICAO MERR definition

The notion of MERR was already introduced in 4.4.2 and 6.2.2.3. In the official source, the MERR acronym means Maximum tolerable ERRor [ICAO, 2006]. Nevertheless, in the literature, other expressions are used when mentioning the MERR as Maximum allowable range ERRor, Maximum allowable pseudorange ERRor [Shively, 1999], Maximum allowable Error in Range [Rife and Phelts, 2008] or Maximum Error Range Residual [Shloss et al., 2002]. It is important to understand that the MERR is defined in the pseudorange domain.

The MERR definition is given in [ICAO, 2006]. The maximum tolerable error for each ranging source  $i$  can be defined for SBAS APV and precision approach as:

$$MERR_i = K_{V,PA} \sqrt{\sigma_{i,UDRE}^2 + \min\{\sigma_{i,UIRE}^2\}} \quad (7-1)$$

where

- $K_{V,PA} = 5.33$  is the multiplier derived from the probability of false alarm equal to  $P_{ffd} = 10^{-7}$ :

$$K_{V,PA} = \sqrt{2} \times \text{erfc}^{-1}(P_{ffd})$$

with

$$\text{erfc}^{-1}(\text{erfc}(x)) = x$$

and

$$\operatorname{erfc}(x) = \frac{2}{\sqrt{\pi}} \int_x^{+\infty} e^{-t^2} dt$$

- $\sigma_{i,UDRE}$  is the standard deviation of the User Differential Range Error (UDRE) for the ranging source  $i$ . It can be seen as the residual range error associated to the corrections provided by the augmentation system. This parameter is estimated by the ground segment of the augmentation system and then sent to the user (via geostationary satellites in SBAS).
- $\min\{\sigma_{i,UDRE}^2\}$  is the minimum possible value of  $\sigma_{i,UIRE}^2$  for any user.  $\sigma_{i,UIRE}^2$  is the standard deviation of the error uncertainty for the ionospheric correction estimated from an ionospheric model using broadcast GIVE (Grid Ionospheric Vertical Error).

*MERR is evaluated at the output of a fault-free user receiver and varies with satellite elevation angle and ground subsystem performance [ICAO, 2006].*

For the sake of simplicity, in the following the term MERR will be used instead of  $MERR_i$ . MERR can be viewed as the lowest value of  $MERR_i$  among all ranging sources.

#### 7.1.1.2 Choice of a targeted MERR value

As it can be understood, the notion of MERR is a key of the SQM analysis and should correspond to a value derived from an integrity analysis. Several derivations of the MERR can be found in the literature:

- The evaluation of the value of the MERR for LAAS can be found in [Shively, 1999] and corresponding values for SBAS can be found in [Phelts, 2001]. In these publications, the MERR depends upon the Ground Accuracy Designator (GAD), the number of monitoring stations and is elevation-dependent. Example of MERR values estimated from models, as a function of the satellite elevation, are shown in [Phelts, 2001]. For a worst case of a satellite at 5° elevation, the typical MERR value is upper-bounded by 3.5 m for SBAS L1 in the case of three monitoring stations (and lower bounded by 0.7 m).
- A simpler MERR formula is provided in [Shloss et al., 2002] for WAAS (single frequency) that only depends upon the UDRE, the User Ionospheric Vertical Error (UIVE) and the obliquity factor. This formula corresponds to a so-called static MERR and is given by:

$$MERR = \frac{5.33}{3.29} \times \sqrt{\sigma_{UDRE}^2 + (F_{PP}\sigma_{UIVE})^2} \leq \frac{5.33}{3.29} \times \sqrt{\sigma_{UDRE}^2 + 9} \quad (7-2)$$

where

- $\sigma_{UDRE}$  and  $\sigma_{UIVE}$  are the standard deviations of the UDRE and GIVE monitors.  $\sigma_{UIVE}$  can be conservatively set to its floor value of 3.
- $F_{PP}$  is the obliquity factor, conservatively set to 1.

Note that this formula changes for a dual-frequency system since the ionospheric term can be removed. The static MERR then becomes:

$$MERR = \frac{5.33}{3.29} \times \sigma_{DFRE} \quad (7-3)$$

where  $\sigma_{DFRE}$  is the standard deviation of the Dual-Frequency Range Error (DFRE).

Table 7-1 provides the values of the static MERR for both WAAS single and dual-frequency cases. Assuming that a SBAS would target a minimum UDRE/DFRE of 4, the static MERR would be 6.08 m in single frequency case and 3.64 m in dual-frequency case.

- Finally, a new derivation of the MERR was proposed in [Rife and Phelts, 2008] where the MERR value also takes into account the actual probability of detection of the SQM as well as the response time of the SQM metric filter and the airborne measurement filter. This MERR is

referred to as time-varying MERR and is associated with a complex computation methodology. It has been applied to WAAS in [Phelts et al., 2013]. This MERR fully protects the user since it takes the filters time response in consideration (which was not the case in the static MERR). It also has the property to have a value that varies as a function of the probability of detection of a given distortion (the MERR becomes higher as the distortion is easier to detect).

UDRE Index (UDREI)	UDRE	MERR for L1-only Users	MERR for Dual- frequency Users
0	0.75	5.01	1.21
1	1	5.12	1.62
2	1.25	5.27	2.03
3	1.75	5.63	2.83
4	2.25	6.08	3.64
5	2.0	6.87	4.86
6	3.75	7.78	6.08
7	4.5	8.76	7.29
8	5.25	9.80	8.51
9	6.0	10.87	9.72
10	7.5	13.09	12.15
11	15	24.78	24.30
12	50	81.15	81.00
13	150	243.06	243.01

**Table 7-1.** Static MERR values for WAAS for L1-only and dual-frequency users [Phelts et al., 2013].

Because the time-varying MERR derivation has not been implemented for the DFMC case in this thesis, it is proposed to use for the MERR the target value of 3.64 m provided for WAAS dual-frequency case in Table 7-1 for an UDRE/DFRE of 4. The value is rounded to 3.5 m in the rest of the document.

This MERR thus represents the maximum tolerable value for an undetected bias on the iono-free measurement which can be caused by a distortion on L1, L5/E5a, or both, then:

- if a bias occurs on L1 (none on L5/E5a), then the resulting absolute differential bias on L1 should be lower than 1.55 m,
- if a bias occurs on L5/E5a (none on L1), then the resulting absolute differential bias on L5/E5a should be lower than 2.78 m,
- if a bias occurs at the same time on L1 and L5, then the resulting differential bias should be such that:

$$|2.26 \cdot \Delta b_{EWF,L_1}^i - 1.26 \cdot \Delta b_{EWF,L_5}^i| < 3.5 \text{ m} \quad (7-4)$$

As a consequence, if one wants to protect a user against an EWF occurring at the same time on the two frequencies, one would have to consider the worstcase where the L1 and L5 biases would add up. It is equivalent to:

$$|2.26 \cdot \Delta b_{EWF,L_1}^i| + |1.26 \cdot \Delta b_{EWF,L_5}^i| < 3.5 \text{ m} \quad (7-5)$$

This means that it would be necessary to put in place an EWF detection process which is better than what would be needed if considering that an EWF can only occur on one frequency at a



time. In this case, the maximum differential bias values for L1 and L5 to respect an iono-free MERR of 3.5 m is plotted in Figure 7-1.

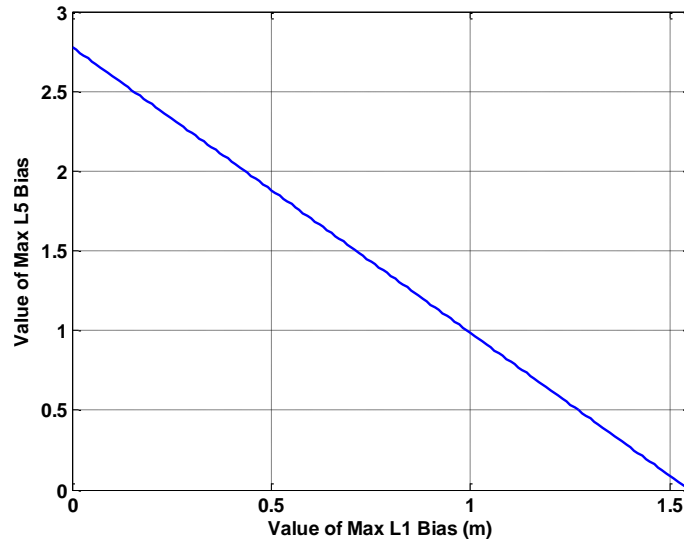


**Figure 7-1.** Acceptable values of maximum L5 and L1 biases for DFMC SBAS.

The above analysis is really associated to a worst-case scenario where the bias on L1 and the bias on L5 combine to create the worst iono-free bias.

In the case of the present analysis, it will be assumed that an EWF can only occur on one frequency at a time. As a consequence, the SQM performance will be limited to the detection (with appropriate  $P_{md}$  and  $P_{ffd}$  requirements) of any EWF that would create:

- a differential bias on a Galileo E1 OS measurement greater than 1.55 m, or
- a differential bias on a Galileo E5a measurement greater than 2.78 m.

This is still a significant first step compared to a 3.5 m MERR for GPS L1 C/A that is classically used in the literature (when used in mono-frequency airborne receivers).

#### 7.1.1.3 Conclusion

To conclude two objectives are targeted on GPS L1 C/A signal: 3.5 m which consists of SBAS L1 requirements and 1.55 m in a DFMC context. Same targets are adopted for Galileo E1C. For Galileo E5a and GPS L5, only one objective is targeted: 2.78 m.

#### 7.1.2 Tests and metrics

SQM consists of a test (noted *Test*) to evaluate if the signal is affected by a distortion or not. SQM methodology has already been described for example in [Irsigler, 2008] or [Phelts and Walter, 2003]. The typical SQM is based on the use of metrics to detect distortions of the correlation function used to track the GNSS signal. A large number of metrics can be designed based on combinations of correlator outputs. These combinations can be simple as with the simple, the difference, the sum ratio metrics or the alpha metric [Phelts et al., 2003] or more tricky as the “squared  $\Delta$ ” metric [Phelts et al.,

2001]. Metrics could also be designed from CDO outputs (see chapter 4 and [Phelts et al., 2013]). The three types of metrics used in this document are:

- *The simple ratio metric* which is the easiest metric to implement and permits to detect all kind of correlation function distortions.

$$metric_x = \frac{I_x}{P} \quad (7-6)$$

- *The difference ratio metric* which permits to detect distortions that affect the correlation function in an asymmetric way (asymmetric from the prompt) more efficiently than the simple ratio metric.

$$metric_{x-x} = \frac{I_{-x} - I_x}{P} \quad (7-7)$$

- *The sum ratio metric* which permits to detect distortions that affect the correlation function in a symmetric way (symmetric from the prompt) more efficiently than the simple ratio metric.

$$metric_{x+x} = \frac{I_{-x} + I_x}{P} \quad (7-8)$$

where

- $I_x$  is the in phase correlator output value at a distance  $x$  (in chip unit) from the prompt.
- $P$  is the value representing the prompt correlator output. In the literature,  $P$  can take two forms:
  - o  $P = I_0$ : in this case  $P$  is the prompt correlator output.
  - o  $P = (I_{-z} + I_z)/2$ : in this case  $P$  is an approximation of the prompt correlator output based on two symmetric correlator outputs.

The use of a virtual prompt for metric normalization has been reported in [Phelts and Walter, 2003] with  $P = (I_{-0.025} + I_{0.025})/2$ . Nevertheless, in WAAS reference stations, a prompt is used. In this Ph.D. thesis, it is decided to use the classical prompt for metrics normalization for Galileo E1C, Galileo E5a, GPS L5 and GPS L1 C/A signals.

The three types of metrics used in this document are elementary. These metrics are looked at for two main reasons:

- the simple ratio and the difference ratio metrics are currently used in SQM implemented in EGNOS [Bruce et al., 2000].
- the theoretical value of  $\sigma_{metric}$  for these three metrics can be derived as shown in appendix B.

The SQM test consists in looking at the way these different metrics are modified with respect to their nominal values (in nominal conditions) to decide if a distortion is present. The test compares the difference between each metric value and its nominal value to a threshold. Mathematically, the test based on a given metric  $j$  (noted  $Test_{metric,j}$ ) can be represented as:

$$Test_{metric,j} = \frac{|metric_{j,dist}^i - metric_{j,nom}|}{th_{metric,j}} \quad (7-9)$$

where

- $metric_{j,dist}^i$  is the current value of the metric  $j$  which can be affected by a distortion. The index  $i$  shows that this value is estimated for the ranging signal  $i$ .

- $metric_{j,nom}$  is the nominal value of the metric  $j$ . For example, the nominal value can consist in the median of that metric across all satellites in view [Phelts et al., 2013]. Another method is to estimate the nominal value of metrics from the average value of that metric for a given PRN using previous measurements known to represent nominal conditions. In the simulations considered in this chapter, the nominal correlation function used to estimate nominal metrics is the ideal filtered correlation function.
- $th_{metric,j}$  is the detection threshold associated to the metric  $j$ , determined according to a required false alarm probability.  
Assuming that the distribution of the noise on the metric  $j$  in the nominal case is Gaussian with a standard deviation  $\sigma_{metric,j}$ , the value of  $th_{metric,j}$  can be deduced from the targeted false alarm probability  $P_{ffd}$  as:

$$th_{metric,j} = K_{ffd} \times \sigma_{metric,j} \quad (7-10)$$

where  $K_{ffd}$  is the multiplier derived from the probability of fault-free detection probability  $P_{ffd}$  defined in 7.1.4.

The Gaussian behavior of the noise affecting correlator outputs was verified in [Irsigler, 2008] and is in general assumed. It is shown in 7.1.5.2 that if the Gaussian behavior on correlator outputs holds true, then the Gaussian behavior on the considered metrics can be assumed.

In order to detect a faulty case in real time, a Neyman Pearson hypothesis test is performed. The monitor which is implemented in reference station is based on the following concept: if  $Test_{metric,j}$  is higher than one, an alarm is triggered, whereas if  $Test_{metric,j}$  is smaller than one the signal is considered as usable. This means that a distortion can be detected by several metrics at the same time.

### 7.1.3 Minimum Detectable Error (MDE) definition

The notion of test threshold is of primary importance because it represents the limit between what is considered as a nominal or a faulty behavior. Nevertheless,  $th_{metric,j}$  is only associated to the probability of false alarm while ICAO imposes requirements regarding the probability of false alarm and the probability of missed detection. This is the reason why it is important to define the notion of Minimum Detectable Error (MDE) which is representative of the minimum detectable metric distortion that allows to fulfil both false alarm and missed detection ICAO requirements. In this part, the definition of MDE is given. Values of MDE are estimated in 7.1.5.

#### 7.1.3.1 MDE definition

In [ICAO, 2006], the MDE and the MDR (Minimum Detectable Ratio) are used to derive the SQM performance. In this manuscript, for the sake of notation,  $MDE_{metric,j}$  is used to name the MDE associated to the metric  $j$ .

Taking back the definition of ICAO, which assumes that the metrics are Gaussian distributed, the  $MDE_{metric,j}$  values used in simulations to assess the minimum metric distortion detectable by the SQM according to required false alarm and missed detection probabilities is:

$$MDE_{metric,j} = (K_{md} + K_{ffd})\sigma_{metric,j} \quad (7-11)$$

## 7. Signal quality monitoring of new signals

where  $K_{md}$  is the missed detection multiplier representing a given missed detection probability defined in 7.1.4.

Figure 7-2 illustrates the difference between the detection threshold  $th_{metric,j}$  and  $MDE_{metric,j}$ . Note that  $th_{metric,j}$  is the true threshold used in the implemented SQM, while the MDE is a theoretical value used to test the SQM performance based on simulations.

To assess the theoretical SQM performance in presence of distortions with respect to the ICAO requirements, it is thus necessary to compare the value of the bias affecting the detector associated to each metric with respect to the corresponding MDE.

Let us define the performance test  $Test_{metric,j\_MDE}$  as:

$$Test_{metric,j\_MDE} = \frac{|metric_{j,dist,no\ noise}^i - metric_{j,nom}|}{MDE_{metric,j}} \quad (7-12)$$

Where  $metric_{j,dist,no\ noise}^i$  now represents the distorted metric without noise (the impact of noise is now absorbed by the MDE value). From this definition, it can be seen that the MDE is more representative of a bias than of an error between the current and the nominal values of the metric.

If  $Test_{metric,j\_MDE} > 1$ , this means that a given distortion is detected by the detector associated to the metric  $j$  with the appropriate ICAO requirements. The estimation of  $MDE_{metric,j}$  is consequently a key to establish SQM performance.

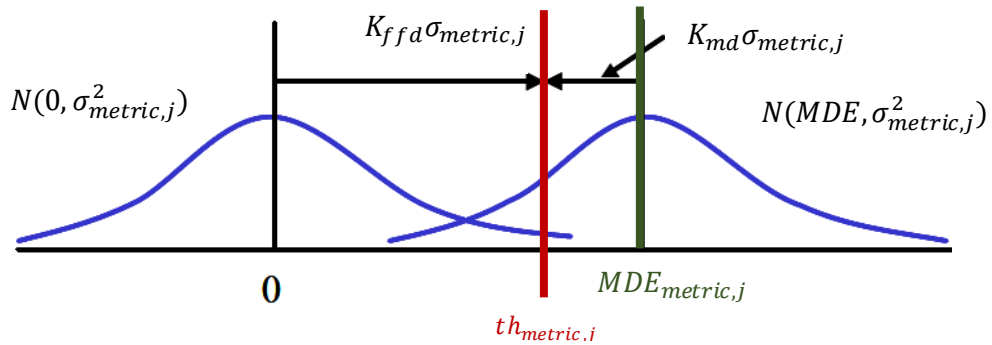


**Figure 7-2.** Difference between the detection threshold and the MDE.

### 7.1.3.2 Case of a test based on several metrics

Based on equation (7-11),  $MDE_{metric,j}$  can be written as:

$$MDE_{metric,j} = K \sigma_{metric,j} \quad (7-13)$$

where  $K = (K_{md} + K_{ffd})$ . In this case,  $K$  is associated to the requirements associated to a given detector associated to metric  $j$ .

If several metrics (and thus detectors) are used by the SQM, it is important to find the appropriate value of  $K$  for each detector so that the global requirement at the global SQM level is fulfilled. Using several dependent metrics entails that the false alarm and missed detection probabilities associated to each metric test are not equal to the probabilities of the global test using all metrics.

In the typical implementation of a SQM, a distortion is said to be detected if any of the detection tests (based on different metrics) detects the distortion. The detection can thus be assessed by looking if the maximum value of  $Test_{metric,j\_MDE}$  over all metrics  $j$  is greater than 1. This is equivalent at looking at the maximum value of  $Test_{metric,j\_MDE}$ :

$$Test_{MDE} = \max_{metric,j} [Test_{metric,j\_MDE}] \quad (7-14)$$

To estimate  $Test_{MDE}$  values in the context of this Ph.D. (use of several metrics of different types):

- $K$  must be evaluated for each detector. Explanations about the  $K$  value are provided in 7.1.5.1.
- $\sigma_{metric}$  has to be assessed for the different metrics that are used in this document. This task is tackled in 7.1.5.2.

#### 7.1.4 Targeted requirements ( $P_{ffd}$ , $P_{md}$ and TTA)

MDE values and SQM performance are dependent upon  $P_{md}$  and  $P_{ffd}$  requirements. In this part probabilities values that are used in the continuation are presented. In addition, a discussion about the TTA and transient SQM problem is undertaken.

##### 7.1.4.1 $P_{ffd}$ , $P_{md}$ in ICAO requirements

The current SBAS L1 requirement regarding SBAS SQM is provided by [ICAO, 2006] and states that the ground segment should be able to detect any EWF-induced differential bias greater than a given MERR, with a  $P_{md}$  of  $1.10^{-3}/\text{test}$  and a  $P_{ffd}$  of  $1.5.10^{-7}/\text{test}$ . These values are for the global SQM performance and not for each individual metric test.

##### 7.1.4.2 $P_{ffd}$ , $P_{md}$ in WAAS

The values taken in WAAS single frequency mentioned in [Phelts et al., 2013] are different from ICAO values and must come from the specific WAAS integrity tree:

- $P_{md}$  of  $10^{-5}/\text{test}$  since the assumed a priori probability of failure for a GPS satellite is  $6.42 \times 10^{-5}/\text{satellite/h}$  and the allocated fault probability in WAAS due to an EWF is  $6.45 \times 10^{-10}/\text{h}$ ,
- $P_{ffd}$  of  $3.2 \times 10^{-8}/\text{test}$  corresponding to one false alarm per satellite per year. It should be noted that this is a conservative value, since the SQM test statistics are highly correlated (over 50 to 100 s) and this value assumes independent exposures to false alarm for each second.

These values are associated to the use of GPS L1 C/A only. In the case of a dual-frequency user, there is a need to monitor both signals on L1/E1C and on L5/E5a. Due to the lack of real knowledge on the dependence between failures occurring on L1 and L5, it can be conservatively assumed that the same probabilities apply for each individual signal.

## 7. Signal quality monitoring of new signals

### 7.1.4.3 Targeted $P_{ffd}$ , $P_{md}$

Each specific system has to derive its own values of  $P_{ffd}$  and  $P_{md}$  that must be applied on tests to meet global required performance. The value of the  $P_{ffd}$  is chosen depending on the service continuity that must be reached. The  $P_{md}$  is chosen depending on the integrity risk (estimated from the integrity risk tree) and the a priori satellite failure rate probabilities. Depending on the architecture of the augmentation system, these probabilities are different. As an example two possible architectures are:

- Architecture 1: each reference station individually provides its assessment of the presence of an EWF. To do so, it bases its decision on the fact that at least one of its detectors flags the presence of a distortion. The decision of each reference station is then sent to the master station. It is assumed that the Central Processing Facility (CPF) then decides to declare the presence of an EWF based on majority voting. This architecture could be associated to the current EGNOS v2 architecture.
- Architecture 2: each reference station sends all its SQM metrics (or correlator outputs) values to the CPF. The CPF then aggregates the information coming from each reference station. This aggregation consists in averaging coherently the corresponding metrics and to decide on the presence of an EWF if at least one of its detectors flags the presence of a distortion. This architecture could be associated to the current WAAS architecture.

Advantages and drawbacks of the two architectures are detailed in [Julien et al., 2016]. In the two cases,  $P_{ffd}$  and  $P_{md}$  defined per test are different.

In this manuscript, it is proposed to use the ICAO  $P_{md}$  of  $1.10^{-3}/\text{test}$  and a  $P_{ffd}$  of  $1.5.10^{-7}/\text{test}$  for the global required SQM performance at the CPF level (thus assuming an Architecture 2 case). Indeed, this is the official document in which the two probabilities are defined. In EGNOS and WAAS, these values will be slightly different, nevertheless, results presented in this chapter can be used to estimate SQM performance at different  $P_{md}$  and  $P_{ffd}$  as it is shown in 7.3.3.2.

### 7.1.4.4 Requirement on the TTA

TTA requirements are provided in chapter 2. For the LPV-200 approach which is targeted by SBAS, TTA is equal to 6.2 s. The TTA is dependent upon three terms:

- the time  $t_{detect}$  to detect a distortion,
- the time  $t_{inf}$  for the information to be sent from the reference station to the user and to be processed.
- the time  $t_{HMI}$  at which the distortion entails a hazardous differential error on the user.

The TTA is then defined by:

$$TTA = t_{inf} + (t_{detect} - t_{HMI}) \quad (7-15)$$

If  $t_{inf}$  is necessarily positive, the term  $(t_{detect} - t_{HMI})$  can be positive or negative. Indeed,  $(t_{detect} - t_{HMI})$  is negative if a distortion is detected at reference level before that this distortion becomes a threat for differential users.

In this manuscript, the TTA requirement is not considered and it is assumed that the monitoring is performed in steady state conditions. This choice is made for two main reasons:

- The TTA is dependent upon transient response of the filter implemented at the user and at the reference level to smooth pseudorange measurements and metric values (reference only). By consequence taking into account the TTA adds three parameters that have an impact on SQM performance and make the interpretation of results more difficult. Note that the notion of time-varying MERR (not used in this manuscript) introduced in section 7.1.1 takes care of the TTA requirements.
- SQM performance estimated taking into account the transient state is assessed by using SQM performance obtained in steady state conditions. In [Pheltset al., 2001] is shown that *the basic transient SQM problem (with TTA = 0 seconds) reduces to a simple comparison of the normalized steady state errors* where the basic transient SQM problem is to consider that the same first order filter is used to filter the detection test and the user differential pseudo range error. If a different filter is used to filter the detection test and to filter user differential pseudorange error, the SQM problem is not reduced to a simple comparison of the normalized steady state. The problem is more complex but SQM performance can still be estimated from the steady state.

To conclude, in this manuscript only the steady state is considered. Indeed, the study of the steady state is necessary before analysing SQM performance in transient state. It is however important to mention that this implies that the user might not be properly covered during transient phases. In future works, transient SQM performance could be assessed based on results provided in this chapter.

### 7.1.5 Theoretical estimation of the MDE

After defining requirements targeted by the SQM in terms of  $P_{ffd}$  and  $P_{md}$ , MDE values are estimated theoretically. First, the value of  $K$  is derived, then values of metrics standard deviations are derived.

#### 7.1.5.1 Estimation of parameter $K$

Let us call  $P_{X\_metric,j}$  ( $X = ffd$  or  $md$ ) the probability associated to one test based on one metric  $j$  and let us assume that the same probability budget is allocated to each sub-test. In this condition,  $P_{X\_metric,j}$  is not dependent upon the index  $j$ . If several metrics are used, as it is envisaged in this study,  $P_{ffd\_metric,j}$  and  $P_{md\_metric,j}$  have to be computed for each metric. Considering that the total test is based on  $N_{test}$  detectors and that an alarm is triggered if at least one metric exceeds its threshold, two extreme cases are imaginable:

- Metrics are totally independent. In this condition, probabilities on one sub-test ( $P_{X\_metric,j}$ ) are related to the global test probability ( $P_X$ ) by:

$$P_{ffd} = \sum_{k=1}^{N_{test}} C_{N_{test}}^k P_{ffd\_metric,j}^k (1 - P_{ffd\_metric,j})^{N_{test}-k} \quad (7-16)$$

$$P_{md} = P_{md\_metric,j}^{N_{test}} \quad (7-17)$$

- Metrics are totally dependent, in this case :

$$P_{ffd} = P_{ffd\_metric,j} \quad (7-18)$$

$$P_{md} = P_{md\_metric,j} \quad (7-19)$$

## 7. Signal quality monitoring of new signals

In real conditions,  $P_{X\_metric,j}$  are between the two above extreme cases. With a precise knowledge about the correlation between each metric, exact  $P_{X\_metric,j}$  and consequently exact  $K_{metric,j} = (K_{md\_metric,j} + K_{ffd\_metric,j})$  could be estimated.  $K_{md\_metric,j}$  is the coefficient multiplier associated to  $P_{md\_metric,j}$  and  $K_{ffd\_metric,j}$  is the coefficient multiplier associated to  $P_{ffd\_metric,j}$ .  $K_{md} = 5.26$  for  $P_{md} = 1.10^{-3}$  and  $K_{ffd} = 3.09$  for  $P_{ffd} = 1.5.10^{-7}$ .

$K_{metric,j}$  is assessed in this document in a conservative way which is obtained when metrics are considered as totally dependent, as shown in Figure 7-3. In red is plotted  $K_{metric,j}$  in the particular case where all metrics are totally dependent and in blue the case where all metrics are totally independent. In real conditions,  $K_{metric,j}$  will take values between the red and the blue curves.

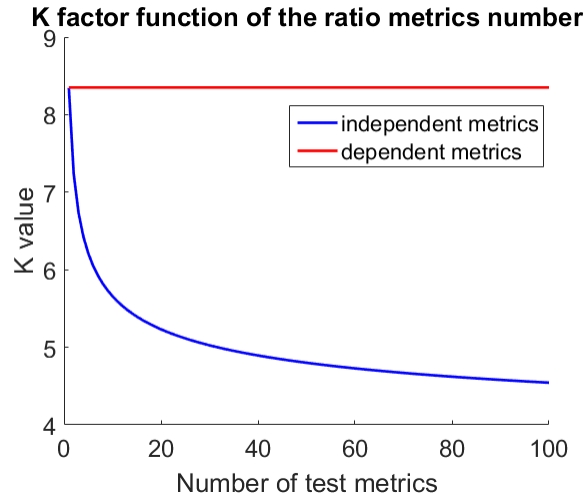


**Figure 7-3.**  $K_{metric,j}$  factors if metrics are totally dependent (red plot) or totally independent (blue plot) function of the sub-tests number.

It entails that even if several metrics are used to define a test, the  $MDE_{metric,j}$  for each individual metric fulfilling the ICAO requirements in terms of  $P_{ffd}$  and  $P_{md}$  can be modeled in a conservative way as:

$$MDE_{metric,j} = 8.35 \times \sigma_{metric,j} \quad (7-20)$$

### 7.1.5.2 $\sigma_{metric}$ estimation

As discussed previously,  $MDE_{metric,j}$  is a function of  $\sigma_{metric,j}$  assuming that the noise distribution on metrics is Gaussian.

$\sigma_{metric,j}$  can be estimated theoretically for the three introduced metrics (simple ratio, sum ratio and difference ratio metrics). Mathematical  $\sigma_{metric,j}$  expressions are given in appendix B assuming that the noise distribution on metrics is Gaussian. This condition is fulfilled when:

- $I_x$  is treated as a Gaussian variable  $N(\mu_x, \sigma_x^2)$ . This property is used in many publications as for instance [Irsigler, 2008], [Brocard et al., 2014] or [Sleewaegen and Boon, 2001].
- $\frac{\mu_x}{\sigma_x}$  tends to infinity, which can be interpreted as a high  $C/N_0$  condition. In this case, the ratio of two such Gaussian random variables tends towards a Gaussian instead of a more complex distribution [Brocard et al., 2014]. It can be considered that these conditions are verified at reference station level [Irsigler, 2008] operating with a 1 s correlation duration.



To verify the theoretical formulas of  $\sigma_{metric,j}$ , a Matlab® program was developed. This program generates a noisy filtered signal and a local replica. Then, the two signals are correlated to obtain a noisy correlation function. Metrics are then built from the noisy correlation functions using Monte Carlo simulations so that  $\sigma_{metric,j}$  can be assessed. As an example, theoretical and simulated  $\sigma_{metric,j}$  values are compared in Figure 7-4 where all metrics are simulated for a *BPSK*(1) signal. In this particular case, the coherent integration time is equal to 1 s, the  $C/N_0$  is equal to 30 dB-Hz and the signal is filtered by the reference filter. One hundred values of a given metric are generated to estimate standard deviations.

From Figure 7-4, it appears that even at a  $C/N_0 = 30$  dB-Hz, the theoretical  $\sigma_{metric,j}$  values match with values obtained in simulations. For lower values of  $C/N_0$ , the derived theoretical  $\sigma_{metric,j}$  may not be representative of the ratio of two Gaussian distributions and results have to be interpreted carefully for  $C/N_0$  lower than 30 dB-Hz. More precisely, for lower  $C/N_0$ , better estimation of theoretical  $\sigma_{metric,j}$  can be derived from formulas defined in [Brocard et al., 2014]. Nevertheless, in the context of this Ph.D., it will be seen that reference stations are operating at  $C/N_0$  higher than 30 dB-Hz.

Note that standard deviations theoretical formulas might not be valid if the noise on correlator outputs is not Gaussian-distributed.

On Figure 7-4 are represented theoretical (continuous plots) and simulated (dotted plots) metrics standard deviations for  $metric_{x-x}$  (in blue),  $metric_{x+x}$  (in purple) and  $metric_x$  (in blue for  $x$  negative and in purple for  $x$  positive). It is shown in appendix B that similar adequacies between theoretical and simulated metrics standard deviations have been obtained for Galileo E1C and E5a signals.

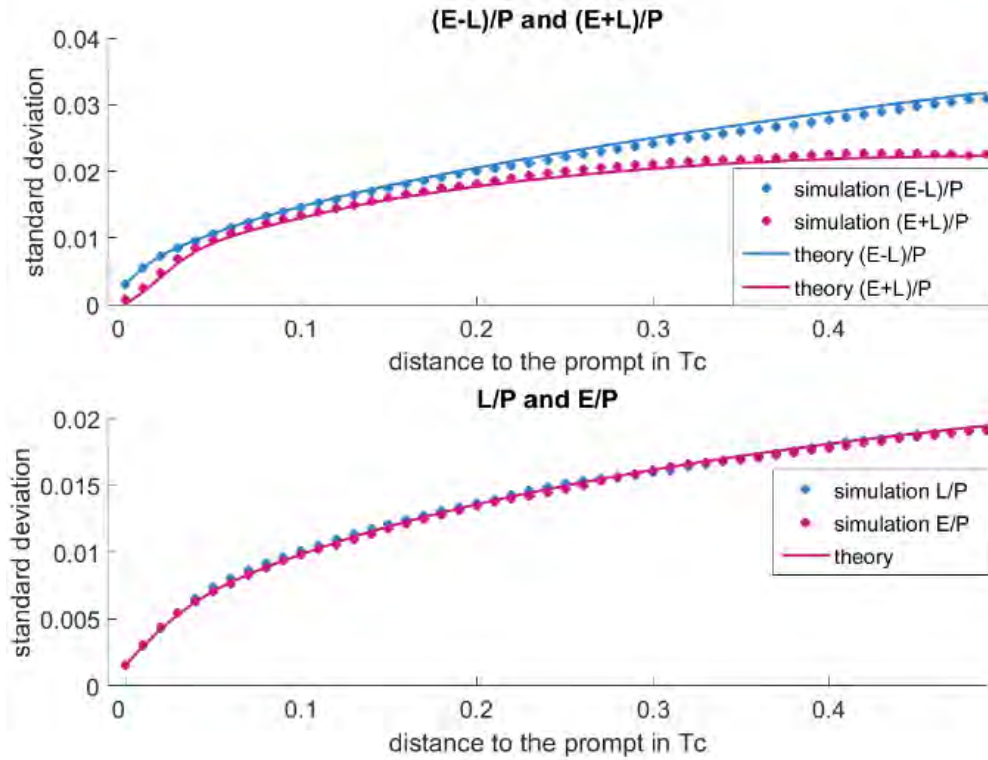


**Figure 7-4.** Theoretical and simulated metrics standard deviations on a *BPSK*(1)-modulated signal for  $C/N_0 = 30$  dB-Hz and  $T_{int} = 1$  s.

## 7.1.6 Conclusions

In this section, notions related to SQM are presented: the MERR, tests, metrics, requirements and MDE. A comparison of the MUDE, MERR and MDE notions is presented in Table 7-2. In spite of their names, this three parameters are referred to as biases more than errors. The bias is the average of errors obtained from one error distribution.

	MERR	MUDE	MDE
Meaning	Maximum tolerable ERRor (or other)	Maximum Undetected Differential Error	Minimum Detectable Error
Domain of application	Pseudorange	Pseudorange	Correlation function (metrics)
Concept	If a distortion leads to a differential tracking bias above MERR for at least one differential user, the distortion has to be detected with the $P_{ffa}$ and $P_{md}$ probabilities.	If a distortion leads to a differential tracking bias above MUDE for at least one differential user, the distortion is detected by the SQM with the $P_{ffa}$ and $P_{md}$ probabilities.	If a distortion leads to a difference between the current value of a metric and the nominal value of the same metric above MDE, the distortion is detected by the SQM with the $P_{ffa}$ and $P_{md}$ probabilities.
Value definition	Depends upon the requirement.	Depends upon the SQM, the $C/N_0$ , considered user receiver configuration, considered reference receiver configuration, considered TM, requirements.	Depends upon the SQM, the $C/N_0$ , considered reference receiver configuration, considered TM, requirements.

**Table 7-2.** Definition of MDE, MERR and MUDE.

Only three types of metrics are assumed used by the SQM: the simple ratio, the sum ratio and the different ratio metrics (from the prompt of the correlation function). These metrics built from correlator outputs are adapted to detect asymmetric as well as symmetric distortions. Moreover, theoretical derivation of the standard deviation for these metrics has been shown to be valid.

One important conclusion is that SQM performance can be assessed using the notion of MDE, which is a function of the ICAO requirements, the number and types of metrics used, and the standard deviation of the metrics used. The expression of  $MDE_{metric,j}$  that is kept in the following is assessed in this section in a conservative way, assuming that a test is based on several metrics, but that all metrics are totally dependent.

## 7.2 Parameters with an influence on SQM performance

Now that the different requirements of the SQM, as well as its performance criteria, have been presented, it is important to expose the testing methodology. To do so, it is important to describe:

- the user receiver and reference station receivers configurations of interest,
- the TM, or in other words, the distortions that must be monitored,
- metrics that are used to design the SQM.

### 7.2.1 Tested distortions

It is clear that SQM performance is dependent upon signal distortions that have to be monitored. The proposed TMs were described in chapter 6, together with a methodology to design them.

In this chapter, SQM performance is tested for GPS L1 C/A based on the grid of points exposed on Table 7-3. For Galileo E1C, E5a and GPS L5, the SQM is tested based on values presented in Table 7-4. For the latter, some differences are noticeable compared to the TM proposed in chapter 6 and are given in bold:

- For Galileo E5a and GPS L5, on area 1, more  $\sigma$  values are tested. Instead of increasing  $\sigma$  by 4 Mnepers/s between each distortion, an increment of 1 Mnepers/s is used to have the same increment as on the large TM-B zone of area 1 on Galileo E1C and the same increment as on the TM-B on GPS L1 C/A. This choice is conservative.
- For Galileo E1C, even if TM-A1 and TM-A2 are considered in the TM-A, the simplified TM-C (which does not include the TM-A2) is used in order to limit the number of tests to perform. The choice of removing TM-A2 from the TM-C is also justified by the fact that no digital distortion was observed on Galileo E1C nominal signals.
- Some TM-B upper bound values are slightly increased to be sure to test all distortions inside the TMs.

The resolutions with which the TMs are tested are kept from chapter 6. Based on the method proposed in the previous chapter, a deeper analysis of the resolution could permit to have more adapted tested distortions. However, this problem is not tackled in this manuscript.

GPS L1 C/A TM-C is tested with a  $f_d$  increment equal to 0.57 MHz in order to test ten different frequencies.

	$\Delta$ (chip)	$\sigma$ (Mnepers/s)	$f_d$ (MHz)
TM A	$[-0.12:0.01:0.12]$	-	-
TM B	-	$[0.8:1:8.8]$	$[4:1:17]$
TM C	$[-0.12:0.01:0.12]$	$[0.8:1:8.8]$	$[7.3:0.57:13]$

**Table 7-3.** GPS L1 C/A TM used to estimate SQM performance.

## 7. Signal quality monitoring of new signals

Simplified TM-C							
TM-B				TM-A			
Area 1		Area 2		TM-A1	TM-A2		
$f_d$ (MHz)	$\sigma$ (Mnepers/s)	$f_d$ (MHz)	$\frac{\sigma}{(f_d)^2}$ (nepers/s/ Hz/MHz)	$\Delta_{min} =$ $-\Delta_{max}$ (chip)	$\Delta_{11min} =$ $-\Delta_{11max}$ (chip)	$\Delta_{61min} =$ $-\Delta_{61max}$ (chip)	
Galileo E1C	1: 1: 4	3: 1: 19	0.07: 0.05: <b>5.07</b>	0: 0.01: 0.12	0: 0.01: 0.1	0: 0.01: 0.08	
	1: 1: 19						
	4: 1: 19						
Galileo E5a and GPS L5	3: 1: 19	4: 1: 19	0.06: 0.075: <b>3.56</b>	0: 0.1: 1.2	/	/	

**Table 7-4.** Galileo E1C, Galileo E5a and GPS L5 TMs used to estimate SQM performance for different signals (in bold differences with proposed TMs from chapter 6).

### 7.2.2 Receiver configurations

SQM performance and more precisely the value of the MUDE and the capability of the reference station to detect distortions are dependent upon the tested users' configurations (that have an influence on the MUDE) and the reference station configuration (that has an influence on the MUDE and the detection capability). The impact of receivers configurations on the MUDE was discussed in part 4.4.3. Table 7-5 summarized receivers configurations that are considered in this chapter to assess SQM performance. They are in line with the latest discussion regarding the future airborne DFMC receiver constraints [Samson, 2015].

	Galileo E1C signal ( <i>CBOC</i> (6.1)) and GPS L1 C/A( <i>BPSK</i> (1))		Galileo E5a and GPS L5 signal ( <i>BPSK</i> (10))	
	reference	user	reference	user
Tracking technique	EML ( <i>BOC</i> (1.1) local replica for Galileo E1C and <i>BPSK</i> (1) for GPS L1)		EML ( <i>BPSK</i> (10) local replica)	
Correlator spacing	0.1 chip	0.08, 0.1 and 0.12 chip	1 chip	0.8, 1 and 1.2 chip
Pre-correlation bandwidth (double-sided)	24 MHz	12, 14, 16, 20, 22, 24 MHz	24 MHz	12, 14, 16, 20, 22, 24 MHz
Equivalent reception filter	6 <sup>th</sup> -order Butterworth	4 filters are tested	6 <sup>th</sup> -order Butterworth	4 filters are tested

**Table 7-5.** Reference receiver and user receiver configurations used to estimate SQM performance for different signals.

The four filters that are tested are the same as described in 6.1.2.1 and more details about these filters are given in appendix E. Tested receivers configurations are similar to configurations tested in chapter 6 to establish the TM. The major difference is that only one filter type is applied at the reference receiver. The consequence is that results provided in this chapter are less conservative than in chapter 6, however, they are more representative of the state-of-the-art [Samson, 2015] and more adapted when testing SQM performance that do not have to be too conservative.

For example, in EGNOS, RIMS-A stations estimate differential corrections while RIMS-C stations, with a different receiver configuration than the one on RIMS-A stations, support the SQM. The concept developed in this chapter can be applied if different stations are used to compute the differential corrections and perform the SQM. The strategy is to estimate the MDE values in the operating conditions of the station used for the SQM and to estimate maximum differential error in the operating conditions of the station which estimates differential conditions. For the sake of simplicity and because of the lack of information, it will be assumed that the SQM and differential corrections are provided by the same station which is referred to as the reference station.

### 7.2.3 Definition of reference SQMs

In this manuscript, SQM designs are based on an assumed baseline reference receiver:

- for Galileo E1C and GPS L1 C/A, SQM designs are based on fifty-one monitored correlator outputs  $I_x$  with  $x = -0.25:0.01:0.25$  in GPS L1 /A chip unit,
- for Galileo E5a and GPS L5, SQM designs are based on twenty-one correlator outputs  $I_x$  with  $x = -1:0.1:1$  in Galileo E5a chip unit.

Figure 7-5 illustrates by green circles correlator outputs that are used on the different correlation functions to design the SQM.

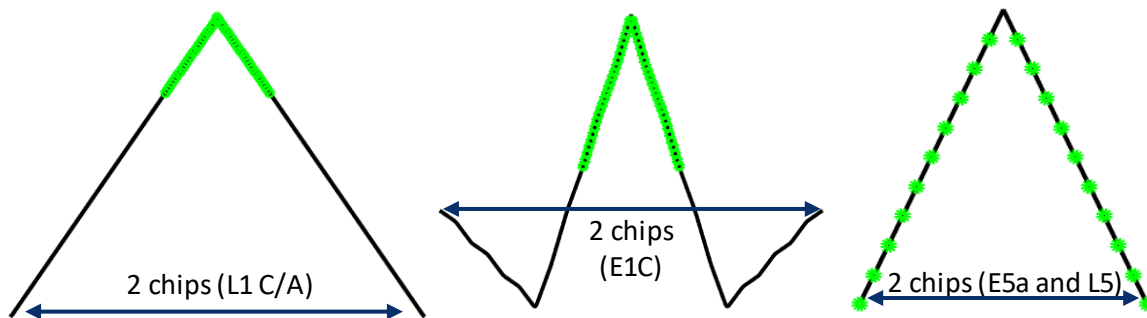


**Figure 7-5.** Correlator outputs used to design the SQM (represented in green).

The limitation to these correlator outputs is justified by three main reasons:

- ICAO-like TM distortions are more visible around the prompt of the correlation function. It is not necessary to monitor the correlation function too far away from the prompt.
- Correlator outputs situated far away from the prompt are more subject to multipath. With the selected correlator outputs range, the impact of multipath is limited.
- A time delay of 10 ns between two correlator outputs is nowadays reachable but lower values of time delays are more difficult to achieve due to a limitation in the sampling frequency of

## 7. Signal quality monitoring of new signals

the analog-to-digital converters. Additionally, denser correlator outputs may be highly correlated, making their observation less interesting for detection purpose.

From these correlator outputs, a reference SQM is defined for each signal. The three types of metrics presented earlier are used (simple, difference and sum ratio metrics) for all monitored correlator outputs.

For Galileo E1C and GPS L1 C/A the reference SQM consists of fifty simple ratio metrics plus twenty-five difference ratio metrics and twenty-five sum ratio metrics. More precisely:

- fifty  $metric_x$  are tested for  $x = -0.25:0.01:-0.01$  and  $x = 0.01:0.01:0.25$  in GPS L1 C/A chip unit,
- twenty-five  $metric_{x+x}$  are tested for  $x = 0.01:0.01:0.25$  in GPS L1 C/A chip unit,
- twenty-five  $metric_{x-x}$  are tested for  $x = 0.01:0.01:0.25$  in GPS L1 C/A chip unit.

For Galileo E5a and GPS L5, the reference SQM consists of forty metrics:

- twenty  $metric_x$  with  $x = -1:0.1:-0.1$  and  $x = 0.1:0.1:1$  in E5a chip unit,
- ten  $metric_{x+x}$  with  $x = 0.1:0.1:1$  in E5a chip unit,
- ten  $metric_{x-x}$  with  $x = 0.1:0.1:1$  in E5a chip unit.

Correlator outputs are estimated from a coherent integration time equal to 1 s and metrics are not smoothed.

### 7.3 SQM performance assessment: example on GPS L1 C/A

SQM performance is estimated by testing if distortions are detected or not (fulfilling the ICAO requirements) and by estimating the worst impact of undetected distortions on the differential tracking bias. In the previous sections, it was seen that SQM performance is dependent upon the TM, considered receivers configurations, the SQM design and the MDE (which is related to the  $C/N_0$  of the monitored signal through the standard deviation of the metrics).

A new representation of the SQM performance is proposed in this section to assess, from one unique figure, its performance at different equivalent theoretical  $C/N_0$ . The new representation and its foundations are introduced in part 7.3.1 and developed in part 7.3.2. To illustrate the concept, the reference SQM introduced in 7.2.3 is used on a GPS L1 C/A signal (fifty simple ratio metrics plus twenty-five difference ratio metrics and twenty-five sum ratio metrics) to detect signal distortions of the ICAO TM.

In addition to the simplification of the assessment of SQM performance, the representation also allows to easily compare several SQMs performance. In section 7.3.4, two designs of SQM are compared still considering a GPS L1 C/A signal.

In section 7.3.3, a strategy is exposed to estimate the equivalent theoretical  $C/N_0$  at which a reference station is operating.

### 7.3.1 A representation to assess SQM performance

In this document, SQM performance is assessed based on the highest differential error (on all tested user/reference receivers configurations) entailed by a distortion from the proposed TM considering only the steady state error. This allows to protect any possible airborne user. To do that, two quantities are computed:

- the detectability of the distortion by the SQM. Knowing the distortion and  $MDE_{metric,j}$ , it is possible to evaluate  $Test_{metric,j\_MDE}$  for each metric and by consequence  $Test_{MDE}$ .  $Test_{MDE}$  is independent from the user receiver and depends upon:
  - o the reference receiver configuration,
  - o the SQM design implemented to the reference,
  - o the  $C/N_0$  of incoming signals which will have a direct impact on  $\sigma_{metric,j}$  and consequently on  $MDE_{metric,j}$  and  $Test_{metric,j\_MDE}$ .

Comparing  $Test_{MDE}$  to 1, it is possible to know if a specific distortion from the TM is detected by the SQM according to the ICAO requirements for a given reference station configuration.

- the highest differential error created by the distortion. Considering all allowed user receiver configurations and the reference station receiver configuration, the highest differential error induced by a given distortion of the TM between different users and the reference can be assessed independently from the SQM. This highest differential error is called the maximum differential error.

Using simulations,  $Test_{MDE}$  and the maximum differential error values can be estimated for each distortion of the TM. As an example, the reference SQM is used.

Figure 7-6 shows the maximum differential error induced by distortions from the TM defined by ICAO for GPS L1 C/A signal, among the tested user configurations, as a function of the  $Test_{MDE}$  value. The  $C/N_0$  of the incoming signal is equal to 35 dB-Hz. This representation is comparable to the representation proposed in [Phelts et al., 2013] except that in this document, the value of  $Test_{MDE}$  is based on the  $P_{md}$  and  $P_{ffd}$  whereas in [Phelts et al., 2013] the value of  $Test_{MDE}$  is derived only from the  $P_{ffd}$ .

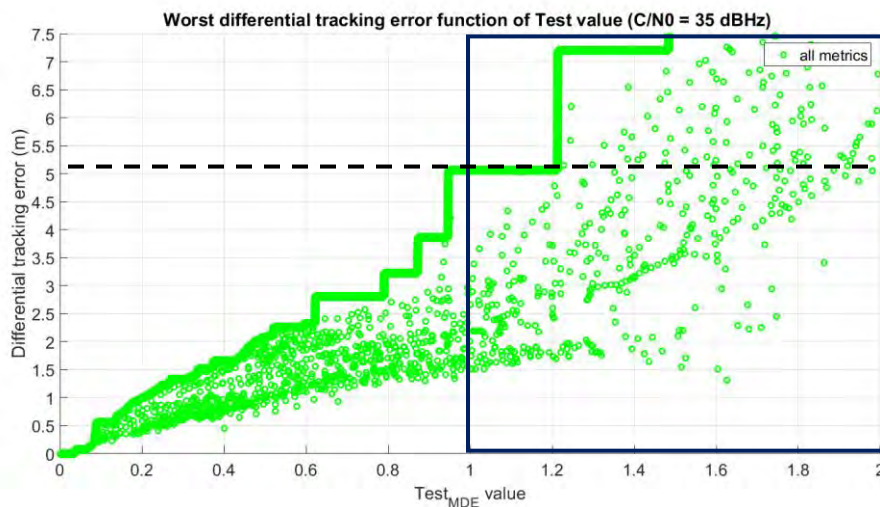


**Figure 7-6.** Example of worst differential tracking errors function of  $Test_{MDE}$ .



## 7. Signal quality monitoring of new signals

Each point of the graph corresponds to one distortion of the TM with the highest impact on tested users. 1326 distortions are represented (12 from TM-A, 126 from the TM-B and 1188 from the TM-C). The continuous line corresponds to the upper bound. The step-wise shape is easier to interpret on Figure 7-8, as discussed in the following section.

Distortions included in the blue square of Figure 7-6 are distortions detected by the defined reference SQM ( $Test_{MDE} > 1$ ) in the described particular case. The MUDE can then be read by taking the largest differential tracking error for  $Test_{MDE} < 1$ . In the conditions of Figure 7-6, the MUDE is equal to 5.1 m.

### 7.3.2 Scale change to assess SQM performance function of $C/N_0$

The MUDE is dependent upon the  $C/N_0$  through the MDE, which is a drawback because MUDE has to be evaluated depending on the  $C/N_0$  at which a reference station is operating as shown in Figure 7-7. On this figure, it can be seen that MUDE is equal to 5.1 m if the reference is operating at a  $C/N_0$  equal to 35 dB-Hz and to 2.9 m if the reference is operating at a  $C/N_0$  equal to 38 dB-Hz.

In this part, it is proposed to adapt the scale on the x-axis in order to have one representation that permits to assess performances of a given SQM at different  $C/N_0$ .

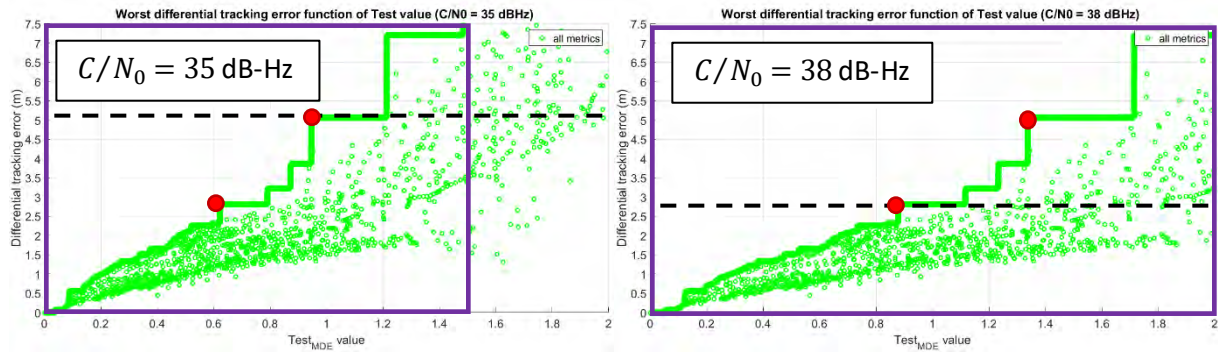


**Figure 7-7.** Comparison of SQM performances considering that the reference station is operating at  $C/N_0 = 35$  dB-Hz (left) and  $C/N_0 = 38$  dB-Hz (right).

In Figure 7-7, purple rectangles encompass the same set of distortions. It can be seen that the fact to operate at a different  $C/N_0$  only entails a dilatation or a compression of the x-axis. Red points represent two distortions for both reception cases. The figure hints that a x-axis scale change could be applied to represent the effect of the  $C/N_0$ . Indeed, there is a relation between  $C/N_0$  and the value of  $Test_{MDE}$  since the  $C/N_0$  has an impact on  $\sigma_{metric}$  which is part of the MDE. Then, a relation exists between  $\sigma_{metric}$  and  $MDE_{metric}$ , or equivalently between  $\sigma_{metric}$  and  $Test_{MDE}$  for a given metric.

Assuming a metric with a Gaussian distribution, the relation between the  $C/N_0$  in decibel-hertz and a  $Test_{metric,j\_MDE}$  can be represented as (see relation between  $C/N_0$  and the metric standard deviation in Appendix B):

$$Test_{metric\_MDE} = \frac{C_{distortion,j}}{MDE_{metric,j}} = \frac{C_{distortion,j}}{K \times \sigma_{metric,j}} = \frac{C_{distortion,j} \times \sqrt{10^{\frac{C/N_0}{10}}}}{C_{metric,j} \times K} \quad (7-21)$$

where



- $C_{metric,j}$  is a factor associated to the metrics with the highest  $Test_{metric,j\_MDE}$  value. This factor is independent from the  $C/N_0$  but is metric-dependent. The expression of this factor can be deduced for the different metrics from formulas derived in appendix B.
- $C_{distortion,j}$  is a factor independent from the  $C/N_0$  but which is distortion and metric-dependent.

As a consequence, for a given distortion entailing a given value of  $C_{distortion}$ , the following relation exists:

$$C/N_0 = 20 * \log_{10} \left( \frac{C_{metric,j} \times K \times Test_{metric\_MDE}}{C_{distortion,j}} \right)$$

The detection (according to the ICAO requirements) of a given distortion being achieved when  $Test_{metric\_MDE}$  is greater than 1, it is possible to find the minimum  $C/N_0$  that allows to have  $Test_{metric\_MDE} = 1$  using:

$$(C/N_0)_{min,detect} = 20 * \log_{10} \left( \frac{C_{metric,j} \times K}{C_{distortion,j}} \right)$$

Figure 7-8 shows the same results as on Figure 7-6 but with the x-axis representing the minimum  $C/N_0$  at which the distortion is detected. The figure can also be interpreted in the following way: assuming a given  $C/N_0$  at which the reference station operates, all the distortions generating a dot in Figure 7-8 that are below the operating  $C/N_0$  shall be detected by the SQM. The blue square in Figure 7-8 is thus still representing distortions detected by the SQM at  $C/N_0 = 35$  dB-Hz.

One of the interests of the representation shown in Figure 7-8 is that MUDE can be assessed for different operating  $C/N_0$  considering that the noise on metrics is Gaussian. The green continuous line has a lot of interest in this representation as it corresponds to the highest differential error that is undetected by a reference station at a given  $C/N_0$ . Horizontal parts of the continuous line are due to the fact that a distortion, which entails the worst differential tracking error at a given  $C/N_0$ , remains the distortion that leads to the worst undetected differential error, even for lower values of  $C/N_0$ , till that a step appears when another distortion leads to a higher differential value for a lower  $C/N_0$ .

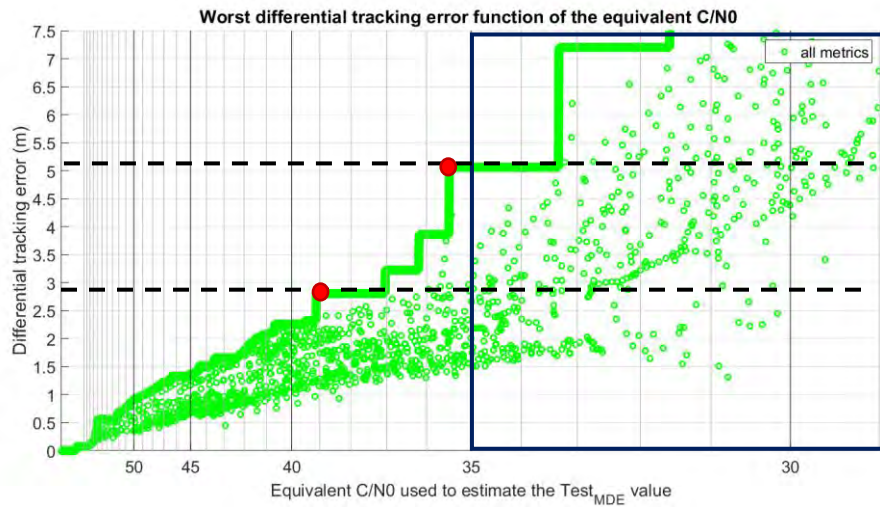


Figure 7-8. Example of worst differential errors function of  $C/N_0$ .

The same results as shown in Figure 7-7 are observed: the MUDE is equal to 5.1 m if the reference is operating at a  $C/N_0$  equal to 35 dB-Hz and to 2.8 m if the reference is operating at a  $C/N_0$  equal to 38 dB-Hz. These limits are represented by dotted black lines. In red are represented distortions at the origin of the value of the MUDE in both cases.

### 7.3.3 Estimation of the equivalent theoretical $C/N_0$ at a reference station

Results that were presented in the previous section are estimated in ideal conditions:

- the noise distribution on metrics is white and Gaussian,
- the coherent integration time is equal to 1 s,
- no multipath is affecting the incoming signal,
- a 6<sup>th</sup>-order Butterworth (24 MHz double-sided) is implemented at the reference level.

To estimate the performance of SQM at a given reference station, it is necessary to know at which  $C/N_0$  the MUDE has to be assessed. In 7.3.3.1, ideal conditions are kept and it is assumed that the noise distribution on metrics is white and Gaussian. Indeed, it is assumed that the integration time and the presence of multipath do not have any influence on the Gaussian characteristic of the noise distribution on metrics: only, the standard deviation of the Gaussian distribution is impacted by the multipath and the integration time.

In 7.3.3.2, a strategy to estimate SQM performance if the noise distribution is not Gaussian is developed.

#### 7.3.3.1 Assuming that the noise on metrics is Gaussian

Figure 7-9 represents, through the dots, some  $\sigma_{metric_x}$  (standard deviation of simple ratio metric  $metric_x$ ) values that have been measured in real conditions. Three examples are proposed:

- The two first cases correspond to a data collection performed at Stanford University with a LAAS integrity test-bed on SV 5 with a 5° elevation angle [Phelts et al., 2003]. Red dots correspond to unsmoothed metrics and green dots to metrics smoothed by a 100 s moving average.
- The last case in blue illustrates  $\sigma_{metric_x}$  obtained from a data collection made by Capgemini with a Novatel GIII receiver. The data collection was one hour long and  $\sigma_{metric_x}$  was estimated from all satellites in view. The worst  $\sigma_{metric_x}$  among satellites is represented by blue dots. The worst case was observed on SV 62. Its elevation angle was equal to 9° at the beginning of the data collection and 33° at the end. The signal  $C/N_0$  was equal to 32.8 dB-Hz at the beginning of the data collect and 42.0 dB-Hz at the end.

Figure 7-9 also shows the theoretical link between  $\sigma_{metric_x}$  and the  $C/N_0$  assuming that only thermal noise is present, according to relations derived in appendix B. One curve corresponds to one  $C/N_0$ .

From Figure 7-9, it can be approximated that the LAAS receiver is working at an equivalent  $C/N_0$  of 35.1 dB-Hz, in the worst case if metrics are unsmoothed, whereas the equivalent  $C/N_0$  is equal to 39 dB-Hz with smoothed metrics. With unsmoothed metrics, standard deviations reported from the Capgemini's data collection correspond in the worst case to an equivalent  $C/N_0 = 35.9$  dB-Hz. This value of 35.9 dB-Hz obtained in the case of the Capgemini's data collection is consistent with

$C/N_0$  values estimated by the receiver. It confirms that equivalent  $C/N_0$  derived from mathematical formula of appendix B are a good approximation of the true signal  $C/N_0$  estimated by a receiver.

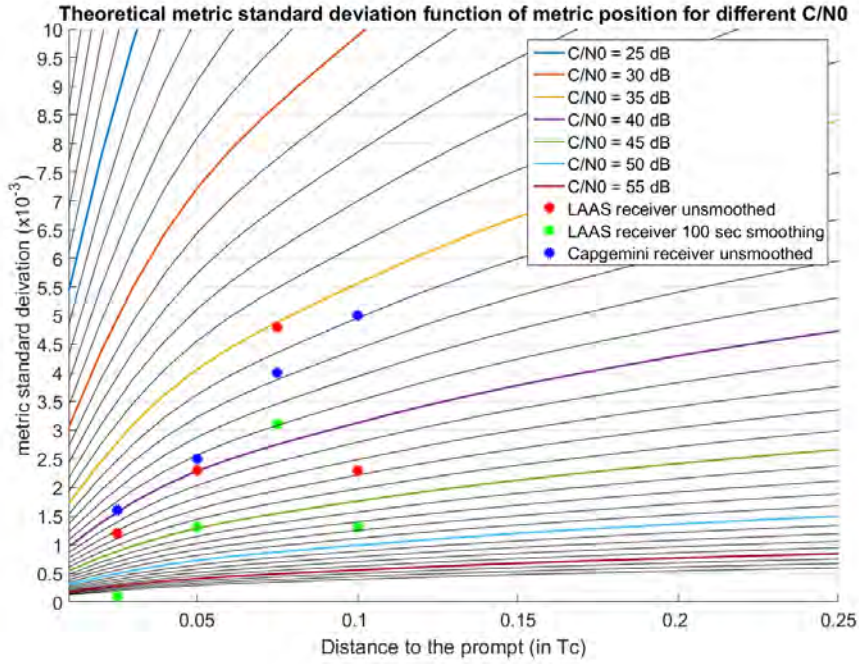


**Figure 7-9.** Example of reference station metrics standard deviations compared to theoretical values. One curve corresponds to one iso- $C/N_0$ .

One important remark is that the 100-second smoothing of the metrics seems to entail only a 4 dB improvement of the equivalent  $C/N_0$  in the real data whereas a 10 dB improvement would be expected if the raw metrics were uncorrelated in time. As a consequence, in practice, the reduction factor to apply on the metrics to consider the effect of the 100-second smoothing filter is only 1.5 to account for correlated errors, such as multipath. Even if this reduction factor was greater on the signals collected by Capgemini, the value of 1.5 (4 dB) can be considered conservative.

### 7.3.3.2 Generalization to Non Gaussian noise on metrics

In order to apply the theoretical SQM performance analysis developed in this chapter, the noise distribution of the metrics would have to be white and Gaussian. In real conditions it can appear that this hypothesis is not true [Thevenon et al., 2014]. One of the consequences is that, at each reference station, the MDE of each metric has to be adjusted to satisfy  $P_{md\_metric,j}$  and  $P_{ffd\_metric,j}$ , and especially avoid too many false alarms. Indeed in non-Gaussian conditions, it is not possible to estimate the  $MDE_{metric,j}$  by multiplying  $\sigma_{metric,j}$  by a multiplier derived from a normal law.

In this case,  $MDE_{metric,j}$  can be determined based on data collections at a given reference station. Indeed, even if the noise distribution on metrics is not Gaussian, it is possible to estimate  $K_{md\_metric,j}$  and  $K_{ffd\_metric,j}$  (and by consequence  $MDE_{metric,j}$ ) from the cumulative distribution function. With the knowledge of the  $MDE_{metric,j}$ , it is then possible to evaluate the equivalent  $\sigma_{metric,j}$  that would lead to the same  $MDE_{metric,j}$  if the metric was Gaussian-distributed. Finally, from this equivalent  $\sigma_{metric,j}$  and an abacus like the one provided in Figure 7-10, it is possible to determine an equivalent theoretical  $C/N_0$  at the reference station. Figure 7-10 represents the value of the MDE as a function

of the equivalent  $C/N_0$  at the reference station and the location of the correlator used in the simple ratio metric (Figure 7-9 multiplied by  $K = 8.35$ ).

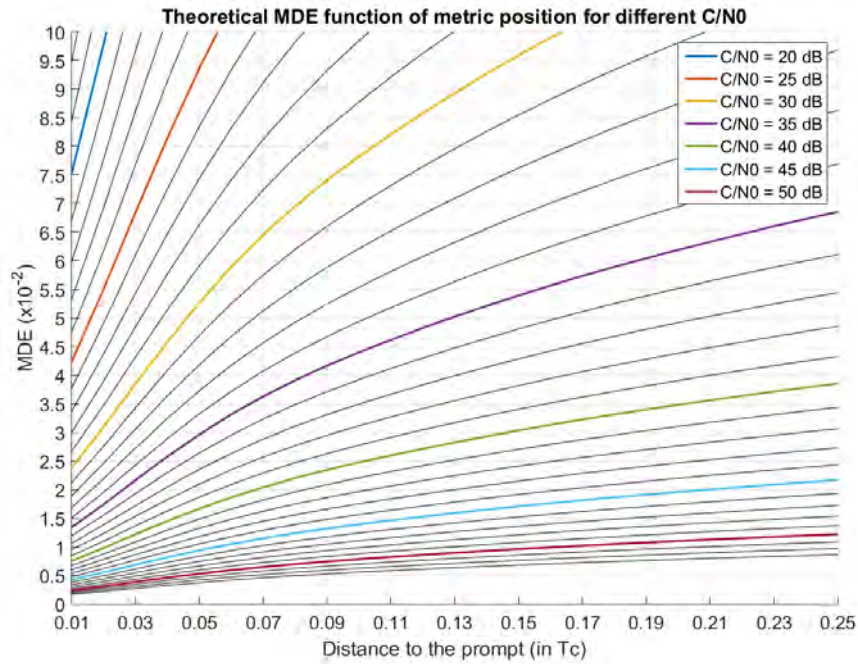


**Figure 7-10.** Simple ratio metrics performance thresholds for different  $C/N_0$  and different distance to the prompt.

As a consequence, even if at a reference station the noise distribution on metrics is not Gaussian, it is possible to find an equivalent theoretical  $C/N_0$  that permits to reduce the problem to an ideal theoretical case. It is then possible to use the innovative representation and to read SQM performance of that reference station for the estimated equivalent theoretical  $C/N_0$ . Nevertheless, if the noise distribution on metrics is far from Gaussian, it might be necessary to ensure that the results correctly bound the actual SQM performance. Due to the lack of data, this abacus is not used in this manuscript but could be of interest for future works.

#### 7.3.4 Comparison of SQMs

Additionally to the fact that the representation proposed in the previous section provides a view of the MUDE as a function of the equivalent theoretical  $C/N_0$ , a second interest of the representation is that performance of different SQMs can be compared independently from the equivalent theoretical  $C/N_0$  at which the reference station is operating.

In this part, a second SQM is introduced: SQM2b. This SQM was studied around 2000 for example in [Phelts et al., 2003] or [Phelts et al., 2000], and is still used nowadays in EGNOS RIMS-C stations [Bruce et al., 2000]. Originally, SQM2b consisted in eleven metrics but only four metrics are used by RIMS-C stations. The second studied SQM is thus based on the four SQM2b metrics:

$$\begin{aligned} &metric_{-0.075} , metric_{0.075} \\ &metric_{0.075-0.075} , metric_{0.1-0.1} \end{aligned}$$



Figure 7-11 gives in red results obtained using the SQM2b and in green using the reference SQM. From these plots, it is clear that the reference SQM has better performance than the SQM2b whatever the  $C/N_0$  is. This result can be read from Figure 7-11 because the red line is higher than the green line for the different values of  $C/N_0$ , i.e. the MUDE of SQM2b is higher than that of the reference SQM for the different values of  $C/N_0$ . This result was expected especially because the reference SQM relies on one hundred metrics whereas SQM2b relies on only four metrics.

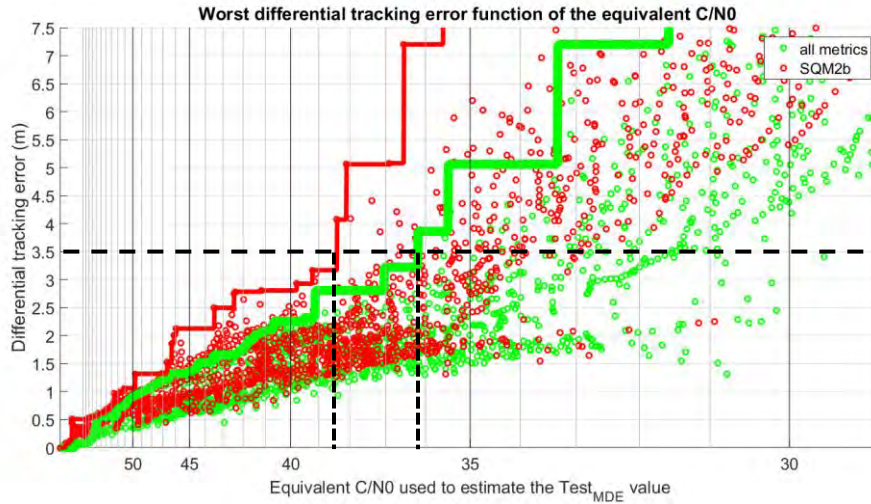


**Figure 7-11.** Comparison of two SQMs performance.

The MERR was fixed to 3.5 m for SBAS L1 civil aviation operations. It can be seen that MUDE is lower than 3.5 m with the SQM2b only if the equivalent  $C/N_0$  is higher than 38.5 dB-Hz, while for the reference SQM, an allowable equivalent  $C/N_0$  is 36.1 dB-Hz.

The results on SQM2b put forward that in this simulation setup, SQM2b does not reach the required performance for signals received with an equivalent  $C/N_0$  lower than 38.5 dB-Hz. This can be interpreted as a reason why a supplementary step in SQM design was proposed in the early 2000s [Phelts et al., 2003]. In order to decrease the metrics standard deviation, which would result in a translation to the right of the red points in Figure 7-11, it was proposed to smooth the metrics using low pass digital filter with a time constant equal to or shorter than 100 s [ICAO, 2006], which corresponds to the airborne measurement smoothing time. Such a smoothing was implemented on WAAS reference stations as defined in [Phelts and Walter, 2003], [Bruce et al., 2000] or [Phelts et al., 2015]. If the noise affecting the metrics was purely white, this smoothing would divide by a factor 10 the metrics standard deviation. However in practice, especially because of multipath, such improvement is not reached.

Considering that no smoothing is applied on metrics, the equivalent theoretical  $C/N_0$  can be as bad as 35 dB-Hz as seen in section 7.3.3.1. In this reception condition, the maximum undetectable differential error (MUDE) is higher than 7.5 m with SQM2b and is equal to 5.1 m with the reference SQM (fifty simple ratio, twenty-five difference ratio and twenty-five sum ratio metrics spread uniformly around the correlation function peak) according to Figure 7-11.

However, if a 100-second moving average window is used to smooth the metrics, the equivalent theoretical  $C/N_0$  would be improved (conservatively) by 4 dB as discussed in section 7.3.3.1. In this case the MUDE would be equal to 3.2 m with the SQM2b and 2.8 m with the reference SQM.

## 7. Signal quality monitoring of new signals

Finally, it is possible to further reduce the equivalent  $C/N_0$  considering that the SQM is taking a decision based on the correlator outputs or the metrics of several reference stations. This is not investigated here, but it can be expected that using data from four reference stations would allow to reduce the standard deviation of the metric by about 2.

From these results, it can be deduced that SQM2b is fulfilling SBAS L1 ICAO requirements (in steady state) even with conservative hypothesis. This conservative hypothesis does not take into account very low  $C/N_0$  that could be seen on some signals as for example on the signal collected by Capgemini at the beginning of the collection. Indeed, the  $C/N_0$  estimated by the receiver was equal to 32.8 dB-Hz.

### 7.3.5 Conclusions

As a conclusion of this section, a new method was proposed to estimate and compare SQM performance independently from the equivalent  $C/N_0$  at which a reference station operates. SQM performance is assessed considering given configurations at user and reference receivers level.

To estimate the SQM performance, two steps are necessary:

- plot the new SQM performance representation as a function of the  $C/N_0$ ,
- find the equivalent theoretical  $C/N_0$  at which a reference station is operating.

The value of the equivalent theoretical  $C/N_0$  is not necessarily representative of the true  $C/N_0$  of signals received by the reference station even if, from the only example available (Capgemini's data collection), equivalent theoretical  $C/N_0$  and true  $C/N_0$  were consistent (no smoothing was applied).

## 7.4 Results on new signals

In this section, SQMs theoretical performance for Galileo E1C, GPS L5 and Galileo E5a is estimated and compared using the methodology developed in the previous section. As described in chapter 6, there are more distortions to test on new GNSS signals than with the ICAO TM defined for GPS L1 C/A since their TS is larger:

- For Galileo E1C, 39455 distortions are generated (12 TM-A1, 80 TM-A2, 1022 TM-B area 1, 1717 TM-B area 2, 14303 TM-C area 1 and 22321 TM-C area 2).
- For Galileo E5a and GPS L5, 21467 distortions are generated (12 TM-A, 425 TM-B area 1, 736 TM-B area 2, 5526 TM-C area 1 and 14768 TM-C area 2).

All abacuses which permit to know the equivalent theoretical  $C/N_0$  at the reference knowing the standard deviation of simple ratio metrics are given for Galileo E5a, GPS L5 and Galileo E1C in section 7.4.1.

Reference SQMs performance is estimated for GPS L5, Galileo E5a and Galileo E1C in section 7.4.2. These SQMs are also called baseline SQMs and are noted  $SQM_{ref}$ .

It will be seen that it is not necessary to use all available metrics to reach the same SQM performance as the reference SQM. In section 7.4.3, a strategy to estimate an optimal SQM in terms of complexity ( $SQM_{optimal}$ ), using a reduced number of metrics, is developed and results obtained from this optimization are presented.

### 7.4.1 Metrics standard deviations vs $C/N_0$ abacuses for new signals

Abacuses which give  $\sigma_{metric_x}$  as a function of an equivalent theoretical  $C/N_0$  for Galileo E5a, GPS L5 (on the right) and Galileo E1C (on the left) signals are provided in Figure 7-12. These abacuses are drawn from equation (B-1) provided in appendix B in the case of simple ratio metrics. The two abacuses are presented to show that they depend upon the correlation function of the considered signal. Moreover, these abacuses permit to estimate at which equivalent theoretical  $C/N_0$  new signals are received at reference station and could be used in future works.

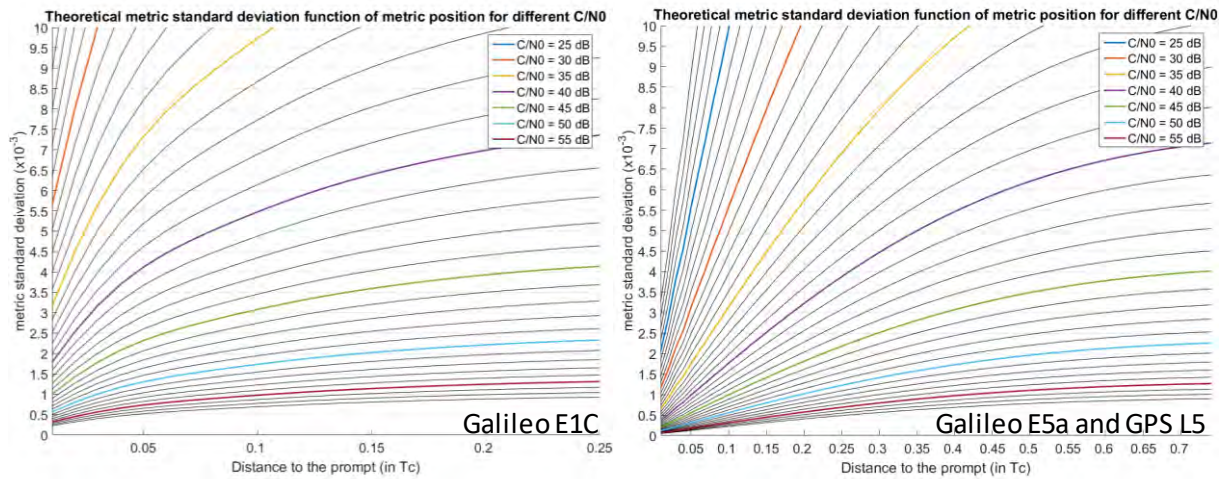


**Figure 7-12.** Metric (simple ratio) standard deviations values. One curve corresponds to one iso- $C/N_0$ . Galileo E1C signal on the left, Galileo E5a (and GPS L5 signal) on the right.

Because of the lack of true measurements on new signals, it is assumed in the following the same conservative equivalent theoretical  $C/N_0$  at typical reference station as in the GPS L1 C/A case:

- considering that no smoothing is applied on metrics, the equivalent theoretical  $C/N_0$  is equal to 35 dB-Hz,
- considering that a 100-second moving average window is applied on metrics, the equivalent theoretical  $C/N_0$  is equal to 39 dB-Hz.

The value of 39 dB-Hz is particularly high. It is reminded that it does not correspond to the true  $C/N_0$  observed from signals but to an equivalent theoretical  $C/N_0$  that takes into account the effect of the smoothing.

### 7.4.2 Performance of a SQM based on all available metrics

In this part, the definition of reference SQMs for Galileo E1C, Galileo E5a and GPS L5 signals are given. It corresponds to a SQM based on all available metrics as presented in 7.2.3. Then performances of the two SQMs are provided.

#### 7.4.2.1 Results on Galileo E1C

The reference SQM for Galileo E1C signal was already presented in 7.2.3 and consists of one hundred metrics:

## 7. Signal quality monitoring of new signals

- fifty simple ratio metrics  $metric_x$  with  $x = -0.25:0.01:-0.01$  and  $x = 0.01:0.01:0.25$  in E1C chip unit,
- twenty-five sum ratio metrics  $metric_{x+x}$  with  $x = 0.01:0.01:0.25$  in E1C chip unit,
- twenty-five difference ratio metrics  $metric_{x-x}$  with  $x = 0.01:0.01:0.25$  in E1C chip unit.

On Figure 7-13 is shown the maximum differential error entailed by distortions of the Galileo E1C TM as a function of the equivalent theoretical reference  $C/N_0$ .

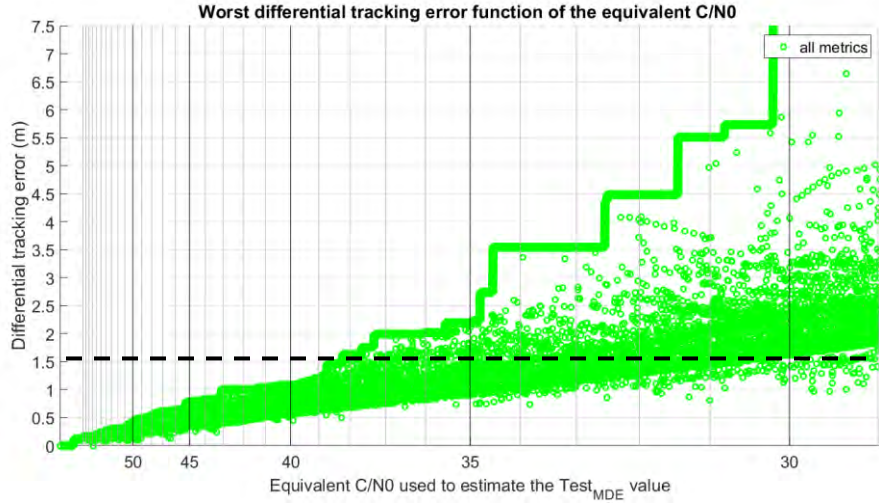


**Figure 7-13.** Reference SQM performance considering the proposed Galileo E1C TM.

From Figure 7-13, it can be seen that to satisfy the requirement on the MUDE of 1.55 m, the equivalent  $C/N_0$  must be higher than 38.4 dB-Hz. This value of 38.4 dB-Hz is considered as reached assuming that a 100-second moving average window is applied on metrics.

A second result is that the MUDE value of 3.5 m is reached for an equivalent theoretical  $C/N_0$  equal to 34.7 dB-Hz on Galileo E1C signal which is better than the 36.1 dB-Hz on GPS L1 C/A signal. It appears that SQM performance is slightly better on Galileo E1C than on GPS L1 C/A using in both cases the reference SQM.

The fact that SQM performance is better on one modulation than on another one can be explained by the fact that the narrower the correlation function peak is, the more the correlation function is affected by the ICAO-like distortions. Therefore, it is easier to detect distortions on sharp correlation function peak.

It is noticeable that the standard deviation of the metrics is higher with the  $BOC(1,1)$  than with the  $BPSK(1)$  because of the variance of the noise which is dependent upon the correlation function slope and the mean value of correlator outputs (see appendix A and appendix B). Nevertheless, it appears that in general, distortions are easier to detect on a  $BOC(1,1)/CBOC(6,1, 1/11, -)$  correlation function than on a  $BPSK(1)$  correlation function.

### 7.4.2.2 Results on Galileo E5a and GPS L5

The reference SQM on Galileo E5a and GPS L5 signals consists of forty metrics:

- twenty  $metric_x$  with  $x = -1:0.1:-0.1$  and  $x = 0.1:0.1:1$  in E5a chip unit,
- ten  $metric_{x+x}$  with  $x = 0.1:0.1:1$  in E5a chip unit,



- ten  $metric_{x-x}$  with  $x = 0.1:0.1:1$  in E5a chip unit.

On Figure 7-14 is shown the maximum differential error entailed by a distortion of the Galileo E5a TM as a function of the equivalent theoretical reference  $C/N_0$ .

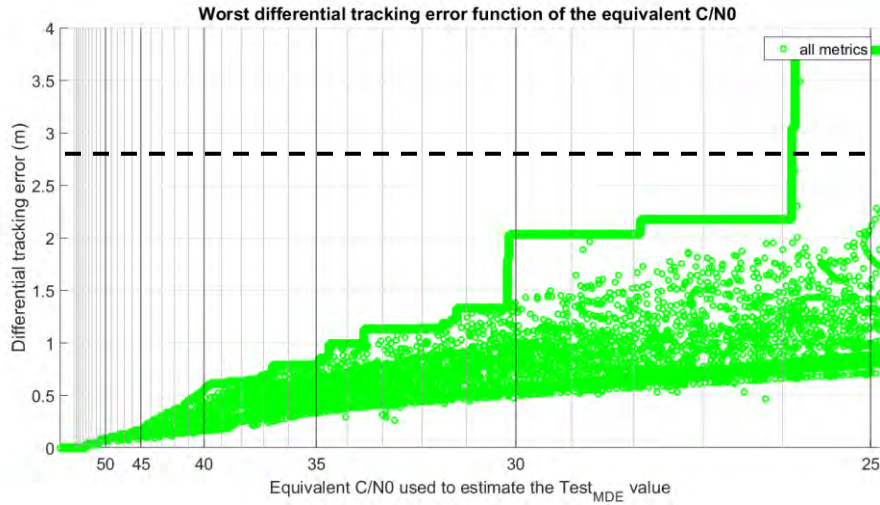


**Figure 7-14.** Reference SQM performance considering the proposed Galileo E5a TM.

To satisfy the requirement on the MUDE of 2.78 m on Galileo E5a and GPS L5, the  $C/N_0$  can be as low as 26 dB-Hz. Such performance is expected to be reached on reference receivers. SQM required performance is clearly easier to reach on Galileo E5a and GPS L5 than on GPS L1 C/A and Galileo E1C. This can also be explained by the fact that correlation function slope is higher with the  $BPSK(10)$  modulation. In addition, differential tracking errors entailed by distortions on this modulation are generally smaller because the correlation function peak is sharper.

It is noticeable that a step is visible around the  $C/N_0 = 26$  dB-Hz. The distortion that leads to this step is a TM-C distortion with  $f_d = 13$  MHz,  $\sigma = 3$  Mnerpers/s,  $\Delta = 0.7$  chip inducing a maximum differential error equal to 3.8 m. The impact of that distortion on the correlation function is represented on Figure 7-15.

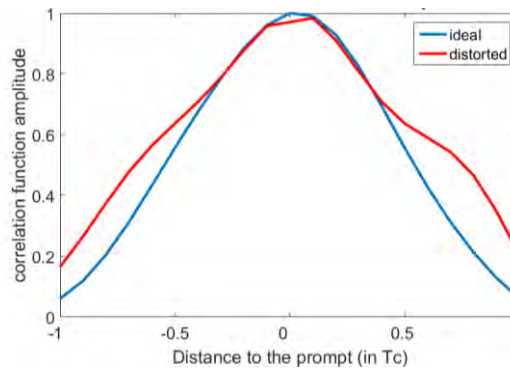


**Figure 7-15.** Distorted correlation function (in red) that induces the step around 26 dB-Hz on Galileo E5a and GPS L5 SQM performance.

### 7.4.3 Optimization of the SQM

In the previous part, the performance that can be reached by the reference SQM ( $SQM_{ref}$ ) built from one hundred metrics on Galileo E1C and from forty metrics on GPS L5 and Galileo E5a have been provided. Such a number of correlators and metrics can appear very high. It is thus interesting to investigate if the same performance can be reached with less correlators and/or less metrics.

#### 7.4.3.1 General results on SQM design

Based on the selected correlator outputs and metric types, SQM performance obtained using all available metrics permits to reach the SQM performance exposed in section 7.4.3. Nevertheless, in [Pagot et al., 2016b] it was shown that some metrics are more able to detect distortions than other. Indeed, [Pagot et al., 2016b] looked at the influence of three parameters on the SQM performance:

- the area covered by the correlator outputs used by the reference SQM,
- the distance between two correlator outputs used by the reference SQM,
- the use of the difference and the sum ratio metrics.

From this study several general results were put forward:

- Distortions detection with metrics based on correlator outputs distant from the correlation function main peak ( $> 200$  ns) is more difficult than with metrics based on correlator outputs close to the prompt. Indeed, second order distortions are attenuated according to the damping factor. Moreover, these correlator outputs will be more affected by multipath which has the consequence to increase metrics standard deviation and thus MDE (in real conditions that are not taken into account in this chapter).
- The use of additional correlator outputs close to each other ( $< 10$  ns) does not increase detection performance. It is due to the fact that the lowest period of ringing effects considered in this document is equal to  $1/(19 \times 10^{-6}) \approx 50$  ns and that high frequency phenomena are filtered out by the RF filter applied on the received signal.
- The difference ratio metric is not able to detect symmetric distortions that can have a threatening impact on differential users.

In the following, the aim of the SQM optimization is to reduce the number of metrics (among available metrics of the reference SQM) while obtaining suitable SQM performance. The definition of suitable performance can depend upon the application but has to be clearly defined to make the optimization relevant.

#### 7.4.3.2 Optimization at a given working point

In this part, the aim of the optimization is to find the SQM based on the lowest number of metrics as possible which is able to detect all distortions that entail a maximum differential tracking error above a given differential error threshold. To be optimal,  $SQM_{optimal}$  has to detect these distortions at same equivalent  $C/N_0$  as the reference SQM,  $SQM_{ref}$ , also called the baseline SQM.

For Galileo E1C, this maximum differential error threshold (MERR) is equal to 1.55 m. For Galileo E5a and GPS L5, this maximum differential error threshold is equal to 2.78 m.

## 7.4.3.2.1 Algorithm of the optimization at a given working point

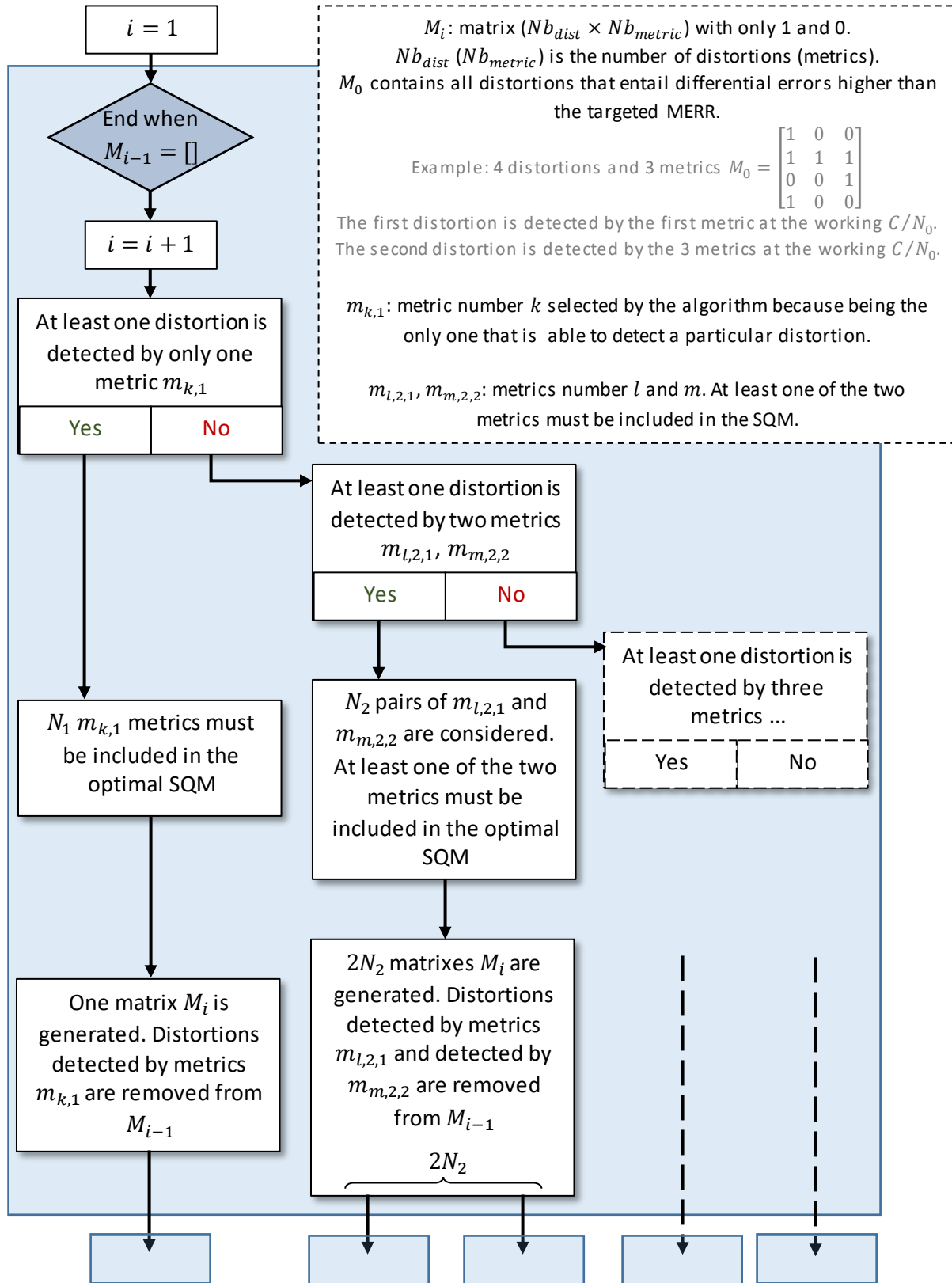


Figure 7-16. Algorithm to optimize the SQM at a given working point.

The block scheme on Figure 7-16 presents the algorithm that has been used to optimize the SQM at a given working point. The blue square corresponds to a basic algorithm step. Several ramifications can start at the end of one basic algorithm step. This algorithm stops when the matrix  $M_{i-1}$  is empty. Optimal SQMs are built from the smallest sets of metrics that have been selected all along the algorithm. Several optimal SQMs can be obtained because several ramifications can be started.

### 7.4.3.2.2 Results on Galileo E1C

It was seen that with the baseline SQM for Galileo E1C (SQM built from all available metrics on E1C signal), the lowest reference equivalent  $C/N_0$  that permits to detect all distortions which entail a maximum differential error higher than 1.55 m is equal to 38.4 dB-Hz.

For Galileo E1C, an optimization is envisaged at this working point.  $SQM_{E1C_{optimal1}}$  is designed to detect all distortions with a maximum impact on the differential error higher than 1.55 m for a reference station operating at an equivalent  $C/N_0 = 38.4$  dB-Hz.

Using the optimization algorithm, it appears that at least six metrics are necessary to design such a SQM. An example of two optimal solutions is given but other solutions are possible: the SQM design is not unique and fifteen different suitable SQMs were found. One possible SQM is the  $SQM_{E1C_{optimal1}}$ , which is composed of the six following metrics (and eleven correlator outputs):

- two simple ratio metrics  $metric_x$  with  $x = -0.01$  and  $x = 0.12$  in E1C chip unit,
- three sum ratio metrics  $metric_{x+x}$  with  $x = 0.02$ ,  $x = 0.05$ ,  $x = 0.07$  in E1C chip unit,
- one difference ratio metric  $metric_{x-x}$  with  $x = 0.20$  in E1C chip unit.

Its performance is represented in red on Figure 7-17

A second possible SQM is the  $SQM_{E1C_{optimal2}}$  represented in blue on Figure 7-17 which is composed of the six following metrics (and nine correlator outputs):

- four simple ratio metrics  $metric_x$  with  $x = -0.01$ ,  $x = 0.01$ ,  $x = 0.12$ , and  $x = 0.21$  in E1C chip unit,
- two sum ratio metrics  $metric_{x+x}$  with  $x = 0.04$ ,  $x = 0.07$  in E1C chip unit.

Its performance is represented in blue on Figure 7-17.

From the two designs, several results are noticeable and tend to confirm outcomes provided in [Pagot et al., 2016b]:

- The most used correlator outputs are situated close to the prompt.
- In general, two correlator outputs spaced by  $0.01 T_c$  are not used in the same SQM design.
- The same correlator output is not used by different metrics for a given SQM design. In other words, correlator outputs are used only once.
- The less used metric is the difference ratio metric.
- Even if different SQM designs are possible, approximatively the same correlator outputs (but different metrics) are used in every optimal SQMs.
- One metric based on correlator outputs far away from the prompt ( $0.21$  and  $0.20 T_c$ ) is present in the two proposed optimal SQMs.

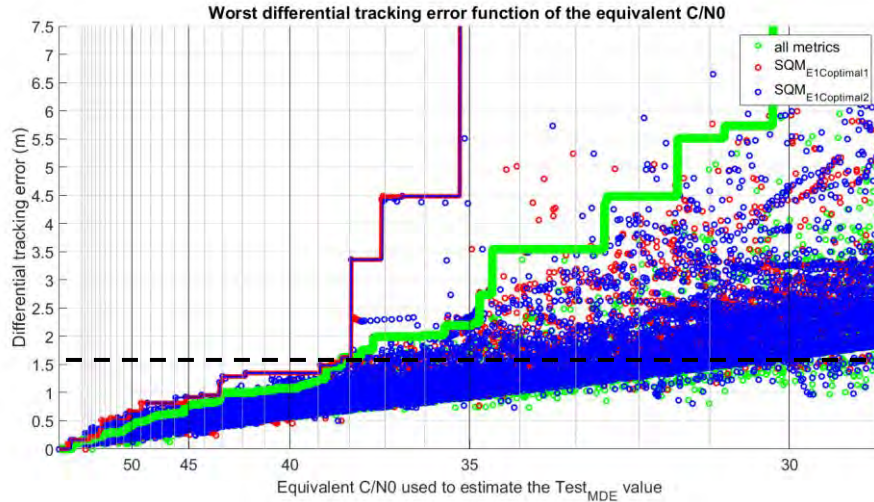


**Figure 7-17.**  $SQM_{E1C\_optimal1}$  (in red) and  $SQM_{E1C\_optimal2}$  (in blue) performances compared to baseline SQM (in green) considering the proposed Galileo E1C TM.

From Figure 7-17, it is clearly visible that the performance of the optimal SQM is equal to performance of the baseline SQM composed of all metrics for  $C/N_0 = 38.4$  dB-Hz. Nevertheless, in general, the bold continuous line corresponding to the highest differential error induced by distortions undetected by a reference station at a given  $C/N_0$  is higher in the optimal SQM case than in the baseline case. It means that the baseline case is more performant (or has equal performance) than the optimal SQMs outside the working operational  $C/N_0$  considered for the optimization. This is a logical result.

#### 7.4.3.2.3 Results on E5a and GPS L5

For GPS L5 and Galileo E5a, the optimal SQM ( $SQM_{E5a\_optimal}$ ) is designed to detect all distortions with a maximum impact on the differential error higher than 2.78 m for a reference station operating at an equivalent  $C/N_0 = 25.3$  dB-Hz. Only three metrics are necessary and twelve SQM designs that permit to reach this performance were found.

As an example, one possible SQM is the  $SQM_{E5a\_optimal1}$  based on the three following metrics (and seven correlator outputs):

- two  $metric_{x+x}$  with  $x = 0.8$  and  $x = 1$  in E5a chip unit,
- one  $metric_{x-x}$  with  $x = 0.1$  in E5a chip unit.

As another example, a second possible SQM is the  $SQM_{E5a\_optimal2}$  based on the three following metrics (and seven correlator outputs):

- two  $metric_x$  with  $x = -0.1$  and  $x = 1$  in E5a chip unit,
- one  $metric_{x+x}$  with  $x = 0.8$  in E5a chip unit.

On Figure 7-18, the two SQMs ( $SQM_{E5a\_optimal1}$  in red and  $SQM_{E5a\_optimal2}$  in blue) are compared to the reference SQM (in green).

It can be seen that all SQMs meet the required performance at the chosen working point, even if the optimal SQMs performance is different elsewhere.

The selection of one particular optimal SQM rather than another one could be made based on a second criterion at a MUDE different from 2.8 m. It is important to notice that for Galileo E5a and GPS L5, the

optimization is realized for an equivalent  $C/N_0 = 25.3$  dB-Hz which is not representative of typical reference station conditions. A second strategy of optimization is also possible: optimized the SQM around an equivalent  $C/N_0$  instead of a value of MUDE. This second strategy is relevant in  $BPSK(10)$ -modulated signal case because the requirement on the maximum differential error (2.8 m) is easily reachable.

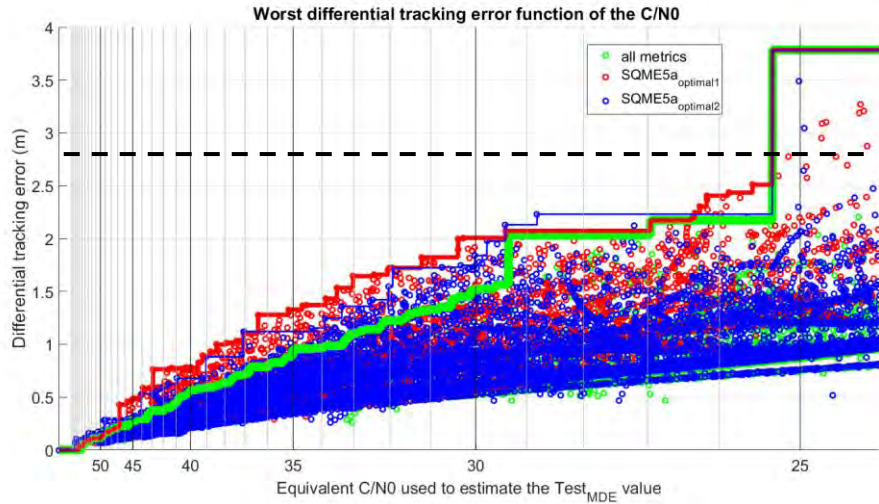


**Figure 7-18.**  $SQM_{E5a\_optimal1}$  and  $SQM_{E5a\_optimal2}$  performances considering the proposed Galileo E5a TM (also valid for GPS L5).  $MUDE = 2.78$  m for  $C/N_0 = 25.3$  dB-Hz.

Assuming now that the reference receiver is operating at an equivalent  $C/N_0 = 39$  dB-Hz (this value was estimated for a GPS L1 C/A signal in part 7.3.3), the MUDE is equal to 0.61 m for the baseline SQM. This performance can be reached by two SQM designs with only three metrics:  $SQM_{E5a\_optimal3}$  and  $SQM_{E5a\_optimal4}$  described below.

$SQM_{E5a\_optimal3}$  is based on the three following metrics (and six correlator outputs):

- one  $metric_x$  with  $x = 0.8$  in E5a chip unit,
- one  $metric_{x+x}$  with  $x = 0.2$  in E5a chip unit,
- one  $metric_{x-x}$  with  $x = 0.1$  in E5a chip unit.

$SQM_{E5a\_optimal4}$  is based on the three following metrics (and five correlator outputs):

- two  $metric_x$  with  $x = 0.1$  and  $x = 0.8$  in E5a chip unit,
- one  $metric_{x+x}$  with  $x = 0.2$  in E5a chip unit.

In the same way, the two optimal SQMs have slightly different performances but the MUDE is equal to 0.61 m for an equivalent  $C/N_0$  equal to 39 dB-Hz.



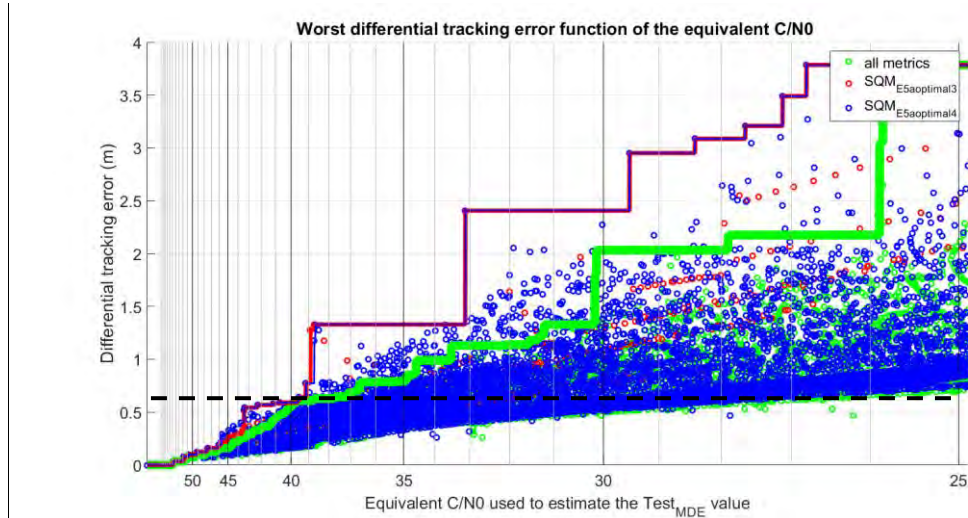


**Figure 7-19.**  $SQM_{E5a\_optimal3}$  and  $SQM_{E5a\_optimal4}$  performances considering the proposed Galileo E5a TM (also valid for GPS L5).  $MUDE = 0.61$  m for  $C/N_0 = 39$  dB-Hz.

From the four optimal SQM designs presented on Galileo E5a signal (and GPS L5 signal), several results are noticeable:

- It is more difficult than on Galileo E1C to find general concepts to design the optimal SQM but less metrics and correlator outputs are necessary to monitor Galileo E5a and GPS L5 signals. The fact that less metrics are necessary to monitor Galileo E5a and GPS L5 signals is mainly justified because, on these signals, the reference SQM is based on less metrics than for Galileo E1C signal.
  - It is also noticeable that with Galileo E5a and GPS L5 signals correlator outputs are not used by different metrics for a given SQM design. In other words, correlator outputs are used only once.
  - Some differences appear between the optimization at  $C/N_0 = 39$  dB-Hz and at  $C/N_0 = 25.3$  dB-Hz:
    - o More correlator outputs close to the prompt are used when the optimization is made at a high  $C/N_0$ .
    - o More SQM designs are possible when the optimization is made at a low  $C/N_0$ .
- It can be justified by the fact that it is easier to optimize at low  $C/N_0$ .

#### 7.4.3.2.4 Conclusions about the SQM optimization at a given working point

The aim of this part is to find a SQM based on the lowest number of metrics as possible without compromise its performance at a given working point with respect to the baseline SQM. Two strategies based on two different criteria were proposed:

- Fix a MUDE, find the lowest equivalent  $C/N_0$  that permits to reach this MUDE with the baseline SQM (SQM built from all available metrics) and find the smallest sets of metrics that permit to reach that MUDE for that lowest  $C/N_0$ .
- Fix an equivalent  $C/N_0$ , find the MUDE obtained at this  $C/N_0$  with the baseline SQM and find the smallest sets of metrics that permit to reach that MUDE for that  $C/N_0$ .

## 7. Signal quality monitoring of new signals

The first strategy is used in the Galileo E1C context for a MUDE equal to 1.55 m (equivalent  $C/N_0 = 38.4$  dB-Hz). Six metrics are sufficient to reach required performance and several SQM designs permit to obtain such performance.

The first strategy is used in the Galileo E5a and GPS L5 context for a MUDE equal to 2.78 m (equivalent  $C/N_0 = 25.3$  dB-Hz). Three metrics are sufficient to reach required performance and several SQM designs permit to obtain such performance.

The second strategy is relevant with Galileo E5a and GPS L5 and is applied for an equivalent  $C/N_0 = 39$  dB-Hz (MUDE = 0.61 m). Three metrics are sufficient to reach required performance and several SQM designs permit to obtain such performance.

Depending on requirements that have to be met, different SQMs can be implemented on a reference station. An additional optimization criterion (for example an additional requirement at a different working point) may be used in order to select one SQM among those that are able to meet the first optimization criterion.

As a conclusion, to obtain SQM performance as good as the baseline SQM at a specific working point, only few metrics (typically around five) are necessary.

### 7.4.3.3 Optimization along all $C/N_0$ values

The SQM optimization proposed at a given working point has the advantage to be optimal at specific critical points and by consequence, only few metrics are necessary to reach performance of the reference SQM for that critical points. This is usually sufficient to ensure that the SQM fulfils a specific requirement. Nevertheless, this approach has one drawback: the optimization is specific to one particular working point and SQM performance can be poor at other points even if it satisfies the targeted requirement. In addition, several SQM designs that satisfy optimization criteria can be found. Indeed, with the strategy used in 7.4.3.2, in general, optimal SQMs are better than other at some equivalent  $C/N_0$  but are worst at other equivalent  $C/N_0$ .

In this part, a second method to design an optimal SQM, free of the first approach drawback, is proposed.

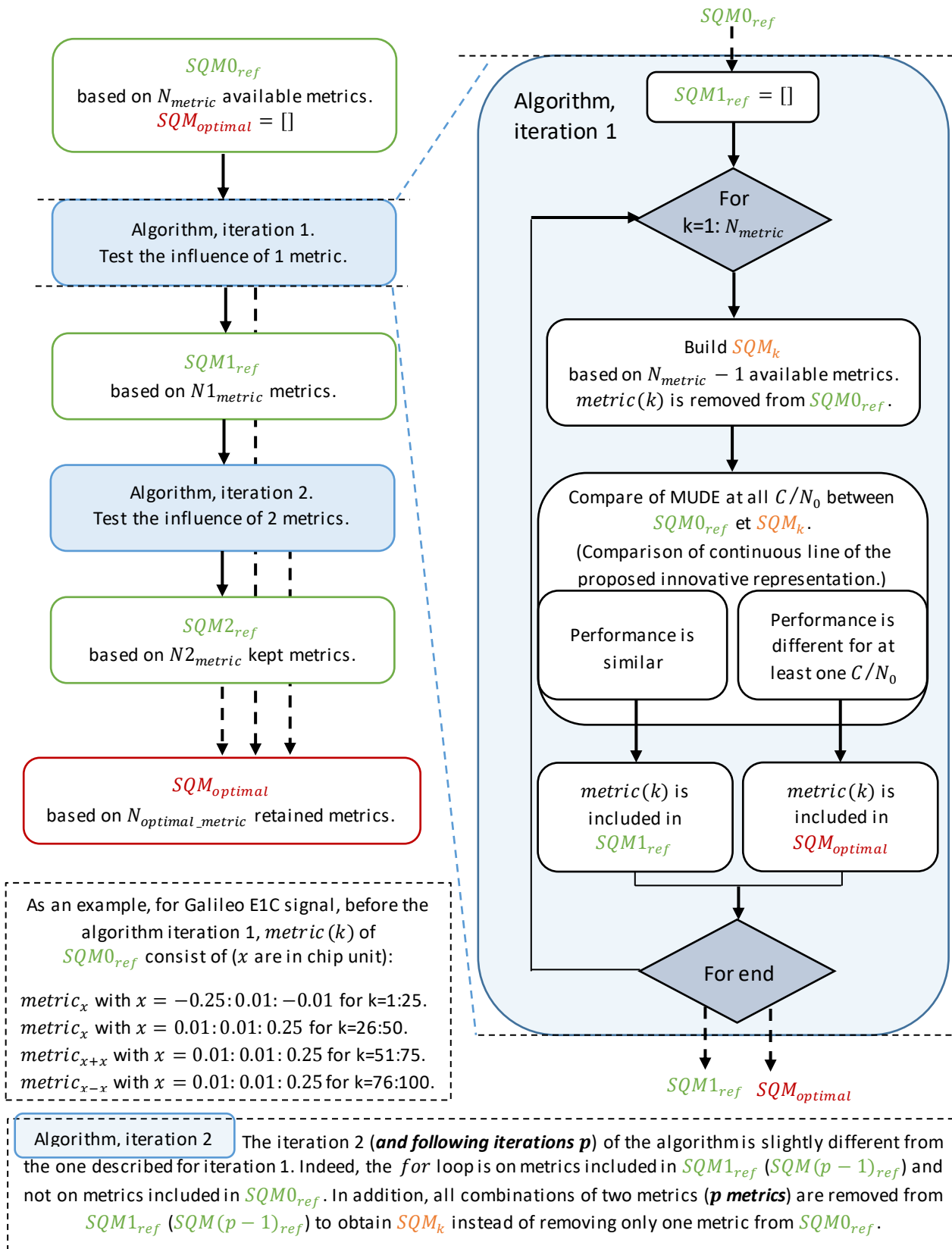
#### 7.4.3.3.1 Algorithm to optimized along all $C/N_0$ values

The optimization criterion consists in finding the smallest set of metrics that permits to reach the performance of the baseline SQM,  $SQM_{ref}$ , whatever the value of the equivalent  $C/N_0$  is. To find this optimal SQM, the principle is represented in Figure 7-20.

The optimization SQM principle is also described below:

- **Step 1.** Generate  $N_{metric}$   $SQM_k$ s where  $N_{metric}$  is the number of all available metrics (or equivalently the number of metrics in  $SQM_{ref}$ ). One  $SQM_k$  is built from  $N_{metric} - 1$  metrics and, for each  $SQM_k$ , one and only one metric is removed from  $SQM_{ref}$ .  $N_{metric} = 100$  for Galileo E1C, and  $N_{metric} = 40$  for Galileo E5a and GPS L5.
- **Step 2.** Compare performance of each  $SQM_k$  with  $SQM_{ref}$ .
- **Step 3.** If the performance of  $SQM_k$  is different from performance of  $SQM_{ref}$ , the metric that has been removed from  $SQM_{ref}$  to obtain this  $SQM_k$  has to be included in  $SQM_{optimal}$ .



Figure 7-20. Algorithm of SQM optimization at all  $C/N_0$  values.

- **Step 4.** It can appear that two (or more) metrics detect the same distortion. In this case, the fact to remove only one metric from the SQM does not change performance of the SQM. The two metrics have to be removed together from the  $SQM_{ref}$  to observe a performance change. It entails that one of the two metrics has to be chosen in the optimal SQM and that optimal SQM design is not unique. The choice of one metric instead of the other does not have any influence on MUDE values. To find metrics which detect same distortions, is it necessary to restart from step 1 by removing two by two (then three by three, etc.) metrics from the  $SQM_{ref}$  and to reiterate step 2 and step 3.

An interpretation of this optimization process is that it removes all redundant metrics from the reference initial set, i.e. metrics that detect distortions already detected by other metrics, and keeps only those metrics who actually define the performance of the baseline SQM. Results obtained on Galileo E1C are provided in section 7.4.3.3.2 and on Galileo E5 and GPS L5 are provided in section 7.4.3.3.3.

#### 7.4.3.3.2 Results on Galileo E1C

For Galileo E1C, an optimal SQM ( $SQM_{E1C\_optimal\_all1}$ ) that reaches performance of the reference SQM is reduced to thirty metrics (and thirty-five correlator outputs):

- twelve  $metric_x$  with  $x = -0.24, -0.11, -0.09, -0.01, 0.02, 0.07, 0.08, 0.09, 0.11, 0.12, 0.13, 0.21, 0.25$  in E1C chip unit,
- fourteen  $metric_{x+x}$  with  $x = 0.01, 0.02, 0.03, 0.04, 0.05, 0.06, 0.07, 0.08, 0.09, 0.10, 0.11, 0.16, 0.24, 0.25$  in E1C chip unit,
- four  $metric_{x-x}$  with  $x = 0.11, 0.12, 0.14, 0.25$  in E1C chip unit.

Figure 7-21 illustrates correlator outputs that are used in the optimal SQM.

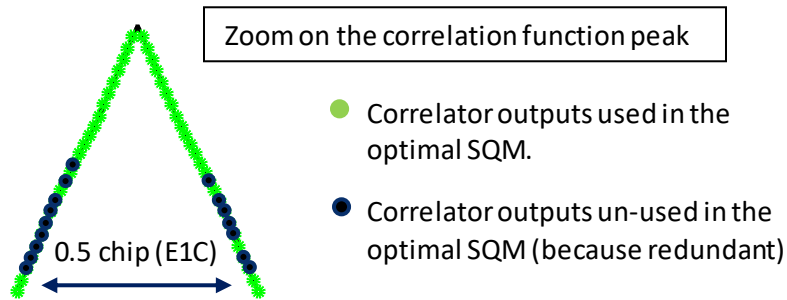


**Figure 7-21.** Correlator outputs used in the optimal SQM (Galileo E1C).

Several differences are noticeable between the SQM design obtained by the optimization at a given working point and the more demanding optimization along all equivalent  $C/N_0$ . These differences are caused by the fact that the design of  $SQM_{E1C\_optimal\_all1}$  has to be more complex than the design of  $SQM_{E1C\_optimal1}$ . In addition to the number of metrics which is five times more important in the case of  $SQM_{E1C\_optimal\_all1}$  compared to  $SQM_{E1C\_optimal1}$ , other differences are observed with  $SQM_{E1C\_optimal\_all1}$ :

- the most used correlator outputs are situated around  $0.1 T_c$  from the prompt and not necessarily close to the prompt,
- in general, two consecutive correlators outputs (spaced by  $0.01 T_c$ ) are used in the same SQM,
- the same correlator outputs can be used by several metrics.

On the other side, some results are comparable between  $SQM_{E1C\_optimal\_all1}$  and  $SQM_{E1C\_optimal1}$ :

- the least used metric is the difference ratio metric,
- some metrics based on correlator outputs far away from the prompt (around  $0.25 T_c$ ) are present in the proposed optimal SQM.

Other optimal SQMs with the same number of metrics exist. From Figure 7-22, it can be seen that, as expected, the MUDE of  $SQM_{E1C\_optimal\_all1}$  is equal to MUDE of the baseline SQM whatever the equivalent  $C/N_0$  is. Indeed, the two continuous lines are superimposed.

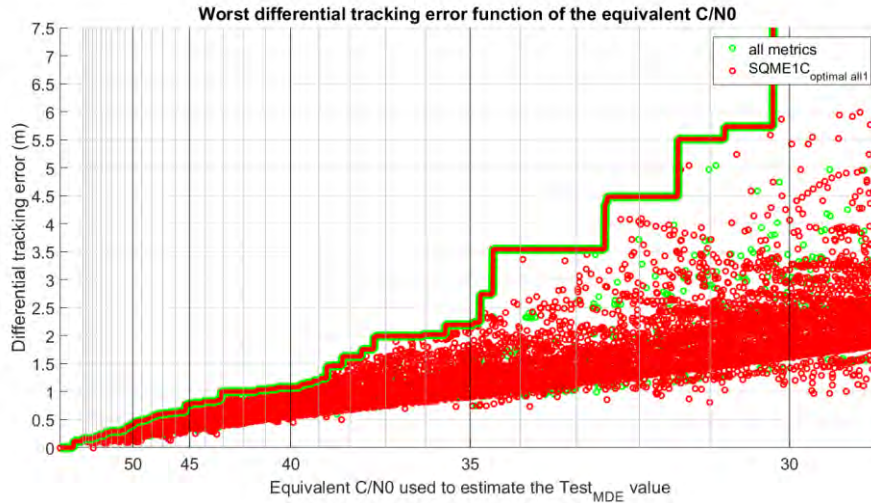


**Figure 7-22.**  $SQM_{E1C\_optimal\_all1}$  performance (in red) compared to the baseline SQM performance (in green).

#### 7.4.3.3.3 Results on Galileo E5a and GPS L5

For GPS L5 and Galileo E5a, an optimal SQM ( $SQM_{E5a\_optimal\_all1}$ ) that reaches performance of the reference SQM is reduced to eleven metrics (and thirteen-one correlator outputs):

- five  $metric_x$  with  $x = -0.1, 0.1, 0.8, 0.9, 1$  in E5a chip unit,
- five  $metric_{x+x}$  with  $x = 0.1, 0.4, 0.6, 0.7, 0.8$  in E5a chip unit,
- one  $metric_{x-x}$  with  $x = 1$  in E5a chip unit.

The same conclusion as with  $SQM_{E5a\_optimal1}$  holds: it is more difficult than on Galileo E1C to find general concept to design the optimal SQM. Nevertheless less metrics and correlator outputs are necessary to monitor Galileo E5a and GPS L5 signals. This is mainly justified because, on these signals, the reference SQM is based on less metrics than to monitor Galileo E1C signal.

Other optimal SQMs with the same number of metrics exist. From Figure 7-23, it can be seen that, as expected, the MUDE of  $SQM_{E5a\_optimal\_all1}$  is equal to the MUDE of the baseline SQM whatever the equivalent  $C/N_0$  is. Indeed, the two continuous lines are superimposed.

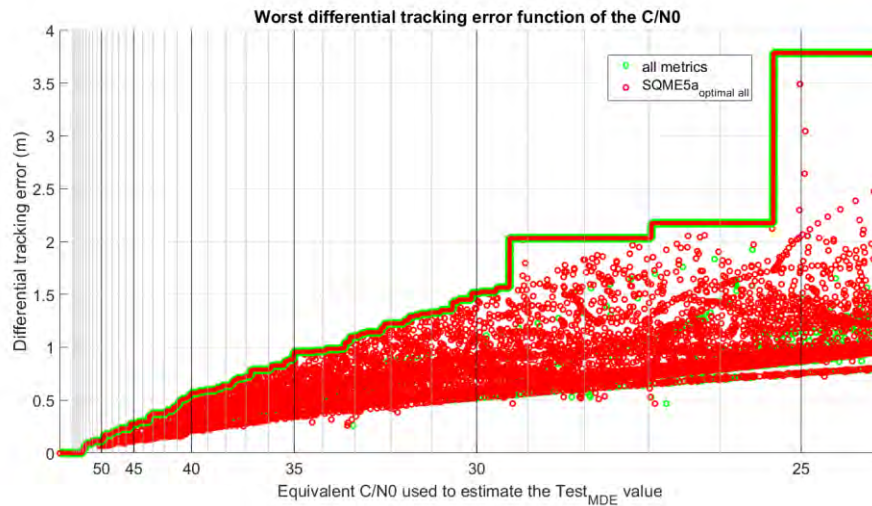


**Figure 7-23.**  $SQM_{E5a\_optimal\_all1}$  performance (in red) compared to the baseline SQM performance (in green).

#### 7.4.4 Conclusions about optimal SQM on new signals

To conclude this section, several methods can be developed to design a SQM with desired performance. Different optimal SQMs are proposed in this section. The main drawback of these approaches is that the SQM is necessarily optimized in given conditions (distortions and receivers configurations have to be given), and is not optimized for other conditions.

The best performance that can be obtained by a reference SQM are summarized in Table 7-6. In grey are presented values that do not correspond to targeted MERR for a given signal. Values in grey are presented for information. The reference SQM consists in:

- fifty simple ratio metrics plus twenty-five difference ratio metrics and twenty-five sum ratio metrics for Galileo E1C and GPS L1 C/A,
- twenty simple ratio metrics plus ten difference ratio metrics and ten sum ratio metrics for Galileo E5a and GPS L5.

MUDE (in meter)	1.55	2.78	3.5
Equivalent $C/N_0$ in dB-Hz (GPS L1 C/A)	44.6	39.1	36.1
Equivalent $C/N_0$ in dB-Hz (Galileo E1C)	38.4	34.7	34.7
Equivalent $C/N_0$ in dB-Hz (GPS L5 and Galileo E5a)	30.2	25.3	25.3

**Table 7-6.** SQM performance considering all available metrics.

The lower the value of  $C/N_0$  is, the easier the required MUDE can be reached. As a consequence, it can be deduced that the SQM based on all available metrics shows better performance on Galileo E5a signal and GPS L5 signal than on Galileo E1C and GPS L1 C/A signals. Moreover, SQM performance is slightly better on Galileo E1C than on GPS L1 C/A. These results have to be carefully interpreted because it is difficult to compare SQM performance of two different modulated signals with different correlation function shapes and different TMs.

It was established in the previous section that the equivalent theoretical  $C/N_0$  can be assumed as equal to 39 dB-Hz considering that metrics are smoothed. In this condition, the reference SQM reaches targeted performance for a MUDE equal to 3.5 m (Galileo E1C and GPS L1 C/A in mono-frequency conditions) and 2.78 m (Galileo E5a and GPS L5 in DFMC conditions). The reference SQM on GPS L1 C/A is not able to reach a MUDE equal to 1.55 m at an equivalent theoretical  $C/N_0$  equal to 39 dB-Hz whereas on Galileo E1C the value of 1.55 m can be achieved (even if with almost no margin).

An optimization process based on the limitation of metrics number is proposed. To reach the performance of the reference SQM at a given MUDE value (MERR equal to 1.55 m), only six metrics are necessary (and nine correlator outputs) on Galileo E1C. On Galileo E5a, with three metrics (and six correlator outputs), it is possible to reach a MUDE equal to 2.78 m at a  $C/N_0 = 25.3$  dB-Hz.

It is also possible to establish optimal SQMs with same MUDE values as the reference SQM whatever the value of the  $C/N_0$  is. In this condition, more metrics and more correlator outputs are necessary: thirty metrics (and thirty-five correlator outputs) for Galileo E1C and twelve metrics (and fourteen correlator outputs) for Galileo E5a and GPS L5.

## 7.5 Conclusions

This chapter tackles the design of SQM in the context of new GNSS signals: Galileo E1C, Galileo E5a and GPS L5. SQM performance is assessed theoretically for different SQM designs. This performance is dependent upon:

- distortions of the TM that have to be detected (presented in 7.2),
- user and reference configurations under discussion (presented in 7.2),
- types of metrics used to design the SQM (presented in 7.1).

In section 7.1, the three types of metrics used to design different SQMs are introduced: the simple ratio, the difference ratio and the sum ratio metrics. It is assumed that metrics are totally dependent in order to estimate SQM performance in a conservative way. In the same section, some SQM notions are exposed. The main issue in SQM study is the determination of requirements and performance thresholds which are proportional to the metrics standard deviation if the noise distribution on metrics is Gaussian. This strong hypothesis was verified in previous works.

In section 7.2, distortions, user/reference receivers configurations and reference SQMs considered for the study are defined for each signal. The reference SQM corresponds to the use of a high number of correlators and represents all available metrics (ratio, difference and sum). This reference SQM is expected to have redundant metrics, and is probably too “expensive”, from a computational point of view, to be implemented in operational reference receivers. However, thanks to its complexity, it is supposed to give the best performance for distortion monitoring.

In section 7.3, the concept of a new representation inspired from [Phelts et al., 2013] to estimate SQM performance is presented using the GPS L1 C/A signal example. This representation permits, based on one single figure, to estimate the theoretical MUDE as a function of the equivalent  $C/N_0$  value at a reference station, for all distortions of a given TM. Even if SQM performance is dependent upon the  $C/N_0$ , the representation gives the possibility to estimate from one figure, the SQM performance at different equivalent  $C/N_0$ .

## *7. Signal quality monitoring of new signals*

From the standard deviation of simple ratio metrics of real collected data, it is then possible to estimate at which theoretical  $C/N_0$  a reference station is operating. It has been seen through examples, that in the worst case, reference stations are operating with an equivalent theoretical  $C/N_0 = 35$  dB-Hz considering unsmoothed metrics and  $C/N_0 = 39$  dB-Hz with a 100-second averaging smoothing on metrics.

It is noteworthy that theoretical concepts are exposed assuming that the noise distribution on metrics is Gaussian. If this hypothesis is not verified, from MDEs estimated in real conditions, SQM performance can still be evaluated from the proposed representation presented in this chapter using an abacus which gives the equivalent theoretical  $C/N_0$  value associated to performance thresholds estimated in real conditions.

In section 7.4, some results about SQM on Galileo E1C, GPS L5 and Galileo E5a signals are established. An optimization process is applied to the reference SQM in order to remove redundant metrics and simplify the computation done by the monitoring process, while still reaching desired performances. It can be seen that SQM shows better performance on GPS L5 and Galileo E5a than on Galileo E1C and GPS L1 C/A. Moreover SQM performance is slightly better on Galileo E1C than on GPS L1 C/A.

To conclude, the work performed in this chapter is realized in a theoretical way and under specific conditions. Even if a method is proposed to adapt theoretical results to real reference station conditions, the provided results must be interpreted carefully and the strategy developed in this chapter has to be applied again at each particular reference station and monitoring station (that can be different). Nevertheless, results presented in this chapter give a solid analysis of expected SQM performance on new GNSS signals.

## 8 Conclusion and recommendations for future works

This chapter aims at drawing conclusions of the work done during this Ph.D. thesis. These conclusions are divided in three main parts: the study of nominal distortions, the study of TM and the study of SQM. Then, several suggestions for future researches in these three areas are listed.

### 8.1 Conclusions

The work performed in this Ph.D. took place in the context of the use of GNSS in civil aviation. It was seen in chapter 2 that a core GNSS constellation cannot be used alone by civil aviation users in some phases of flight. Indeed, the four criteria that define performance of the GNSS service (accuracy, integrity, availability and continuity) cannot be met together when requirements are too stringent. This is the reason why augmentation systems are deployed, such as SBAS, the augmentation system that was targeted in this study, to increase performance of the GNSS service. GNSS service improvement supported by SBAS is today provided only for the GPS L1 C/A signal.

This Ph.D. takes place in a European context. By consequence the European SBAS system, EGNOS, was looked at. EGNOS v3 will augment both GPS and Galileo on L1 and L5 frequency bands and will support civil aviation DFMC users.

For SBAS to meet civil aviation requirements, any source of potential service degradations has to be accounted for. Despite the fact that several sources of errors can be present on GNSS signals, this Ph.D. was focused on one potential source of degradation: GNSS signal distortions due to the satellite payload. These distortions can manifest in two ways: nominal distortions that are generated by healthy satellites due to payload imperfections and non-nominal distortions that are triggered by a satellite payload failure.

To summarize, the purpose of this thesis was to investigate GNSS distortions induced by the payload on Galileo E1C, Galileo E5a pilot component, GPS L5 pilot component and GPS L1 C/A signals in the SBAS context.

#### **Conclusions about nominal distortions**

The investigation on nominal distortions observed on real data was performed using two methods. The first method was to look at the impact of nominal distortions on signals collected with high-gain dish antennas. This method was applied to GPS L1 C/A and to Galileo E1C signals. The second method was to look at the impact of nominal distortions on signals collected with an omnidirectional antenna.

The first method has permitted to confirm distortions features in the chip domain and in the differential tracking error domain. It appeared that nominal digital distortions are consistent with results provided in the state-of-the-art but that it is more difficult to observe consistent analog distortions. The reason of the difference visible on the analog distortion is caused by an imperfect

calibration of high-gain dish antenna as underlined in [Wong, 2014]. Among other results, nominal distortions observed on Galileo E1C signals collected with a high-gain dish antenna are represented. It confirms that no digital distortions are visible on Galileo E1C signals and it puts forward the ringing phenomenon of 24 MHz generated most likely by the payload.

The problem of calibration exists on signals collected with high-gain antennas because only one signal is captured at a given time and it is by consequence difficult to extract the distortion component induced by the receiver. Nevertheless, this issue is mitigated on signals collected with omnidirectional antennas and this is the reason why measurements from omnidirectional antenna were also collected on GPS L1 C/A. The advantage of omnidirectional antennas is that several signals are captured at a given time. As the signal distortion induced by the receiver affects all collected signals at a given time, it is possible, subtracting the mean value of observed signal distortions, to remove the signal distortion component induced by the receiver. Applying this technique, the inter-PRN bias (parameter defined in the pseudorange domain and which effectively affects the receiver) was estimated on some signals collected with an omnidirectional antenna. Values of inter-PRN bias are of the order of tens of centimeters assuming that signals are tracked with an EML discriminator. It appeared that the inter-PRN bias is consistent with results provided in the state-of-the-art and by consequence, seemed to be an interesting parameter to characterize the impact of nominal distortions on users.

To summarize, nominal distortions are difficult to characterize because their impact on users depends upon several parameters. Even if high-gain antenna data collections give the possibility to observe precisely nominal distortions, omnidirectional data collections are more adequate to characterize the impact of nominal distortions on users via the inter-PRN bias.

### **Conclusions about non-nominal distortions**

In this Ph.D., three TMs were proposed: one for Galileo E5a and GPS L5 pilot components (the same modulation is considered), one for Galileo E1C and one for GPS L1 C/A signals. If a new TM was proposed for GPS L1 C/A signal, it was not to question the current ICAO TM, but rather to compare the TM obtained from the developed strategy to the ICAO TM.

It was seen that it is of primary importance to define a TM that is able to characterize signal distortions that could appear on GNSS signals to protect users of these threats. Even if TM consists only in a model with its possible imperfections, its simplicity of use makes it a necessary tool to establish a common and agreed framework for signal distortions monitoring performance.

Based on the observation of nominal distortions, on previous works done regarding TM on GPS L1 C/A signal, and due to the lack of knowledge about payload components, it was decided to design TMs for new signals using same parameters as on GPS L1 C/A to characterize threatening distortions: a damping factor, a ringing frequency, and a delay between rising and falling PRN transitions zero-crossings. As for GPS L1 C/A ICAO TM, three sub-TMs were designed: TM-A, TM-B and TM-C. The TM-A (digital distortion), defined by the delay between rising and falling PRN transitions, was easy to generalize to Galileo E5a and GPS L5 because these two signals have similarities with the GPS L1 C/A signal. On the contrary, the Galileo E1C signal possesses two sub-carrier components that can be both affected by digital distortions. This is the reason why two TM-A were defined on Galileo E1C signal. The TM-B (analog distortion), defined by the ringing frequency and the damping factor, can be modeled by a second order filter that can be applied no matter the signal modulation.

Then, the approach to limit the TM-A and TM-B is based on keeping only signal distortions with:



- an impact higher than  $\Delta_{err\_max} = 1$  m for differential users in a specific receiver configurations range. This value is fixed by requirement.
- an impact smaller than 20 m on a reference station absolute pseudorange measurement.

Then the TM-C consists in a combination of TM-A and TM-B.

It was assumed that distortions which do not satisfy the first point are not a threat for differential (dual-frequency) users, whereas distortions which do not satisfy the second point will be detected by an assumed separate monitor implemented at the reference station to be defined. These TMs are interesting because they take into account all possible threats for all the user/reference configurations considered in this Ph.D.. Proposed TMs were larger than the ICAO TM defined for GPS L1 C/A signal. Even if large values of  $\sigma$  have to be considered, it was assessed that the number of distortions to test can be substantially limited.

### Conclusions about SQM

After defining TMs, the strategy was to design a monitor (SQM) that is able to detect distortions of the TMs which entail threatening behaviors on differential users. As it is done nowadays in SBAS, in this Ph.D. the SQM was built from correlator outputs. Using a large number of correlator outputs (fifty-one for GPS L1 C/A and Galileo E1C and twenty one for Galileo E5a), three metrics were tested to design the SQM: simple ratio, difference ratio and sum ratio metrics normalized by the prompt. SQM performance was assessed theoretically, in a conservative way, as the maximum differential error entailed by a distortion, as a function of the value of the highest metric test for that distortion. SQM performance is dependent upon several parameters:

- distortions of the TM that have to be detected,
- user and reference configurations under discussion,
- types of metrics used to design the SQM,
- $C/N_0$  of the signal that has to be monitored.

A new representation was proposed to assess, from one representation, performance of the SQM independently from an equivalent  $C/N_0$  value. In addition to this representation, a strategy to evaluate the equivalent theoretical  $C/N_0$  in given reference station conditions was exposed. The equivalent  $C/N_0$  in reference station operating conditions was estimated equal to 39 dB-Hz (considering that metrics are smoothed). Using the innovative representation SQMs performances were assessed for the different signals and it appeared that the signal quality monitoring is easier to perform on Galileo E5a (and GPS L5) signal than on GPS L1 C/A signal or on Galileo E1C signal. In particular, at an equivalent  $C/N_0$  equal to 39 dB-Hz, the Maximum Undetected Differential Error (MUDE) obtained with a SQM based on all available metrics is equal to 0.6 m on Galileo E5a, 1.3 m on Galileo E1C and 2.8 m on GPS L1 C/A. Finally, different optimal SQMs were proposed on new signals. The purpose was to decrease the number of metrics on which the SQM relies still reaching required performances targeted in this Ph.D.: a MUDE equal to 1.55 m for Galileo E1C signal and equal to 2.78 m for Galileo E5a and GPS L5 signals. On new signals, typically around five metrics are sufficient to reach targeted performances.

## 8.2 Recommendations for future work

Further works can be conducted from investigations made in this Ph.D. on the three axes that are: nominal distortions, non-nominal distortions and SQM. Recommendations on these three points are detailed.

It is noteworthy that the work performed in this thesis in an EGNOS context is valid for SBAS but could be generalized to GBAS applying some adjustments.

### **Perspectives on nominal distortions**

One of the conclusions about nominal distortions is the difficulty to characterize them. When studying nominal distortions, a particular care must be taken to define precisely the setup that is used to process signals. Significant resources should now be used to estimate more precisely nominal distortions: data collections at the same time and on the same signal with several different antennas, and this, on all signals and all satellites. This would permit to isolate in a better way the signal distortion components induced by the antenna and the receiver.

In addition, only signal distortions on GPS L1 C/A and three Galileo E1C signals were observed. This observation must be done on other signals, especially on Galileo E5a and GPS L5 signals.

Even if the purpose of the study of nominal distortions is to quantify their impact on the users tracking error (and differential tracking error), the S-curve zero-crossing observable is not the unique observable of interest. Indeed, the chip domain observable gives another point of view on signal distortions that may be of interest when distortions are not visible on the correlation function because averaged on the entire signal (during the coherent integration time) but are visible on some particular parts of the signal (for example on rising transitions or on falling transitions).

Nominal signal distortions are currently studied as parameters of interest in the ARAIM context ([European Commission, 2016]). Links between the observation methodology/results and the models used in ARAIM should be established to benefit from the work done in this study.

### **Perspectives on non-nominal distortions**

TMs proposed for Galileo E1C, Galileo E5a and GPS L5 are conservative but were defined considering a limited number of receiver configurations. Consequently, depending on the RF front-end filter technology and bandwidth, and depending on the receiver tracking, TMs could be slightly different. It is noticeable that group delays tested in this manuscript are only equal to 0 ns or 150 ns. In WAAS, filters were tested with a 30 ns increments [Phelts, 2001]. Then, an important remark is that before using these TMs, it is necessary to know if the context permits to use these TMs.

It is noticeable that the TM is limited by the impact of a distortion on a differential user and the impact of a distortion on a reference station. In this Ph.D., it was considered that differential errors higher than 1 m were threatening, but increase this value would reduce the TM. Moreover, it was considered that the reference station will be able to detect tracking bias higher than 20 m but decrease this value would reduce the TM. The adjustment of these two limits will change the TS. For a given application, TM could be re-estimated and should be included in the proposed conservative TM.

Regarding digital distortions, TM-A are taken into account conservatively as potential threats for Galileo signals but it was observed that such distortions do not affect signals in nominal conditions. Further investigations could maybe demonstrate that it is not necessary to consider this threat on a

Galileo signal. More generally, observation of non-nominal distortions and knowledges about payload functioning could help to design TMs.

An important issue regarding TM is about the resolution with which the TM is tested. In this manuscript, a proposition to deal with this problem is introduced and is used to compare the number of tests to perform with different TMs. This method could be applied to optimize the study of non-nominal distortions. It is noteworthy that the TM grid (that represents tested TM distortions) that is used in this manuscript regarding the GPS L1 C/A ICAO TM is coarser than the one used to test WAAS monitors. Thinner TM grids than the ones used in this manuscript could be defined in the future to test the different proposed TMs.

Finally, the entire concept of TM could be reworked. Even if TM is a very useful concept, it cannot be denied that it does not represent all signal distortions that could appear on a GNSS signal. Other strategies could be investigated as an augmented version of the Most EWF concept.

### **Perspectives on SQM**

Assuming a given TM, SQM performance estimated in this Ph.D. is dependent upon:

- user and reference configurations under discussion,
- types of metrics used to design the SQM.

It means that to be defined precisely, SQM performance must be assessed considering exact receiver configurations at user and reference levels. SQM performance could then be estimated in different conditions.

Moreover, in this thesis, only three types of metrics were investigated but more can be studied. Making correlator outputs combination, tens of metrics could be designed as the alpha metric or the “squared  $\Delta$  test”. The chip domain also has potential to better detect signal distortions.

A method was proposed to estimate SQM performance in a conservative theoretical way. One of the most conservative assumption is to consider that all metrics are totally dependent. A more accurate metrics model, taking into account that metrics are correlated, could be considered in the future. In addition, in real conditions, the metric standard deviation is dependent upon the tracking error caused by the noise on the correlation function. This phenomenon was not considered in this manuscript but have to be taken into account in the future to estimate precisely SQM performance.

In this manuscript SQM performance was assessed in steady state conditions. The transient problem could be investigated based on results estimated in steady state conditions.

Finally, the study that is proposed is based on theory. The next step will be to adapt the method developed in this thesis to estimate precisely SQM performance at a given reference station. In particular, the fact that the reference stations that provide differential corrections are different from stations that support the SQM have to be considered.



# References

- [Adams, 1999] C. Adams, *Beware of Evil Waveforms*, published in Avionics Magazine, Sep. 1999.
- [Avila Rodriguez, 2008] J.S. Avila Rodriguez, *Generalized Signal Waveforms for Satellite Navigation*, Ph.D Thesis, University FAF Munich, Germany, 2008.
- [Bastide et al., 2002] F. Bastide, O. Julien, C. Macabiau and B. Roturier, *Analysis of L5/E5 acquisition, tracking and data demodulation thresholds*, in Proceedings of ION GPS, Portland, Oregon, Sep. 2002, pp. 2196–2207.
- [Betz and Kolodziejski, 2000] J.W. Betz and K.R. Kolodziejski, *Extended Theory of Early-Late Code Tracking for a Bandlimited GPS Receiver*, published in NAVIGATION, Journal of The Institute of Navigation, May 2000, pp. 211–226.
- [Brenner et al., 2009] M. Brenner, F. Liu, K. Class, R. Reuter and P. Enge, *Natural Signal Deformations Observed in New Satellites and their Impact on GBAS*, in Proceedings of ION GNSS, Savannah, Georgia, Sep. 2009, pp. 1100–1111.
- [Brocard et al., 2000] D. Brocard, T. Maier and C. Busquet, *EGNOS Ranging and Integrity Monitoring Stations (RIMS)*, in Proceedings of GNSS 2000 Conference, Edinburgh, Scotland, May 2000, pp. 1055–1068.
- [Brocard et al., 2014] P. Brocard, P. Thevenon, O. Julien, D. Salos and M. Mabillean, *Measurement Quality Assessment in Urban Environments Using Correlation Function Distortion Metrics*, in Proceedings of ION GNSS+, Tampa, Florida, Sep. 2014, pp. 2684–2697.
- [Bruce et al., 2000] A.S. Bruce, A.J. Van Dierendonck, A. Jakab, J. Wiebe and B. Townsend, *Detection of GPS Satellite Signal Failures in Satellite Based Augmentation Systems (SBAS)*, in Proceedings of ION GPS 2000, Salt Lake City, Utah, Sep. 2000, pp. 189–198.
- [Chatre, 2003] E. Chatre, *GNSS Development Status and Future Work - GNSS Panel Agenda Item 6 - Presentation*, Sep. 2003.
- [Dragunas and Borre, 2011] K. Dragunas and K. Borre, *Multipath Mitigation Based on Deconvolution*, published in the Journal of Global Positioning Systems, Jun. 2011, vol. 10, pp. 79–88.
- [Edgar et al., 1999] C. Edgar, F. Czopek and B. Barker, *A Co-operative Anomaly Resolution on PRN-19*, in Proceedings of ION GPS, Nashville, Tennessee, Sep. 1999, pp. 2269–2271.
- [Enge et al., 1999] P. Enge, R.E. Phelts and A.M. Mitelman, *Detecting Anomalous signals from GPS satellites*, in Proceedings of ICAO, GNSS/P, Toulouse, France, 1999.
- [ESA, 2015] ESA, *ESA website available at <http://www.esa.int/ESA>*, 2015.
- [European Commission, 2016] European Commission, *Release of EU-US Cooperation on Satellite Navigation, Working Group C - ARAIM Technical Subgroup, Milestone III Report - website available at <http://ec.europa.eu/growth>*, Feb. 2016.

## References

- [FAA, 2008] FAA, *GPS WAAS performance standard, 1st edition*, Oct. 2008.
- [FAA, 2016a] FAA, *Satellite Navigation - Ground Based Augmentation System (GBAS)*. FAA website available at <http://www.faa.gov/>, May 2016.
- [FAA, 2016b] FAA, *WAAS Technical Reports*. FAA website available at <http://www.nstb.tc.faa.gov/DisplayDiscrepancyReport.htm>, Sep. 2016.
- [Fan et al., 2008] T. Fan, V.S. Lin, G.H. Wang and P.A. Dafesh, *Study of signal combining methodologies for future GPS flexible navigation payload (Part II)*, in Proceedings of IEEE/ION PLANS, Monterey, California, May 2008, pp. 1079–1089.
- [Fenton and Jones, 2005] P.C. Fenton and J. Jones, *The theory and performance of NovAtel Inc.'s vision correlator*, in Proceedings of ION GNSS, Long Beach, California, Sep. 2005, pp. 2178–2186.
- [Fernow, 2005] J. Fernow, *WAAS Integrity Risks: Fault Tree, "Threats", and Assertions - Presentation*, Jun. 2005.
- [Fontanella et al., 2010] D. Fontanella, M. Paonni and B. Eissfeller, *A novel evil waveforms threat model for new generation GNSS signals: Theoretical analysis and performance*, in Proceedings of IEEE/Navitech, Noordwijk, the Netherlands, Dec. 2010, pp. 1–8.
- [GALILEO LA, 2015] GALILEO LA, *EGNOS System Architecture and Service Area | Galileo Information Centre for Latin America*. Website available at <http://www.galileoic.org/node/145>, 2015.
- [Gisbert et al., 2012] J.V.P. Gisbert, N. Batzilis, G. Lopez-Risueno and J.A. Rubio, *GNSS payload and signal characterization using a 3m dish antenna*, in Proceedings of ION GNSS, Nashville, Tennessee, Sep. 2012, pp. 347–356.
- [Gleason, 2009] S. Gleason, *GNSS applications and methods - Book*, 2009.
- [GPS.gov, 2000] GPS.gov, *ICD-GPS-200C with revisions till IRN-200C-004, Navstar GPS Space Segment/Navigation User Interfaces*, Apr. 2000.
- [GPS.gov, 2012] GPS.gov, *Interface specification IS-GPS-705C, Navstar GPS Space Segment/User Segment L5 Interfaces*, Sep. 2012.
- [GPS.gov, 2015] GPS.gov, *GPS.gov website available at http://www.gps.gov/systems/gps/*, 2015.
- [GPS.gov, 2016] GPS.gov, *Working Group C - ARAIM Technical Subgroup, Milestone 3 Report, Final Version*, Feb. 2016.
- [GSA, 2010] GSA, *European GNSS (Galileo) Open Service, Signal In Space Interface Control Document*, Feb. 2010.
- [GSA, 2014] GSA, *EGNOS Open Service (OS), Service Definition Document*, Dec. 2014.
- [Gunawardena, 2014] S. Gunawardena, *A Universal GNSS Software Receiver Toolbox*, published in Inside GNSS, Aug. 2014, pp. 58–67.
- [Gunawardena and van Graas, 2012a] S. Gunawardena and F. van Graas, *Analysis of GPS Pseudorange Natural Biases using a Software Receiver*, in Proceedings of ION GNSS, Nashville, Tennessee, Sep. 2012, pp. 2141–2149.

- [Gunawardena and van Graas, 2012b] S. Gunawardena and F. van Graas, *High Fidelity Chip Shape Analysis of GNSS Signals using a Wideband Software Receiver*, in Proceedings of ION GNSS, Nashville, Tennessee, Sep. 2012, pp. 874–883.
- [Gunawardena, 2015] S. Gunawardena, *GPS-SPS Inter-PRN Pseudorange Biases compared for Transversal SAW and LC Filters using Live Sky Data and ChipShape Software Receiver Processing*, in Proceedings of ION ITM, Dana Point, California, Jan. 2015, pp. 393–403.
- [Gunawardena et al., 2015] S. Gunawardena, M. Carroll, J. Raquet and F. Van Graas, *High-Fidelity Signal Deformation Analysis of Live Sky Galileo E1 Signals using a ChipShape Software GNSS Receiver*, in Proceedings of ION GNSS+, Tampa, Florida, Sep. 2015, pp. 3325–3334.
- [Gunawardena and van Graas, 2013] S. Gunawardena and F. van Graas, *An Empirical Model for Computing GPS SPS Pseudorange Natural Biases Based on High Fidelity Measurements from a Software Receiver*, in Proceedings of ION GNSS+, Nashville, Tennessee, Sep. 2013, pp. 1341–1358.
- [Gunawardena and Van Graas, 2014] S. Gunawardena and F. Van Graas, *Analysis of GPS-SPS Inter-PRN Pseudorange Biases due to Receiver Front-End Components*, in Proceedings of ION GNSS+, Tampa, Florida, Sep. 2014.
- [Haines et al., 2012] B. Haines, W. Bertiger, N. Desai, A. Sibois and J. Weiss, *IGS Workshop - Characterizing the GPS Satellite Antenna Phase- and Group-Delay Variations (poster)*, Jul. 2012.
- [ICAO, 2006] ICAO, *ICAO Convention - Annex 10: Aeronautical Telecommunications - Volume 1: Radio Navigation Aids*, 2006.
- [Irsigler, 2008] M. Irsigler, *Multipath Propagation, Mitigation and Monitoring in the Light of Galileo and the Modernized GPS*, Ph.D Thesis, Universität der Bundeswehr München, Germany, 2008.
- [Julien, 2006] O. Julien, *Design of Galileo L1F receiver tracking loops*, Ph.D Thesis, University of Calgary, Canada, 2006.
- [Julien et al., 2006] O. Julien, C. Macabiau, L. Ries and J.-L. Issler, *1-Bit processing of composite BOC (CBOC) signals*, in Proceedings of CNES-ESA Workshop, Toulouse, France, Oct. 2006.
- [Julien et al., 2016] O. Julien, J.-B. Pagot and I. Selmi, *Report on the Assessment of critical hypothesis - Internal document*, Oct. 2016.
- [Julien et al., 2017] O. Julien, I. Selmi, J.-B. Pagot, J. Samson and F. Amarillo-Fernandez, *Extension of EWF Threat Model and Associated SQM*, in Proceedings of ION ITM, Monterey, California, Jan. 2017.
- [Kaplan and Hegarty, 2006] E.D. Kaplan and C.J. Hegarty, *Understanding GPS: principles and applications - Book*, 2006.
- [Laxton and DeVilbiss, 1997] M.C. Laxton and S.L. DeVilbiss, *GPS multipath mitigation during code tracking*, in Proceedings of American Control Conference/IEEE, Albuquerque, New Mexico, Jun. 1997, vol. 3, pp. 1429–1433.
- [Lestarquit et al., 2012] L. Lestarquit, Y. Gregoire and P. Thevenon, *Characterising the GNSS correlation function using a high gain antenna and long coherent integration - Application to signal quality*

## References

- monitoring*, in Proceedings of IEEE/ION PLANS, Myrtle Beach, South Carolina, Apr. 2012, pp. 877–885.
- [Liu et al., 2006] F. Liu, M. Brenner and C.Y. Tang, *Signal deformation monitoring scheme implemented in a prototype local area augmentation system ground installation*, in Proceedings of ION GNSS, Fort Worth, Texas, Sep. 2006, pp. 367–380.
- [Macabiau and Chatre, 2000] C. Macabiau and E. Chatre, *Signal quality monitoring for protection of GBAS users against evil waveforms*, in Proceedings of ION GPS, Salt Lake City, Utah, Sep. 2000, pp. 1202–1211.
- [Macabiau et al., 2003] C. Macabiau, L. Ries, F. Bastide and J.-L. Issler, *GPS L5 receiver implementation Issues*, in Proceedings of ION GPS/GNSS, Portland, Oregon, Sep. 2003, pp. 153–164.
- [Marquis and Shaw, 2011] W. Marquis and M. Shaw, *GPS III. Bringing New Capabilities to the Global Community*, published in Inside GNSS, Oct. 2011, pp. 34–48.
- [Martineau, 2008] A. Martineau, *Performance of Receiver Autonomous Integrity Monitoring (RAIM) for Vertically Guided Approaches*, Ph.D Thesis, University of Toulouse, France, 2008.
- [Mitelman, 2004] A.M. Mitelman, *Signal quality monitoring for GPS augmentation systems*, Ph.D Thesis, Stanford University, California, 2004.
- [Mitelman et al., 1999] A.M. Mitelman, J. Jung and P. Enge, *LAAS Monitoring For A Most Evil Satellite Failure*, in Proceedings of ION ITM, San Diego, California, Jan. 1999, pp. 129–134.
- [Montloin, 2014] L. Montloin, *GNSS Integrity Monitoring in the Presence of Singular Events*, Ph.D Thesis, University of Toulouse, France, 2014.
- [Murphy et al., 2007] T. Murphy, P. Geren and T. Pantaskie, *GPS Antenna Group Delay Variation Induced Errors in GNSS Based Precision Approach and Landing Systems*, in Proceedings of ION GNSS, Fort Worth, Texas, Sep. 2007, pp. 2974–2989.
- [Navipedia, 2015] Navipedia, *Navipedia website available at <http://www.navipedia.net/>*, 2015.
- [NovAtel Inc., 2012] NovAtel Inc., *WAAS Reference Receiver – Third generation (WAAS G-III) Summary of the linear transformation between vision SQM and chip shape*, Apr. 2012.
- [Oehler et al., 2006] V. Oehler, F. Luongo, H.L. Trautenberg, J.-P. Boyero, J. Krueger and T. Rang, *The galileo integrity concept and performance*, in Proceedings of ION GNSS, Fort Worth, Texas, Sep. 2006.
- [OHb System, 2012] OHb System, *Galileo System Key Features*. OHb website available at [https://www.ohb-system.de/tl\\_files/system/images/mediathek/downloads/pdf/120830\\_OHB\\_10604\\_Messe\\_Galileo\\_2012.pdf](https://www.ohb-system.de/tl_files/system/images/mediathek/downloads/pdf/120830_OHB_10604_Messe_Galileo_2012.pdf), 2012.
- [Pagot et al., 2016a] J.-B. Pagot, O. Julien, P. Thevenon, F. Amarillo-Fernández and M. Cabantous, *Signal Quality Monitoring Design for Galileo E5a and Galileo E1C signals*, in Proceedings of Navitec, Noordwijk, the Netherlands, Dec. 2016.



- [Pagot et al., 2016b] J.-B. Pagot, O. Julien, P. Thevenon, F. Amarillo-Fernández and D. Maillard, *Threat Model Design for new GNSS signals*, in Proceedings of ION ITM, Monterey, California, Jan. 2016, pp. 970–982.
- [Pagot et al., 2015] J.-B. Pagot, O. Julien, P. Thevenon, Y. Gregoire, F. Amarillo-Fernández and D. Maillard, *Estimation of GNSS Signals' Nominal Distortions from Correlation and Chip Domain*, in Proceedings of ION ITM, Dana Point, California, Jan. 2015, pp. 415–427.
- [Pagot et al., 2016c] J.-B. Pagot, O. Julien, P. Thevenon, F. Amarillo-Fernández and D. Maillard, *SQM for new GNSS signals*, in Proceedings of ION GNSS+, Portland, Oregon, Sep. 2016.
- [Parkinson and Spilker, 2006] B.W. Parkinson and J.J. Spilker, *GPS: Theory and Application - Book*, 2006.
- [Phelts et al., 2000] R.E. Phelts, D.M. Akos and P. Enge, *Robust signal quality monitoring and detection of evil waveforms*, in Proceedings of ION GPS, Salt Lake City, Utah, Sep. 2000, pp. 1180–1190.
- [Phelts et al., 2006] R.E. Phelts, D.M. Akos and others, *Effects of signal deformations on modernized GNSS signals*, published in Global Positioning Systems, 2006, vol. 5, pp. 2–10.
- [Phelts et al., 2015] R.E. Phelts, E. Altshuler, T. Walter and P. Enge, *Validating Nominal Bias Error Limits Using 4 years of WAAS Signal Quality Monitoring Data*, in Proceedings of ION PNT, Honolulu, Hawaii, Apr. 2015, pp. 956–963.
- [Phelts et al., 2001] R.E. Phelts, A.M. Mitelman, S. Pullen, D.M. Akos and P. Enge, *Transient performance analysis of a multicorrelator signal quality monitor*, in Proceedings of ION GPS, Salt Lake City, Utah, Sep. 2001, pp. 1700–1710.
- [Phelts and Walter, 2003] R.E. Phelts and T. Walter, *Practical Signal Quality Monitoring for Augmentation Systems*, in Proceedings of the International Symposium of GNSS, Tokyo, Japan, Nov. 2003.
- [Phelts et al., 2003] R.E. Phelts, T. Walter and P. Enge, *Toward real-time SQM for WAAS: improved detection techniques*, in Proceedings of ION GNSS+, Portland, Oregon, Sep. 2003, pp. 2739–2749.
- [Phelts et al., 2009] R.E. Phelts, T. Walter and P. Enge, *Characterizing nominal analog signal deformation on GNSS signals*, in Proceedings of ION GNSS, Savannah, Georgia, Sep. 2009, pp. 1343–1350.
- [Phelts et al., 2013] R.E. Phelts, T. Walter, P. Enge and G. Wong, *Signal Deformation Monitoring for Dual-Frequency WAAS*, in Proceedings of ION ITM, San Diego, California, Jan. 2013, pp. 93–106.
- [Phelts et al., 2014] R.E. Phelts, G. Wong, T. Walter and P. Enge, *IWG 26 - Signal Deformation Proposal - Presentation*, Feb. 2014.
- [Phelts, 2001] R.E. Phelts, *Multicorrelator techniques for robust mitigation of threats to GPS signal quality*, Ph.D Thesis, Stanford University, California, 2001.
- [Pini and Akos, 2007] M. Pini and D.M. Akos, *Exploiting GNSS signal structure to enhance observability*, published in IEEE Transactions on Aerospace and Electronic Systems, Oct. 2007, vol. 43, pp. 1553–1566.

## References

- [Pullen, 2009] S. Pullen, *Providing Integrity for Satellite Navigation: Lessons Learned (Thus Far) from the Financial Collapse of 2008-2009*, in Proceedings of ION GNSS, Savannah, Georgia, Sep. 2009, pp. 1305–1316.
- [Pullen, 2011] S. Pullen, *Augmented GNSS: Fundamentals and Keys to Integrity and Continuity*, ION GNSS 2011 Tutorial - Presentation, Sep. 2011.
- [Rajan and Irvine, 2005] J. Rajan and J. Irvine, *GPS IIR-M and IIF: Payload Modernization*, in Proceedings of ION NTM, San Diego, California, Jan. 2005, pp. 508–514.
- [Rebeyrol, 2007] E. Rebeyrol, *Optimisation des signaux et de la charge utile Galileo*, Ph.D Thesis, Télécom ParisTech, France, 2007.
- [Ries and Perello Gisbert, 2006] L. Ries and J.V. Perello Gisbert, *Bitgrabber 2 - Operating Manual*, Oct. 2006.
- [Rife and Phelts, 2008] J. Rife and R.E. Phelts, *Formulation of a time-varying maximum allowable error for Ground-Based Augmentation Systems*, published in IEEE Transactions on Aerospace and Electronic Systems, Apr. 2008, vol. 44, pp. 548–560.
- [Rohde and Schwarz, 2014] Rohde and Schwarz, *R&S FSQ, Signal Analyzer, Operating Manual*, 2014.
- [Roturier et al., 2001] B. Roturier, E. Chatre and J. Ventura-Traveset, *The SBAS integrity concept standardised by ICAO-application to EGNOS*, in Proceedings of European Navigation Conference GNSS, Seville, Spain, 2001, vol. 49, pp. 65–77.
- [RTCA, 2004] RTCA, *DO 245A - Minimum Aviation System Performance Standards for the LAAS*, Dec. 2004.
- [RTCA, 2006] RTCA, *DO 229D - MOPS for GPS/WAAS Airborne Equipment*, Dec. 2006.
- [RTCA, 2008] RTCA, *DO 253C - MOPS for GPS Local Area Augmentation System Airborne Equipment*, Dec. 2008.
- [RTCA, 2009] RTCA, *DO 316 - MOPS for GPS/ABAS Airborne Equipment*, Apr. 2009.
- [Salos, 2012] D. Salos, *Integrity monitoring applied to the reception of GNSS signals in urban environments*, Ph.D Thesis, University of Toulouse, France, 2012.
- [Samson, 2015] J. Samson, *Assumption on the DFMC SBAS MOPS - draft*, Oct. 2015.
- [SBAS IWG, 2014] SBAS IWG, *SBAS Interoperability Working Group, Global SBAS Status - Presentation*, Jun. 2014.
- [Sekar et al., 2012] S.B. Sekar, S. Sengupta and K. Bandyopadhyay, *Analysis of secondary short codes for satellite navigation*, in Proceedings of IEEE National Conference on Communications, Apr. 2012.
- [Shivaramaiah and Dempster, 2009] N.C. Shivaramaiah and A.G. Dempster, *The Galileo E5 AltBOC: understanding the signal structure*, in Proceedings of the International Symposium of GNSS, Gold Coast, Australia, Dec. 2009.

- [Shively, 1999] C. Shively, *Derivation of Acceptable Error Limits For Satellite Signal Faults in LAAS*, in Proceedings of ION GPS, Nashville, Tennessee, Sep. 1999, pp. 761–770.
- [Shloss et al., 2002] P. Shloss, R.E. Phelts, T. Walter and P. Enge, *A Simple Method of Signal Quality Monitoring for WAAS LNAV/VNAV*, in Proceedings of ION GPS, Portland, Oregon, Sep. 2002, pp. 800–808.
- [Sleewaegen and Boon, 2001] J.-M. Sleewaegen and F. Boon, *Mitigating short-delay multipath: a promising new technique*, in Proceedings of ION GPS, Salt Lake City, Utah, Sep. 2001, pp. 204–213.
- [Smitham, 2014] M. Smitham, *Global Positioning Systems Directorate - GPS Program Update to ION GNSS+ 2014 - Presentation*, in Proceedings of , Tampa, Florida, Sep. 2014.
- [Springer and Dilssner, 2009] K. Springer and F. Dilssner, *SVN 49 and Other GPS Anomalies*, published in Inside GNSS, Aug. 2009, pp. 32–36.
- [SSF, 2008] SSF, *Skybridge Spectrum Foundation, Federal Radionavigation Plan*, 2008.
- [Suard, 2010] N. Suard, *PRN1/SVN049 L5 payload drawback and PRN27 outage on the 30th of June 2009: GNSS receiver reactions and lessons learnt*, in Proceedings of ION GNSS, Portland, Oregon, Sep. 2010, pp. 1975–1983.
- [Thevenon et al., 2014] P. Thevenon, J.-B. Pagot, O. Julien and Q. Tessier, *Processing Technique and Performance of the Observation of Evil Waveform in the Chip Domain*, in Proceedings of Navitec, Noordwijk, the Netherlands, Dec. 2014.
- [Thoelert et al., 2009] S. Thoelert, S. Erker and M. Meurer, *GNSS Signal Verification with a High Gain Antenna – Calibration Strategies and High Quality Signal Assessment*, in Proceedings of ION ITM, Anaheim, California, Jan. 2009, pp. 289–300.
- [Thoelert et al., 2014] S. Thoelert, M. Vergara, M. Sgammini, C. Enneking, F. Antreich, M. Meurer, D. Brocard and C. Rodriguez, *Characterization of Nominal Signal Distortions and Impact on Receiver Performance for GPS (IIF) L5 and Galileo (IOV) E1/E5a Signals*, in Proceedings of ION GNSS+, Tampa, Florida, Sep. 2014, vol. 3113–3128.
- [Townsend et al., 2000] B. Townsend, J. Wiebe and A. Jakab, *Results and analysis of using the MEDLL receiver as a multipath meter*, in Proceedings of ION NTM, Anaheim, California, Jan. 2000, pp. 73–79.
- [Vezinet, 2014] J. Vezinet, *Study of Future On-board GNSS/INS Hybridization Architectures*, Ph.D Thesis, University of Toulouse, France, 2014.
- [Walter et al., 2012] T. Walter, P. Enge and B. DeCleene, *GNSS: Report of a Joint Workshop of the National Academy of Engineering and the Chinese Academy of Engineering - Chapter: Integrity Lessons from the WAAS Integrity Performance Panel - Book*, 2012.
- [Westbrook et al., 2000] J. Westbrook, A. Rérolle, H. Blomenhofer, I. McAnany, J. Cosmen, W. Wemer and others, *An Introduction to the EGNOS Central Processing Facility (CPF)*, in Proceedings of the IAIN World Congress and the 56th Annual Meeting of The ION, San Diego, California, Jun. 2000, pp. 6–13.

## References

- [Wong, 2014] G. Wong, *Impact of Nominal Signal Deformations on Satellite Navigation Systems*, Ph.D Thesis, Stanford University, California, 2014.
- [Wong et al., 2010] G. Wong, R.E. Phelts, T. Walter and P. Enge, *Characterization of signal deformations for GPS and WAAS satellites*, in Proceedings of ION GNSS, San Diego, California, Sep. 2010, pp. 3143–3151.
- [Wong et al., 2011] G. Wong, R.E. Phelts, T. Walter and P. Enge, *Alternative characterization of analog signal deformation for GNSS-GPS satellites*, in Proceedings of ION ITM, San Diego, California, Jan. 2011, pp. 497–507.

# Appendix A. Correlator outputs and CDO standard deviations

This appendix aims at describing the model that is used in the Ph.D. to estimate the standard deviation and the covariance of correlator outputs and the standard deviation of bin values at the origin of the CDO.

This appendix is divided in two sections. Firstly, a theoretical derivation of standard deviations is presented. Secondly, theoretical values are compared with results obtained by simulations.

The second part of the appendix has two purposes:

- validate theoretical CDO and correlator outputs standard deviations with simulations,
- validate the signal processing that is used to observe nominal distortions on the CDO and on the correlation function.

## A.1 Theoretical derivation of standard deviations

In the first section of the appendix, a correlator output model is derived in order to find the expression of the standard deviation and the covariance that affect correlator outputs. Then, the same concept is applied to the chip domain to derive the bins standard deviation.

### A.1.1 Correlation function observable

From equation (3-34), the correlator output can be modeled as:

$$I = \sqrt{\frac{P}{2}} R_s(\varepsilon_\tau) D \frac{\sin(\pi \varepsilon_f T_{int})}{\pi \varepsilon_f T_{int}} \cos(\varepsilon_\phi) + n_I(\varepsilon_\tau) \quad (A-1)$$

where

- $R_s$  is the correlation function of the local replica and the filtered received signal code,
- $\varepsilon_\tau$  is the group delay error in second,
- $\varepsilon_\phi$  is the carrier phase delay error in radian,
- $\varepsilon_f$  is the carrier phase Doppler error in hertz,
- $D$  is the sign of the data bit,
- $n_I$  is the noise on the in-phase component.

The expression of  $R_s$  is given using the Wiener Lee relation:

$$R_s(\tau) = \int_{-\infty}^{+\infty} H_{RF}(f) S(f) S_{local}^*(f) e^{2i\pi f \tau} df = FT^{-1}[H_{RF}(f) S(f) S_{local}^*(f)] \quad (A-2)$$

where

- $S(f)$  is the Fourier transform of the received signal,
- $S_{local}(t)$  is the Fourier transform of the local replica signal,
- $H_{RF}(f)$  is the RF filter transfer function (assuming to be equal to the pre-correlation filter),
- $FT^{-1}$  is the inverse Fourier transform.

It is now assumed that  $\varepsilon_f$  and  $\varepsilon_\phi$  are negligible. In this condition, the correlator output can be modeled as:

$$I = \sqrt{\frac{P}{2}} DR_s(\varepsilon_\tau) + n_I(\varepsilon_\tau) \quad (A-3)$$

It is noticeable from this relation that this formula can be applied for different group delay errors ( $\varepsilon_\tau$ ). By consequence, correlator outputs can be estimated for different group delay errors. In the following, the group delay error is called  $x$  instead of  $\varepsilon_\tau$  and is expressed in chip unit. An index  $x$  is put on  $I$  to give the expression of  $I$  for a receiver tracking the signal with a group delay error equal to  $x$ . Moreover, considering that the data bit is evaluated and corrected,  $D$  can be removed from the expression. The model becomes:

$$I_x = \sqrt{\frac{P}{2}} R_s(x) + n_{I_x} \quad (A-4)$$

In [Julien, 2006], a model for the noise correlation function at correlator output was proposed:

$$\begin{aligned} R_{n_I}(\tau) &= \frac{N_0}{4T_{int}} \int_{-\infty}^{+\infty} |H_{RF}(f)|^2 S_{local}(f) S_{local}^*(f) e^{2i\pi f \tau} df \\ &= \frac{N_0}{4T_{int}} FT^{-1}[|H_{RF}(f)|^2 S(f) S_{local}^*(f)] \end{aligned} \quad (A-5)$$

where

- $N_0 = k_b T_{sys}$  is the noise Gaussian density when the noise is considered white and Gaussian in decibel/watt/hertz,
- $k_b$  is the Boltzmann constant equal to  $-228.6$  dBW/K/Hz,
- $T_{sys}$  is the system noise temperature in degree on the Kelvin scale,
- $T_{int}$  is the coherent integration time in second.

To simplified notations used in equation (A-5), the correlation function  $R_N$  is introduced and is linked to  $R_{n_I}$  by:

$$R_{n_I}(\tau) = \frac{N_0}{4T_{int}} R_N(\tau) \quad (A-6)$$

The standard deviation of the correlator output value is then given by:

$$\sigma(n_I) = \sqrt{\frac{P_{n_I}}{P_s}} = \sqrt{\frac{R_{n_I}(0)}{I^2}} = \sqrt{\frac{2R_{n_I}(0)}{P \times R_s^2(0)}} \quad (A-7)$$

The carrier to noise density is finally introduced. Using  $C'/N_0 = 10^{\frac{C/N_0}{10}}$  in hertz with  $C/N_0$  given in decibel-hertz, the correlator output standard deviation expression becomes:

$$\sigma(n_I) = \sqrt{\frac{1}{2 C' / N_0 \times T_{int}} \times \frac{R_N(0)}{R_S^2(0)}} \quad (A-8)$$

The same concept can be applied for different group delay errors. It leads to:

$$\sigma(n_{I_x}) = \sqrt{\frac{R_{n_I}(0)}{I_x^2}} = \sqrt{\frac{1}{2 C' / N_0 \times T_{int}} \times \frac{R_N(0)}{R_S^2(x)}} \quad (A-9)$$

An important remark is that  $\sigma(n_x)$  are given for equivalent correlator outputs amplitude equal to one. The average of the correlator outputs at a delay  $x$  from the prompt is noted  $\mu_x$ .

$$\sigma(n_{I_x}) = \sqrt{\frac{\mu_x = 1}{2 C' / N_0 T_{int}} \times \frac{R_N(0)}{R_S^2(x)}} \quad (A-10)$$

This model is equivalent to the model presented in [Sleewaegen and Boon, 2001]. The only difference is that in this appendix, there is no approximation on noise and tracked correlation functions. It is also possible to choose another normalization to better visualize these results on a correlation function. In this second normalization an index 1 is added to parameters, which gives:

$$\begin{aligned} \mu_{1I_x} &= R_S(x) \sqrt{2 C' / N_0 T_{int}} \\ \sigma_1(n_{I_x}) &= \sqrt{R_N(0)} \end{aligned} \quad (A-11)$$

In order to estimate different metrics standard deviations using formula presented in appendix B,  $cov(n_{I_x}, n_{I_y})$  as to be estimated. This covariance can directly be obtained from the noise correlation function.

$$\begin{aligned} cov(n_{I_x}, n_{I_y}) &= E[n_{I_x} n_{I_y}] - E[n_{I_x}] E[n_{I_y}] = E[n_{I_x} n_{I_y}] = \frac{R_{n_I}(x - y)}{I_x I_y} = \frac{\frac{N_0}{4 T_{int}} R_N(x - y)}{I_x I_y} \\ &= \frac{1}{2 C' / N_0 \times T_{int}} \times \frac{R_N(x - y)}{R_S(x) R_S(y)} \end{aligned}$$

The following equation can be written:

$$cov(n_{I_x}, n_{I_y}) = \frac{1}{2 C' / N_0 \times T_{int}} \times \frac{R_N(x - y)}{R_S(x) R_S(y)} \quad (A-12)$$

To conclude, all parameters necessary to evaluate theoretical standard deviations for different metrics can be modeled as:

$$\begin{aligned} \mu_{1I_x} &= R_S(x) \sqrt{2 C' / N_0 T_{int}} \\ \sigma_1(n_{I_x}) &= \sqrt{R_N(0)} \\ cov_1(n_{I_x}, n_{I_y}) &= R_N(x - y) \end{aligned}$$

### A.1.2 Chip Domain Observable

After deriving the standard deviation of correlator outputs and the covariance between two correlator outputs, the standard deviation in the chip domain is estimated theoretically.

The GNSS signal  $s(t)$  passes through the analog section of the receiver before being processed to estimate the CDO (see 3.2). Without considering the sampling process to simplify notations, the resulting signal, filtered by the antenna and the RF front-end is noted  $\tilde{s}(t)$ . During this operation the noise is also filtered. If the noise is considered as white and Gaussian, and if the filter is assumed as an ideal brick wall with a double-sided bandwidth  $BW$  in hertz, the noise power ( $P_n$ ) on the filtered in-phase channel can be modeled as:

$$P_n = \int_{-\frac{BW}{2}}^{\frac{BW}{2}} \frac{N_0}{2} df = \frac{N_0 BW}{2} \quad (A-13)$$

The chip domain observable is directly estimated from the filtered signal  $\tilde{s}(t)$ . In one bin is the average of  $N_{CDO}$  samples defined in equation (4-4). Consequently, the power in one bin can be assessed by:

$$P_{bin} = P N_{CDO} \quad (A-14)$$

with

$$N_{CDO} = F_s \Delta_{bin} \frac{T_{obs}}{T_{code}} N_{observed\_part\_code}$$

- $F_s$  the sampling frequency in hertz,
- $T_{obs}$  the observation time in second,
- $T_{code}$  the code period in second,
- $N_{observed\_part\_code}$  is the number of the wanted observed sections per code period,
- $\Delta_{bin}$  is the size of the bin in second,
- $P$  is the power of the received signal in watt.

Assuming that the amplitude in bins is equal to one, it is possible to estimate theoretical noise standard deviation in a bin by:

$$\sigma(n_{CDO}) = \sqrt{\frac{P_n}{P_{bin}}} = \sqrt{\frac{N_0 BW}{2 P N_{CDO}}} = \sqrt{\frac{BW/F_s}{2 C'/N_0 \Delta_{bin} T_{obs} N_{observed\_part\_code}}} \quad (A-15)$$

with  $C'/N_0 = 10^{\frac{C/N_0}{10}}$  the carrier to noise density in decibel-hertz.

One important remark is that if no filter is considered at the RF front-end the expression of the standard deviation of the noise is still valid with  $BW = F_s$ .



## A.2 CDO and correlator outputs standard deviations estimated from simulations

In simulation, the CDO and the correlation function observables are derived in several steps:

- A signal is generated by the program with a sampling frequency  $F_s$ . A noise is added to the signal with a given  $C/N_0$ . The signal can also be filtered at the end of this step.
- The signal is processed by the GNSS receiver software, as described in 5.1.2. The acquisition is followed by the tracking. CDO and correlator outputs are estimated every  $T_{obs}$  s on  $T_{tot}$  s.  $T_{obs}$  corresponds to the time during which samples are accumulated in bins to estimate the CDO. It also corresponds to the time during which samples are convolved with the local replica to estimate correlator outputs. The integration time ( $T_{int} = 1$  s) used for the tracking, may be different from the observation time  $T_{obs}$ . The CDO is estimated on  $N_{bin}$  bins and correlation observable on  $N_{corr\_out}$  correlator outputs. After a period of time  $T_{tot}$ ,  $N$  draws of each bin and correlator output are saved with  $N = T_{tot}/T_{obs}$ .
- Then CDO and correlator outputs are post-processed. The standard deviation is estimated from the  $N$  saved draws of the  $N_{bin}$  bins and the  $N_{corr\_out}$  correlator outputs.

Results presented in this appendix are obtained using parameters presented in Table A-1. Six different cases are tested.

	Case 1	Case 2	Case 3	Case 4	Case 5	Case 6
$C/N_0$	60 dB-Hz					
$T_{obs}$	20 ms					
$T_{tot}$	4 s					
$N$	200					
$N_{bin}$	/	1000	100	/	1000	100
$N_{corr\_out}$	801	/	/	801	/	/
$F_s$	12 MHz			40 MHz		
Filter	No filter			Brick wall filter (15 MHz bandwidth)		

**Table A-1.** Description of the different tested cases.

On Figure A-1 is plotted correlation function results averaged on  $T_{tot}$  in the case 1. It means that  $N = 200$  epochs are averaged together. On the top, eight hundred and one averaged correlator outputs are shown and the standard deviation is estimated, on the bottom, for the eight hundred and one correlator outputs.

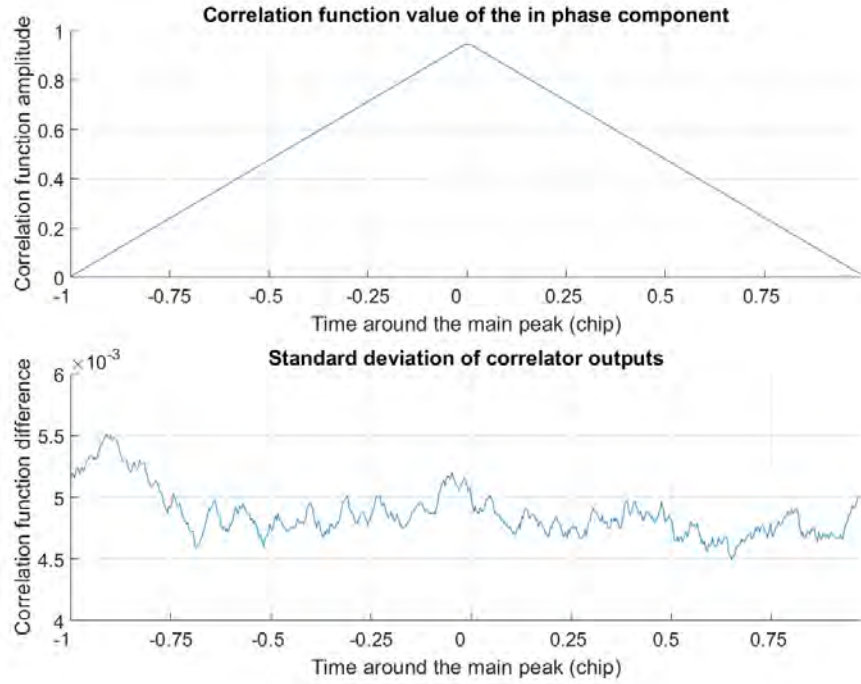


**Figure A-1.** Correlator outputs and associated standard deviation in case 1.

On Figure A-2 is plotted the chip domain results averaged on  $T_{tot}$  in the case 2. It means that  $N = 200$  epochs are averaged together. On the top, one thousand averaged bins values are shown and the standard deviation is estimated, on the bottom, for the one thousand bins. Only rising transitions are averaged.

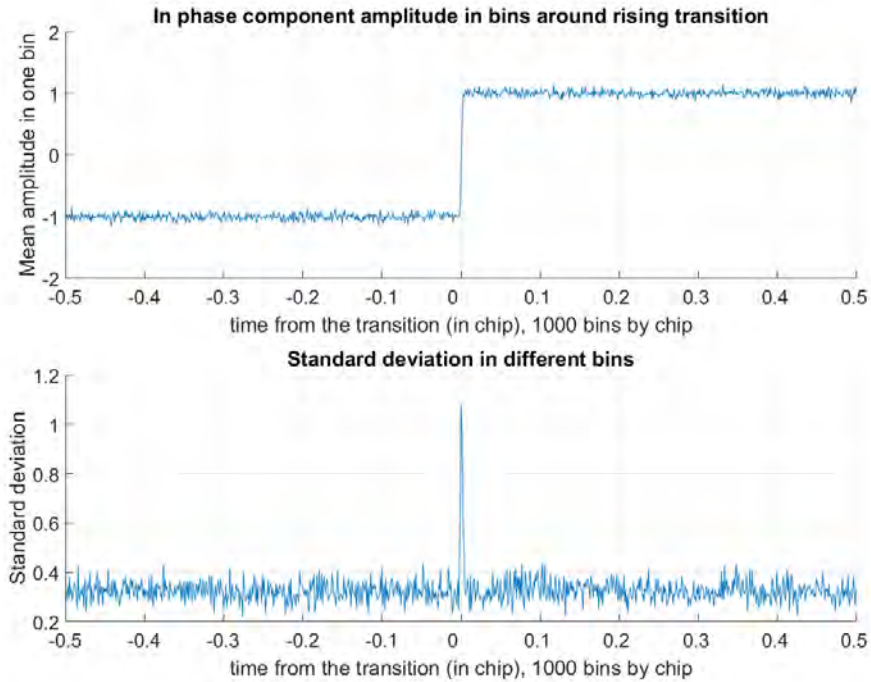


**Figure A-2.** Bins value and associated standard deviation in case 2.

On Figure A-3 is plotted the chip domain results averaged on  $T_{tot}$  in the case 3. It means that  $N = 200$  epochs are averaged together. On the top, one hundred averaged bins values are shown and the

standard deviation is estimated, on the bottom, for the one hundred bins. Only rising transitions are averaged.

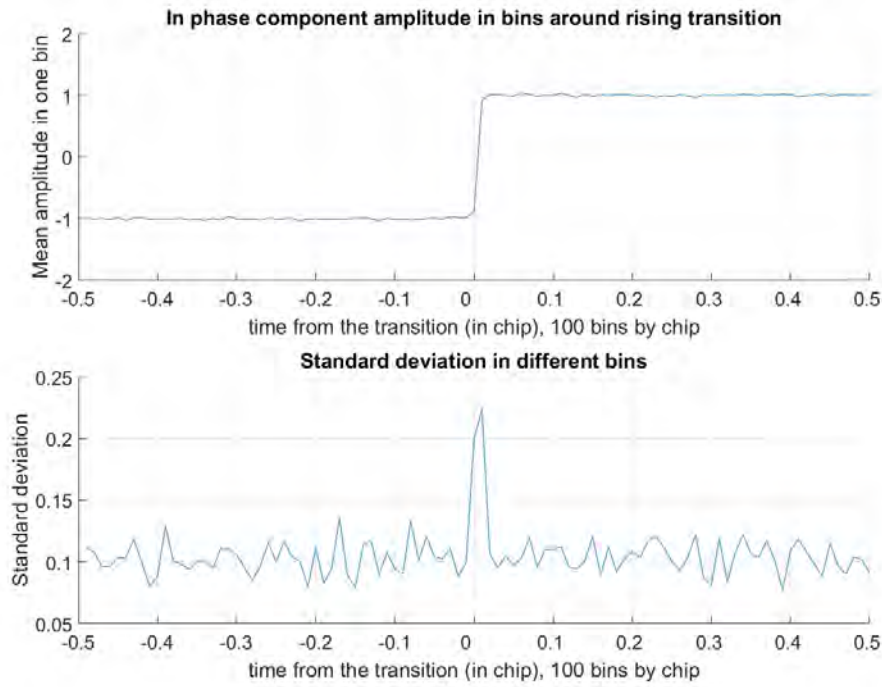


**Figure A-3.** Bins value and associated standard deviation in case 3.

To have a better estimation of the standard deviation of correlator outputs and bins, the standard deviation is averaged among the different correlator outputs and the different bins. It means that  $N_{corr\_out}$  correlator outputs standard deviations are averaged and  $N_{bin}$  bins standard deviations are averaged.

Results provided in Table A-2 validate theoretical formulas of standard deviations (on the correlation function and the chip domain) as well as the Matlab® program. Indeed, Table A-2 proposes a comparison between theoretical standard deviation values and standard deviation obtained by simulation for the six different cases.

	Theory	Simulation
Case 1 $\sigma_{corr}$	$5.0 \times 10^{-3}$	$4.9 \times 10^{-3}$
Case 2 $\sigma_{cdo}$	$3.1 \times 10^{-1}$	$3.3 \times 10^{-1}$
Case 3 $\sigma_{cdo}$	$9.9 \times 10^{-2}$	$1.0 \times 10^{-1}$
Case 4 $\sigma_{corr}$	$5.0 \times 10^{-3}$	$5.4 \times 10^{-3}$
Case 5 $\sigma_{cdo}$	$1.9 \times 10^{-1}$	$1.9 \times 10^{-1}$
Case 6 $\sigma_{cdo}$	$6.1 \times 10^{-2}$	$6.6 \times 10^{-2}$

**Table A-2.** Description of the different tested cases.

Even if the Table A-2 corresponds to particular random draws and particular cases, it is noticeable that values obtained by simulations are consistent with theoretical values whether filtering is applied or not.

These results are of primary importance for two reasons:

- it validates theoretical standard deviation formulas derived in the previous section of this appendix,
- it validates the Matlab® program which tracks the signal and estimates the CDO and correlation function observables.

## Appendix B. Theoretical and simulated metrics standard deviations

The first section of this appendix aims at providing theoretical formulas of several metrics standard deviations. Three metrics are considered: the simple, the difference and the sum ratio metrics normalized by the prompt. The second section compares theoretical metrics standard deviations to standard deviations estimated by simulation.

### B.1 Theoretical derivation of some metrics standard deviations

In this section, standard deviations of different metrics are expressed theoretically. Taking back results from [Brocard et al., 2014], the formulas of the standard deviations of simple ratio, difference ratio and sum ratio metrics normalized by the prompt are remained.

In [Brocard et al., 2014] the standard deviation was estimated for two metrics, the simple ratio metric  $metric_x = (I_x/I_z)$  and the differential ratio metric  $metric_{x-y} = ((I_x - I_y)/I_z)$ . These theoretical standard deviations are valid for long integration time ( $T_{int} \geq 1$  s). Mathematical approximations of the two metrics standard deviations are recalled:

$$\sigma\left(\frac{I_x}{I_z}\right) = \sqrt{\frac{\mu_x^2}{\mu_z^2} \left[ \frac{\sigma^2(n_x)}{\mu_x^2} + \frac{\sigma^2(n_z)}{\mu_z^2} - 2 \frac{cov(n_x n_z)}{\mu_z \mu_x} \right]} \quad (B-1)$$

$$\sigma\left(\frac{I_x - I_y}{I_z}\right) = \sqrt{\frac{(\mu_x - \mu_y)^2}{\mu_z^2} \left[ \frac{\sigma^2(n_z)}{\mu_z^2} + \frac{\sigma^2(n_x) + \sigma^2(n_y) - 2cov(n_y n_x)}{(\mu_x - \mu_y)^2} - 2 \frac{cov(n_x n_z) - cov(n_y n_z)}{\mu_z (\mu_x - \mu_y)} \right]} \quad (B-2)$$

It can also be demonstrated in the same way that the standard deviations of sum ratio metrics  $metric_{x+y} = ((I_x + I_y)/I_z)$  can be modeled as:

$$\sigma\left(\frac{I_x + I_y}{I_z}\right) = \sqrt{\frac{(\mu_x + \mu_y)^2}{\mu_z^2} \left[ \frac{\sigma^2(n_z)}{\mu_z^2} + \frac{\sigma^2(n_x) + \sigma^2(n_y) + 2cov(n_y n_x)}{(\mu_x + \mu_y)^2} - 2 \frac{cov(n_x n_z) + cov(n_y n_z)}{\mu_z (\mu_x + \mu_y)} \right]} \quad (B-3)$$

## B.2 Theoretical VS simulated $\sigma_{metric}$

In Figure B-1, Figure B-2 and Figure B-3 are given theoretical (in continuous plot) and simulated (in dotted plot) metrics standard deviations for  $metric_{x-x}$  (in blue),  $metric_{x+x}$  (in purple) and  $metric_x$  (in blue for  $x$  negative and in purple for  $x$  positive). Figure B-1 presents standard deviations for a GPS L1 C/A signal ( $BPSK(1)$  modulation). Figure B-2 corresponds to results for a Galileo E1C signal (the received signal is  $CBOC(6,1,1/11, -)$ -modulated and the local replica is  $BOC(1,1)$ -modulated). Figure B-3 gives standard deviations for a Galileo E5a signal ( $BPSK(10)$  modulation).

Plots were obtained for a  $C/N_0 = 30$  dB-Hz and a 1 s integration time (no smoothing). The sampling frequency is equal to 112 MHz for GPS L1 C/A and Galileo E1C signals, and 400 MHz for Galileo E5a signal. All signals are filtered by a 6<sup>th</sup>-order Butterworth filter with a 24 MHz double-sided bandwidth.

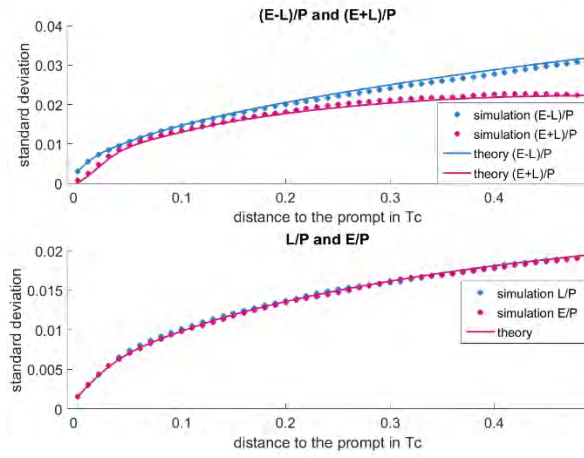


**Figure B-1.** Theoretical (continuous line) and simulated (dotted line) metrics standard deviations on  $BPSK(1)$  signal.

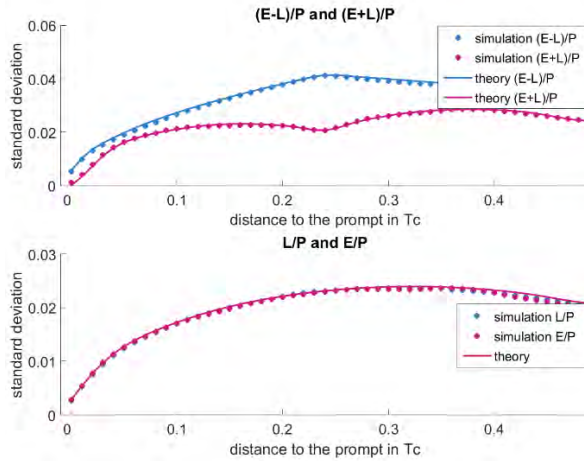


**Figure B-2.** Theoretical (continuous line) and simulated (dotted line) metrics standard deviations on  $CBOC(6,1,1/11)$  signal.

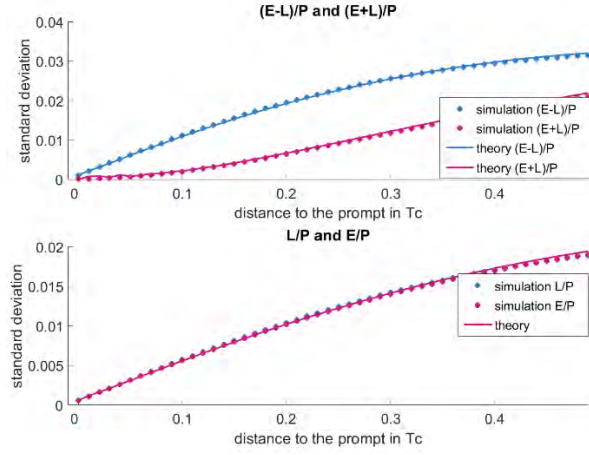


**Figure B-3.** Theoretical (continuous line) and simulated (dotted line) metrics standard deviations on BPSK(10) signal.

Figure B-1, Figure B-2 and Figure B-3 show that theoretical metrics standard deviations match with simulations.

To conclude, it can be deduced that different SQMs can be tested by simulations applying theoretical formulas established in this appendix to estimate  $\sigma_{metric}$ . Results given by this approach are valid:

- assuming that the noise on correlator outputs has a Gaussian distribution [Irsigler, 2008],
- for high enough integration time ( $T_{int} > 1$  s). In this condition,  $\sigma_{metric}$  can be estimated theoretically according to formulas given in this appendix and in appendix A. [Brocard et al., 2014] [Julien, 2006]





## Appendix C. List of signals collected from high-gain dish antennas

This appendix presents the different signals that were collected with high-gain dish antennas to assess the impact of nominal distortions. The day and the hour of data collections are provided.

Data were collected at Leeheim by the DLR with an antenna owned by the German administration. Data were collected at Toulouse by CNES with an antenna owned by CNES. Data were collected at Noordwijk by ENAC with an antenna owned by ESA. Details about different data collections are given in 5.1.1. Data were collected during time periods varying from 10 s to 10 min.

In Table C-1 are presented GPS L1 C/A collected signals whereas in Table C-2 are presented Galileo E1C collected signals. Data collected by CNES are highlighted in blue.

PRN	Block	Antenna	Data collection date (mm/dd/yy)	Time at the beginning of data collection (hour:min)
1	GPS BII-F	Leeheim	03/14/2012	08:34
2	GPS BII-R	Toulouse	05/13/2014	09:17
4	GPS BII-A	Leeheim	03/14/2012	11:14
5	GPS BII-RM	Leeheim	03/13/2012	15:31
7	GPS BII-RM	Leeheim	03/13/2012	15:15
12	GPS BII-RM	Toulouse	07/16/2014	11:26
13	GPS BII-R	Leeheim	03/14/2012	14:11
13	GPS BII-R	Toulouse	04/18/2014	09:57
17	GPS BII-RM	Leeheim	03/14/2012	09:54
17	GPS BII-RM	Toulouse	07/16/2014	11:02
23	GPS BII-R	Leeheim	03/14/2012	10:13
23	GPS BII-R	Toulouse	05/13/2014	08:40
24	GPS BII-F	Toulouse	07/18/2014	11:14
25	GPS BII-F	Toulouse	07/18/2014	11:19
26	GPS BII-A	Toulouse	05/13/2014	11:33
29	GPS BII-RM	Toulouse	07/17/2014	17:15
32	GPS BII-A	Leeheim	03/14/2012	08:38

**Table C-1.** Information about GPS L1 C/A data collections. In blue are highlighted signals collected by CNES.

PRN	block	antenna	Data collection date ( <i>mm/dd/yy</i> )	Time at the beginning of data collection ( <i>hour:min</i> )
14	Galileo-FOC FM-2	Noordwijk	09/29/2015	14:47
18	Galileo-FOC FM-1	Noordwijk	Mars 2015	/
22	Galileo-FOC FM-4	Noordwijk	09/29/2015	10:51

**Table C-2.** *Information about Galileo E1C data collections.*

## Appendix D. Nominal distortion parameters

In this appendix, nominal distortions observed on GPS L1 C/A collected signals are characterized from the four parameters defined in 4.1.1.3.2. For each parameter, definition and associated overbound value obtained in [Phelts et al., 2009] by high resolution measurements are given in brackets.

- *Rise time/Fall time* (25 ns): It is the time it takes for the rising (falling) edge of the signal to increase from the preceding zero-crossing to the ideal amplitude.
- *Peak time* (45 ns): It is the time it takes for the rising edge of the signal to increase from the preceding zero-crossing to the first peak value.
- *Settling time* (180 ns (at 10 % convergence)): It is the time measured from the zero-crossing preceding a positive (or negative) chip to when the signal response first enters and then remains within a band whose width is computed as a percentage of amplitude for the remaining duration of the chip width.
- *Peak overshoot ratio* (35 %): It is the difference of the amplitude of the first peak and the ideal amplitude, divided by the ideal amplitude.

In Table D-1 results obtained from rising transitions are provided, whereas in Table D-2 results obtained from falling transitions are exposed. In blue are highlighted results obtained from CNES measurements.

PRN	Rise time (ns)	Overshoot ratio (%)	Peak time (ns)	Settling time (ns)
1 (L)	15	30	31	60
2 (T)	14	30	30	42
4 (L)	12	32	28	59
5 (L)	13	36	28	65
7 (L)	13	37	28	64
12 (T)	13	32	29	44
13 (L)	11	33	27	64
13 (T)	12	32	29	43
17 (L)	12	34	28	64
17 (T)	14	39	29	85
23 (L)	13	31	28	66
23 (T)	12	27	29	60
24 (T)	16	36	33	45
25 (T)	15	34	32	53
26 (T)	13	32	30	44
29 (T)	13	36	28	43
32 (L)	12	32	28	61

**Table D-1.** Information about GPS L1 C/A data collections. In blue are highlighted results obtained from CNES measurements.

PRN	Fall time (ns)	Overshoot ratio (%)	Peak time (ns)	Settling time (ns)
1 (L)	14	27	30	59
2 (T)	13	30	30	43
4 (L)	12	33	28	63
5 (L)	12	36	27	62
7 (L)	10	37	25	63
12 (T)	11	33	27	44
13 (L)	10	34	26	64
13 (T)	12	32	28	42
17 (L)	11	35	26	61
17 (T)	13	37	29	43
23 (L)	10	31	26	66
23 (T)	11	28	28	41
24 (T)	13	32	30	46
25 (T)	12	32	29	43
26 (T)	13	33	29	44
29 (T)	13	36	28	61
32 (L)	13	34	28	60

**Table D-2.** Information about GPS L1 C/A data collections. In blue are highlighted results obtained from CNES measurements.

## Appendix E. Features of tested filters

To take into account the diversity of filters that can be implemented on civil aviation users, four filters are used in this Ph.D.:

- Filter1: 6<sup>th</sup>-order Butterworth.
- Filter2: resonator filter type with a constant group delay equal to zero.
- Filter3: resonator filter type with a concave group delay and a 150 ns differential group delay.
- Filter4: 6<sup>th</sup>-order Butterworth for the amplitude and the smallest order Butterworth filter leading to a differential group delay higher than 150 ns for the phase.

This appendix illustrates the amplitude, the phase and the differential group delay of each filter considering a 24 MHz bandwidth (double-sided).

On Figure E-1 are presented characteristics of Filter1: 6<sup>th</sup>-order Butterworth (24 MHz double-sided).

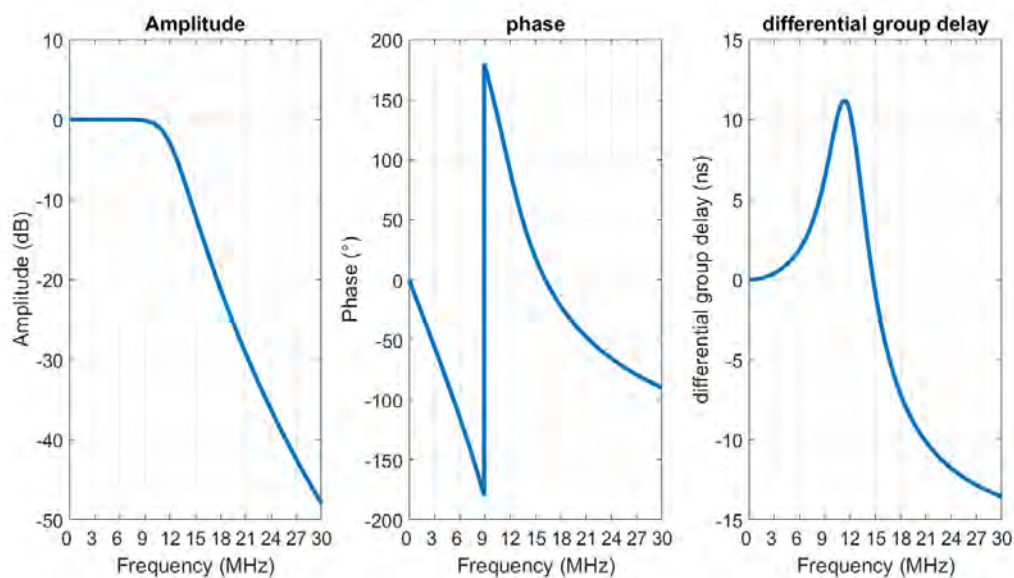


**Figure E-1.** Amplitude, phase and differential group delay of the 6<sup>th</sup>-ordre Butterworth filter used in simulations.

On Figure E-2 are presented characteristics of Filter2: resonator filter type with a constant group delay equal to zero (24 MHz double-sided).

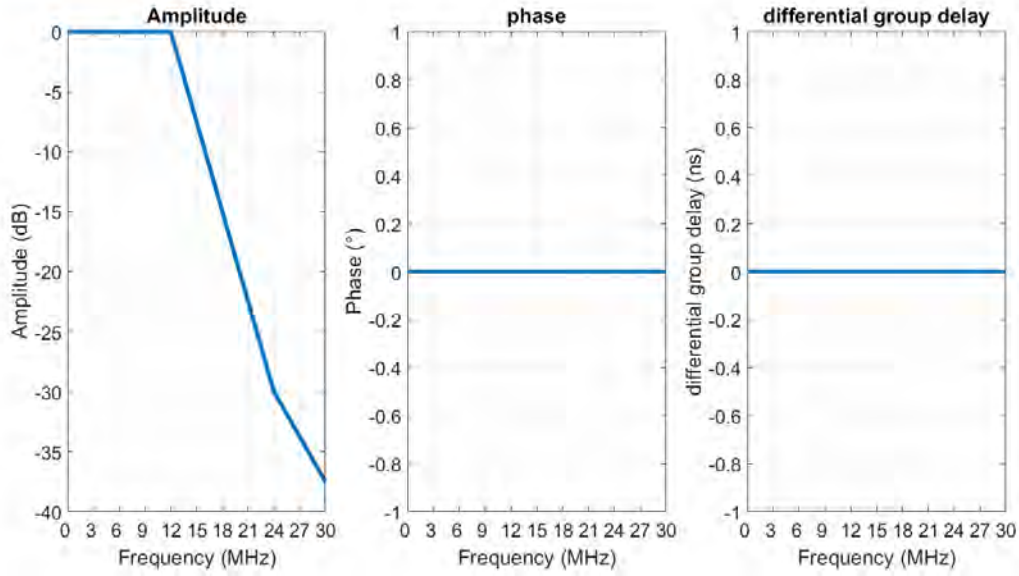


**Figure E-2.** Amplitude, phase and differential group delay of resonator filter type with a constant group delay equal to zero used in simulations.

On Figure E-3 are presented characteristics of Filter3: resonator filter type with a concave group delay and a 150 ns differential group delay (24 MHz double-sided).

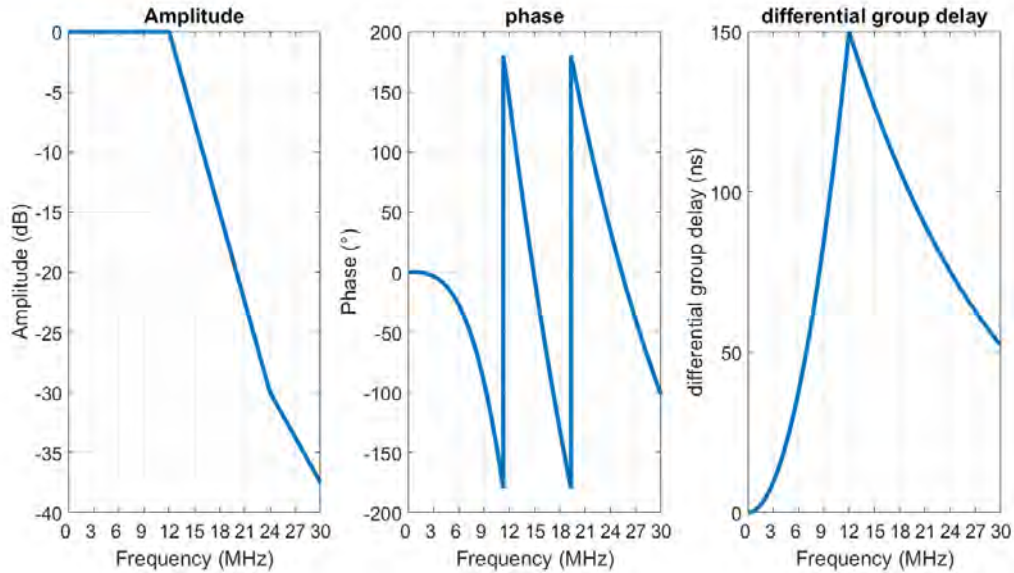


**Figure E-3.** Amplitude, phase and differential group delay of resonator filter type with a concave group delay and a 150 ns differential group delay used in simulations.

On Figure E-4 are presented characteristics of Filter4: 6<sup>th</sup>-order Butterworth for the amplitude and the smallest order Butterworth filter leading to a differential group delay higher than 150 ns for the phase (24 MHz double-sided).

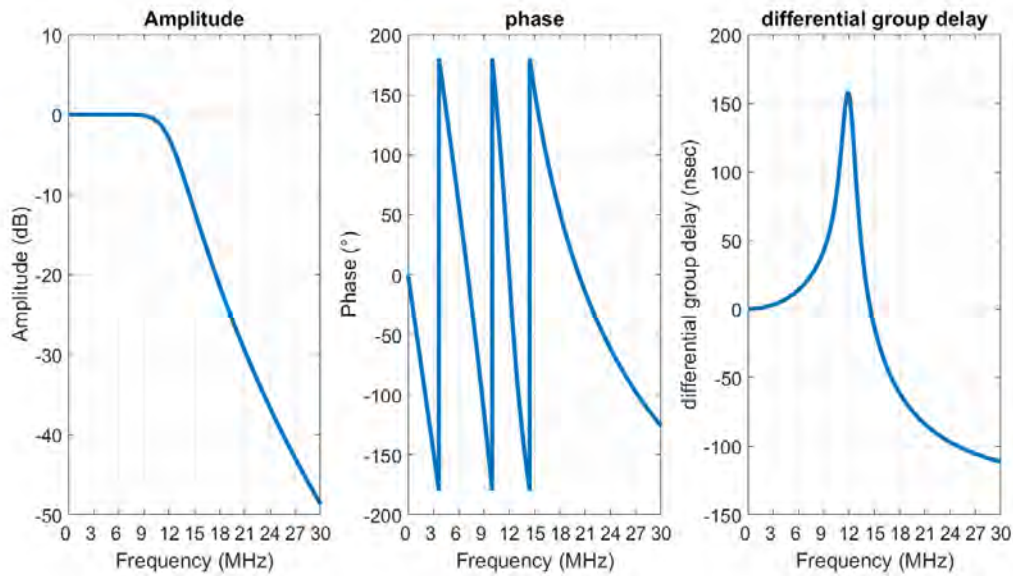


**Figure E-4.** Amplitude, phase and differential group delay of a 6<sup>th</sup>-order Butterworth filter for the amplitude and the smallest order Butterworth filter leading to a differential group delay higher than 150 ns for the phase used in simulations.

On Figure E-5 is shown the chip distortion induced by the four filters. This distortion can be interpreted as the impulse response of the filter.

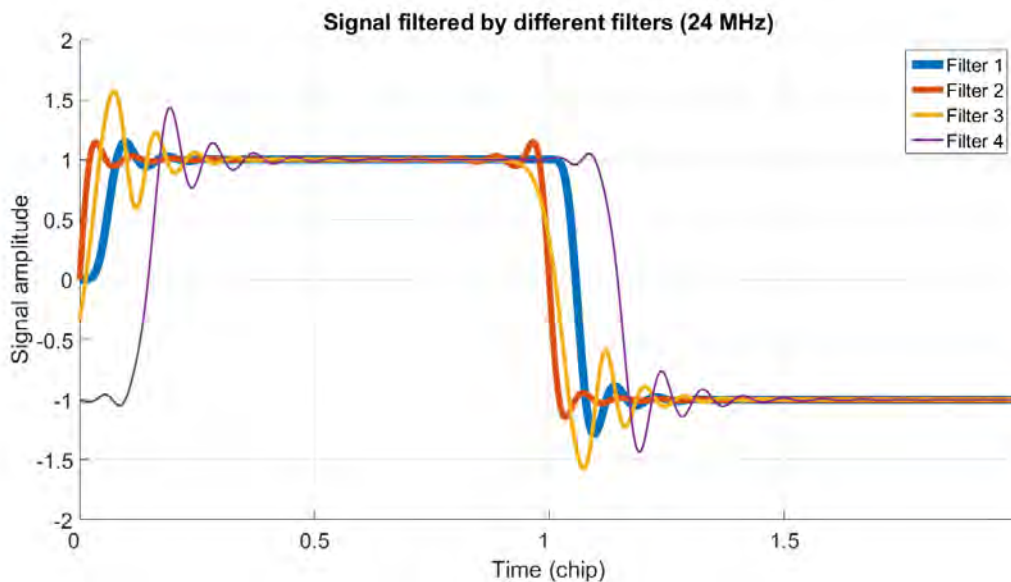


**Figure E-5.** Chip distortion induces by the four different filters.





## Appendix F. Distortions to test on the proposed TMs

A strategy is exposed in section 6.4.3 to assess how many more distortions have to be tested on proposed TMs than on the ICAO TM defined for GPS L1 C/A.

A parameter  $\Delta_{err\_dist}$  was introduced and is representative of the tracking error difference observed between two consecutive tested distortions. The concept to define an appropriate  $\sigma$  spacing between two consecutive distortions is to consider that only low enough  $\Delta_{err\_dist}$  values are tolerable.  $\Delta_{err\_dist}$  obtained with a reference sampling of the GPS L1 C/A current TS was estimated equal to 2.8 m. This is the approximate limit that has to be reached in the worst case when sampling the TS for the different studied signals.

In section 6.4.3, the concept is applied to estimate the number of distortions to test on the Galileo E1C TM-B area 1. In this appendix, the same reasoning is applied on area 2 of the Galileo E1C TM-B and to other signals.

### F.1 Number of tests on area 1 for Galileo E5a, GPS L5 and GPS L1 C/A

First the number of distortions to test on area 1 for Galileo E5a and GPS L5 signals is assessed. Then the number of distortions to test on area 1 of GPS L1 C/A signals is assessed.

#### F.1.1 Galileo E5a and GPS L5 area 1

The same principle as on Galileo E1C area 1 can be applied on Galileo E5a and GPS L5 signals. However, with these signals, it is not necessary to define different zones. One of the consequences is that less tests have to be performed.

The proposed grid presented in Figure F-1 contains 119 distortions. This grid has been created using the following parameters:  $f_d = 3:1:19$  MHz and  $\sigma = 0.05:4:24$  Mnepers/s.

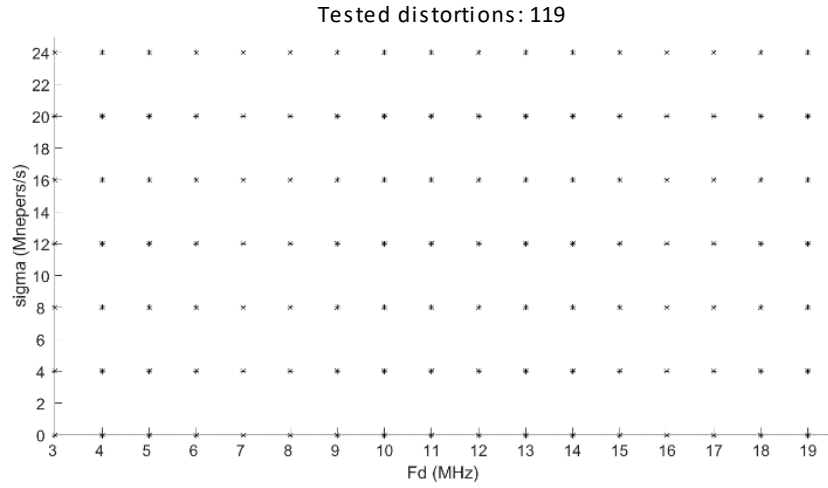


**Figure F-1.** Example of TS grid (Galileo E5a and GPS L5, area 1 of the proposed TM).

Associated  $\Delta_{err\_dist}$  are presented in Figure F-2:

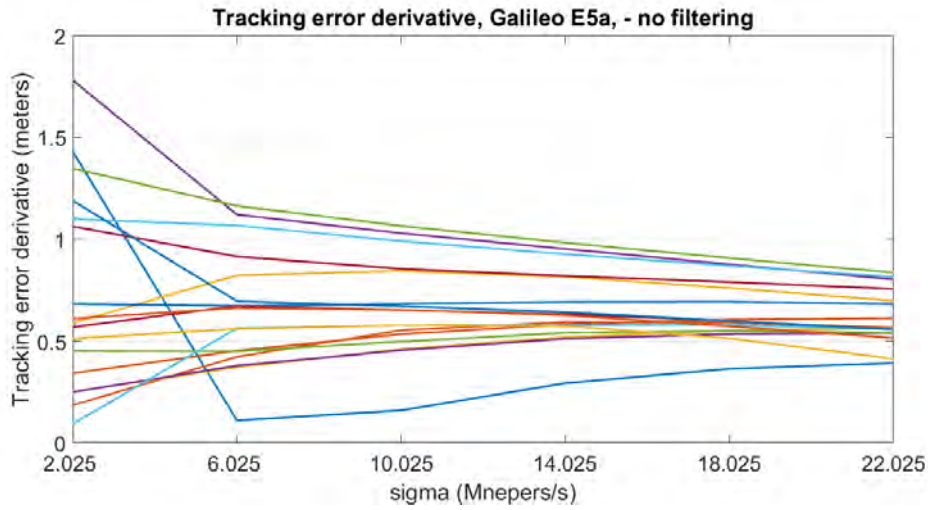


**Figure F-2.**  $\Delta_{err\_dist}$  associated to the selected TS grid (Galileo E5a and GPS L5, area1 of the proposed TM).

For the grid proposed on Figure F-1, the maximum value of  $\Delta_{err\_dist}$  (equal to 1.8 m) has the same order of magnitude (and is even smaller) as in the GPS L1 C/A ICAO TM case (see Figure F-2). It entails that the number of simulations to cover Galileo E5a and GPS L5 area 1 is approximatively the same ( $\approx 119/126$ ) as the number of simulations necessary to cover the GPS L1 C/A ICAO TM with an equivalent resolution.

### F.1.2 GPS L1 C/A area 1

The same principle can be applied on GPS L1 C/A signal.

The area 1 can be decomposed in four tested zones resulting in 1040 different distortions:

- Zone 1 to study low  $f_d$ . The grid consists of  $f_d = 1:1:4$  MHz and  $\sigma = 1:0.2:28$  Mnepers/s. This zone is included in the red square on Figure F-3.

- Zone 2 to study low  $\sigma$ . The grid consists of  $f_d = 3:1:19$  MHz and  $\sigma = 0.05:0.2:1$  Mnepers/s. It is noticeable that distortions with  $\sigma$  lower than 0.05 Mnepers/s cannot be studied without increasing dramatically the number of tests. This is why the lower bound of 0.05 Mnepers/s is set. This zone is included in the green square on Figure F-3.
- Zone 3 to study low  $\sigma$  and  $f_d$ . The grid consists of  $f_d = 1:1:3$  MHz and  $\sigma = 0.05:0.025:1$  Mnepers/s. This zone is included in the orange square on Figure F-3.
- Zone 4 to study the rest of the TS. The grid consists of  $f_d = 4:1:19$  MHz and  $\sigma = 1:1:28$  Mnepers/s. This zone is included in the blue square on Figure F-3.

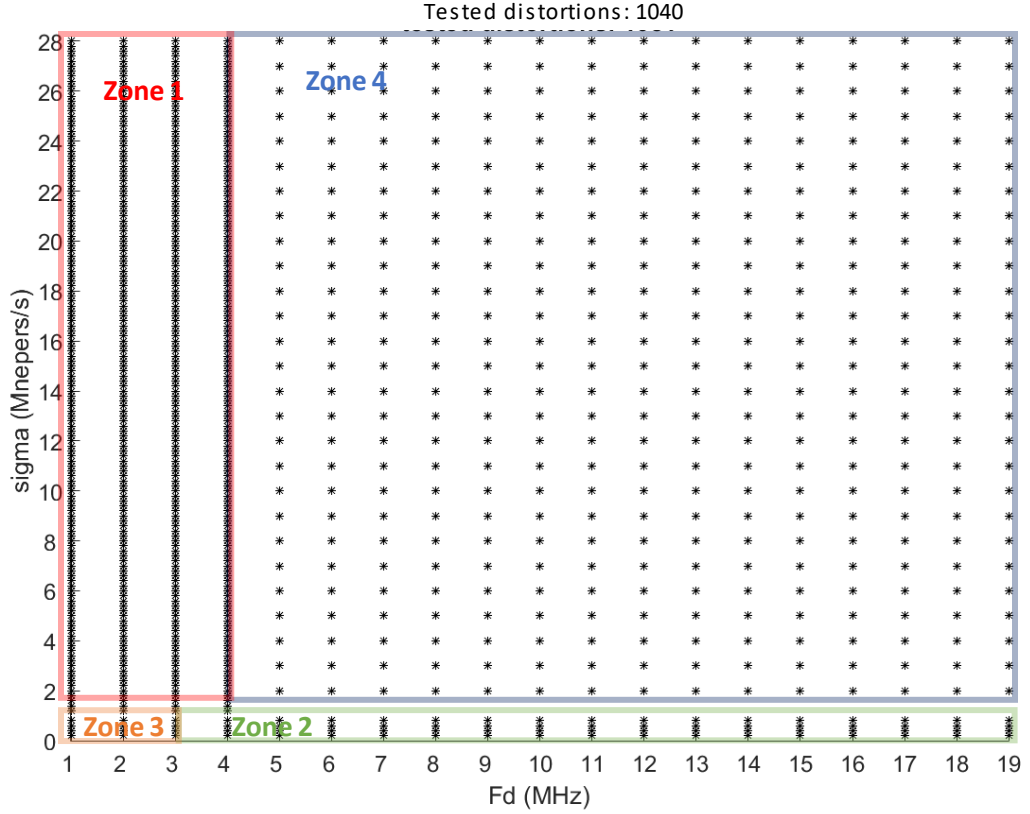


Figure F-3. Example of TSs grid (GPS L1 C/A, area 1 of the proposed TM).

$\Delta_{err\_dist}$  estimated for zone 1, zone 2 and zone 3 are presented in Figure F-4 (no filter is applied at receiver level). Results for zone 4 are not presented because from Figure 6-24, it was seen that with the selected grid on zone 4, the highest  $\Delta_{err\_dist}$  value is equal to 2.8 m.

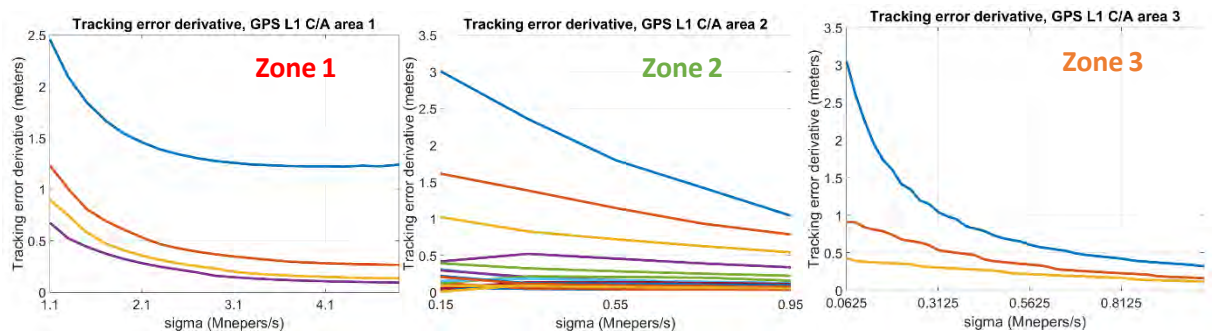


Figure F-4.  $\Delta_{err\_dist}$  associated to the selected TS grid for GPS L1 C/A area 1. On the left it corresponds to zone 1, on the middle to zone 2 and on the right to zone 3.

For the grid proposed on Figure F-3, the maximum value of  $\Delta_{err\_dist}$  (equal to 3.1 m) has the same order of magnitude as in the GPS L1 C/A ICAO TM case (see Figure F-4). It entails that the number of simulations to cover GPS L1 C/A area 1 has to be multiplied by 8.3 ( $\approx 1040/126$ ) compared to the number of simulations necessary to cover the GPS L1 C/A ICAO TM with the same resolution.

## F.2 Number of tests on area 2

Distortions in the area 2 of the TS must also be tested. The same strategy as the strategy used to define the number of distortions to test on area 1 is applied in this section to estimate the number of distortions to test on area 2 for Galileo E1C, Galileo E5a, GPS L5 and GPS L1 C/A signals.

### F.2.1 Galileo E1C area 2

In the Galileo E1C area 2, with the same mesh as in zone 3 of area 1 ( $f_d = 3:1:19$  MHz and  $\sigma/(f_d)^2 = 0.07:1:5$  Mnepers/MHz/MHz/s),  $\Delta_{err\_dist}$  are higher for high frequencies because a lot of  $\sigma$  values are omitted in the  $\sigma/(f_d)^2$  representation. This is why it is necessary to reduce the mesh in area 2 to reach the same resolution as on area 1. Regarding the Galileo E1C signal, it is decided to use a mesh twenty times thinner on the y-axis for area 2 as illustrated in Figure F-5 and Figure F-6. Figure F-5 corresponds to the TS grid in the  $\sigma/(f_d)^2$  representation whereas Figure F-6 is given in the  $\sigma$  representation.

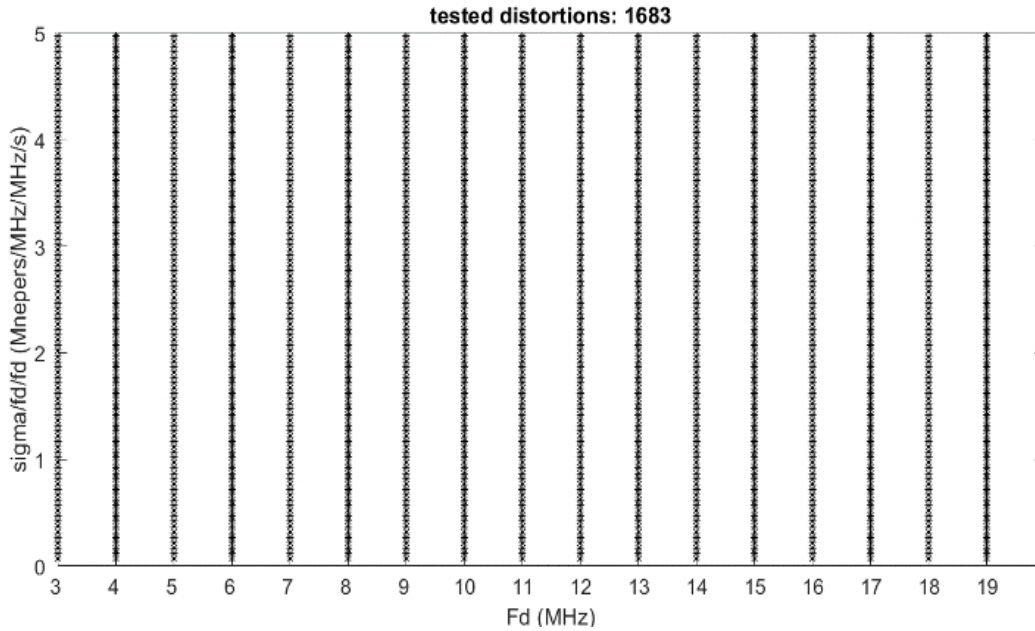
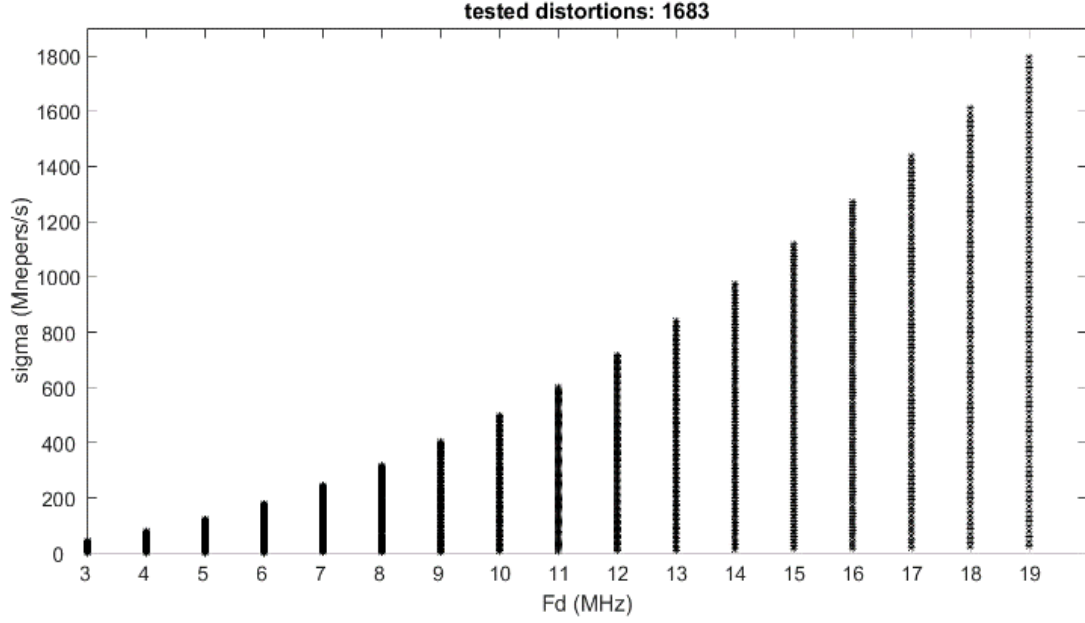
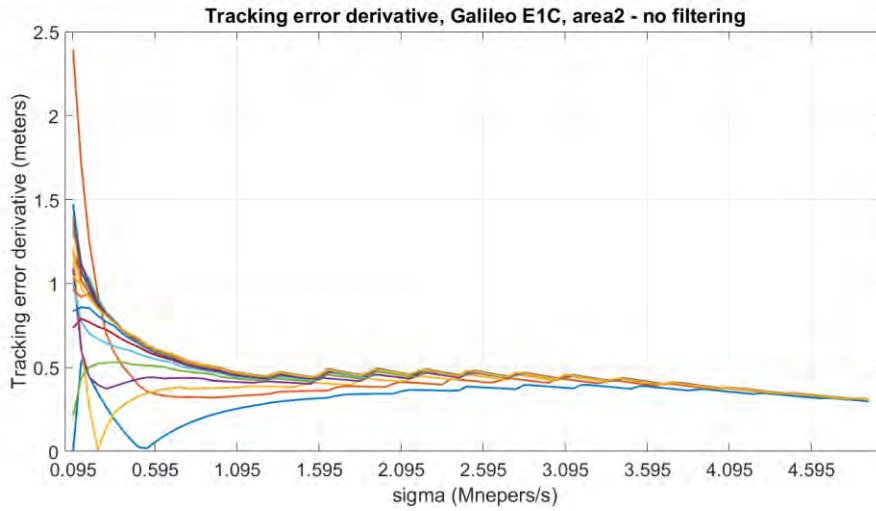


Figure F-5. Example of a TS grid in the  $\frac{\sigma}{(f_d)^2}$  representation (Galileo E1C, area2 of the proposed TM).



**Figure F-6.** Example of a TS grid in the  $\sigma$  representation (Galileo E1C, area2 of the proposed TM).

$\Delta_{err\_dist}$  is given Figure F-7 for this proposed grid. Different curves correspond to the seventeen tested  $f_d$  (from 3 MHz to 19 MHz). The x-axis gives the  $\sigma/(f_d)^2$  mean value of the two consecutive  $\sigma/(f_d)^2$  tested values (at fixed  $f_d$ ) at the origin of the  $\Delta_{err\_dist}$  computation.



**Figure F-7.**  $\Delta_{err\_dist}$  associated to the TS grid from Figure F-6 (Galileo E1C, area2 of the proposed TM).

From Figure F-7, it can be seen that with a thinner mesh ( $\sigma/(f_d)^2 = 0.07:0.05:5$  Mnepers/MHz/MHz/s), the maximum value of  $\Delta_{err\_dist}$  (equal to 2.4 m) has the same order of magnitude as in the GPS L1 C/A ICAO TM case. It means that an equivalent resolution is obtained if the number of tested distortions in area 2 is multiplied by 13.4 ( $\approx 1683/126$ ) compared to the number of tests necessary to cover the current ICAO TM.

### F.2.2 Galileo E5a and GPS L5 area 2

The same concept can be applied on Galileo E5a and GPS L5. Figure F-8 represents  $\Delta_{err\_dist}$  values for  $f_d = 4: 1: 19$  MHz. At each  $f_d$  value corresponds one curve. It is decided to use a mesh fifteen times thinner in ordinate than for area 1 ( $\sigma/(f_d)^2 = 0.06: 0.075: 3.5$  Mnepers/MHz/MHz/s).

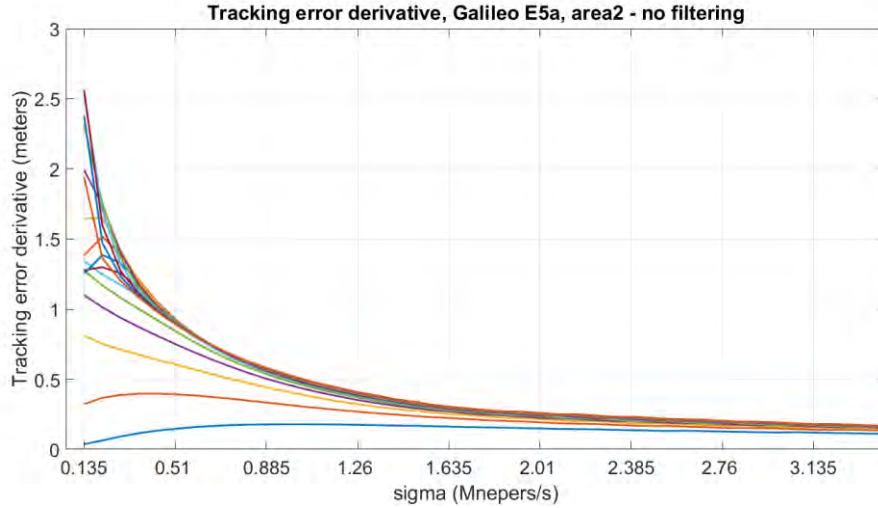


**Figure F-8.**  $\Delta_{err\_dist}$  values (Galileo E5a and GPS L5, area2 of the proposed TM).

As observed for Galileo E1C, for this grid, the maximum value of  $\Delta_{err\_dist}$  (equal to 2.6m) has the same order of magnitude as in the GPS L1 C/A ICAO TM case. It means that an equivalent resolution is obtained if the number of tested distortions in Galileo E5a and GPS L5 area 2 is multiplied by 6.7 ( $\approx 840/126$ ) compared to the number of tests necessary to cover the current ICAO TM.

### F.2.3 GPS L1 C/A area 2

The same concept can be applied on GPS L1 C/A. Figure F-9 represents  $\Delta_{err\_dist}$  values for  $f_d = 4: 1: 19$  MHz. At each  $f_d$  value corresponds one curve. It is decided to use a mesh ten times thinner on the y-axis than for zone 4 of area 1 ( $\sigma/(f_d)^2 = 0.07: 0.1: 1.8$  Mnepers/MHz/MHz/s).

For the proposed grid on area 2, the maximum value of  $\Delta_{err\_dist}$  (equal to 2.8 m) has the same order of magnitude as in the GPS L1 C/A ICAO TM case (see Figure F-9). It means that an equivalent resolution is obtained if the number of tested distortions in GPS L1 C/A area 2 is multiplied by 2.7 ( $= 342/126$ ) compared to the number of tests necessary to cover the current ICAO TM.

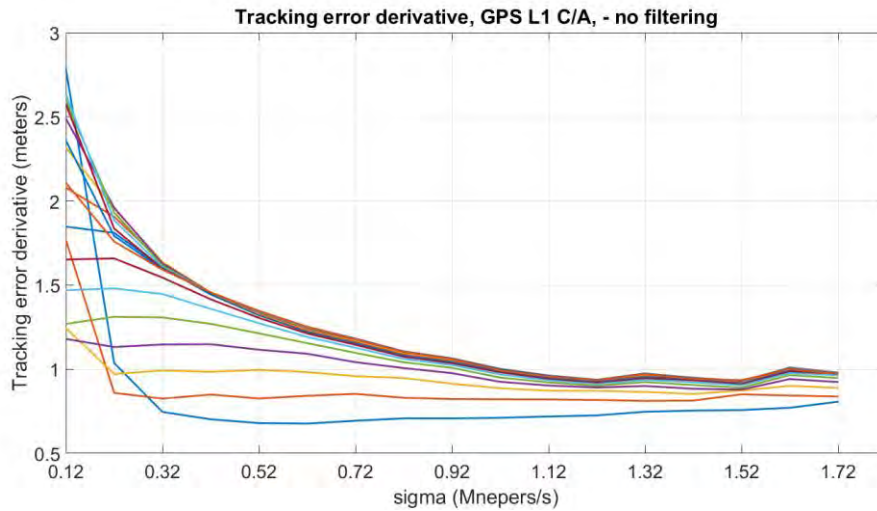


**Figure F-9.**  $\Delta_{err\_dist}$  values (GPS L1 C/A, area2 of the proposed TM).

### F.3 Conclusion about the number of distortions to test

To conclude, it has been seen in this section that longer simulations are required to cover the wide proposed TSs. However, to obtain approximatively the resolution with which the TS is examined in the GPS L1 C/A ICAO TM case, the number of simulations can be limited to:

- $13.4 + 8 = 21.4$  times the number of simulations compared to the current ICAO TM for Galileo E1C.
- $6.7 + 1 = 7.7$  times the number of simulations compared to the ICAO current TM for Galileo E5a.
- $8.3 + 2.7 = 11$  times the number of simulations compared to the ICAO current TM for GPS L1 C/A.

These three values are reasonable considering GNSS signal distortions context.





## Appendix G. Properties of TM-B distortions at $\sigma/f_d$ and $\sigma/(f_d)^2$ constant

In this appendix, two important properties of analog signal distortions are described. More precisely, two ratios defined from TM-B parameters have interesting properties:

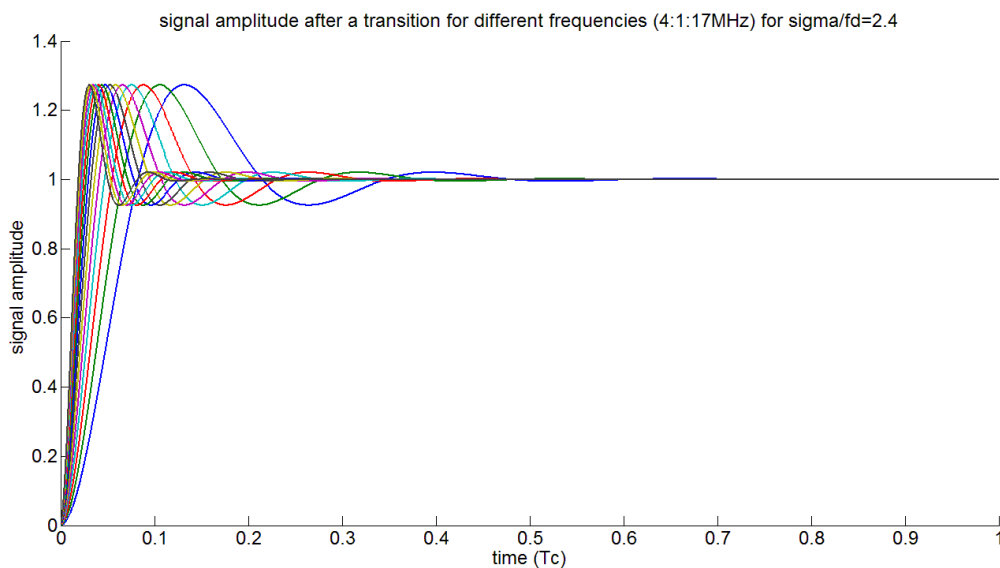
- $\sigma/f_d$  ratio defines the amplitude of the first peak overshoot caused by a distortion in the signal domain,
- $\sigma/(f_d)^2$  ratio defines the global shape of the correlation function.

The property of the second ratio is of primary interest because it can permit to reduce the number of distortions to test. Indeed, instead of testing all values of  $\sigma$  and  $f_d$  which lead to the same  $\sigma/(f_d)^2$  ratio and the same distorted correlation function, only one value of  $\sigma$  and  $f_d$  can be tested to take into account this distorted correlation function.

### G.1 $\sigma/f_d$ ratio

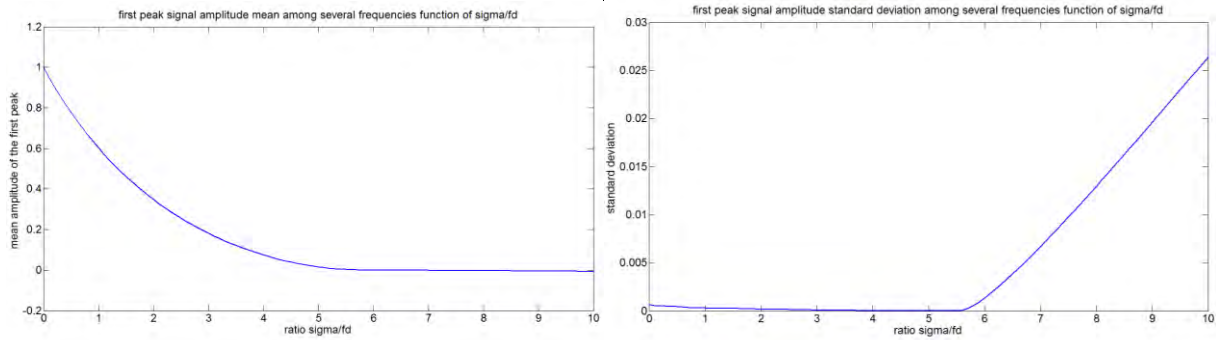
$\sigma/f_d$  value defines the signal distortion first peak overshoot.

Figure G-1 shows the signal amplitude after a transition applying a TM-B distortion. Different plots correspond to different  $f_d$  (from 4 MHz to 17 MHz with a 1 MHz increment). In this case,  $\sigma/f_d = 2.4$  nepers/Hz. It is visible that the maximum amplitude is the same for all  $f_d$  and is equal to 27 % of the chip amplitude.



**Figure G-1.** Signal shape for different  $f_d$  but the same  $\sigma/f_d$ . GPS L1 C/A.

Figure G-2 shows the average distortion first peak overshoot in % (left) and the standard deviation associated to this mean (right) for different  $\sigma/f_d$  ratios.

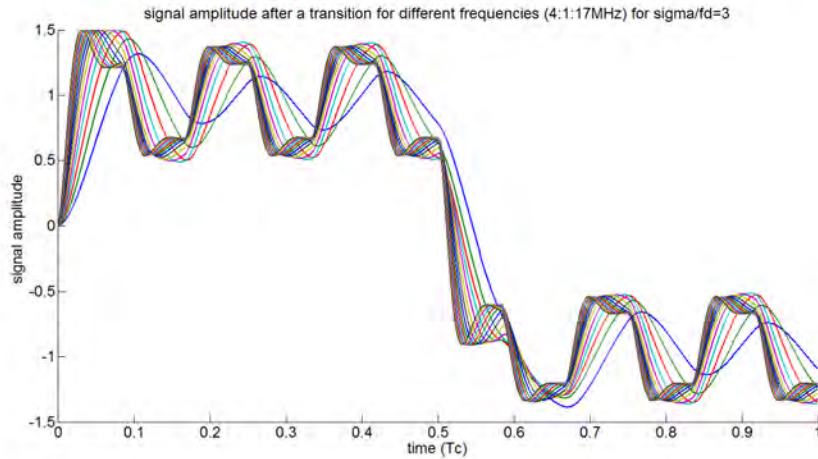


**Figure G-2.** Average distortion first peak overshoot in % (left) and standard deviation associated to the average (right) function of  $\sigma/f_d$ . GPS L1 C/A.

For  $\sigma/f_d < 5$  nepers/Hz, the overshoot of the first peak is not dependent on  $f_d$  but only on the ratio. For higher ratios, some  $f_d$  do not reach the chip amplitude, this is why the standard deviation increases. These results also highlight that from a certain ratio value, the distortion is strongly attenuated.

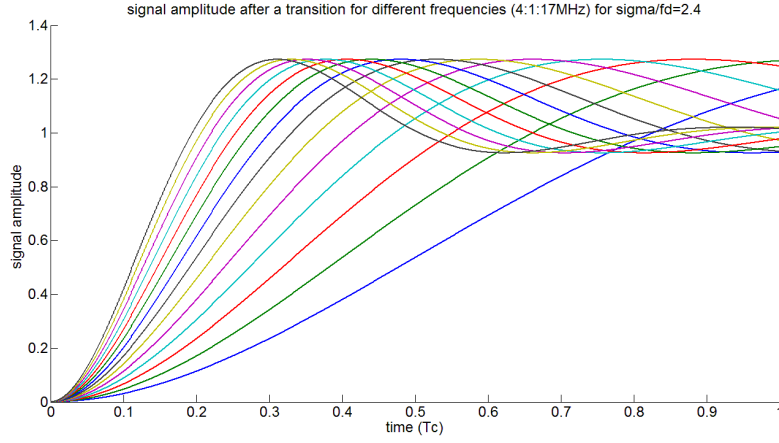
It appears that the first signal peak overshoot equal to 27 % of the chip amplitude is obtained for:

- $\sigma/f_d = 3$  nepers/Hz for Galileo E1C. For this ratio, the first peak amplitude is equal to  $1.48 - 1.23 = 0.25$  (1.23 is the high crenel sub-chip amplitude in the nominal case) as illustrated in Figure G-3.



**Figure G-3.** Signal shape for different  $f_d$  but the same  $\sigma/f_d = 3$  nepers/Hz. Galileo E1C.

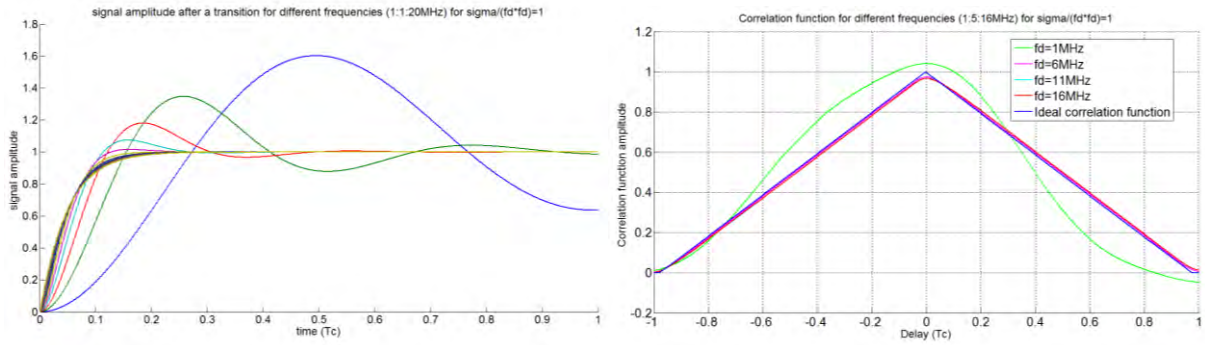
- $\sigma/f_d = 2.4$  nepers/Hz for Galileo E5a (as expected). For this ratio, the first peak overshoot is equal to  $1.27 - 1 = 0.27$  as illustrated in Figure G-4.



**Figure G-4.** Signal shape for different  $f_d$  but the same  $\sigma/f_d = 2.4$  nepers/Hz. Galileo E5a.

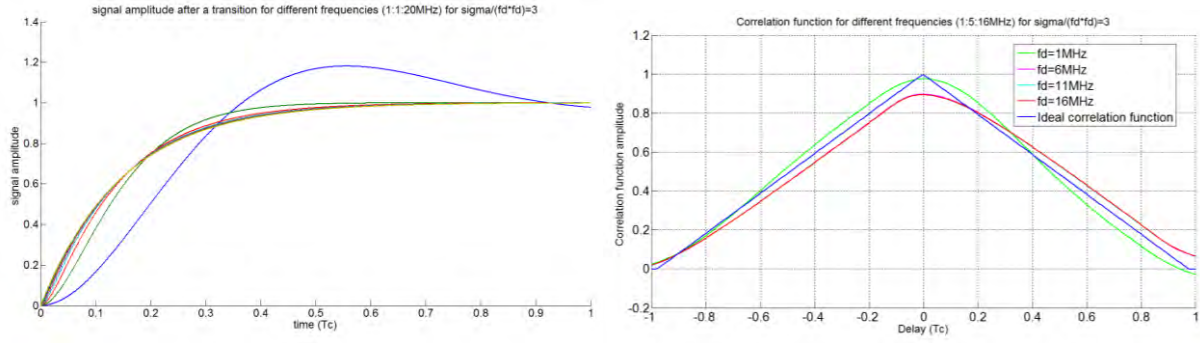
## G.2 $\sigma/(f_d)^2$ ratio

Figure G-5 illustrates signal (left) and correlation function (right) distortions for  $\sigma/(f_d)^2 = 1$  nepers/s/Hz/MHz and different  $f_d$  values. On the left,  $f_d$  are tested considering values of  $f_d$  from 1 MHz to 20 MHz with a 1 MHz increment. On the right, only four values of  $f_d$  are tested (1 MHz in green, 6 MHz in pink, 11 MHz in light blue and 16 MHz in red).



**Figure G-5.** Signals (left) and correlation functions (right) for several  $f_d$  but the same  $\sigma/(f_d)^2 = 1$  nepers/s/Hz/MHz. GPS L1 C/A signal.

Figure G-6 illustrates signal (left) and correlation function (right) distortions for  $\sigma/(f_d)^2 = 3$  nepers/s/Hz/MHz and different  $f_d$  values. Same colors as on Figure G-5 are used.



**Figure G-6.** Signals (left) and correlation functions (right) for several  $f_d$  but the same  $\sigma/(f_d)^2 = 3$  nepers/s/Hz/MHz. GPS L1 C/A signal.

Two conclusions are deduced from Figure G-5 and Figure G-6:

- $\sigma/(f_d)^2$  represents the general shape of the correlation function excepted for low  $f_d$ . It is noteworthy that for  $\sigma/(f_d)^2 = 3$  nepers/s/Hz/MHz, all correlation functions, affected by 6 MHz to 16 MHz  $f_d$ , have the same shape.
- Even correlation functions affected by highly attenuated distortions can lead to threatening tracking error. For  $\sigma/(f_d)^2 = 3$  nepers/s/Hz/MHz, apart from the 1 MHz signal distortion, the chip amplitude is not reached at the end of the chip. This phenomenon grows when the ratio  $\sigma/(f_d)^2$  increases. The consequence on the correlation function is that the peak is totally rounded and an asymmetry is visible.

Galileo E1C (left) and Galileo E5a (right) distorted correlation functions are presented in Figure G-7 for  $\sigma/(f_d)^2 = 1$  nepers/s/Hz/MHz and for different  $f_d$  (1 MHz in green, 6 MHz in pink, 11 MHz in light blue and 16 MHz in red).

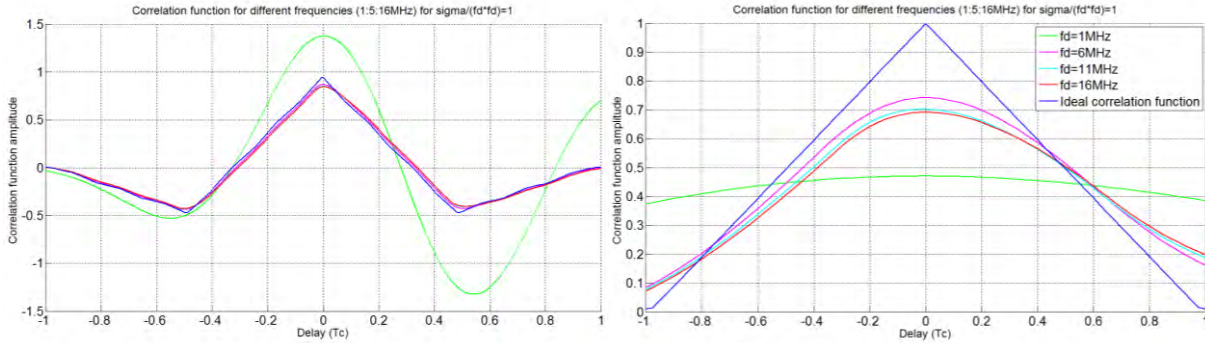


**Figure G-7.** Correlation function distortions for several  $f_d$  (1 : 5 : 16 MHz) but the same  $\sigma/(f_d)^2 = 1$  nepers/s/Hz/MHz. Galileo E1C on the right and Galileo E5a on the left.

The same phenomenon appears on new signals (from a certain  $f_d$ , the correlation function shape is only dependent on  $\sigma/(f_d)^2$ ). It is noticeable that highly attenuated signals distortions for new modulations are also fully visible and the asymmetry is stronger when  $\sigma/(f_d)^2$  is higher. The consequence is that the tracking bias entailed by these distortions is more important. This phenomenon is illustrated in Figure G-8 for a Galileo E1C signal. The plot is also shown in section 6.4.1.2.

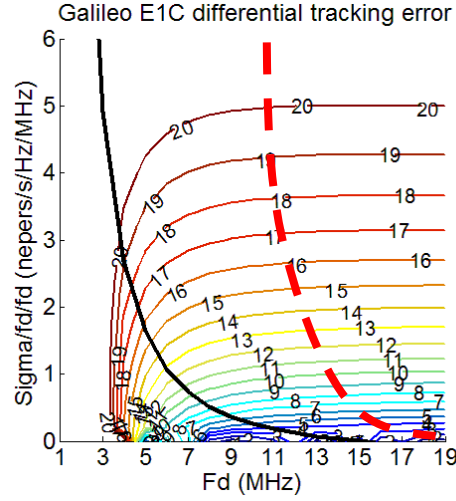


**Figure G-8.** Differential tracking error on a Galileo E1C signal in the  $\sigma/(f_d)^2$  representation.

Another important observation is that from a certain  $f_d$ , for a given  $\sigma/(f_d)^2 = cst$ , the tracking error is constant. If these results are visible, this is due to the fact that the correlation function distortion is constant for distortions satisfying  $\sigma/(f_d)^2 = cst$ . The saturation phenomenon illustrated by Figure G-8 is visible from the  $\sigma/(f_d)^2$  representation when the tracking error is independent from the frequency. This remark could simplify a lot the study of highly attenuated signal distortions: instead of considering all distortion parameters, it is possible to take into account only the first parameters set ( $f_d$  and  $\sigma$ ) leading to a particular distortion. These limit parameters sets can be approximatively considered on the red dashed line.

In the  $\sigma/(f_d)^2$  representation, it seems possible to include in the TM only distortions below the red dashed curve and the red dotted line (20 m limit). This would allow to reduce considerably the TM.





## **Modeling and monitoring of new GNSS signal distortions in the context of civil aviation**

GNSS is used nowadays in various fields for navigation and positioning including safety-of-life applications. Among these applications is civil aviation that requires a very high quality of service for the most demanding phases of flight in terms of integrity, accuracy, availability and continuity. To meet these requirements any source of potential service degradations has to be accounted for. One such example is GNSS signal distortions due to the satellite payload which can manifest in two ways: nominal distortions that are generated by healthy satellites due to payload imperfections and non-nominal distortions that are triggered by a satellite payload failure. The thesis first looks at the nominal distortions through GPS L1 C/A and Galileo E1C signals. Different types of observations are used based on correlation or chip domain visualization, and using high-gain and omnidirectional antennas. After the observation of nominal distortions, the dissertation investigates the non-nominal distortions due to the payload failure. Supported by the groundwork performed by civil aviation on signal distortion for the GPS L1 C/A signal, this dissertation aims at proposing new distortions models associated to the new GPS and Galileo signals that will be used by civil aviation after 2020. In particular, new TMs for new signals (GPS L5, Galileo E5a and Galileo E1C) are proposed. Finally, in this dissertation is built an appropriate monitor, referred to as SQM that is able to detect any distortion from the proposed TMs (for new signals) that could lead to a position integrity failure. Regarding GPS L1 C/A signal monitoring, such SQM is today implemented in GNSS augmentation systems including GBAS and SBAS. The current monitors are based on the analysis of the correlation function.

**Keywords:** *GNSS, signal processing, signal distortions, signal quality monitoring.*

---

## **Modélisation et surveillance des distorsions pour les nouveaux signaux GNSS dans le contexte de l'aviation civil**

Le GNSS est actuellement présent dans de nombreux domaines et permet le positionnement et la navigation. Parmi ces domaines, l'aviation civile a besoin d'une qualité de service élevée, notamment pendant les phases de vol les plus exigeantes en termes d'intégrité, de précision, de disponibilité et de continuité. Afin de satisfaire ces exigences, toutes les sources de dégradations potentielles du service doivent être prises en compte. Les distorsions des signaux GNSS générées par la charge utile du satellite sont un exemple de problème qui doit être pris en compte par l'aviation civile. Elles peuvent se manifester de deux manières différentes: les distorsions nominales générées par les satellites en fonctionnement normal et les distorsions non nominales générées lors d'une panne de la charge utile. Tout d'abord, cette thèse aborde le problème des déformations nominales affectant les signaux GPS L1 C/A et Galileo E1C. Différentes observations sont réalisées à partir de la visualisation de la fonction de corrélation ou du signal et par l'utilisation d'antennes à haut gain et d'une antenne omnidirectionnelle. Après l'observation des distorsions nominales, cette thèse aborde le sujet des distorsions non nominales du signal. En utilisant les travaux réalisés dans le passé par l'aviation civile dans le cadre du signal GPS L1 C/A, le but est de proposer de nouveaux modèles de distorsions associés aux nouveaux signaux GPS et Galileo qui vont être utilisés par l'aviation civile après 2020. Dans cette optique, de nouveaux modèles de menace (appelés TMs) pour les nouveaux signaux (GPS L5 et Galileo E5a et E1C) sont proposés. La dernière étape de cette thèse se focalise sur l'étude d'une technique capable de protéger un utilisateur de l'aviation civile contre les TMs proposés pour les nouveaux signaux. Cette technique appelée SQM est aujourd'hui implémentée dans les systèmes GBAS et SBAS pour détecter les distorsions de la fonction de corrélation dans le cadre des signaux GPS L1 C/A.

**Mots-clés:** *GNSS, traitement du signal, distorsions du signal, détection de distorsions.*